

HARNESSING RADICAL REACTIVITY WITH PARAMAGNETIC
ORGANOMETALLIC CHROMIUM COMPLEXES

by

Kenneth Cory MacLeod

B.Sc., The University of Prince Edward Island, 2007

A THESIS SUBMITTED IN PARTIAL FULFILLMENT OF
THE REQUIRMENTS FOR THE DEGREE OF

DOCTOR OF PHILOSOPHY

in

THE COLLEGE OF GRADUATE STUDIES

(Chemistry)

THE UNIVERSITY OF BRITISH COLUMBIA

(Okanagan)

April 2012

© Kenneth Cory MacLeod, 2012

Abstract

First-row transition metal complexes are increasingly being investigated as catalysts for organic synthesis. In addition to being more abundant, less expensive, and often less toxic compared to their second and third-row analogues, first-row complexes often exhibit complementary reactivity in the form of single-electron reaction pathways. One way of avoiding this complementary reactivity has been to use redox noninnocent ligands to enforce two-electron chemistry. An alternative is to embrace the radical reactivity of first-row metals.

Keeping this in mind, a CpCr β -diketiminato ligand platform, where Cp = cyclopentadienyl, was used to study Cr–C bond homolysis with a series of well-defined paramagnetic Cr(III) hydrocarbyl complexes. The results of that investigation led to the development of the first example of a single-component Cr initiator/mediator for organometallic mediated radical polymerization. Carbon–carbon bond forming reactions for organic synthesis were also targeted. A protocol was established for the Cr-catalyzed radical cyclization of bromo and chloroacetals, in which the first example of chloroacetal cyclization under catalytic conditions is reported. A tertiary phosphine was also prepared by radical C–P bond formation using a Cr catalyst.

Like many low-valent transition metal complexes, the Cr(II) compounds reported herein were extremely air-sensitive, leading to the formation of oxidation products containing strong Cr–O bonds. Methods were developed to selectively break the Cr–O bonds to convert the oxidized species back to catalytically relevant compounds and to reduce the need for stringent oxygen-free reaction conditions.

The final chapter examines the use of well-defined Cr compounds for C–C bond forming reactions that occur at the metal centre, as opposed to the free radical mechanisms discussed in the other chapters. Replacing the β -diketiminato ligand with a deprotonated benzylamine provided a ligand platform that was structurally similar to the CpCr β -diketiminato system, but incorporated a reactive Cr–C bond that was used to study reductive elimination reactions for C–C bond formation. Initial results indicate that reductive elimination from a Cr(IV) intermediate is achieved by single-electron oxidation of a Cr(III) complex.

Preface

The majority of the results presented in Chapter 2 have been published and some figures were reproduced with permission from: MacLeod, K. C.; Conway, J. L.; Tang, L.; Smith, J. J.; Corcoran, L. D.; Ballem, K. H. D.; Patrick, B. O.; Smith, K. M. *Organometallics* **2009**, 28, 6798–6806 (© 2009 American Chemical Society) and MacLeod, K. C.; Conway, J. L.; Patrick, B. O.; Smith, K. M. *J. Am. Chem. Soc.* **2010**, 132, 17325–17334 (© 2010 American Chemical Society). Preliminary syntheses of compounds **2.1**, **2.1b**, **2.2**, **2.2b**, **2.6**, **2.7**, **2.9**, and **2.14** were performed by the following Smith group researchers: Dr. Liming Tang (postdoctoral), Julia L. Conway (undergraduate), Joshua J. Smith (undergraduate), and Jeffrey A. Therrien (undergraduate). X-ray data collection was performed by Dr. Brian O. Patrick and Anita Lam at the University of British Columbia, Vancouver.

The majority of the results presented in Chapter 3 have been published and some figures were reproduced with permission from: MacLeod, K. C.; Patrick, B. O.; Smith, K. M. *Inorg. Chem.* **2012**, 51, 688–700 (© 2011 American Chemical Society). Preliminary syntheses of compounds **3.1**, **3.3**, **3.3c**, and **3.7** were performed by the following Smith group undergraduate researchers: Julia L. Conway and Katherine H. D. Ballem. Preliminary studies of **3.1** with Ph_3PI_2 were performed by Addison N. Desnoyer, an undergraduate researcher in the Smith group. X-ray data collection was performed by Dr. Brian O. Patrick and Anita Lam at the University of British Columbia, Vancouver.

The results presented in Chapter 4 have been published and some figures were reproduced with permission from: Champouret, Y.; MacLeod, K. C.; Ulrich, B.; Patrick, B. O.; Smith, K. M.; Poli, R. *Organometallics* **2010**, 29, 167–176 (© 2009 American Chemical Society) and Champouret, Y.; MacLeod, K. C.; Smith, K. M.; Patrick, B. O.; Poli, R. *Organometallics* **2010**, 29, 3125–3132 (© 2010 American Chemical Society). X-ray data collection was performed by Dr. Brian O. Patrick and Anita Lam at the University of British Columbia, Vancouver.

The haloacetal cyclization results in Chapter 5 have been published and some figures were reproduced with permission from: MacLeod, K. C.; Patrick, B. O.; Smith, K. M. *Organometallics* **2010**, 29, 6639–6641 (© 2010 American Chemical Society). X-ray data collection was performed by Dr. Brian O. Patrick and Anita Lam at the University of British Columbia, Vancouver.

Table of Contents

Abstract	ii
Preface	iii
Table of Contents.....	iv
List of Tables.....	vi
List of Figures	vii
List of Abbreviations	xi
Acknowledgements	xiii
Chapter 1 Radical Chemistry of the Transition Metals.....	1
1.1 Oxidative Addition to Transition Metal Complexes.....	1
1.2 Transition Metal Mediated Single-Electron Oxidative Addition in Organic Synthesis	3
1.3 Reversible Metal–Carbon Bond Formation	5
1.4 Controlled Radical Polymerization.....	6
1.5 Thesis Objectives	7
Chapter 2 Exploring Cr–C Bond Homolysis with CpCr[(ArNCMe)₂CH](R) Complexes ..	9
2.1 Attempted Synthesis of Cp*Cr[(XylNCMe) ₂ CH]	11
2.2 Alkyl Halide Activation	12
2.3 Synthesis of Cr(III) Halide Complexes	13
2.4 Synthetic Routes to CpCr[(ArNCMe) ₂ CH](R) Compounds	15
2.5 Steric Effects on the Synthesis of CpCr[(ArNCMe) ₂ CH](R) Compounds.....	19
2.6 Electronic Effects: Cyanomethyl and Benzyl Compounds.....	22
2.7 Phenyl, Alkenyl and Alkynyl Compounds	23
2.8 Solvent C–H Atom Abstraction	23
2.9 UV-visible Spectroscopy	25
2.10 X-ray Crystallography	27
2.11 Exploring Cr(III)–R Bond Homolysis	29
2.12 Exploring Cr(III)–R Photolysis	34
2.13 Experimental Section	35
Chapter 3 Reactivity of CpCr[(ArNCMe)₂CH](X) Complexes.....	49
3.1 Synthesis of {CpCr[(XylNCMe) ₂ CH]} ₂ (μ-O).....	50
3.2 Reactivity of {CpCr[(XylNCMe) ₂ CH]} ₂ (μ-O).....	52
3.3 Synthesis of Cr(III) Benzoate and Acetate Complexes	54
3.4 Synthesis of a Cr(III) Enolate Complex	54
3.5 Synthesis of Cr(III) Alkoxide Complexes	55
3.6 Manganese Reactivity with Cr(III) Compounds.....	56
3.7 Synthesis and Reactivity of a Cr(III) Fluoride Compound.....	58
3.8 C–F Bond Formation with CpCr[(XylNCMe) ₂ CH](F).	65
3.9 OAT Reactivity: PPh ₃ Oxidation.....	67

3.10	HAT Reactivity.....	69
3.11	Synthesis of $\{\text{CpCr}[(\text{HIPTNCMe})_2\text{CH}]\}_2(\mu\text{-O})$	72
3.12	Catalytic HAT.....	74
3.13	Synthesis and Reactivity of a Cr(III) Nitrosoarene Complex.....	76
3.14	Experimental Section.....	78
Chapter 4	Controlled Radical Polymerization of Vinyl Acetate.....	95
4.1	A Single-Component Chromium Reagent for OMRP.....	96
4.2	Identification of the Deactivated Complex, and Mechanistic Implications.....	101
4.3	ATRP of Vinyl Acetate.....	104
4.4	Reverse ATRP of Vinyl Acetate.....	105
4.5	Stoichiometric Reactions with $\text{CpCr}[(\text{XylNCMe})_2\text{CH}]$	107
4.6	Experimental Section.....	111
Chapter 5	Carbon-based Radicals for C–C and C–P Bond Formation.....	117
5.1	Radical Cyclization of Haloacetals.....	117
5.2	Chromium Catalyst Regeneration in Haloacetal Cyclization.....	124
5.3	C–C Bond Formation with Benzyl Radicals.....	126
5.4	Addition of Alkyl Radicals to Substituted Olefins.....	129
5.5	Chromium Catalyzed C–P Bond Formation.....	133
5.6	Experimental Section.....	135
Chapter 6	Synthesis and Reductive Elimination from CpCr Aryl Complexes.....	150
6.1	Synthesis of $\text{CpCr}(\text{C}_6\text{H}_4\text{CH}_2\text{NMe}_2)$	151
6.2	Single-Electron Oxidation of $\text{CpCr}(\text{C}_6\text{H}_4\text{CH}_2\text{NMe}_2)$	153
6.3	Synthesis of $\text{CpCr}(\text{C}_6\text{H}_4\text{CH}_2\text{NMe}_2)(\text{R})$ Complexes.....	155
6.4	Comparison of $\text{CpCr}(\text{C}_6\text{H}_4\text{CH}_2\text{NMe}_2)$ with $\text{CpCr}[\text{C}(\text{Ph})\text{C}(\text{Ph})\text{C}_6\text{H}_4\text{CH}_2\text{NMe}_2]$	158
6.5	Oxidatively Induced Reductive Elimination.....	160
6.6	Experimental Section.....	162
Chapter 7	Conclusions and Future Work.....	167
References.....		169
Apendices.....		180
Appendix A.	Supplementary X-ray Data.....	180
Appendix B.	^1H NMR Spectrum of Compound 5.3	189

List of Tables

Table 2.1. Selected bond lengths and angles for CpCr[(ArNCMe) ₂ CH](R) complexes.	27
Table 2.2. Comparison of rate constants for CpCr[(ArNCMe) ₂ CH](R) bond homolysis.	32
Table 3.1. HAT reactions for the conversion of γ -terpinene to <i>p</i> -cymene.	75
Table 4.1. Selected bond lengths (Å) and bond angles (deg) for complexes 3.3 , 3.3c , and 3.4	102
Table 5.1. Chromium-catalyzed radical cyclization of bromo and chloro acetals.	122
Table 5.2. Optimization experiments to reduce the air-sensitivity of haloacetal cyclizations.	125
Table 5.3. Addition of alkyl radicals to enones.	132
Table A.1. Crystal data and refinement parameters for X-ray structures of 2.1a , 2.2a , 2.3 , 2.3a , 2.3b , and 2.4	181
Table A.2. Crystal data and refinement parameters for X-ray structures of 2.6a , 2.6b , 2.7a , 2.7b , 2.7c , and 2.8	182
Table A.3. Crystal data and refinement parameters for X-ray structures of 2.10 , 2.10c , 2.11 , 2.11a , 2.13 , and 2.14a	183
Table A.4. Crystal data and refinement parameters for X-ray structures of 2.14b , 2.14c , 2.15 , 2.16 , 2.17 , and 2.18	184
Table A.5. Crystal data and refinement parameters for X-ray structures of 2.19 , 3.2 , 3.4 , 3.5 , and 3.6	185
Table A.6. Crystal data and refinement parameters for X-ray structures of 3.8 , 3.10 , 3.11 , 3.12 , and 4.3	186
Table A.7. Crystal data and refinement parameters for X-ray structures of 5.2 , 6.1 , 6.2 , 6.6 , and 6.7	187
Table A.8. Crystal data and refinement parameters for X-ray structures of 6.9 , 6.10 , and 6.11	188

List of Figures

Figure 1.1. Synthesis of aqueous Cr(III) alkyl compounds via radical C–H activation.	3
Figure 1.2. Proposed cycle for Cr-catalyzed Nozaki-Hiyama-Kishi reaction.	4
Figure 2.1. Synthesis of cyclopentadienyl chromium 2,6- ⁱ Pr ₂ C ₆ H ₃ (Dpp) substituted β-diketiminato compounds.	9
Figure 2.2. A list of the CpCr[(ArNCMe) ₂ CH](R) compounds and their halide precursors presented in this chapter.	11
Figure 2.3. Attempted synthesis of a Cp*Cr[(XylNCMe) ₂ CH] complex.	12
Figure 2.4. Comparison of the observed rate constants for the activation of Me ₃ SiCH ₂ I with compounds 2.1 (diamonds) and 2.1b (squares).	13
Figure 2.5. Thermal ellipsoid diagrams (50%) of Cr(III) chloride complexes 2.3 (a), 2.3a (b), and 2.3b (c).	14
Figure 2.6. Synthesis of the Cr(III) bromide complex CpCr[(XylNCMe) ₂ CH](Br) (2.5).	15
Figure 2.7. Thermal ellipsoid diagrams (50%) of Cr(III) tosylate complexes 2.6a (a) and 2.6b (b).	15
Figure 2.8. Synthetic routes to CpCr[(ArNCMe) ₂ CH](R) complexes.	16
Figure 2.9. Thermal ellipsoid diagrams (50%) of the Cr(III) methyl complex 2.2a (a) and Cr(III) trimethylsilylmethyl complexes 2.7a (b), 2.7b (c), and 2.7c (d).	17
Figure 2.10. Synthesis of 2.7 from Me ₃ SiCH ₂ I and Mn (method C).	18
Figure 2.11. Attempted synthesis of Cr(III)–CH ₂ CMe ₂ Ph complexes.	19
Figure 2.12. Thermal ellipsoid diagrams (50%) of 2.8 (a) and 2.1a (b).	20
Figure 2.13. Thermal ellipsoid diagrams (50%) of Cr(III) isobutyl complexes 2.10 (a) and 2.10c (b).	20
Figure 2.14. Thermal ellipsoid diagrams (50%) of Cr(III) neopentyl complexes 2.11 (a) and 2.11a (b).	21
Figure 2.15. Thermal ellipsoid diagrams (50%) of the Cr(III) cyanomethyl complex 2.13 (a), and Cr(III) benzyl complexes 2.14a (b), 2.14b (c), and 2.14c (d).	22
Figure 2.16. Thermal ellipsoid diagrams (50%) of Cr(III) phenyl (2.15 (a)), alkenyl (2.16 (b)), and alkynyl (2.17 (c)) complexes.	23
Figure 2.17. Reaction of 2.11 with benzylic C–H bonds to produce 2.14 and 2.18 , and a thermal ellipsoid diagram (50%) of 2.18 with all H atoms omitted for clarity.	24
Figure 2.18. UV-vis spectra of the Cr(II) complex 2.1 , and the Cr(III) neopentyl (2.11b),	

benzyl (2.14), and SPh (2.19) complexes in hexanes (1.1×10^{-4} M).	25
Figure 2.19. Use of radical trap X_2 to quantify Cr(III)–R bond homolysis.	30
Figure 2.20. Thermal ellipsoid diagram (50%) of 2.19	30
Figure 2.21. UV-vis decay curve for the conversion of Cr(III) neopentyl 2.11 to Cr(III)–SPh 2.19 ($k_{\text{obs}} = 3.54 \times 10^{-3} \text{ s}^{-1}$).	31
Figure 2.22. UV-vis decay curve (560 nm) for the Cr(III) isobutyl compounds 2.10 (a) and 2.10c (b) and pseudo-first-order rate constants k_{obs}^{-1} plotted against $[\text{PhSSPh}]^{-1}$ for compounds 2.11 (c), 2.14 (d), 2.14a (e), 2.14b (f), 2.14c (g), and 2.18 (h).	33
Figure 2.23. Decay curve for the conversion of 2.2 to 2.19 with light exposure ≥ 400 nm.	35
Figure 3.1. Proposed conversion of μ -oxo complex 3.1 back to the Cr(II) complex 2.1	49
Figure 3.2. Interconversion of CpCr β -diketiminate complexes.	51
Figure 3.3. UV-vis spectra monitoring reaction of the Cr(II) compound 2.1 [1.10×10^{-4} M] with air.	52
Figure 3.4. Conversion of μ -oxo compound 3.1 to Cr(III)–X species.	53
Figure 3.5. Thermal ellipsoid diagram (50%) of 3.5	54
Figure 3.6. Thermal ellipsoid diagram (50%) of 3.6	55
Figure 3.7. Thermal ellipsoid diagram (50%) of 3.8	59
Figure 3.8. Reaction of the Cr(III)–F (3.8) and Cr(III)–BF ₄ (3.9) complexes with Mn.	59
Figure 3.9. UV-vis spectra of the Cr(III)–BF ₄ complex 3.9 [4.91×10^{-5} M] in (a) Et ₂ O and (b) THF/Et ₂ O (9:1).	60
Figure 3.10. Reaction of the Cr(III) fluoride complex 3.8 with silanes.	61
Figure 3.11. Reaction of the Cr(III) tosylate complex 2.6 with Na[HB(Et) ₃], and subsequent air exposure to form the Cr(III) ethyl species.	62
Figure 3.12. Reaction of CpCr[(XylNCMe) ₂ CH](I) with BEt ₃ and O ₂	63
Figure 3.13. Reaction of Cr(III) fluoride complex 3.8 with BEt ₃ and O ₂	65
Figure 3.14. Reaction of the Cr(II) compound 2.1 with Ph ₃ CCl.	66
Figure 3.15. Conversion of Ph ₃ CCl to Ph ₃ CF with compound 3.8 as the F atom source.	66
Figure 3.16. Proposed mechanism for C–F bond formation.	67
Figure 3.17. Formation of OPPh ₃ from the μ -oxo complex 3.1	68
Figure 3.18. Thermal ellipsoid diagram (50%) of 3.2	70
Figure 3.19. Proposed mechanism for the formation of the Cr(III) hydroxide 3.2 from the μ -oxo complex 3.1	70
Figure 3.20. Reaction of the Cr(II) complex 2.1b with pyridine <i>N</i> -oxide.	71

Figure 3.21. Thermal ellipsoid diagram (50%) of 3.10 .	72
Figure 3.22. Synthesis of a HIPT substituted CpCr β -diketiminate complex and its reactivity with pyridine <i>N</i> -oxide.	73
Figure 3.23. Thermal ellipsoid diagram (50%) of 3.11 .	73
Figure 3.24. Nitrosoarene binding modes in transition metal compounds.	76
Figure 3.25. Thermal ellipsoid diagram (50%) of 3.12 .	77
Figure 3.26. Reaction of nitrosobenzene compound 3.12 with H atom sources.	78
Figure 4.1. Initiation and controlled polymerization with a single-component organometallic species	97
Figure 4.2. Conversion as a function of time for the VAc polymerization initiated by compound 2.11 .	98
Figure 4.3. Evolution of the UV-vis properties during the VAc polymerization controlled by compound 2.11 (conditions as shown in Figure 4.2).	99
Figure 4.4. Comparison of the radical polymerization of styrene, VAc, and MA using compound 2.11 as initiator.	100
Figure 4.5. Thermal ellipsoid diagram (50%) of 3.4 .	101
Figure 4.6. Proposed mechanism for the β -acetate transfer deactivation process.	102
Figure 4.7. Proposed mechanism for the OMRP of VAc with compound 2.11 .	103
Figure 4.8. Conversion as a function of time for the VAc polymerization initiated by MeCH(Cl)COOMe (In-Cl) in the presence of compound 2.1 (diamonds) or 2.1c (squares).	105
Figure 4.9. Conversion as a function of time for the VAc polymerization initiated by V-70 in the presence of compound 2.3c .	106
Figure 4.10. Conversion as a function of time for the VAc polymerization initiated by V-70 in the presence of compound 3.4 .	107
Figure 4.11. Reaction of the Cr(II) compound 2.1 with 0.5 equivalents of MeCH(Cl)COOMe.	108
Figure 4.12. Thermal ellipsoid diagram (50%) of the Cr(III) enolate complex 4.2 .	108
Figure 4.13. Proposed mechanism of ATRP and reverse ATRP for the polymerization of VAc using CpCr β -diketiminate complexes as polymerization mediators.	110
Figure 4.14. Reaction of the Cr(II) compound 2.1 with AIBN.	111
Figure 5.1. Oxidative addition of 5.1a with the Cr(II) compound 2.1 .	118
Figure 5.2. Thermal ellipsoid diagram (50%) of compound 5.2 .	118

Figure 5.3. Steric hindrance and Cr–R bond homolysis in Cr(III) alkyl complexes.	119
Figure 5.4. Photolysis of the Cr(III) alkyl compound 5.2	120
Figure 5.5. Proposed mechanism for the chromium-catalyzed radical cyclization of haloacetals.	123
Figure 5.6. Proposed catalytic cycle for the chromium-catalyzed synthesis of bibenzyl from PhCH ₂ Cl and ClMgCH ₂ Ph.	127
Figure 5.7. Proposed catalytic cycle for the chromium-catalyzed synthesis of bibenzyl from PhCH ₂ Cl with Mn as a reducing agent.	128
Figure 5.8. Conversion of Cr(III) enolate species to Cr(III) halides and reduction to Cr(II). ..	131
Figure 6.1. Chromium-catalyzed alkyne trimerization.	150
Figure 6.2. Previously reported synthesis and reactivity of CpCr(C ₆ H ₄ CH ₂ NMe ₂) (6.1).	152
Figure 6.3. Synthesis of compound CpCr(C ₆ H ₄ CH ₂ NMe ₂) (6.1).	152
Figure 6.4. Synthesis of compound CpCr[C(Ph)C(Ph)C ₆ H ₄ CH ₂ NMe ₂] (6.2).	153
Figure 6.5. Synthesis of Cr(III) CpCr(C ₆ H ₄ CH ₂ NMe ₂)(X) compounds by single-electron oxidation of CpCr(C ₆ H ₄ CH ₂ NMe ₂) (6.1).	154
Figure 6.6. Thermal ellipsoid diagrams (50%) of the Cr(III) alkoxide compound 6.6 (a) and the Cr(III)–SPh compound 6.7 (b).	155
Figure 6.7. Thermal ellipsoid diagram (50%) of 6.9	157
Figure 6.8. Synthesis of compound CpCr(C ₆ H ₄ CH ₂ NMe ₂)(C ₆ H ₄ Me) (6.10).	157
Figure 6.9. Synthesis of Cr(III) CpCr[C(Ph)C(Ph)C ₆ H ₄ CH ₂ NMe ₂](X) compounds by single-electron oxidation of CpCr[C(Ph)C(Ph)C ₆ H ₄ CH ₂ NMe ₂] (6.2).	158
Figure 6.10. Thermal ellipsoid diagram (50%) of 6.11	159
Figure A.1. Thermal ellipsoid diagram (50 %) of 3.11	180
Figure B.1. ¹ H NMR (400.1 MHz, CDCl ₃) spectrum of compound 5.3	189

List of Abbreviations

δ	chemical shift
ϵ	extinction coefficient
AIBN	2,2'-azobis(isobutyronitrile)
Ar	aryl
ATRP	atom transfer radical polymerization
BDE	bond dissociation energy
Col	collidine (2,4,6-trimethylpyridine)
Cp	cyclopentadienyl
Cp*	1,2,3,4,5-pentamethylcyclopentadienyl
CRP	controlled radical polymerization
Dep	2,6-diethylphenyl
Dpp	2,6-diisopropylphenyl
en	ethylenediamine
Et	ethyl
FRP	free radical polymerization
HAT	hydrogen atom transfer
HIPT	(2,4,6,2'',4'',6''-hexaisopropyl-1,3':5',1''-terphenyl)
In-Cl	methyl 2-chloropropionate [MeCH(Cl)COOMe]
Lut	lutidine (2,6-dimethylpyridine)
MA	methyl acrylate
Me	methyl
Mes	2,4,6-trimethylphenyl
M_n	number average molecular weight
$M_{n(th)}$	theoretical number average molecular weight
M_w	weight average molecular weight
M_w/M_n	molecular weight distribution
NHK	Nozaki-Hiyama-Kishi
OAT	oxygen atom transfer
OMRP	organometallic mediated radical polymerization
OTf	trifluoromethanesulfonate
OTs	<i>p</i> -toluenesulfonate
Pc	phthalocyaninate

Ph	phenyl
PMA	poly(methyl acrylate)
ppm	parts per million
PS	polystyrene
PVAc	poly(vinyl acetate)
py	pyridine
pz'H	3- <i>tert</i> -butyl-5-methylpyrazole
saloph	<i>N,N'</i> -bis(salicylidene)- <i>o</i> -phenylenediaminate
SEC	size exclusion chromatography
TBAT	tetrabutylammonium difluorotriphenylsilicate
TEMPO	(2,2,6,6-tetramethylpiperidin-1-yl)oxyl
THF	tetrahydrofuran
tmtaa	tetraaza[14]annulene (7,16-dihydro-6,8,15,17-tetramethyldibenzo[<i>b,i</i>][1,4,8,11]tetraazacyclotetradecinate)
TPP	5,10,15,20-tetraphenylporphyrinate
Tp ^{tBu,Me}	hydrotris(3- <i>tert</i> -butyl-5-methylpyrazolyl)borate
TPyEA	tris(2-pyrazol-1-ylethyl)amine
V-70	2,2'-azobis(4-methoxy-2,4-dimethylvaleronitrile)
VAc	vinyl acetate
Xyl	2,6-dimethylphenyl

Acknowledgements

I would like to thank my supervisor, Professor Kevin M. Smith, for his guidance and often infectious enthusiasm for scientific research. I am also inclined to thank my undergraduate research supervisor, the late Professor Robert I. Haines, for instilling in me the belief that rate laws are not something to be feared. I would also like to thank the past and present members of the Smith and McNeil lab groups for making the laboratory an environment that was rarely lacking in intellectually stimulating conversation. I would also like to thank Professor Stephen McNeil and Dr. James Bailey for helpful discussions, Professor Paul Shipley for always being willing to assist with NMR experiments, and Dr Brian Patrick for his patience in dealing with the seemingly endless learning curve that is X-ray crystallography.

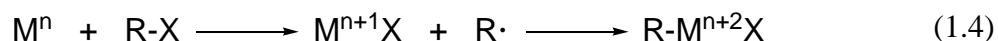
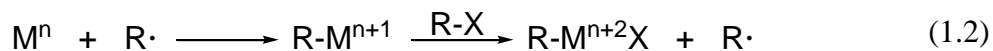
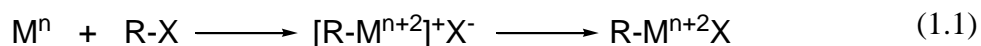
Finally, I would like to thank my family and friends for their support. In particular, I would like to thank my wife for her endless support, with whom I will soon be joining in the real world.

Chapter 1 Radical Chemistry of the Transition Metals

The study of well-defined transition metal compounds provides an opportunity to better understand reactions involving those complexes.¹ Structural modification of ligand systems can have pronounced implications on reactivity of the transition metal complexes involved. Structural elucidation of these compounds allows for an increased understanding into the steric and electronic factors that accompany such ligand modifications. Increasing our understanding of structure-activity relationships will allow the field of inorganic chemistry to progress towards the idea of rational catalyst design to both improve and further elaborate catalyst reactivity. The focus of this thesis is, therefore, the preparation and study of well-defined chromium compounds with a specific interest towards radical reactions.

1.1 Oxidative Addition to Transition Metal Complexes

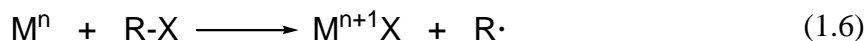
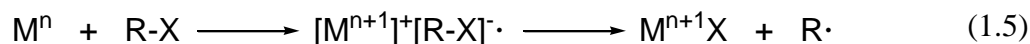
Oxidative addition reactions of transition metal compounds with alkyl halides (R-X) can proceed by a variety of different mechanisms.² Mechanisms involving the formal two-electron oxidation of the metal centre are shown in eq 1.1-1.4, where n indicates the oxidation state of the metal centre (M).² Eq 1.1 describes the S_N2 mechanism, where the metal centre acts as a nucleophile to attack the alkyl halide. This reaction proceeds by the formation of ionic intermediates and no radical species are formed during this process. Alternatively, the mechanisms in eq 1.2-1.4 involve the formation of radical intermediate species. All three reactions are described by two sequential single-electron oxidation events at the metal centre.



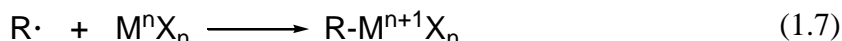
The distinction between eq 1.3 and 1.4 is the difference in the nature of the initial electron transfer. In the case of outer-sphere electron transfer (eq 1.3), an electron is transferred from the metal centre to the alkyl halide to form an ionic pair, which is followed by formation of the alkyl radical and the metal-halide complex. The inner-sphere mechanism (eq 1.4) involves halide atom transfer from the alkyl halide to the transition metal, resulting in the formation of the Mⁿ⁺¹X intermediate and the alkyl radical (R·). The C-based radical is then trapped by the Mⁿ⁺¹X

intermediate to form the organometallic product $R-M^{n+2}X$. The oxidative addition reactions described above are most common in second and third-row transition metal compounds because stable oxidation states of those metals are characteristically separated by two electrons.

First-row transition metals, on the other hand, are capable of easily accessing adjacent oxidation states. As a result, oxidative addition of organic halides with first-row transition metal complexes often leads to the formal single-electron oxidation of the metal centre, as opposed to the two-electron oxidations described above.³ The oxidative addition can proceed by either the outer-sphere (eq 1.5) or inner-sphere (eq 1.6) mechanisms. In both cases the oxidized $M^{n+1}X$ complex and an organic radical $R\cdot$ is generated. Because these reactions are limited to single-electron oxidations of the metal centre, the radical is not trapped by the $M^{n+1}X$ species and, therefore, can react with a second equivalent of the transition metal starting material.

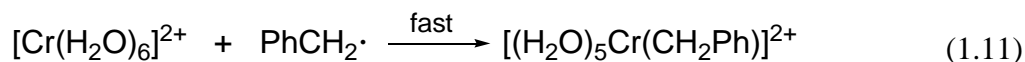
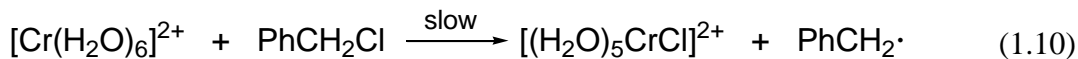


In general, organic radicals can react with transition metal compounds to form a metal–carbon bond, as shown in eq 1.7, or electron transfer between the radical and the transition metal may occur (eq 1.8).³ A third possibility involves ligand transfer from the transition metal to the organic radical (eq 1.9).³



Early examples of single-electron oxidation of transition metal compounds for the reduction of organic halides included $[Co(CN)_5]^{3-}$ and aqueous Cr(II). Reaction between Me–I and $[Co(CN)_5]^{3-}$ formed the Co(III) species $[Co(CN)_5(I)]^{3-}$ and the organic radical $Me\cdot$ according to the mechanism shown in eq 1.6.^{2a} A second equivalent of the Co starting material is then capable of trapping $Me\cdot$ to form the Co(III) species $[Co(CN)_5(Me)]^{3-}$ according to eq 1.7. The reduction of benzyl chloride ($PhCH_2Cl$) with aqueous Cr(II) provided the expected Cr(III) species $[(H_2O)_5CrCl]^{2+}$ and $[(H_2O)_5Cr(CH_2Ph)]^{2+}$.⁴ The single-electron oxidative addition of chloroform ($CHCl_3$) was also reported to provide the aqueous Cr(III) chloride species and the

organochromium compound $[(\text{H}_2\text{O})_5\text{Cr}(\text{CHCl}_2)]^{2+}$.⁵ Subsequent work by Kochi described the mechanism for the oxidative addition of PhCH_2Cl with aqueous $\text{Cr}(\text{II})$ as a two step process.⁶ The first step involved the rate determining inner-sphere electron transfer, shown in eq 1.10, to generate the $\text{Cr}(\text{III})$ chloride species and a benzyl radical. The benzyl radical then reacted with a second equivalent of $\text{Cr}(\text{II})$ to form the organochromium species in a second fast step (eq 1.11).



The rate determining oxidative addition step with aqueous $\text{Cr}(\text{II})$ was limited to highly activated alkyl halides. The rate of reaction was enhanced by addition of N-donor ligands such as ethylenediamine (en).⁷ Radical clock experiments were conducted to provide further evidence for the mechanism involving organic radical intermediates, and allowed for determination of the rate constant for trapping the organic radical with the $[\text{Cr}(\text{en})_2]^{2+}$ complex.⁷ The rate constants for trapping organic radicals with $[\text{Cr}(\text{en})_2]^{2+}$ was on the order of $10^7 \text{ M}^{-1}\text{s}^{-1}$.

The use of H_2O_2 ⁸ and pulse radiolysis⁹ to generate reactive $\cdot\text{OH}$ radicals in situ, which are then able to abstract H atoms from organic substrates was used to prepare organic radicals and study the trapping of such radicals with aqueous $\text{Cr}(\text{II})$ (Figure 1.1). The radical trapping by aqueous $\text{Cr}(\text{II})$ is also extremely rapid, approaching the diffusion control limit at 10^7 to $10^8 \text{ M}^{-1}\text{s}^{-1}$, and is relatively constant regardless of the nature of the organic radical.¹⁰

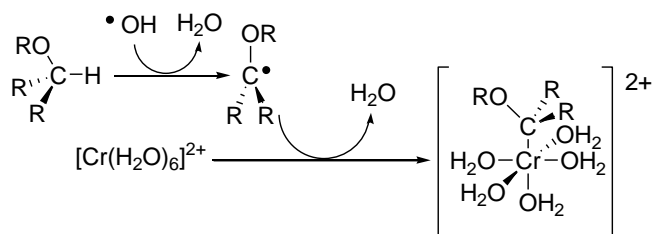


Figure 1.1. Synthesis of aqueous $\text{Cr}(\text{III})$ alkyl compounds via radical C–H activation.

1.2 Transition Metal Mediated Single-Electron Oxidative Addition in Organic Synthesis

Single-electron oxidative addition reactions of chromium have received extensive use for the coupling of organic halides with aldehydes. Hiyama and co-workers reported the use of CrCl_2 in THF for the coupling of allyl halides and aldehydes to provide allyl alcohols.¹¹ This reaction proceeds by single-electron oxidation of the allyl halide to form the $\text{Cr}(\text{III})$ halide species and an allyl radical. The allyl radical is then trapped by a second equivalent of CrCl_2 to

form a Cr(III) allyl species, which undergoes insertion of the aldehyde into the Cr–C bond to form a Cr(III) alkoxide species, which is hydrolyzed to obtain the allyl alcohol products. Nozaki and Kishi later reported that catalytic amounts of NiCl_2 could be used to increase the substrate scope by activating alkenyl or aryl halides.¹² The first report of a Nozaki-Hiyama-Kishi (NHK) reaction that proceeded with a catalytic amount of Cr was developed by Fürstner and Shi.¹³ The proposed catalytic cycle shown in Figure 1.2 used Me_3SiCl to break the Cr–O bond and Mn powder as the stoichiometric reductant to recycle the Cr.

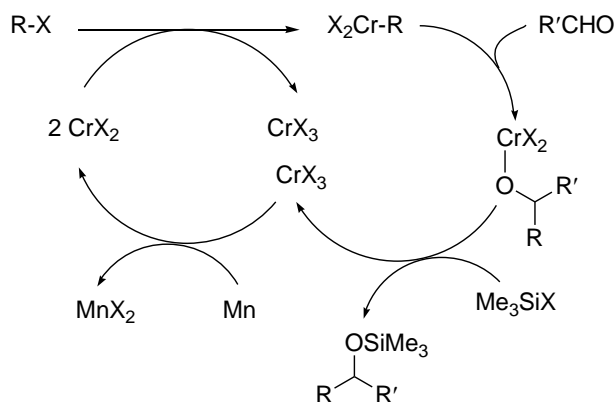
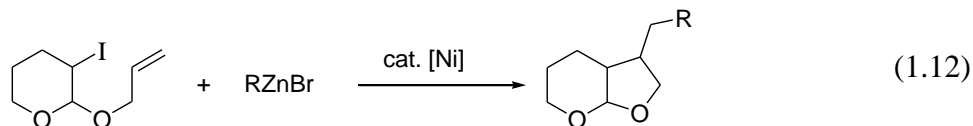


Figure 1.2. Proposed cycle for Cr-catalyzed Nozaki-Hiyama-Kishi reaction.

The chiral alcohol formed upon coupling of an organic halide with an aldehyde or ketone in these reactions typically leads to a mixture of enantiomers. The development of catalytic asymmetric Cr-mediated coupling reactions has allowed for the preparation of enantiomerically enriched products.¹⁴ Kishi and co-workers have developed Cr sulfonamide catalysts and applied them in natural product total synthesis of increasingly complex molecules. They recently reported the total synthesis of halichondrin C using seven individual Cr-mediated coupling reactions for the installation of a new C–C bond in each reaction.¹⁵ The total synthesis of a series of halichondrins and their synthetic intermediates by Kishi and co-workers led to the discovery of the anticancer drug Eribulin, which is a synthetic analogue of halichondrin B.¹⁶ Previous to the total synthesis reported by Kishi and co-workers, the full scale drug discovery and development of halochondrins had been limited by the ability to obtain the compounds in sufficiently large quantities from natural sources, despite the known high antitumor activity of the compounds. Due to the sheer structural complexity of the halochondrins and Eribulin, the ability to prepare the compounds in an economically feasible manner will ultimately determine the potential for success in this area, with Cr catalyzed asymmetric coupling reactions playing a key role.¹⁶

First-row transition metals are increasingly being investigated for their use in catalytic C–C bond forming reactions.¹⁷ These compounds often display complementary reactivity compared to their second and third-row analogues, which is often manifested in radical reactivity. In particular, the development of Ni, Co, and Fe catalysts for cross-coupling reactions has led to an increased appreciation for the prevalence of radical reactivity in reactions involving alkyl substrates, with secondary alkyl halides being particularly prone to radical reactivity.¹⁸ Ni-catalyzed alkyl-alkyl Negishi coupling reactions are proposed to proceed by single-electron reduction of the alkyl halide to form a Ni iodide species and an alkyl radical.¹⁹ Work by Hu and co-workers used radical clocks to establish the presence of alkyl radicals in Ni-catalyzed alkyl-alkyl Kumada coupling reactions.²⁰ Alkyl halides capable of undergoing intramolecular radical C–C bond formation have also been used as substrates in Ni²¹ and Co²² catalyzed cross-coupling reactions to achieve multiple C–C bond forming processes in a single reaction sequence. An example is shown in eq 1.12, where oxidative addition of the alkyl halide with the Ni catalyst generates the alkyl radical, which then undergoes rapid intramolecular radical cyclization and the resulting bicyclic radical is then trapped by the Ni. Transmetalation between the Zn and Ni installs the R group on the Ni and reductive elimination provides the coupled product.²¹



Fu and co-workers recently reported the asymmetric Suzuki cross-coupling for activated alkyl halides using chiral Ni catalysts.²³ These reactions convert racemic organic halides into chiral products by taking advantage of the presence of planar radical intermediates, which are trapped by the chiral Ni catalyst to reductively eliminate enantioenriched products.

1.3 Reversible Metal–Carbon Bond Formation

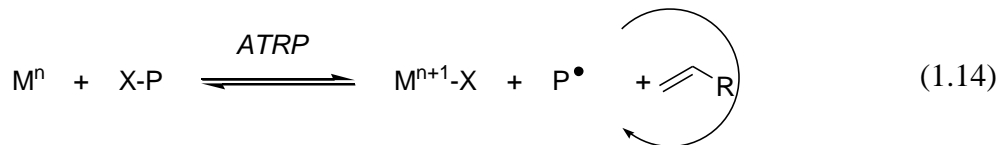
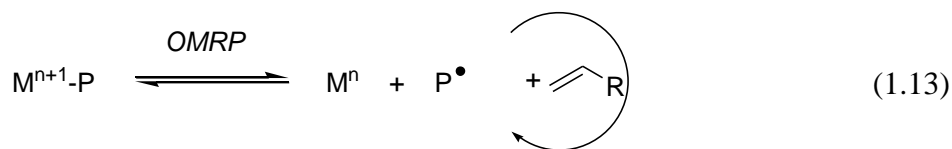
Homolytic metal–carbon (M–C) bond cleavage is the microscopic reverse of eq 1.7, involving the formation of an organic radical species. Perhaps the most widely studied example of M–C bond homolysis is that of cobalamin (vitamin B₁₂). Halpern and co-workers first reported the study of homolytic bond cleavage in synthetic cobalamin analogues in 1982.²⁴ Their work described kinetic methods for the quantitative determination of homolysis rate constants, and through a full kinetic analysis M–C bond dissociation energies (BDEs) were reported. A review was later published by Halpern describing, in detail, the experimental procedures that had been developed for the determination of M–C bond homolysis rate constants

and BDEs.²⁵ Cr–C bond homolysis was also studied in the aqueous Cr(III) alkyl compounds described above.²⁶ Teuben and Luinstra also reported the observation of Ti–C bond homolysis in substituted titanocene alkyl compounds.²⁷ In the same year, Finke and Daikh described a Co macrocycle complex that reversibly formed a Co–C bond with a benzyl radical.²⁸ The complex was reported to undergo rapid and reversible M–C bond homolysis in solution, and yet the complex persisted in solution unless a radical trap was introduced to quench the benzyl radicals. Finke termed this stability of radical intermediates as the persistent radical effect (PRE). This term refers to the fact that even though benzyl radical coupling to form bibenzyl is extremely rapid ($10^9 \text{ M}^{-1} \text{ s}^{-1}$), the resulting Co(II) complex is stable in solution. Therefore, the concentration of Co(II) builds up initially in solution, which leads to a decrease in the benzyl radical concentration and effectively prevents further decomposition of the organic radicals by bimolecular coupling reactions.

1.4 Controlled Radical Polymerization

Controlled radical polymerization (CRP) is a relatively recent advancement in polymer chemistry, which has led to the development of materials that are not easily prepared by other polymerization techniques. In particular, the development of CRP has provided improved methods for polymerizing polar monomers to provide polymeric materials with uniform molecular weights.²⁹ Chain growth occurs by attack of the radical species on the double bond of a monomer to form a new C–C bond. This process is selective for radical attack on the least substituted C atom of the double bond, and, therefore, as the polymer chain continues to grow the same radical is generated with each sequential addition of a monomer unit.

The fundamental principle behind CRP relies on the ability to sufficiently reduce the effective concentration of radical species in solution during the polymerization process as a means of avoiding unwanted radical coupling termination events.³⁰ Reducing the concentration of radical species in these reactions is achieved by reversible trapping of the growing polymer chains. First-row transition metal complexes are particularly well suited to this task due to easily accessible adjacent oxidation states. Two major strategies have been developed for transition metal-mediated CRP: organometallic-mediated radical polymerization (OMRP), where the growing polymer chains ($\text{P}\cdot$) are reversibly trapped by a transition metal species to form a M–C bond (eq 1.13); and atom transfer radical polymerization (ATRP), where an M–X compound (X is typically a halogen atom) is used to reversibly transfer X to the growing polymer chains, forming X-capped dormant polymers (eq 1.14).²⁹



Both processes rely on the persistent nature of the metal complex. In OMRP the metal complex acts as a radical trap to reduce the effective concentration of growing radical chains in solution. While ATRP relies on the same fundamental principal of reducing the radical concentration in solution, this is achieved by reversibly capping the growing polymer chains with a halogen atom. In both cases the radical process must be initiated. This is most often achieved by the addition of a radical initiator. For OMRP, azo initiators are most commonly used to initiate the radical polymerization process. These initiators are thermally decomposed to generate reactive radical intermediates in situ.

ATRP initiators are typically activated alkyl halides, which react rapidly in a single-electron oxidative addition reaction (eq 1.5 and 1.6) with the metal complex to generate the oxidized $M^{n+1}-X$ species and an organic radical.³¹ The organic radical can then either react with the oxidized metal species to reform the organic halide, or react with monomer to initiate the polymer chain growth process. The $M^{n+1}X$ species generated in situ is now present in solution and will reversibly transfer the halide atom to the growing polymer chains (eq 1.14).

An alternative is to start with a metal complex in the oxidized $M^{n+1}-X$ state and to add an azo initiator to start the polymerization process. This technique of starting with a well-defined $M^{n+1}-X$ as the control agent is referred to as reverse ATRP. This process reduces the possibility of unwanted side reactions between the reduced M^n species and the radical initiator, and also forces ATRP conditions at the beginning of the polymerization process because there is no M^n species in solution at the outset of the reaction.

1.5 Thesis Objectives

The main focus of this thesis was to evaluate the ability of well-defined Cr compounds to control radical reactions. Despite the previously established reactivity between Cr(II) and organic halides, Cr-mediated reduction of organic halides is rarely studied with well-defined Cr compounds. In the present study, a series of Cr(II) CpCr β -diketiminato compounds, where Cp =

cyclopentadienyl, were prepared as a means of studying the reactivity between organic halides and Cr(II). The ancillary Cp and β -diketiminato ligands reported herein consistently remained tightly bound to the metal centre facilitating characterization of both starting materials and reaction products of the Cr(II)/Cr(III) redox couple. Additionally, the electron-donating Cp and β -diketiminato ligands, in combination with the coordinatively unsaturated Cr(II) metal centre provided highly reactive isolable compounds for this study.

In Chapter 2 a series of CpCr β -diketiminato hydrocarbyl compounds were synthesized and fully characterized, and kinetics studies were performed to evaluate the propensity for Cr–C bond homolysis. The main objective of Chapter 3 was to establish methods of regenerating viable CpCr β -diketiminato compounds from air-exposed decomposition products. This was achieved by studying different methods for selectively breaking strong Cr–O bonds. The potential for CpCr β -diketiminato compounds to be used as control agents for radical polymerization under both OMRP and ATRP reaction conditions was evaluated in Chapter 4. Extending the range of catalytic applications to organic synthesis is the topic of Chapter 5. In Chapters 4 and 5, C–C bond formation was achieved by generating radical intermediates in solution. The focus of Chapter 6 was to form C–C bonds at the metal centre as an alternative to relying on free radical processes. As a result, the β -diketiminato ligand was replaced with a deprotonated benzylamine ligand in order to incorporate a reactive Cr–aryl bond into the half-sandwich compounds.

Chapter 2 Exploring Cr–C Bond Homolysis with CpCr[(ArNCMe)₂CH](R) Complexes

The single-electron reduction of organic halides by transition metal compounds has been widely studied. The inner-sphere mechanism involves an electron transfer to the alkyl halide (R–X) to form a metal–halide bond and an alkyl radical shown in eq 1.6. The radical can be subsequently trapped by a second equivalent of metal to form an organometallic species (eq 1.7).³ Recently there have been a host of C–C bond forming reactions catalyzed by first-row transition metals that are proposed to involve C-based radical intermediates.¹⁸

The synthesis of CpCr[(DppNCMe)₂CH] (**2.1c**), where Dpp = 2,6-*i*Pr₂C₆H₃, was initially reported by the Smith group³² by reacting NaCp with the Cr(II) dimer {[(DppNCMe)₂CH]Cr(THF)(μ-Cl)}₂ of Gibson and co-workers shown in Figure 2.1.³³ A more convenient route was later reported for the preparation of CpCr[(XylNCMe)₂CH], where Xyl = (2,6-Me₂C₆H₃) **2.1**, directly from CrCl₂ by sequential addition of NaCp followed by Li[(XylNCMe)₂CH].³⁴ This procedure was found to be generally applicable for the synthesis of a variety of CpCr(II) β-diketiminate compounds of the form CpCr[(ArNCMe)₂CH], where Ar = Xyl (**2.1**), Mes (2,4,6-Me₃C₆H₂) (**2.1a**), Dep (2,6-Et₂C₆H₃) (**2.1b**), Dpp (**2.1c**), and a series of mixed-aryl β-diketiminate ligands (eq 2.1).^{35,36}

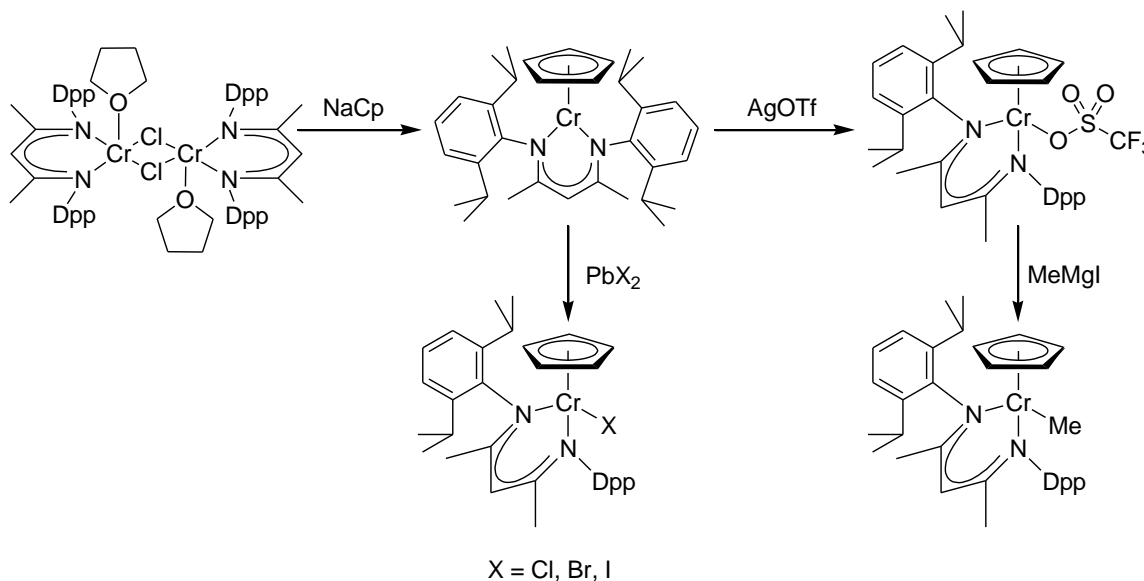
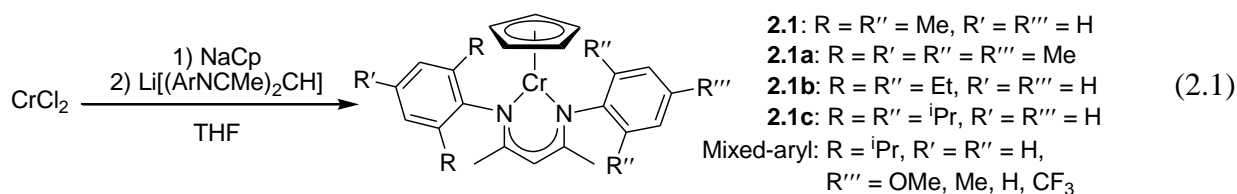


Figure 2.1. Synthesis of cyclopentadienyl chromium 2,6-*i*Pr₂C₆H₃ (Dpp) substituted β-diketiminate compounds.



The activation of iodomethane (MeI) with the well-defined Cr(II) compounds **2.1-2.1c** formed a mixture of the corresponding Cr(III) iodide and Cr(III) methyl species.³⁵ The steric reduction observed for these compounds upon changing from Dpp to the smaller N-aryl substituents Xyl, Mes, and Dep did not result in any significant increase of the rate constants for MeI activation. One unexpected benefit of the steric reduction was observed during the independent synthesis of the products of MeI activation, the Cr(III) iodide and methyl compounds. While the Cr(III) methyl compound CpCr[(DppNCMe)₂CH](Me) was prepared by salt metathesis from the triflate precursor and one equivalent of MeMgI (Figure 2.1),³² the corresponding compounds with smaller β-diketiminato ligands CpCr[(ArNCMe)₂CH](Me), where Ar = Xyl (**2.2**), Mes (**2.2a**), and Dep (**2.2b**), were conveniently prepared directly from the Cr(III) chloride precursors CpCr[(ArNCMe)₂CH](Cl), where Ar = Xyl (**2.3**), Mes (**2.3a**), and Dep (**2.3b**), under similar reaction conditions.³⁵

The rate constants for (iodomethyl)trimethylsilane (Me₃SiCH₂I) activation with the Cr(II) compounds **2.1** and **2.1b** are presented herein. Additionally, a series of Cr(III) hydrocarbyl compounds with Cp and the 2,6-dimethylphenyl (Xyl) β-diketiminato ligands were prepared (shown in Figure 2.2), including full characterization and structural elucidation. Selected examples of the Cr(III)–R compounds were prepared with all four β-diketiminato ligands to examine the effects of varying the N-aryl substituents. The CpCr[(XylNCMe)₂CH](X) compounds are numbered sequentially from **2.2** through **2.19** and a letter suffix is used to signify variation of the N-aryl substituents for Mes (**a**), Dep (**b**), and Dpp (**c**). The Cr(III) hydrocarbyl compounds were subjected to reaction with the radical trapping agent diphenyl disulfide (PhSSPh) to determine rate constants for Cr–C bond homolysis. The fate of the Cr species upon bond homolysis in the presence of PhSSPh was identified as CpCr[(ArNCMe)₂CH](SPh). The steric and electronic factors influencing the rates of bond homolysis will also be discussed.

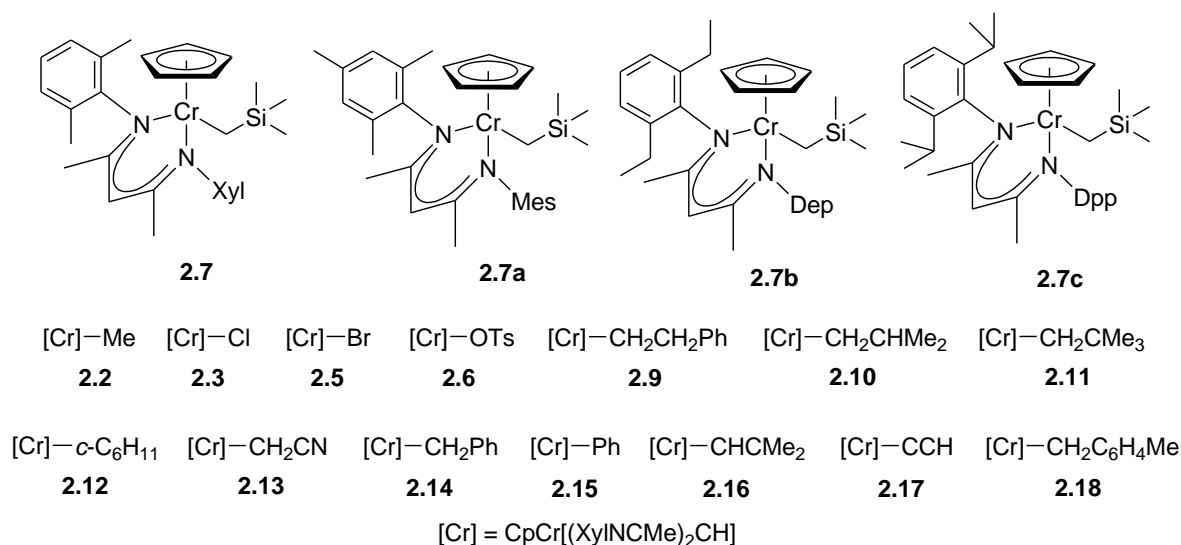


Figure 2.2. A list of the $CpCr[(ArNCMe)_2CH](R)$ compounds and their halide precursors presented in this chapter.

2.1 Attempted Synthesis of $Cp^*Cr[(XylNCMe)_2CH]$

It was previously established that the Cr(II) compound **2.1c** could be prepared by the sequential addition of NaCp and $Li[(DppNCMe)_2CH]$ to $CrCl_2$, or by the addition of $Li[(DppNCMe)_2CH]$ followed by NaCp. Attempts to prepare a pentamethylcyclopentadienyl (Cp^*) analogue of compound **2.1** by both methods of sequential addition were unsuccessful. In both cases, no tractable products were isolated from the reactions. In an attempt to facilitate synthesis of a Cp^* complex, the chloride ligands of $CrCl_2$ were replaced with better leaving groups.

The addition of $Li[(XylNCMe)_2CH]$ to $CrCl_2$ followed by the addition of NaO_2CPh formed an orange-brown solution. Removal of the ionic by-products followed by the addition of AgOTf, where OTf = trifluoromethanesulfonate, resulted in the formation of a silver mirror on the reaction vessel, indicating oxidation of the Cr to form a putative $[(XylNCMe)_2CH]Cr(O_2CPh)(OTf)$ complex. Removal of the silver metal followed by addition of $LiCp^*$ caused a colour change from red-yellow to brown (red transmitted). Crystallization provided X-ray quality crystals of a Cr(II) bridging benzoate dimer $\{[(XylNCMe)_2CH]Cr\}_2(\mu-O_2CPh)_2$ (**2.4**) (Figure 2.3). Compound **2.4** has Cr–N and Cr–O bond lengths of 2.0343(17)–2.0356(16) Å and 1.9863(15)–2.0186(14) Å, respectively. As expected for a 4-coordinate Cr(II) compound, **2.4** deviates only slightly from a square planar geometry at the two Cr centres with an average dihedral angle of 15°, where 0° indicates a perfectly square planar geometry and 90° is tetrahedral.³⁷ The solid-state molecular structure of **2.4** is similar to the previously reported

Cr(II) amidinate dimer complex $\{\text{Cr}[\text{}^t\text{BuNC}(\text{Me})\text{NEt}]\}_2[\mu_2\text{}^t\text{BuNC}(\text{Me})\text{NEt}]_2$, where two of the amidinate ligands are bound in a κ^2 -fashion and the other two are bridging across the two Cr atoms.³⁸ The small amidinate ligands allow for the formation of a short Cr–Cr bond that is not observed in **2.4**. Similar bimetallic Pd compounds were recently reported by Ritter and co-workers where bridging acetate and succinate ligands were found to hold the Pd atoms within proximity to one another to establish a bimetallic reductive elimination mechanism for Pd catalyzed C–X bond formation.³⁹ No further attempts were made to prepare a $\text{Cp}^*\text{Cr}[(\text{XylNCMe})_2\text{CH}]$ complex or to optimize the synthesis of **2.4**.

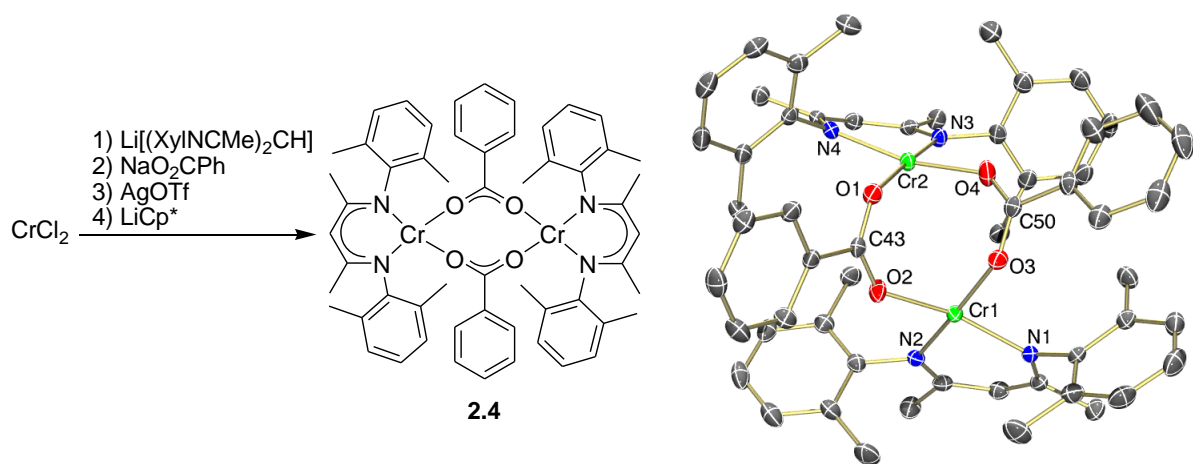
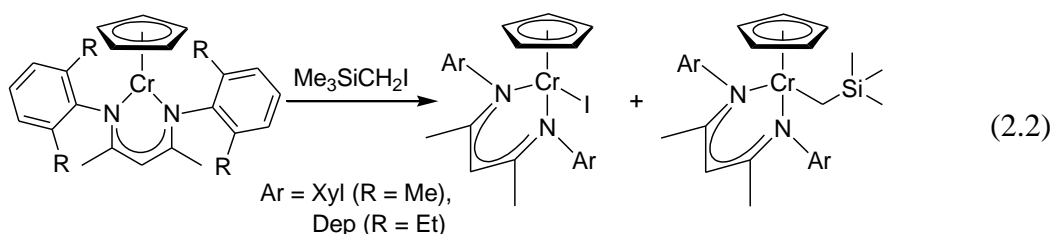


Figure 2.3. Attempted synthesis of a $\text{Cp}^*\text{Cr}[(\text{XylNCMe})_2\text{CH}]$ complex. Thermal ellipsoid diagram (50%) of complex **2.4** with all H atoms omitted for clarity.

2.2 Alkyl Halide Activation

The activation of $\text{Me}_3\text{SiCH}_2\text{I}$ with compounds **2.1** and **2.1b** was found to proceed smoothly providing a mixture of the Cr(III)–I and Cr(III)– CH_2SiMe_3 compounds (eq 2.2). The independent synthesis of the Cr(III) iodide compounds has been previously reported.³⁵ Synthesis and characterization of the Cr(III)– CH_2SiMe_3 compounds is presented in section 2.4. The reactions were monitored by UV-visible spectroscopy at a wavelength of 427 nm to track the decreasing concentration of the Cr(II) starting material. When conducted with a large excess of $\text{Me}_3\text{SiCH}_2\text{I}$ compared to Cr(II) the UV-visible decay curve was fit to a first-order model. The



reactions were conducted with 5 different concentrations of excess $\text{Me}_3\text{SiCH}_2\text{I}$ and the observed rate constants were plotted as a function of $[\text{Me}_3\text{SiCH}_2\text{I}]$ (Figure 2.4) to obtain the second-order rate constants (slope = $2k_1$) for compounds **2.1** ($k_1 = 4.4(4) \times 10^{-1} \text{ M}^{-1}\text{s}^{-1}$) and **2.1b** ($k_1 = 3.7(3) \times 10^{-1} \text{ M}^{-1}\text{s}^{-1}$)

These results suggest that there is an effect on the rate of $\text{Me}_3\text{SiCH}_2\text{I}$ activation when varying the N-aryl substituents of the β -diketiminate ligand. This is in contrast to the results for MeI activation by these compounds, which did not exhibit a steric influence on the rate constants.³⁵ The difference in reactivity can be rationalized by the steric bulk imparted by the trimethylsilyl substituent of the substrate in combination with the N-aryl substituents of the ligands now introducing a steric influence on the rate of alkyl iodide activation.

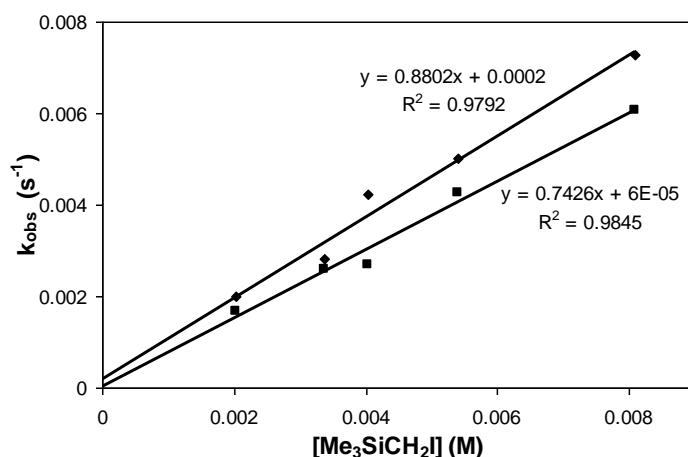
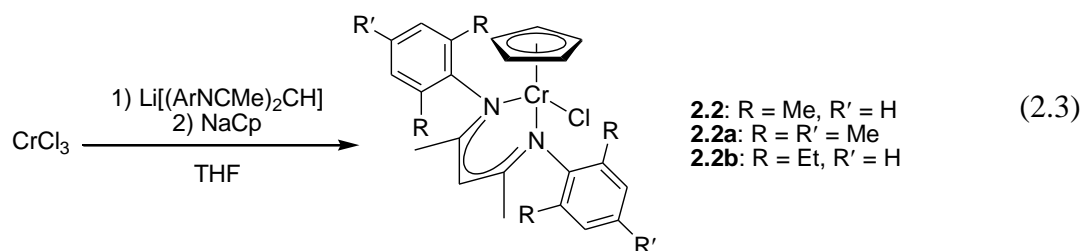


Figure 2.4. Comparison of the observed rate constants for the activation of $\text{Me}_3\text{SiCH}_2\text{I}$ with compounds **2.1** (diamonds) and **2.1b** (squares).

2.3 Synthesis of Cr(III) Halide Complexes

The Cr(III) halide compounds $\text{Cr}[(\text{DppNCMe})_2\text{CH}](\text{X})$, where $\text{X} = \text{Cl}$, Br , and I , were previously prepared by reacting the Cr(II) precursor with 0.5 equivalents of the appropriate PbX_2 salt.³² Synthesis of the smaller $\text{CpCr}[(\text{PhNCMe})_2\text{CH}](\text{Cl})$ complex was reported by Jin and co-workers by reacting $\text{Li}[(\text{PhNCMe})_2\text{CH}]$ with $\text{CpCrCl}_2(\text{THF})$; they also reported that the $\text{CpCr}[(\text{DppNCMe})_2\text{CH}](\text{Cl})$ complex could not be readily prepared by this method.⁴⁰

Alternatively, the Cr(III) chloride complexes $\text{CpCr}[(\text{ArNCMe})_2\text{CH}](\text{Cl})$, where $\text{Ar} = \text{Xyl}$ (**2.3**), Mes (**2.3a**), and Dep (**2.3b**), were prepared directly from CrCl_3 in a two-step, one-pot synthesis shown in eq 2.3. $\text{Li}[(\text{ArNCMe})_2\text{CH}]$ was added to a THF suspension of anhydrous CrCl_3 resulting in a red-brown solution, consistent with the formation of $\text{Cr}[(\text{ArNCMe})_2\text{CH}](\text{Cl})_2(\text{THF})_2$ previously reported by Gibson³³ and Theopold.⁴¹ Subsequent



treatment of the reaction mixture with NaCp caused a rapid colour change to green (orange transmitted). Crystallization of the Cr(III) chloride compounds **2.3** - **2.3b** provided X-ray quality crystals in good yields. The solid-state molecular structures of **2.3** - **2.3b** are shown in Figure 2.5. The structures all exhibit very similar geometrical parameters with Cr–Cl and Cr–N bond lengths in the ranges of 2.2972(11) – 2.3090(7) Å and 2.0078(19) – 2.023(3) Å, respectively, similar to the previously reported CpCr[(DppNCMe)₂CH](Cl)³² and CpCr[(PhNCMe)₂CH](Cl).⁴⁰

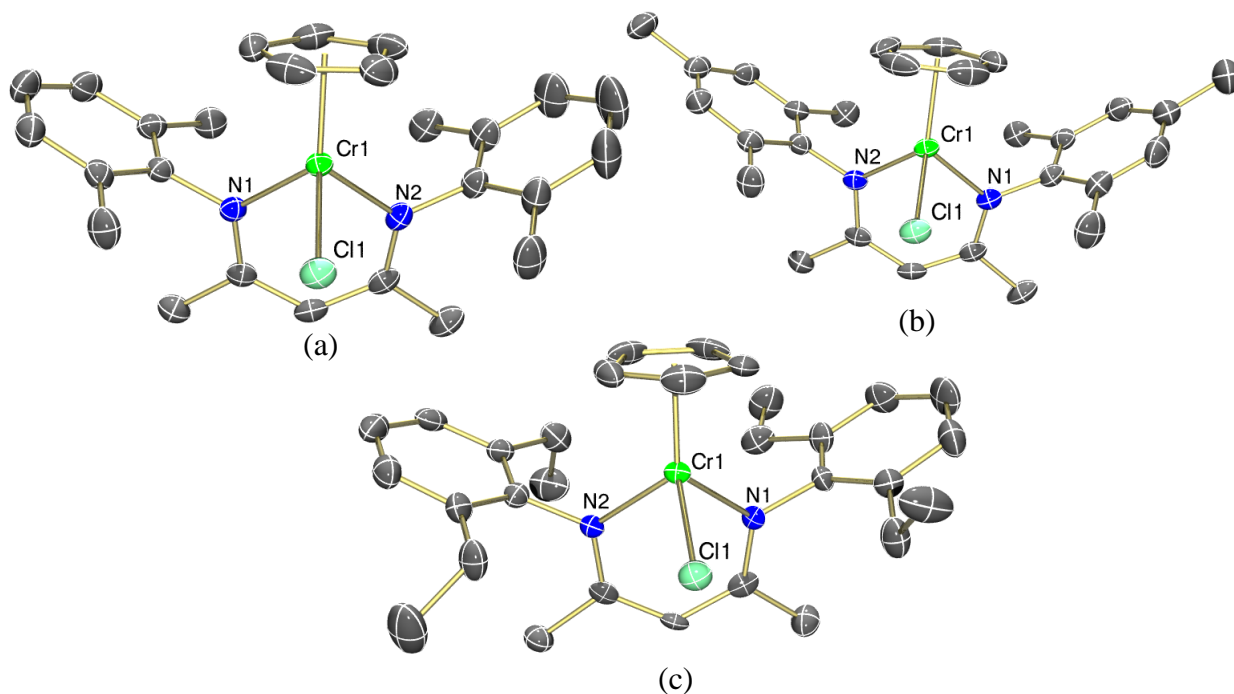


Figure 2.5. Thermal ellipsoid diagrams (50%) of Cr(III) chloride complexes **2.3** (a), **2.3a** (b), and **2.3b** (c). All H atoms and one half-molecule of hexanes (**2.3** only) are omitted for clarity. Additionally, **2.3** crystallizes with a disordered Cp ligand that was modeled in two orientations, **2.3a** crystallizes as a racemic twin with both enantiomers present in the crystal, and **2.3b** crystallizes with one disordered ethyl group (C14 and C15) that was modeled in two orientations; in all cases only one orientation is shown for clarity.

A Cr(III) bromide complex was prepared by a method similar to the synthesis of $\text{CpCr}[(\text{DppNCMe})_2\text{CH}](\text{Br})$.³² The synthesis of $\text{CpCr}[(\text{XylNCMe})_2\text{CH}](\text{Br})$ (**2.5**) was achieved by generating the Cr(II) compound **2.1** in situ followed by oxidation with PbBr_2 to produce an analytically pure black crystalline material in good yield (Figure 2.6).

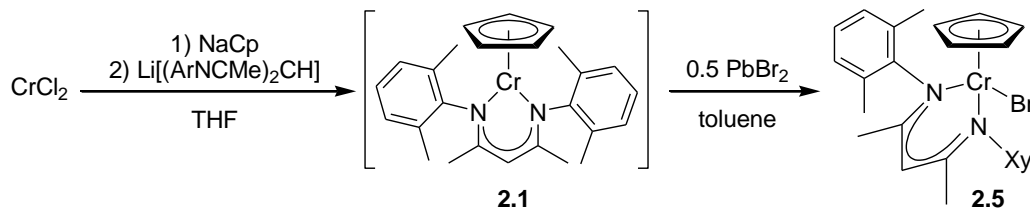


Figure 2.6. Synthesis of the Cr(III) bromide complex $\text{CpCr}[(\text{XylNCMe})_2\text{CH}](\text{Br})$ (**2.5**).

The pseudo-halide Cr(III) compounds $\text{CpCr}[(\text{ArNCMe})_2\text{CH}](\text{OTs})$, where Ar = Xyl (**2.6**), Mes (**2.6a**), and Dep (**2.6b**), were prepared by substitution of the chloride ligand of compounds **2.3** – **2.3b** for a tosylate group using AgOTs . The solid-state molecular structures of **2.6a** and **2.6b**, shown in Figure 2.7, exhibit bonding parameters very similar to their chloride analogues and have Cr–O bond lengths of 1.9872(13) Å for **2.6a** and 1.9835(10) Å for **2.6b**.

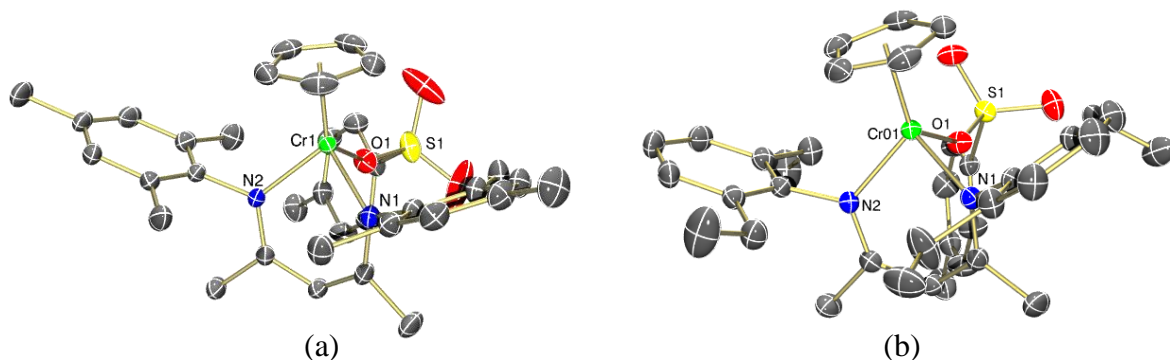


Figure 2.7. Thermal ellipsoid diagrams (50%) of Cr(III) tosylate complexes **2.6a** (a) and **2.6b** (b). All H atoms are omitted for clarity.

2.4 Synthetic Routes to $\text{CpCr}[(\text{ArNCMe})_2\text{CH}](\text{R})$ Compounds

Both the Cr(III) chloride and Cr(III) tosylate precursors were used to prepare $\text{CpCr}[(\text{ArNCMe})_2\text{CH}](\text{R})$ complexes, where Ar = Xyl, Mes, or Dep, by salt metathesis, as shown in Figure 2.8. The more convenient route was method A, by reacting the Cr(III) chloride precursors with commercial Grignard reagents RMgX , where X = Cl, Br, or I, followed by the addition of commercial anhydrous 1,4-dioxane and Celite filtration to remove the $\text{MgX}_2(\text{dioxane})$ precipitate. Recrystallization of the Cr(III) hydrocarbyl compounds from

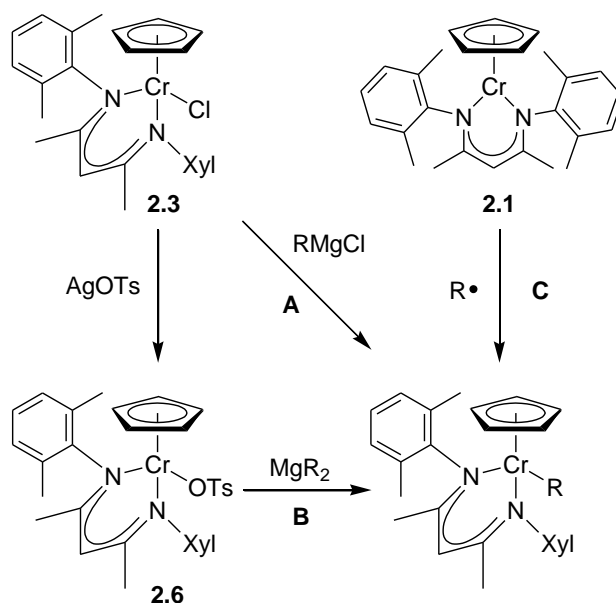


Figure 2.8. Synthetic routes to $\text{CpCr}[(\text{ArNCMe})_2\text{CH}](\text{R})$ complexes.

hexanes at $-35\text{ }^{\circ}\text{C}$ provided the desired compounds in high purity. For example, the Cr(III) methyl complex $\text{CpCr}[(\text{MesNCMe})_2\text{CH}](\text{Me})$ (**2.2a**) was readily prepared by reaction of the Cr(III) chloride compound **2.3a** with the Grignard reagent MeMgI . Compound **2.2a** was obtained in high yield as X-ray quality crystals (Figure 2.9a).

The previously reported $\text{CpCr}[(\text{DppNCMe})_2\text{CH}](\text{Me})$ complex required the use of a better leaving group than chloride and thus was prepared from the known Cr(III) triflate derivative (Figure 2.1).³² This was rationalized by the steric congestion of the large Dpp substituted β -diketiminato. In cases where the N-aryl and R substituents reported herein resulted in sufficient steric bulk to hinder the salt metathesis, the alternative method **B** was used. For example, the synthesis of $\text{CpCr}[(\text{XylNCMe})_2\text{CH}](\text{CH}_2\text{SiMe}_3)$ (**2.7**) was achieved by Method **A**, and could also be achieved by reacting the Cr(III) tosylate precursor **2.6** with the appropriate RMgX , but the synthesis was found to proceed to completion much faster when the halide-free method **B** was used. When using the Cr(III) tosylate precursor, the RMgX reagent remained too sluggish to perform the salt metathesis reaction due to a competing side reaction of Cr(III) halide formation resulting from ligand exchange between the Cr-OTs and Mg-X prior to alkylation.

The Mes and Dep N-aryl substituted versions of compound **2.7**, $\text{CpCr}[(\text{MesNCMe})_2\text{CH}](\text{CH}_2\text{SiMe}_3)$ (**2.7a**) and $\text{CpCr}[(\text{DepNCMe})_2\text{CH}](\text{CH}_2\text{SiMe}_3)$ (**2.7b**), were also prepared by reacting the Cr(III) tosylate precursors **2.6a** and **2.6b**, respectively, with $\text{Mg}(\text{CH}_2\text{SiMe}_3)_2 \cdot 1.05(1,4\text{-dioxane})$. Interestingly, the sterically demanding Dpp analogue

CpCr[(DppNCMe)₂CH](CH₂SiMe₃) (**2.7c**) was also readily prepared by reaction of the Cr(III) triflate precursor CpCr[(DppNCMe)₂CH](OTf) with the dialkyl Grignard reagent. The solid-state molecular structures of compounds **2.7a**, **2.7b**, and **2.7c** are shown in Figure 2.9.

Method C in Figure 2.8 highlights the ability of Cr(II) to trap carbon-based radicals. As discussed in section 2.2, the activation of Me₃SiCH₂I with the Cr(II) compound **2.1** produces a mixture of the Cr(III)–I and Cr(III)–CH₂SiMe₃ (**2.7**) compounds. By reacting compound **2.1** with 1.5 equivalents of Me₃SiCH₂I and an excess of Mn powder, compound **2.7** was cleanly prepared and isolated in >70% yield (Figure 2.10). While Zn and Mg are also capable of reducing the Cr(III) iodide back to Cr(II), they did not lead to the clean formation of **2.7** by this method, as determined by UV-vis spectroscopic analysis of the crude reaction mixtures. A similar reaction was reported using Zn as a stoichiometric reductant for the production of an organochromium(III) compound by single-electron reduction of CHCl₃ with Cr(II).⁴² An in depth discussion of the use of Mn as a stoichiometric reductant both in this work and in the literature is presented in Chapter 3.

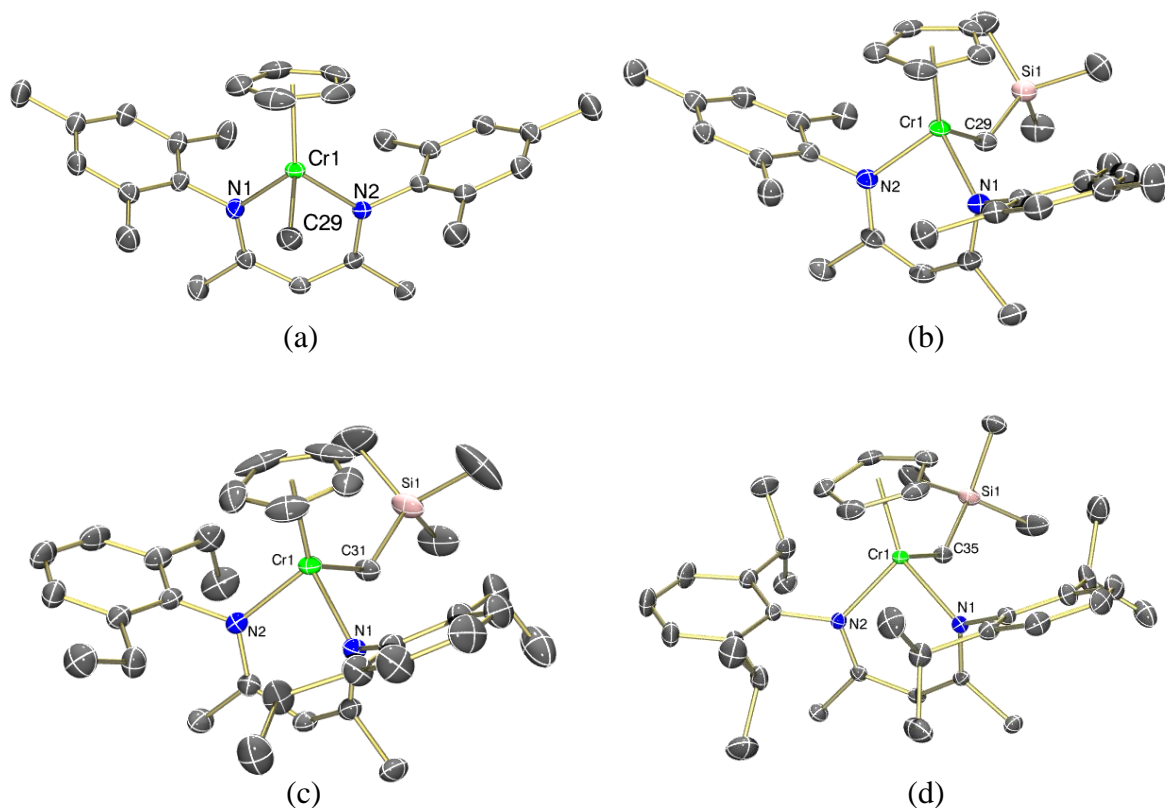


Figure 2.9. Thermal ellipsoid diagrams (50%) of the Cr(III) methyl complex **2.2a** (a) and Cr(III) trimethylsilylmethyl complexes **2.7a** (b), **2.7b** (c), and **2.7c** (d). Complex **2.7b** crystallizes with one disordered ethyl group (C12 and C13) that was modeled in two orientations and complex **2.7c** crystallizes with two independent molecules in the asymmetric unit; in both cases only one is shown, and all H atoms are omitted for clarity.

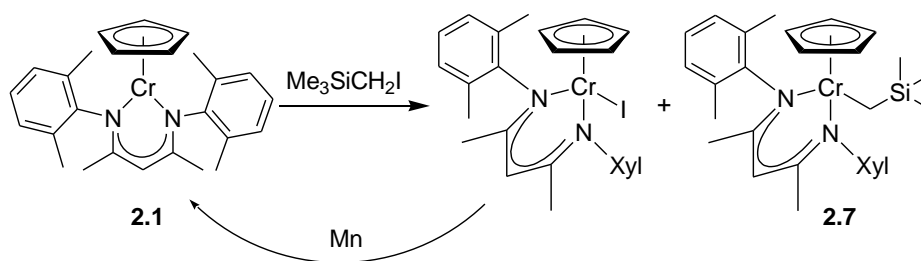
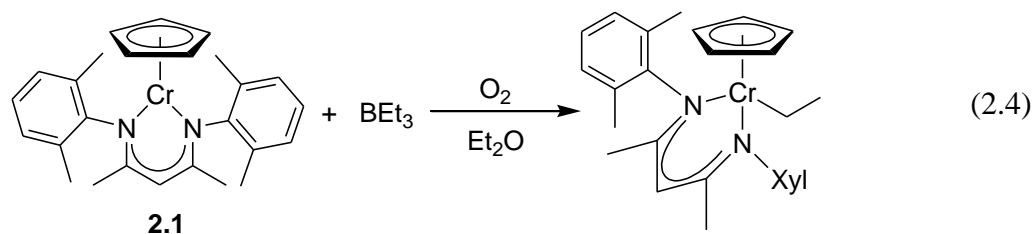


Figure 2.10. Synthesis of **2.7** from $\text{Me}_3\text{SiCH}_2\text{I}$ and Mn (method C).

Another example of method C is shown in eq 2.4 for the synthesis of $\text{CpCr}[(\text{XylNCMe})_2\text{CH}](\text{Et})$. Simply mixing the Cr(II) compound **2.1** with BEt_3 does not induce any reaction, as determined by UV-vis spectroscopy. However, air exposure of the UV-vis sample induced a reaction to cleanly form the Cr(III) ethyl compound in situ, despite the highly air-sensitive nature of compound **2.1** (discussed in Chapter 3). Comparison of the final UV-vis spectrum to an authentic sample prepared by method A confirmed the formation of the Cr(III) ethyl compound. Treatment of both trialkylboranes and *B*-alkylcatecholboranes with O_2 is known to induce release of alkyl radicals.⁴³ This strategy was also adopted by McNeil and co-workers for the preparation of a Co(III)–Et complex that was not readily prepared by other more conventional alkylation methods.⁴⁴



2.5 Steric Effects on the Synthesis of $\text{CpCr}[(\text{ArNCMe})_2\text{CH}](\text{R})$ Compounds

Extending method **B** to more sterically demanding R groups beyond CH_2SiMe_3 initially proved challenging. The attempted synthesis of Cr(III) neophyl ($\text{CH}_2\text{CMe}_2\text{Ph}$) complexes by method **B** did not provide the desired products $\text{CpCr}[(\text{ArNCMe})_2\text{CH}](\text{CH}_2\text{CMe}_2\text{Ph})$, shown in Figure 2.11. The reactions of Cr(III) tosylate compounds **2.6** and **2.6a** with the halide-free Grignard reagent provided crystalline products in low yields. The isolated products were characterized by single-crystal X-ray diffraction, revealing that the Cr(II) compound **2.1a** was isolated from the reaction with **2.6a** starting material and a Cp-free ortho-metallated product **2.8** was isolated from the reaction with **2.6** (Figure 2.12).⁴⁵ It was reported that the same reaction protocol carried out with the Cr(III) triflate compound $\text{CpCr}[(\text{DppNCMe})_2\text{CH}](\text{OTf})$ in THF solvent provided a Cr(III) species of the form $\text{CpCr}[(\text{DppNCMe})_2\text{CH}](\text{C}_4\text{H}_7\text{O})$ that formed by activation of the THF reaction solvent, also isolated in low yield.⁴⁶ Due to the low isolated yields of the products observed in the reactions shown in Figure 2.11, it was assumed that there was a mixture of products formed in both cases and that different compounds preferentially crystallized out of solution for the different β -diketiminate ligands. No further attempts were made to improve the reactions with $\text{Mg}(\text{CH}_2\text{CMe}_2\text{Ph})_2$.

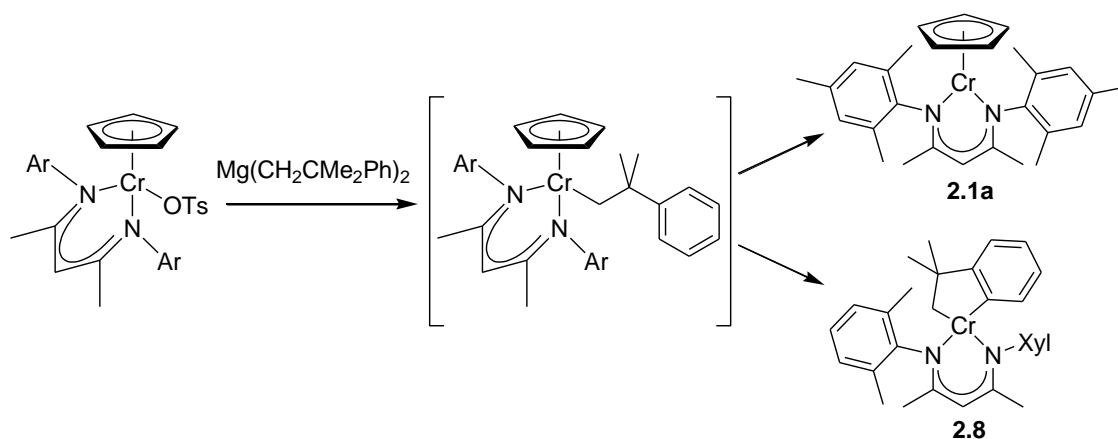


Figure 2.11. Attempted synthesis of Cr(III)–CH₂CMe₂Ph complexes.

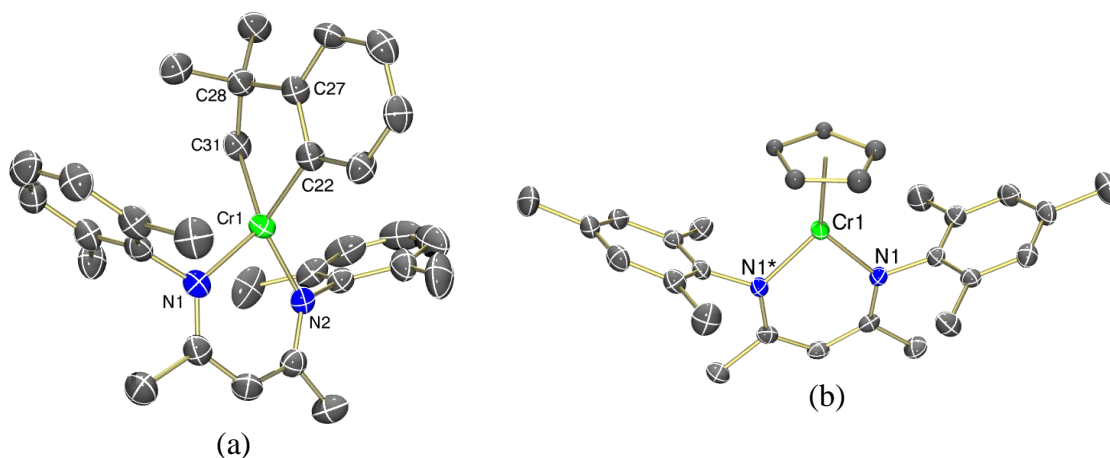


Figure 2.12. Thermal ellipsoid diagrams (50%) of **2.8** (a) and **2.1a** (b). Complex **2.8** crystallizes with two independent molecules in the asymmetric unit and **2.1a** crystallizes with one half-molecule residing on a two-fold axis of rotation with a disordered Cp ligand that was modeled in four orientations; in both cases only one orientation is shown, and all H atoms are omitted for clarity.

Interestingly, it appears that the formation of a metallated product is limited to compound **2.8** since the less sterically hindered compound $\text{CpCr}[(\text{XylNCMe})_2\text{CH}](\text{CH}_2\text{CH}_2\text{Ph})$ (**2.9**) was readily prepared by method **A** from reaction of the Cr(III) chloride precursor **2.3** with $\text{ClMgCH}_2\text{CH}_2\text{Ph}$. Removing the phenyl substituent of the neophyl ligand also greatly facilitated the synthesis of Cr(III)–alkyl compounds. Reaction of **2.3** with $\text{ClMgCH}_2\text{CHMe}_2$ provided the Cr(III) compound $\text{CpCr}[(\text{XylNCMe})_2\text{CH}](\text{CH}_2\text{CHMe}_2)$ (**2.10**) in good yield. Preparation of the isobutyl compound using the more sterically congested Dpp N-aryl substituted ligand proceeded smoothly using method **B** by reaction of the Cr(III) triflate precursor with $\text{Mg}(\text{CH}_2\text{CHMe}_2)_2$. Crystallization of the product provided X-ray quality crystals of $\text{CpCr}[(\text{DppNCMe})_2\text{CH}](\text{CH}_2\text{CHMe}_2)$ (**2.10c**). The solid-state molecular structures of **2.10** and

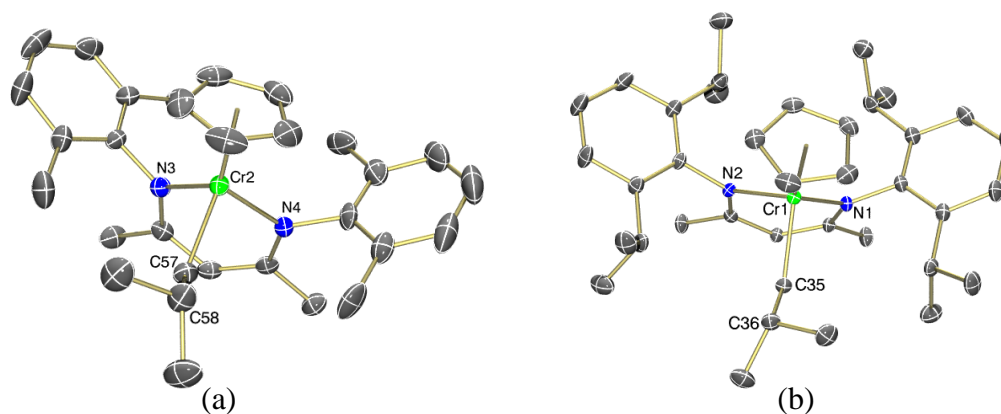


Figure 2.13. Thermal ellipsoid diagrams (50%) of Cr(III) isobutyl complexes **2.10** (a) and **2.10c** (b). Both complexes crystallize with two independent molecules in the asymmetric unit; only one is shown, and all H atoms are omitted for clarity.

2.10c are shown in Figure 2.13. These results indicate that replacing either the methyl or the phenyl substituents of the neophyl ligand with typically very reactive β -hydrogen atoms actually increases the stability of the resulting Cr(III)–R compounds. The highly stable nature of 15 valence electron Cr(III) alkyl compounds with respect to β -hydrogen elimination has precedence in the literature.⁴⁷

While CH_2SiMe_3 and neopentyl (CH_2CMe_3) substituents at first glance appear very similar, it has been shown that there are significant differences in reactivity.⁴⁸ In particular organometallic compounds with neopentyl ligands are typically much less stable than their CH_2SiMe_3 analogues. In light of these differences in reactivity, the synthetic target of a well-defined Cr(III) neopentyl complex appeared to be a worthy endeavour. Gratifyingly, the synthesis of $\text{CpCr}[(\text{ArNCMe})_2\text{CH}](\text{CH}_2\text{CMe}_3)$, where Ar = Xyl (**2.11**), Mes (**2.11a**), and Dep (**2.11b**), were achieved by method **B**. Unfortunately, attempts to prepare the Dpp N-aryl substituted analogue resulted in reduction to the Cr(II) species **2.1c**. Single-crystal X-ray diffraction of compounds **2.11** and **2.11a** confirmed the formation of the desired Cr(III) neopentyl compounds (Figure 2.14).

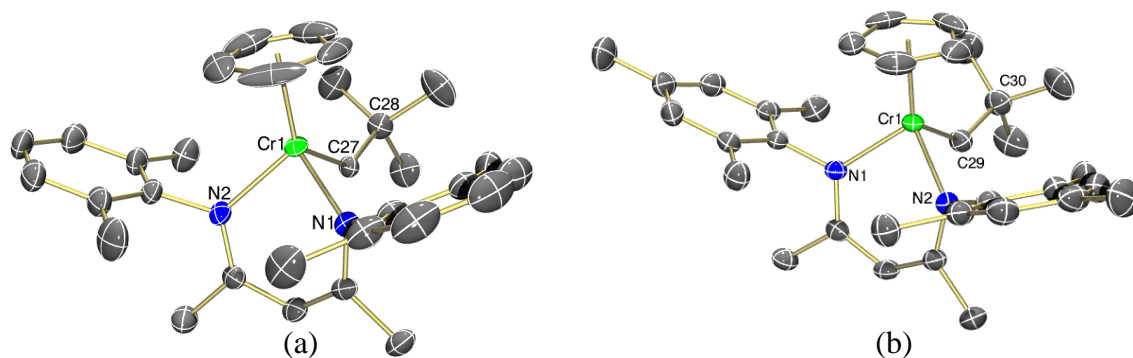


Figure 2.14. Thermal ellipsoid diagrams (50%) of Cr(III) neopentyl complexes **2.11** (a) and **2.11a** (b). Complex **2.11** crystallizes with two independent molecules in the asymmetric unit; only one is shown, and all H atoms are omitted for clarity.

A Cr(III) compound with a secondary alkyl cyclohexyl ($c\text{-C}_6\text{H}_{11}$) ligand was also prepared by method **B**. Reaction of the Cr(III) tosylate precursor **2.6** with the dialkyl Grignard reagent $\text{Mg}(c\text{-C}_6\text{H}_{11})_2$ provided the $\text{CpCr}[(\text{XylNCMe})_2\text{CH}](c\text{-C}_6\text{H}_{11})$ (**2.12**) compound as an analytically pure material. Single-crystal X-ray diffraction of isolated **2.12** resulted in structural characterization of the Cr(II) compound **2.1**, presumably a result of the transportation and storage of the crystals prior to analysis. Compound **2.12** was also found to rapidly convert to **2.1** in solution at concentrations of 10^{-4} M suitable for UV-visible spectroscopic analysis.

2.6 Electronic Effects: Cyanomethyl and Benzyl Compounds

Having prepared a series of Cr(III) alkyl compounds with varying amounts of steric congestion, we were also interested in alkyl group electronic effects. Both cyanomethyl (CH_2CN) and benzyl (CH_2Ph) groups contain substituents that stabilize the $\cdot\text{CH}_2\text{CN}$ and $\cdot\text{CH}_2\text{Ph}$ radicals, respectively. The increased stability of the radical species should lead to a decreased stability of the Cr(III)–R compounds by weakening the Cr–R bonds.²⁹ The cyanomethyl compound $\text{CpCr}[(\text{XylNCMe})_2\text{CH}](\text{CH}_2\text{CN})$ (**2.13**) was prepared by reacting the Cr(III) chloride precursor **2.3** with in situ generated KCH_2CN .⁴⁹ Single-crystal X-ray diffraction confirmed the connectivity of the cyanomethyl ligand as being C-bound to the metal centre (Figure 2.15a),⁵⁰ as opposed to an N-bound keteniminate complex.⁵¹

The Cr(III) benzyl complexes $\text{CpCr}[(\text{ArNCMe})_2\text{CH}](\text{CH}_2\text{Ph})$, where Ar = Xyl (**2.14**), Mes (**2.14a**), and Dep (**2.14b**), were prepared by method A from the Cr(III) chloride precursors and ClMgCH_2Ph . The larger $\text{CpCr}[(\text{DppNCMe})_2\text{CH}](\text{CH}_2\text{Ph})$ (**2.14c**) complex was also readily prepared from the Cr(III) triflate precursor. The solid-state molecular structures of compounds **2.14a** and **2.14b**, shown in Figure 2.15b and c respectively, display the benzyl substituents as being aligned symmetrically between the flanking ortho N-aryl substituents; compound **2.14b**

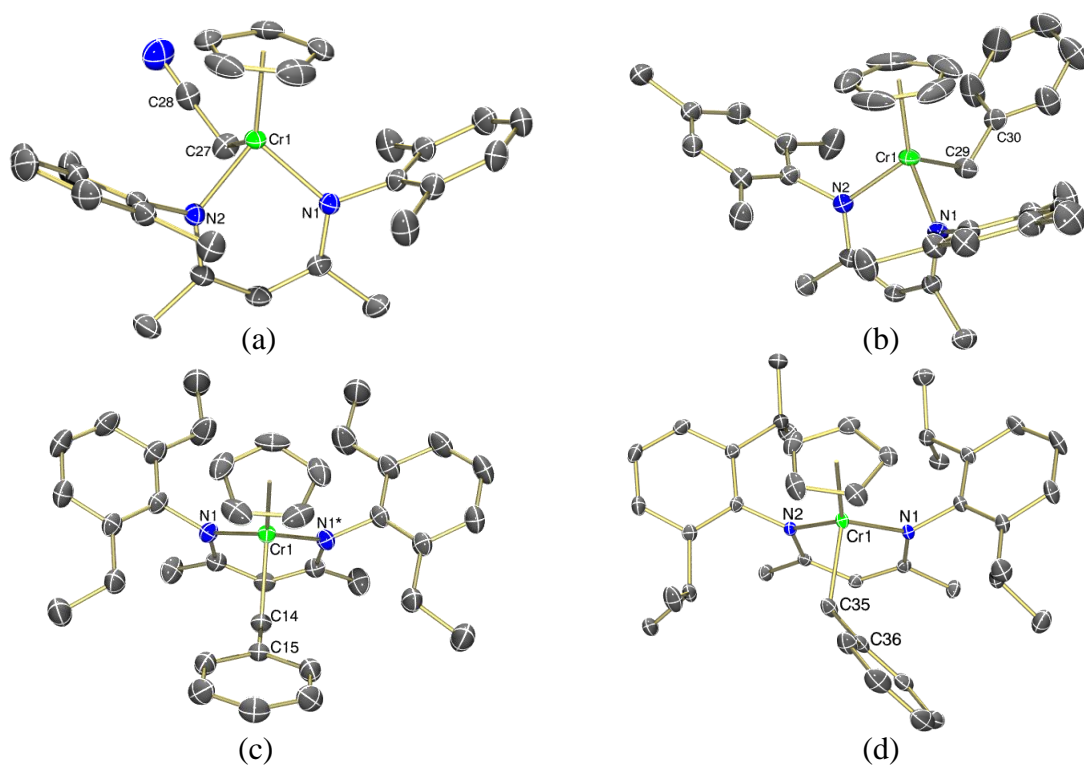


Figure 2.15. Thermal ellipsoid diagrams (50%) of the Cr(III) cyanomethyl complex **2.13** (a), and Cr(III) benzyl complexes **2.14a** (b), **2.14b** (c), and **2.14c** (d). All H atoms are omitted for clarity. Additionally, complex **2.14b** crystallizes on a mirror plane with one half-molecule in the asymmetric unit.

contains a crystallographically imposed mirror plane. In compound **2.14c**, with the more sterically congested β -diketiminato ligand, the phenyl substituent is turned to one side (Figure 2.15c) suggesting that the observed orientations of the benzyl ligand in these compounds may be due to intermolecular interactions within the crystal lattice.

2.7 Phenyl, Alkenyl and Alkynyl Compounds

While the cyanomethyl and benzyl groups form stabilized radical intermediates, aryl and vinyl groups form extremely reactive radical species. The Cr(III) phenyl (Ph) complex $\text{CpCr}[(\text{XylNCMe})_2\text{CH}](\text{Ph})$ (**2.15**) was prepared by method **B**. The less sterically demanding alkenyl complex $\text{CpCr}[(\text{XylNCMe})_2\text{CH}](\text{CH}=\text{CMe}_2)$ (**2.16**) and an alkynyl complex $\text{CpCr}[(\text{XylNCMe})_2\text{CH}](\text{C}\equiv\text{CH})$ (**2.17**) were readily prepared by method **A**. The X-ray structures of compounds **2.15** – **2.17** are shown in Figure 2.16.

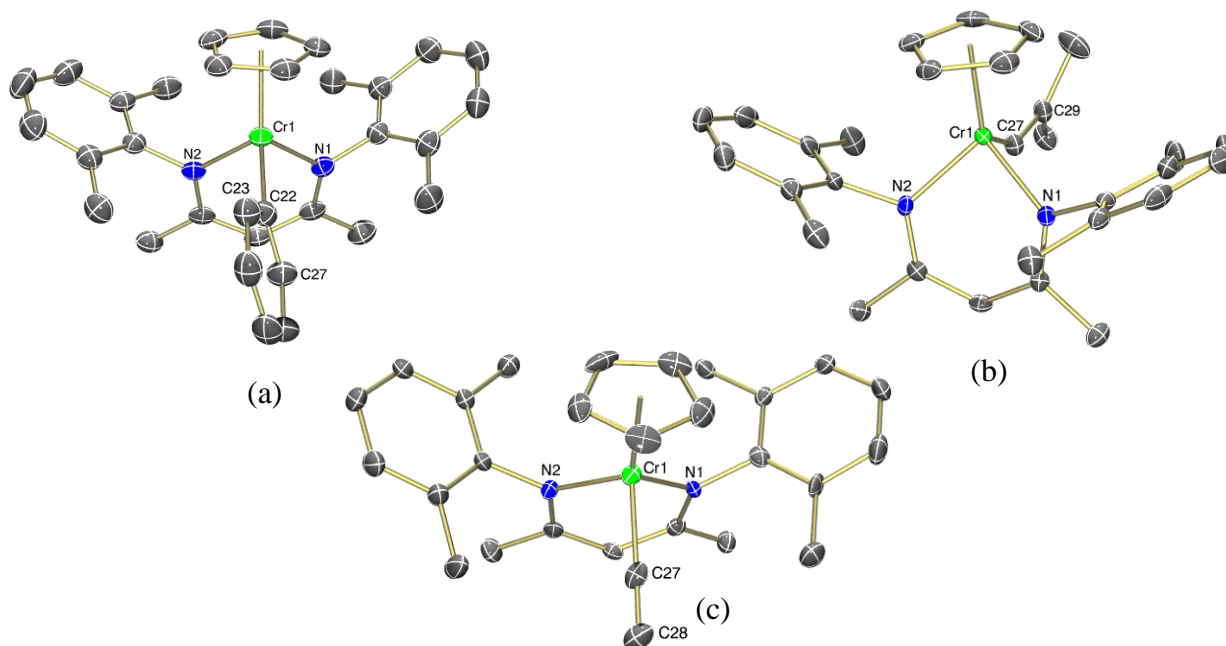


Figure 2.16. Thermal ellipsoid diagrams (50%) of Cr(III) phenyl (**2.15** (a)), alkenyl (**2.16** (b)), and alkynyl (**2.17** (c)) complexes. Complex **2.16** crystallizes with two independent molecules in the asymmetric unit; only one is shown, and all H atoms are omitted for clarity.

2.8 Solvent C–H Atom Abstraction

When dissolved in toluene, the Cr(III) neopentyl complex **2.11** cleanly converted to the Cr(III) benzyl compound **2.14** at room temperature. A similar reaction was observed in a 10:1 mixture of benzene/*p*-xylene to yield $\text{CpCr}[(\text{XylNCMe})_2\text{CH}](\text{CH}_2\text{C}_6\text{H}_4\text{Me})$ (**2.18**). Single-crystal X-ray diffraction of the isolated product confirmed the connectivity as being bound

though one of the methyl substituents of the *p*-xylene (Figure 2.17). The formation of **2.14** and **2.18** in these reactions suggested a radical C–H bond activation mechanism due to the observed preference for benzylic versus aromatic C–H bonds.⁵² The proposed mechanism shown in Figure 2.17 involves initial Cr–C bond homolysis of compound **2.11** to generate a neopentyl radical, which abstracts a benzylic H atom generating a stabilized benzylic radical. The radical is then trapped by the Cr(II) species **2.1** that was generated as a result of the initial Cr–C bond homolysis. Preparation of the Cr(III) phenyl compound **2.15** indicated that a Cr–C(sp²) bond is readily accessible should the Cr(III) neopentyl compound **2.11** undergo a nonradical C–H bond activation reaction, which are known to favour strong C–H bonds due to the thermodynamically favourable formation of M–C(sp²) bonds.⁵³ Furthermore, the addition of **2.11** to benzene in the absence of *p*-xylene showed no evidence of C–H bond activation to form the Cr(III) phenyl compound **2.15**; the only observed reaction was the conversion of **2.11** to the reduced Cr(II) compound **2.1**, as determined by UV-vis spectroscopy. Additionally, the Cr(III) phenyl compound **2.15** was stable in THF and benzene solutions at concentrations of 10^{−4} M, with no signs of decomposition after 4 days at room temperature.

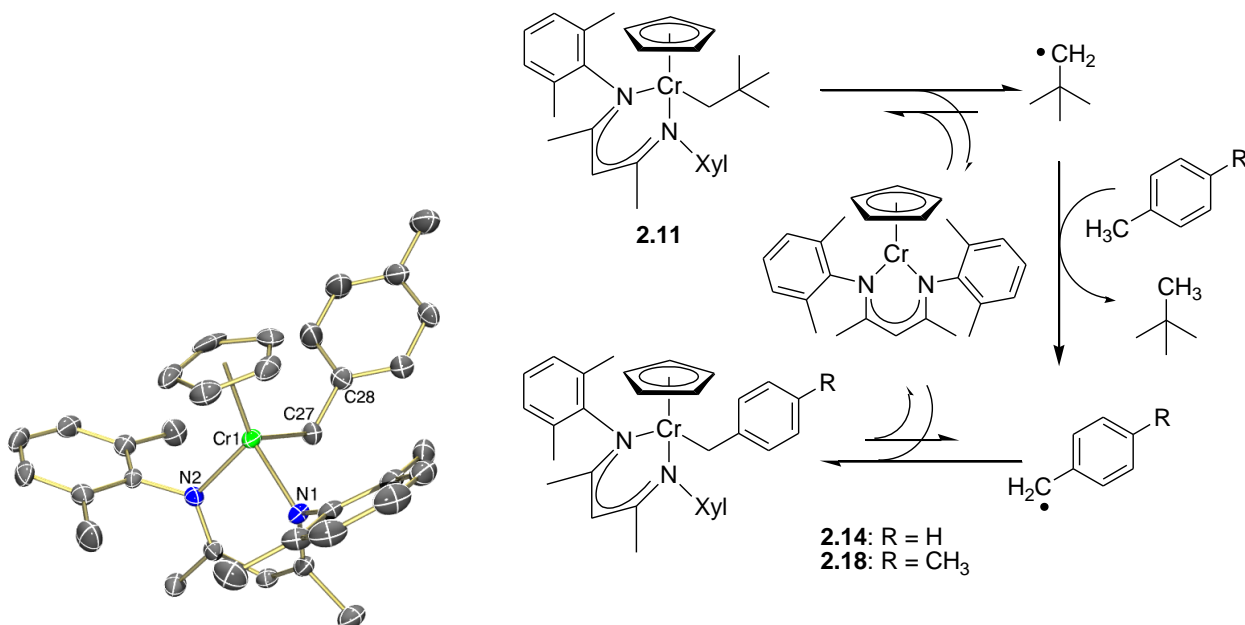


Figure 2.17. Reaction of **2.11** with benzylic C–H bonds to produce **2.14** and **2.18**, and a thermal ellipsoid diagram (50%) of **2.18** with all H atoms omitted for clarity.

2.9 UV-visible Spectroscopy

The Cr(III) halide compounds $\text{CpCr}[(\text{XylNCMe})_2\text{CH}](\text{X})$, where $\text{X} = \text{Cl}$ (**2.3**), Br (**2.5**), and I , exhibit an interesting trend in their UV-vis spectra. The compounds have two absorption bands in the UV-vis spectra, with a strong absorption at ~ 425 nm and a weaker absorption at ~ 585 nm. The higher energy peak becomes red shifted as the halide ligand is changed from Cl to I , with $\text{Cl} = 418$ nm, $\text{Br} = 423$ nm, and $\text{I} = 431$ nm. This trend was also found to apply to the Cr(III) fluoride analogue (presented in section 3.6), which exhibits an absorption band at 402 nm. The pseudo-halide Cr(III) tosylate compounds **2.6** – **2.6b** also have similar UV-vis spectra, with a strong absorption band at 412 nm and a weaker absorption at ~ 570 nm. All of the $\text{CpCr}[(\text{ArNCMe})_2\text{CH}](\text{R})$ compounds also display two strong absorption bands in their UV-vis spectra with λ_{max} in the ranges 395–436 nm and 535–582 nm (Figure 2.18), similar to the Cr(III) halide compounds.

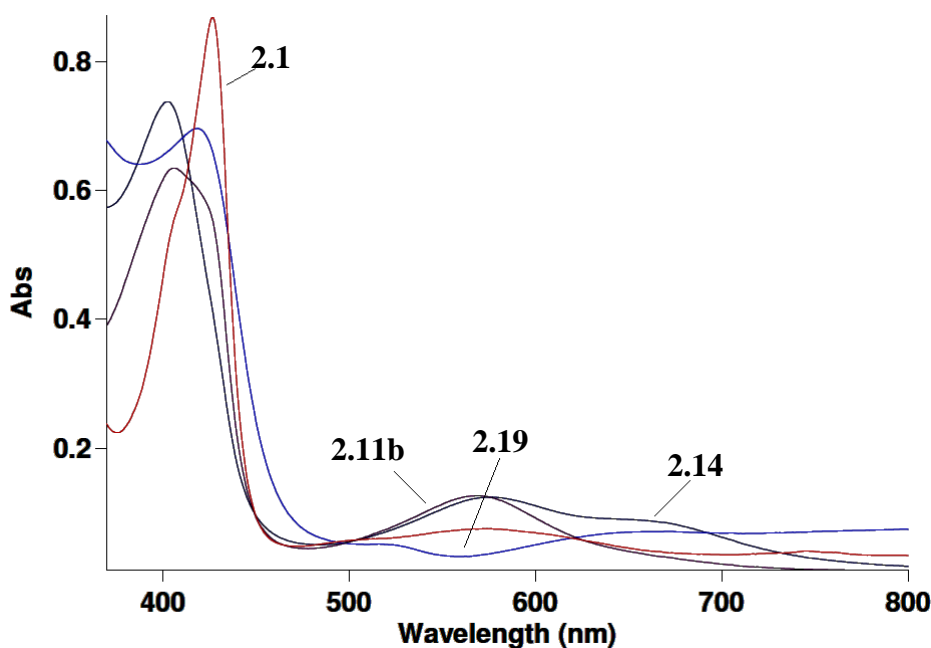
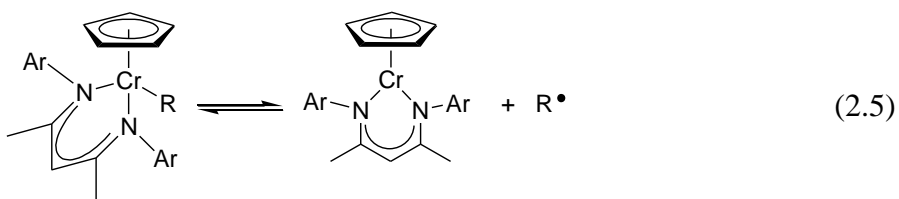


Figure 2.18. UV-vis spectra of the Cr(II) complex **2.1**, and the Cr(III) neopentyl (**2.11b**), benzyl (**2.14**), and SPh (**2.19**) complexes in hexanes (1.1×10^{-4} M).

While all of the CpCr β -diketiminate compounds reported in this chapter were found to exhibit strong absorption bands at similar wavelengths, the Cr(III)–R compounds display very different extinction coefficients (ϵ) compared to their Cr(III)–X precursors. The ϵ values of the Cr(III)–X compounds are approximately double compared to the Cr(III)–R compounds for the high energy peak at ~400 nm but they have much smaller ϵ values for the low energy peak at ~550 nm. These very distinct differences in the UV-vis spectra proved to be extremely valuable in using UV-vis spectroscopy as a preliminary characterization technique during synthesis.

Small differences in the UV-vis spectra of the compounds are accompanied by visible colour differences. The Cr(II) analogue **2.1** has two absorption bands in the UV-vis region at 427 nm and 573 nm (Figure 2.18) and is green to incident light and magenta to transmitted light. The Cr(III) chloride (**2.3**–**2.3b**), bromide (**2.5**), and tosylate (**2.6**–**2.6b**) compounds are green to incident light and orange to transmitted light. Many of the Cr(III) hydrocarbyl compounds are purple to both incident and transmitted light with some exceptions: the Cr(III)–CH₂CN compound **2.13** is green (red transmitted) and the Cr(III)–CH₂Ph compounds **2.14**–**2.14c** are green-blue; both have a distinctive shoulder absorption in their UV-vis spectra at 650 nm (Figure 2.18). The Cr(III)–CH₂SiMe₃ compounds **2.7**–**2.7c** are also slightly different with a violet to transmitted colour, and the Cr(III)–CH=CMe₂ (**2.16**) and –C \equiv CH (**2.17**) compounds are red and orange-red, respectively.

As discussed in the previous section, the Cr(III) neopentyl compound **2.11** was found to convert to the Cr(III) benzyl complex when dissolved in toluene. Compounds **2.11**–**2.11b** were also found to convert to the Cr(II) compounds **2.1**–**2.1b**, respectively, upon dilution in hexanes to concentrations appropriate for UV-vis analysis (10^{–4} M), even though **2.11**–**2.11b** were initially isolated by recrystallization from concentrated hexanes solutions. The concentration dependence of the stability of **2.11** is a result of the equilibrium that is established in solution (eq 2.5), with high dilution causing the equilibrium to shift to the dissociated side. The cyclohexyl compound **2.12** underwent rapid conversion to Cr(II) when diluted in hexanes for UV-vis analysis. None of the other Cr(III) hydrocarbyl compounds reported herein showed any appreciable buildup of Cr(II) during UV-vis sample preparation.



2.10 X-ray Crystallography

Single-crystal X-ray diffraction was used throughout this work as a means of definitively identifying each of the paramagnetic $\text{CpCr}[(\text{ArNCMe})_2\text{CH}](\text{R})$ compounds. Table 2.1 lists the selected bond lengths and angles for the crystallographically characterized $\text{CpCr}[(\text{ArNCMe})_2\text{CH}](\text{R})$ compounds reported in this chapter. Two sets of values are listed in Table 2.1 in cases where the compounds crystallized with two independent molecules in the asymmetric unit. In most cases the observed bonding parameters were found to correlate with the observed chromium–alkyl bond homolysis.

Table 2.1. Selected bond lengths and angles for $\text{CpCr}[(\text{ArNCMe})_2\text{CH}](\text{R})$ complexes.

	Ar	R	Cr–C (Å)	Cr–C–E(deg)	Cr–N(1) (Å)	Cr–N(2) (Å)
2.2a	Mes	Me	2.0645(17)	-	2.0245(13)	2.0231(13)
2.7a	Mes	CH_2SiMe_3	2.1031(17)	131.89(9)	2.0186(15)	2.0334(14)
2.7b	Dep	CH_2SiMe_3	2.1098(15)	130.31(8)	2.0355(12)	2.0390(13)
2.7c	Dpp	CH_2SiMe_3	2.111(2)	135.71(11)	2.0572(17)	2.0411(17)
			2.118(2)	134.71(11)	2.0400(17)	2.0519(17)
2.10	Xyl	CH_2CHMe_2	2.121(5)	126.5(4)	2.033(4)	2.042(4)
			2.125(5)	126.6(4)	2.031(4)	2.038(4)
2.10c	Dpp	CH_2CHMe_2	2.1269(15)	126.15(11)	2.0394(13)	2.0275(13)
			2.1199(15)	126.49(11)	2.0415(13)	2.0393(13)
2.11	Xyl	CH_2CMe_3	2.136(3)	135.1(2)	2.046(2)	2.051(2)
			2.145(3)	134.9(2)	2.040(2)	2.043(2)
2.11a	Mes	CH_2CMe_3	2.128(2)	134.37(16)	2.0411(17)	2.0337(17)
2.13	Xyl	CH_2CN	2.126(2)	114.67(16)	2.0143(16)	2.0217(17)
2.14a	Mes	CH_2Ph	2.1384(19)	120.66(14)	2.0231(17)	2.0320(16)
2.14b	Dep	CH_2Ph	2.144(2)	121.63(14)	2.0377(13)	-
2.14c	Dpp	CH_2Ph	2.1239(13)	126.30(9)	2.0309(10)	2.0577(10)
2.15	Xyl	Ph	2.098(3)	124.8(3)	2.033(2)	2.027(2)
2.16	Xyl	CHCMe_2	2.050(4)	142.1(3)	2.025(3)	2.037(3)
			2.038(4)	142.4(3)	2.029(3)	2.023(3)
2.17	Xyl	CCH	2.009(5)	176.6(5)	2.016(4)	2.011(4)
2.18	Xyl	$\text{CH}_2\text{C}_6\text{H}_4\text{Me}$	2.131(4)	124.3(3)	2.029(3)	2.031(3)

Typical Cr–C bond lengths were in the range of 2.10 – 2.13 Å. As expected, the Cr(III) methyl compound **2.2a** had the shortest Cr–C bond for the Cr(III) alkyl compounds at 2.0645(17) Å. The Cr(III) phenyl compound **2.15** had a surprisingly short bond at 2.098(3) Å and the Cr(III) alkenyl (**2.16**) and alkynyl (**2.17**) have even shorter bonds at 2.044(4) Å (average) and 2.009(5) Å, respectively, due to the decreased steric influence of the R groups. Conversely, the Cr(III) neopentyl compound **2.11** lies on the long end of the Cr–C bond lengths range with an average bond length of 2.140(3) Å. Differences in the Cr–C bond length as a result of varying

the N-aryl substituents were observed for the $\text{CpCr}[(\text{ArNCMe})_2\text{CH}](\text{CH}_2\text{SiMe}_3)$ compounds. The expected trend of increasing steric bulk of the Ar substituents ($\text{Xyl} \approx \text{Mes} < \text{Dep} < \text{Dpp}$) tracks with the observed trend in Cr–C bond lengths, with **2.7a** < **2.7b** < **2.7c**. This trend was also observed in the Cr β -diketimate Cr–N bond lengths of the Cr(III)– CH_2SiMe_3 compounds.

The Cr(III) alkynyl compound **2.17** contains the shortest Cr–N bonds with an average bond length of 2.014(4) Å, only slightly shorter than the Cr(III)– CH_2CN compound **2.13** (2.0180(17) Å average). At the other end of the range of Cr–N bond lengths, the Cr(III) neopentyl compound **2.11** has an average bond length of 2.045(2) Å and the Dpp substituted Cr(III)– CH_2SiMe_3 compound **2.7c** has a similar average bond length of 2.0476(17) Å, with the remaining Cr(III) hydrocarbyl compounds falling within the Cr–N bond length range of 2.02 – 2.04 Å.

Perhaps the most unexpected bond length trends are those of the Cr(III) benzyl compounds. While there is a large variation in the Cr–C bond lengths of the benzyl compounds, from 2.1239(13) – 2.144(2) Å, the observed trend ($\text{Dpp} < \text{Mes} < \text{Dep}$) does not follow the expected increase with increasing steric bulk of the Ar substituents ($\text{Mes} < \text{Dep} < \text{Dpp}$) but the trend is observed with the average Cr–N bond lengths of those compounds. The electronic stabilization of the benzylic ligand causes a weakening of the Cr–C bond which is consistent with the relatively long Cr–C bonds in compounds **2.14a** – **2.14c** despite the relatively small steric considerations of the CH_2Ph ligand. The relatively weak Cr–C bonds of the Cr(III) benzyl compounds in combination with the observed trend in Cr–C bond lengths in the solid state (or lack thereof) suggest that crystal packing effects are the governing factors influencing the observed Cr–C bond lengths. In other words, the decrease in energy obtained from optimal crystal packing outweighs the increase in energy due to distortion of the Cr–C bond length. These findings are in agreement with a computational study that examined the ability of the $\text{CpCr}[(\text{ArNCMe})_2\text{CH}]$ system to trap radicals ($\text{R}\cdot$).⁵⁴ The calculated transition states had very long Cr–C bond lengths of 3.440 and 3.396 Å, where Ar = Xyl and Dpp respectively, and low barriers for Cr(II) trapping the $\text{R}\cdot$.

Large differences in the Cr–C–C bond angles were also observed for the Cr(III) benzyl compounds. The Mes (**2.14a**) and Dep (**2.14b**) substituted analogues had very similar bond angles of 120.66(14) and 121.66(14) degrees, respectively, while the Dpp substituted analogue **2.14c** had a bond angle approximately 5° larger (126.30(9)°). Interestingly, the cyanomethyl derivative **2.13** had a significantly smaller angle of 114.67(16)°, while the sterically congested Cr– CH_2SiMe_3 and neopentyl compounds all had bond angles > 130°, indicative of significant

steric strain. Even the alkenyl compound **2.16** had a larger than expected Cr–C–C bond angle of 142.2(3)° (average).

2.11 Exploring Cr(III)–R Bond Homolysis

The observed formation of the Cr(III) benzyl compound **2.14** and the Cr(III) *para*-methylbenzyl compound **2.18** from the Cr(III) neopentyl compound **2.11** indicated Cr–C bond homolysis. The Cr(III) hydrocarbyl compounds presented herein were subjected to study of the rates of Cr–C bond homolysis. Preliminary studies focused on conversion of the Cr(III) neopentyl compound **2.11** to the reduced Cr(II) compound **2.1**. The conversion was monitored in hexanes solutions of **2.11** (10^{-4} M) using UV-vis spectroscopy. The reaction showed clean conversion to the reduced Cr(II) over a period of 14 h at room temperature. Interestingly, the reaction did not go to completion in benzene solvent under the same reaction conditions; after 2 days there was approximately a 1:1 mixture of Cr(III):Cr(II). The solvent dependence was attributed to the difference in C–H BDE between the hexanes and benzene,⁵² limiting the ability of the $\cdot\text{CH}_2\text{CMe}_3$ radical to undergo C–H activation of the benzene.

The use of 9,10-dihydroanthracene as a radical trap, due to the relatively weak C–H bonds, provided similar results to that of the hexanes experiments. Unfortunately, no valuable kinetic information could be extracted from the data due to the build up of the persistent Cr(II) product, which acted as an extremely efficient radical trapping agent.²⁸ One alternative was to perform the experiment under pseudo-first-order reaction conditions by adding an excess of a radical trapping agent that only reacts with $\text{R}\cdot$ (in this case 9,10-dihydroanthracene), and an excess of the reduced metal complex (in this case compound **2.1**).²⁴ These types of experiments often require extended reaction times to reach completion due to the presence of an excess of the reduced metal complex. Monitoring the reaction by UV-vis spectroscopy can also be difficult due to the absorption associated with the presence of a large excess of the reduced metal complex. Alternatively, the use of a radical trapping agent (X_2) that reacts with both the organic radical and the reduced metal complex (Figure 2.19) allows the experiments to be performed under pseudo-first-order conditions without the need for an excess of the reduced metal complex.²⁵

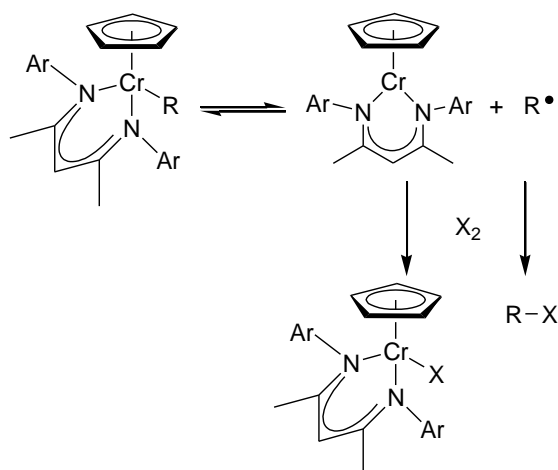


Figure 2.19. Use of radical trap X_2 to quantify Cr(III)–R bond homolysis.

(2,2,6,6-Tetramethylpiperidin-1-yl)oxyl (TEMPO) was initially considered as a suitable radical trapping agent because of the well established reactivity with organic radicals.⁵⁵ It was also found to react rapidly with the Cr(II) compound **2.1**, the other prerequisite for use as a radical trap, but the proposed product of the reaction, a Cr(III)–TEMPO complex, could not be isolated or fully characterized from the reaction mixture. Diphenyl disulfide (PhSSPh) has also been well established as an efficient trapping agent for organic radicals: alkyl radicals react with PhSSPh with rate constants of $1.7 \times 10^5 \text{ M}^{-1} \text{ s}^{-1}$.⁵⁵ PhSSPh is also known to react with Cr(II) compounds by single-electron oxidation,⁵⁶ and was found to react cleanly with the Cr(II) compound **2.1** to form the Cr(III)–SPh compound $\text{CpCr}[(\text{XylNCMe})_2\text{CH}](\text{SPh})$ (**2.19**). The solid-state molecular structure of **2.19**, shown in Figure 2.20, displays a typical Cr(III)–S bond length of 2.3707(6) Å and a Cr–S–C bond angle of 110.66(7)°, ⁵⁶ as well as Cr–N bond lengths of 2.0238(16) and 2.0322(16) Å that are similar to the other CpCr β -diketiminate compounds reported herein.

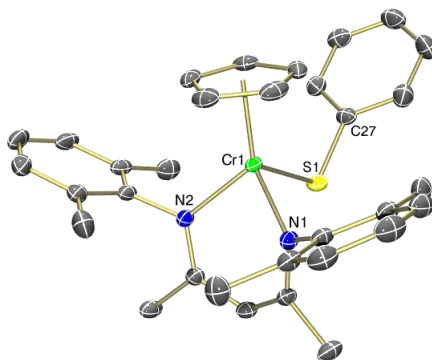


Figure 2.20. Thermal ellipsoid diagram (50%) of **2.19**. All H atoms are omitted for clarity.

The reaction between the Cr(II) compound **2.1** and PhSSPh resulted in the rapid formation of **2.19**, even at a concentration of 1×10^{-4} M of **2.1** the reaction with 6 equivalents of PhSSPh was complete in the time required to transfer the UV-vis cell from the glovebox to the spectrophotometer for analysis (~3 min). In addition to the rapid formation and high stability of **2.19**, it also has a minimum absorption in the UV-vis spectrum at 560 nm where the Cr(III)–R compounds absorb strongly (Figure 2.18), making PhSSPh an ideal radical trapping agent for these kinetic studies.

The Cr(III) neopentyl compound **2.11** reacted cleanly with an excess of at least 10 equivalents of PhSSPh at room temperature. The reaction was monitored by UV-vis at 560 nm and the resulting spectrum was fit to first-order decay. A sample spectrum is shown in Figure 2.21. The reaction was monitored at high concentrations of PhSSPh where saturation kinetics was observed. The first-order rate constant for the Cr–C bond homolysis, $k = 3.6(3) \times 10^{-3} \text{ s}^{-1}$, was extracted from the plot of k_{obs}^{-1} vs $[\text{PhSSPh}]^{-1}$ (shown in Figure 2.22c). A list of rate constants for the Cr–C bond homolysis of the Cr(III) hydrocarbyl compounds is presented in Table 2.2; the graphs of k_{obs}^{-1} vs $[\text{PhSSPh}]^{-1}$ for these compounds are in Figure 2.22.

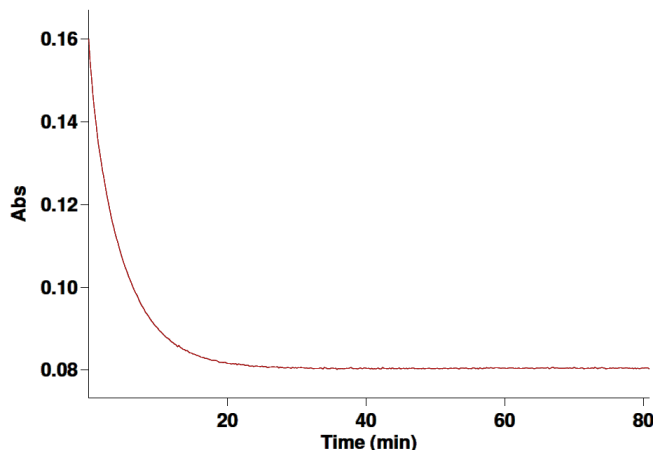


Figure 2.21. UV-vis decay curve for the conversion of Cr(III) neopentyl **2.11** to Cr(III)–SPh **2.19** ($k_{\text{obs}} = 3.54 \times 10^{-3} \text{ s}^{-1}$). Conditions: initial $[\mathbf{2.11}] = 1.74 \times 10^{-4} \text{ M}$; $[\text{PhSSPh}] = 1.80 \times 10^{-2} \text{ M}$; monitored at 560 nm in hexanes at room temperature.

A seemingly small change in the steric profile of the hydrocarbyl group, neopentyl vs isobutyl, resulted in a large decrease in the rate constant by more than two orders of magnitude, from $3.6(3) \times 10^{-3} \text{ s}^{-1}$ to $\sim 1 \times 10^{-5} \text{ s}^{-1}$. Interestingly, the rate constant for Cr(III) benzyl compound **2.14** ($3.2(5) \times 10^{-3} \text{ s}^{-1}$) was very similar to the neopentyl species **2.11**, indicative of electronic destabilization of the Cr–C bond of **2.14** due to the increased stability of the $\text{PhCH}_2\cdot$ radical formed upon bond cleavage. By comparison, the rate constant for Cr–C bond homolysis in the aqueous compound $[(\text{H}_2\text{O})_5\text{Cr}(\text{CH}_2\text{Ph})]^{2+}$ was reported to be $2.6 \times 10^{-3} \text{ s}^{-1}$.⁵⁷ Further

evidence of electronic effects on the rate of homolysis were observed by comparison of the rate constants for the benzyl (**2.14**) and *para*-methylbenzyl (**2.18**) compounds. A two-fold increase in the rate constant was observed with the *p*-methyl substituted benzyl, consistent with the increased stability of benzyl radicals upon addition of a *p*-methyl substituent.⁵⁸

Table 2.2. Comparison of rate constants for CpCr[(ArNCMe)₂CH](R) bond homolysis.

	Ar	R	Rate constant k (s ⁻¹)
2.10	Xyl	CH ₂ CHMe ₂	$\sim 1 \times 10^{-5}$ ^a
2.10c	Dpp	CH ₂ CHMe ₂	$\sim 5 \times 10^{-5}$ ^a
2.11	Xyl	CH ₂ CMe ₃	$3.6(3) \times 10^{-3}$
2.14	Xyl	CH ₂ Ph	$3.2(5) \times 10^{-3}$
2.14a	Mes	CH ₂ Ph	$3.2(4) \times 10^{-3}$
2.14b	Dep	CH ₂ Ph	$1.1(7) \times 10^{-2}$
2.14c	Dpp	CH ₂ Ph	$9(2) \times 10^{-3}$
2.18	Xyl	CH ₂ C ₆ H ₄ Me	$7.8(7) \times 10^{-3}$

^a Estimated from single point experiments at high [PhSSPh].

Direct comparison of the four Cr(III) benzyl compounds **2.14** – **2.14c** displayed a distinct trend in the steric effect of the different β -diketiminato ligands (Xyl \approx Mes < Dep \approx Dpp). The Xyl and Mes substituted ligands had the same rate constants, as expected based on the similar steric profile of the two ligands. Additionally, the presence of the *p*-methyl substituents of the Mes substituted ligand did not have any effect on the rate constant compared to the Xyl substituted analogue. The more sterically congested Dep and Dpp substituted ligands caused a three-fold increase in the rate constant compared to the Xyl and Mes derivatives, a trend that was also observed with the isobutyl compounds **2.10** and **2.10c**.

The remaining Cr(III) hydrocarbyl compounds **2.2**, **2.7**, **2.9**, **2.13**, **2.15**, **2.16**, **2.17**, and the ethyl compound CpCr[(XylNCMe)₂CH](Et) were all subjected to the same reaction conditions as those described above but were not found to undergo Cr–C bond homolysis at appreciable rates at room temperature. The Cr(III)–CH₂SiMe₃ compound **2.7** did not react with a large excess of PhSSPh when subjected to the same reaction conditions as compound **2.11** when monitored by UV-vis spectroscopy. Unexpectedly, the stock solution of the kinetic experiment of **2.7** that was stored in the glovebox did react to form the expected Cr(III)–SPh compound **2.19** over the same time period. Upon leaving the sample from the UV-vis spectrometer to stand under ambient laboratory light it also cleanly converted to **2.19**. Further investigation revealed that all of the CpCr[(ArNCMe)₂CH](R) compounds reported herein, except for the alkynyl compound **2.17**, also cleanly formed the Cr(III)–SPh analogues in the presence of PhSSPh when exposed either to

sunlight or ambient laboratory light. Compound **2.17** was a unique case that led to complete decomposition of the Cr species, presumably due to the highly reactive nature of a putative $\text{HC}\equiv\text{C}\cdot$ radical generated as a result of Cr–C bond homolysis.

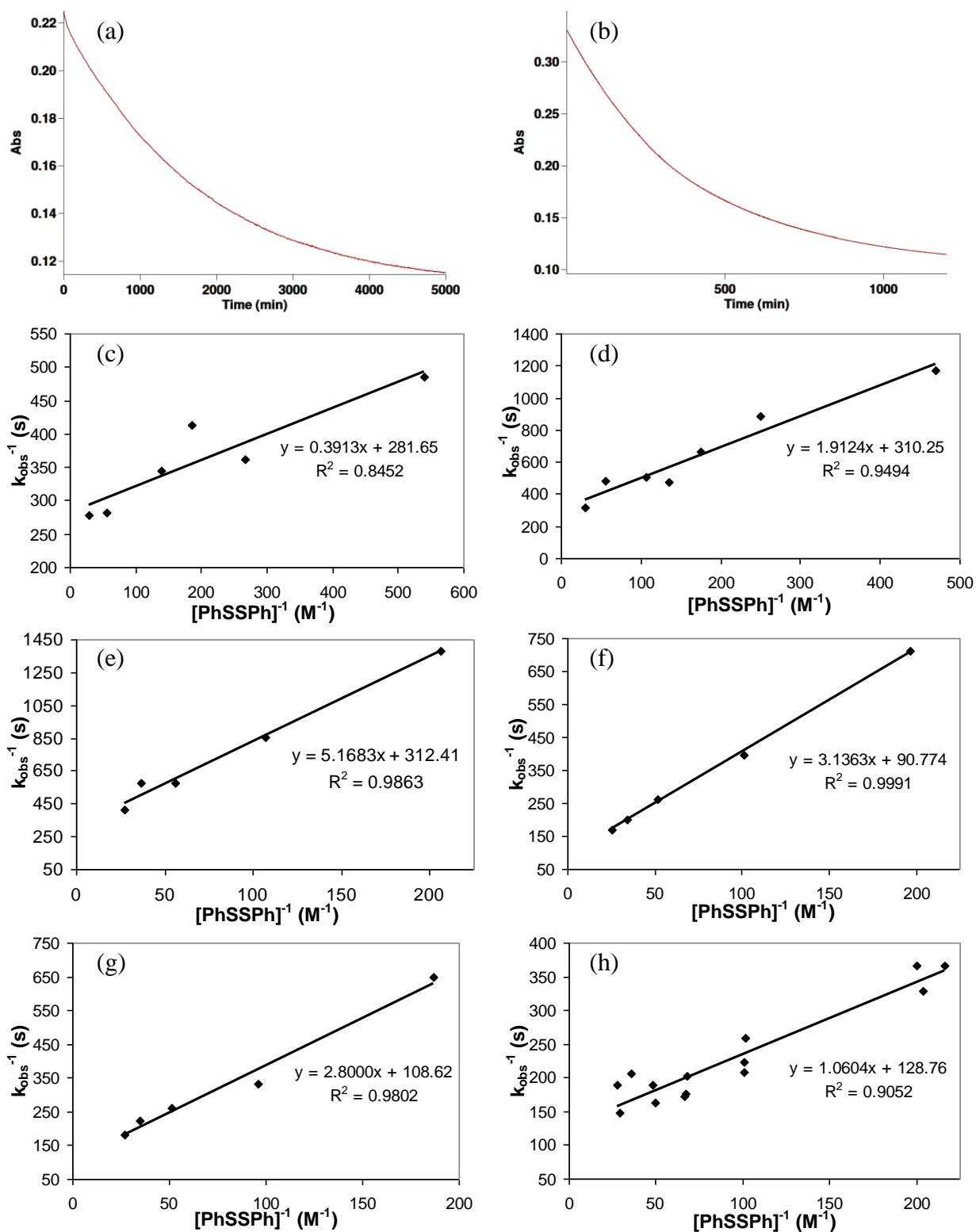


Figure 2.22. UV-vis decay curve (560 nm) for the Cr(III) isobutyl compounds **2.10** (a) and **2.10c** (b) and pseudo-first-order rate constants k_{obs}^{-1} plotted against $[\text{PhSSPh}]^{-1}$ for compounds **2.11** (c), **2.14** (d), **2.14a** (e), **2.14b** (f), **2.14c** (g), and **2.18** (h).

2.12 Exploring Cr(III)–R Photolysis

Photolytically induced M–R bond homolysis has been well established in the literature, especially for organocobalt compounds.⁵⁹ Although the photochemistry of octahedral Cr(III) coordination compounds has also been studied,⁶⁰ the observed photolytically induced bond homolysis of the Cr(III) hydrocarbyl compounds was surprising. During the preparation of the Cr(III)–R compounds there was no evidence to suggest that photolysis was occurring. As discussed earlier, the Cr(II) CpCr[(ArNCMe)₂CH] compounds have been shown to be extremely efficient radical trapping agents. During light exposure it is possible that small amounts of the Cr(II) species builds up in solution which subsequently prevents further decomposition due to the persistent nature of the Cr(II) radical trap. Only by adding the radical trap PhSSPh that consumed both the Cr(II) and the organic radical was the photolytically induced bond homolysis reactivity fully appreciated.

The Cr(III) methyl compound **2.2** was examined to determine the specific wavelengths of light responsible for inducing bond homolysis. The Cr(III) hydrocarbyl compounds all exhibit two strong absorption bands in the UV-vis spectrum. The lower energy band was first examined by preparing a 10^{−4} M hexanes solution of **2.2** containing a large excess of PhSSPh. Exposure to light ≥ 500 nm in a fluorometer over a period of 30 min did not induce bond homolysis, as no change in the UV-vis spectrum was observed over that time period. Exposure of the reaction mixture to light ≥ 400 nm did induce bond homolysis causing compound **2.2** to convert to the Cr(III)–SPh compound **2.19**. The clean formation of **2.19** from **2.2** was essentially complete after 5 h of light exposure over a 2 day period; after 94 min of light exposure the reaction was stored with the strict exclusion of light for 24 h before re-exposure to complete the reaction, decay curve shown in Figure 2.23. No reaction was observed during the 24 h period without light exposure, demonstrating the need for continual exposure to induce bond homolysis. The results indicated that the higher energy absorption (395–436 nm) of the Cr(III) hydrocarbyl compounds was responsible for the Cr–C bond homolysis.

A 10^{−4} M hexanes solution of Cr(III) methyl complex **2.2** was also subjected to air exposure while monitoring the UV-vis spectrum of the solution. Interestingly, the solution of **2.2** was found to be completely air-stable over a period of 3 h when protected from light, with no change to the UV-vis spectrum during air exposure. Conversely, the Cr(III) benzyl compound **2.14** decomposes under similar conditions within minutes of air exposure, due to the presence of Cr–C bond homolysis for compound **2.14** in the absence of light. The Cr(II) species that is formed upon bond homolysis is extremely air-sensitive and therefore the observed air-sensitivity

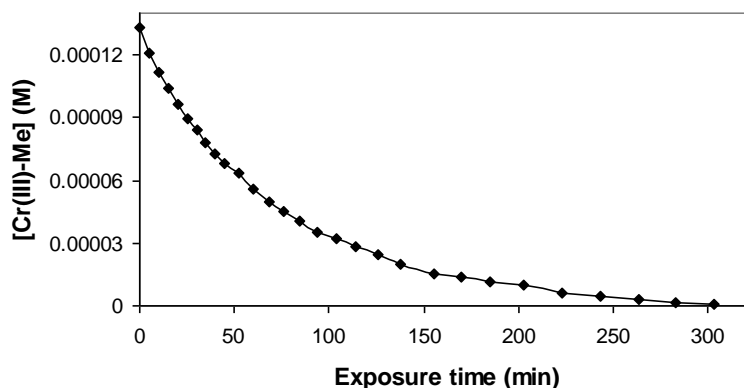


Figure 2.23. Decay curve for the conversion of **2.2** to **2.19** with light exposure ≥ 400 nm. Conditions: initial **2.2** = 1.91×10^{-4} M; [PhSSPh] = 1.99×10^{-2} M; monitored at 560 nm in hexanes at room temperature.

of the Cr(III) hydrocarbyl compounds is apparently limited to the ability of O_2 to function as a radical trapping agent. The similarity in photolytic reactivity between PhSSPh and O_2 is consistent with the mechanism shown in Figure 2.19, where the O_2 acts as a radical trap for both the organic radical and Cr(II).

In summary, the Cr(III) hydrocarbyl compounds that do not undergo bond homolysis at room temperature in the absence of light are air-stable as solids and in solution in the absence of light. Therefore, the Cr(III) hydrocarbyl compounds that are thermally stable with respect to bond homolysis can be considered air-stable in the absence of light, and light-stable in the absence of air.

2.13 Experimental Section

General considerations. Unless otherwise indicated, all reactions were carried out under nitrogen using standard Schlenk and glovebox techniques. Hexanes, toluene, dichloromethane, Et_2O , and THF were purified by passage through activated alumina and deoxygenizer columns from Glass Contour Co. (Laguna Beach, CA, USA). Benzene was dried over sodium/benzophenone, purified by vacuum distillation, degassed by three freeze-vacuum-thaw cycles and stored under nitrogen. Celite (purchased from Aldrich) was dried overnight at $120^\circ C$ before being evacuated and then stored under nitrogen.

Characterization. UV-visible spectroscopic data was collected on Varian Cary 100 Bio or Shimadzu UV-2550 UV-visible spectrophotometers in a specially constructed cell for air-sensitive samples: a Kontes Hi-Vac Valve with PTFE plug was attached by a professional glassblower to a Hellma 10 mm path length quartz absorption cell with a quartz-to-glass graded seal. 1H NMR spectra were recorded on a Varian Mercury Plus 400 spectrometer. 1H NMR

spectra were referenced to the residual solvent peak. Solution magnetic susceptibilities were determined by the method of Evans.⁶¹ Elemental analyses were performed by Guelph Chemical Laboratories, Guelph, ON, Canada or by the UBC Department of Chemistry microanalytical services.

Materials. Acetonitrile, 1,4-dioxane, butyllithium (1.6 M in hexanes), chromium(III) chloride (anhydrous), lead(II) bromide, manganese powder, phenyl disulfide, potassium bis(trimethylsilyl)amide, *p*-xylene (anhydrous), silver *p*-toluenesulfonate, silver trifluoromethanesulfonate, sodium benzoate, sodium cyclopentadienylide (2.0 M in THF), and all Grignard reagents were purchased from Aldrich and used as received. Chromium(II) chloride was purchased from Strem or Aldrich and used as received. 1,2,3,4,5-Pentamethylcyclopentadiene and (iodomethyl)trimethylsilane were purchased from Aldrich, degassed by three freeze-vacuum-thaw cycles, and stored under nitrogen prior to use. Compounds **2.1**,³⁴ **2.1b**,⁵⁴ **2.2**,³⁵ CrCl₂(tmeda),^{45b} H[(XylNCMe)₂CH],⁶² H[(MesNCMe)₂CH],⁶³ H[(DepNCMe)₂CH],⁶³ and CpCr[(DppNCMe)₂CH](OTf)³² were prepared according to literature procedures. The Grignard reagents: Mg(CH₂CMe₃)₂·*x*(1,4-dioxane), Mg(CH₂SiMe₃)₂·*x*(1,4-dioxane), Mg(CH₂CHMe₂)₂·*x*(1,4-dioxane), Mg(CH₂CMe₂Ph)₂·*x*(1,4-dioxane), Mg(*c*-C₆H₁₁)₂·*x*(1,4-dioxane), and Mg(Ph)₂·*x*(1,4-dioxane) were also prepared based on literature procedures.⁶⁴

Synthesis of CpCr[(MesNCMe)₂CH] (2.1a). Following a procedure similar to that previously reported for compound **2.1**,³⁴ H[(MesNCMe)₂CH] (744 mg, 2.23 mmol) was dissolved in THF (12 mL). *n*-BuLi (1.60 mL of 1.6 M solution in hexanes, 2.56 mmol, 1.15 equiv) was added dropwise and the resulting yellow solution was stirred for 0.5 h at room temperature. In a separate Schlenk flask, CrCl₂(tmeda) (531 mg, 2.22 mmol, 1 equiv) was suspended in THF (35 mL) followed by the addition of NaCp (1.25 mL, 2.50 mmol, 1.13 equiv). The resulting mixture was stirred for 30 min at room temperature. To this solution, the lithium salt prepared above was added dropwise and the mixture was stirred at room temperature overnight. The solvent was evaporated under reduced pressure and the residue was extracted with hexanes, followed by filtration through Celite. The solvent was again removed under reduced pressure and the complex was dissolved in hexanes (20 mL), filtered, and cooled to -35 °C for several days to yield black crystals of **2.2a** (730 mg, 73%) in two crops. μ_{eff} (Evans, C₆D₆): 4.8 μ_B . Anal. Calcd. for C₂₈H₃₄CrN₂: C, 74.64; H, 7.61; N, 6.22. Found: C, 74.83; H, 7.96; N, 6.42. UV-vis (hexanes; λ_{max} , nm (ϵ , M⁻¹cm⁻¹)): 308 (11700), 427 (7210), 573 (376).

Synthesis of CpCr[(MesNCMe)₂CH](Me) (2.2a). To a solution of **2.3a** (105 mg, 0.216 mmol) in Et₂O (20 mL) was added MeMgI (0.080 mL of 3.0 M solution in Et₂O, 0.24 mmol) and the mixture was allowed to stir at room temperature overnight. To the resulting purple solution was added an excess of 1,4-dioxane (0.20 mL) and allowed to stir for 1 hr at which time the reaction mixture was filtered over Celite. The solvent was removed under reduced pressure, the residue was extracted with hexanes (1 mL), filtered over Celite, and cooled to -35 °C to yield black crystals of **2.2a** (77.5 mg, 77%) isolated in two crops over several days. Anal. Calcd. for C₂₉H₃₇N₂Cr: C, 74.81; H, 8.01; N, 6.02. Found: C, 75.14; H, 8.33; N, 6.18. UV-vis (hexanes; λ_{max} , nm (ϵ , M⁻¹cm⁻¹)): 416 (5580), 542 (1600).

Synthesis of CpCr[(XylNCMe)₂CH](Cl) (2.3). Compound H[(XylNCMe)₂CH] (1.43 g, 4.67 mmol) was added to a Schlenk flask, dissolved in THF (30 mL) and cooled to 0 °C in an ice-water bath. *n*-BuLi (3.20 mL of 1.6 M solution in hexanes, 5.12 mmol, 1.10 equiv) was added dropwise and the resulting yellow solution was allowed to warm to room temperature while stirring for 1 hour. The lithium salt was then cannulated into a suspension of CrCl₃ (744 mg, 4.70 mmol, 1.00 equiv) in THF (20 mL) and stirred at room temperature overnight. NaCp (2.60 mL, 5.20 mmol, 1.11 equiv) was added to the solution which was again stirred at room temperature overnight. The solvent was evaporated under reduced pressure and the residue was extracted with 40 mL of a hexanes/dichloromethane mixture (3:1), filtered over Celite and rinsed with hexanes (3 × 5 mL). The green (orange transmitted) filtrate was concentrated and cooled to -20 °C to yield dark green crystals of **2.3** (1.66 g, 78%) over several days in three crops. Anal. Calcd. for C₂₆H₃₀CrN₂Cl: C, 68.19; H, 6.60; N, 6.12. Found: C, 67.88; H, 6.50; N, 5.73. UV-vis (hexanes; λ_{max} , nm (ϵ , M⁻¹cm⁻¹)): 418 (7220), 581 (504).

Synthesis of CpCr[(MesNCMe)₂CH](Cl) (2.3a). Using a procedure identical to that described above for compound **2.3**, compound **2.3a** was prepared from H[(MesNCMe)₂CH] (2.35 g, 7.03 mmol), *n*-BuLi (4.90 mL of 1.6 M solution in hexanes, 7.84 mmol), CrCl₃ (1.13 g, 7.15 mmol) and NaCp (3.90 mL of 2.0 M solution in THF, 7.80 mmol). Dark green crystals of **2.3a** (2.55 g, 75%) were isolated over several days in four crops. Anal. Calcd. for C₂₈H₃₄N₂CrCl: C, 69.19; H, 7.05; N, 5.76. Found: C, 69.17; H, 7.43; N, 5.43. UV-vis (hexanes; λ_{max} , nm (ϵ , M⁻¹cm⁻¹)): 419 (8060), 583 (798).

Synthesis of CpCr[(DepNCMe)₂CH](Cl) (2.3b). Using a similar procedure to that described above for compound **2.3**, compound **2.3b** was prepared from H[(DepNCMe)₂CH] (3.65 g, 10.1 mmol), *n*-BuLi (6.90 mL of 1.6 M solution in hexanes, 11.0 mmol), CrCl₃ (1.60 g, 10.1 mmol) and NaCp (5.50 mL of 2.0 M solution in THF, 11.0 mmol). Upon work up the

residue was extracted with 120 mL of a hexanes/Et₂O/dichloromethane mixture (2:1:1), filtered over Celite and rinsed with hexanes (2 × 10 mL). Black crystals of **2.3b** (4.11 g, 79%) were isolated over several days in three crops. Anal. Calcd. for C₃₀H₃₈N₂CrCl: C, 70.09; H, 7.45; N, 5.45. Found: C, 69.82; H, 7.17; N, 5.07. UV-vis (hexanes; λ_{max}, nm (ε, M⁻¹cm⁻¹)): 420 (8670), 585 (875).

Synthesis of [(XylNCMe)₂CH]Cr₂(μ-O₂CPh)₂ (2.4). To a solution of H[(XylNCMe)₂CH] (307 mg, 1.00 mmol, 1.03 equiv) in THF, *n*-BuLi (0.69 mL of 1.6 M solution in hexanes, 1.1 mmol, 1.1 equiv) was added dropwise and the resulting yellow solution was allowed to stir for 0.5 h at room temperature. In a separate Schlenk flask, CrCl₂ (119 mg, 0.968 mmol) was suspended in THF (20 mL) and cooled to -35 °C followed by the dropwise addition of the lithium salt prepared above. The resulting orange-brown reaction mixture was allowed to stir overnight at room temperature followed by the addition of a THF (8 mL) suspension of NaO₂CPh (140 mg, 0.972 mmol, 1.00 equiv). The reaction mixture was again stirred overnight before removal of the solvent under reduced pressure. The residue was extracted with Et₂O (~15 mL) and filtered over Celite followed by the addition of AgOTf (251 mg, 0.978 mmol, 1.01 equiv). Upon stirring overnight the reaction solution turned red-yellow in colour and the reaction vessel became coated with a thin film of Ag metal, at which point the solvent was removed under reduced pressure, the residue extracted with THF (~10 mL), and filtered over Celite, followed by the addition of a THF solution of NaCp* (142 mg, 0.997 mmol, 1.03 equiv). The reaction mixture was allowed to stir for 5 days at which point the solvent was removed under reduced pressure, the residue extracted with hexanes, filtered over Celite. The solvent was again removed under reduced pressure, the residue extracted with a minimum of hexanes (3 mL), filtered over Celite, and the brown solution (red transmitted) was cooled to -35 °C for several days to yield X-ray quality crystals of **2.4** (30 mg, 6%). Anal. Calcd. for C₅₆H₆₀N₄O₄Cr₂: C, 70.28; H, 6.32; N, 5.85. Found: C, 69.93; H, 7.05; N, 5.85.

Synthesis of CpCr[(XylNCMe)₂CH](Br) (2.5). In a Schlenk flask, H[(XylNCMe)₂CH] (2.19 g, 7.16 mmol, 1.03 equiv) was dissolved in THF (30 mL) and cooled in an ice bath at which point *n*-BuLi (4.60 mL of 1.6 M solution in hexanes, 7.36 mmol, 1.03 equiv) was added dropwise. The resulting yellow solution was allowed to warm to room temperature while stirring for 45 min. In a separate Schlenk flask, CrCl₂(THF)₂ (1.86 g, 6.97 mmol) was suspended in THF (40 mL) followed by the addition of NaCp (3.70 mL of 2.0 M solution in THF, 7.40 mmol, 1.06 equiv). The resulting mixture was stirred for 45 min at room temperature. The lithium salt prepared above was then transferred by cannula to the Schlenk containing the

chromium and the resulting green solution (magenta transmitted) was stirred overnight. The solvent was removed under reduced pressure and the residue was extracted with hexanes (50 mL), filtered over Celite, rinsed with hexanes (3×5 mL) and the solvent was again removed under reduced pressure. The residue was dissolved in toluene (30 mL) and transferred by cannula to another Schlenk flask containing a suspension of PbBr_2 (1.30 g, 3.54 mmol, 0.508 equiv.) in toluene (10 mL). After stirring overnight, the reaction mixture was filtered over Celite. The Celite was rinsed with toluene (2×5 mL) and the green solution (orange transmitted) was concentrated to a volume of 30 mL and cooled to -20°C to yield black crystals of **2.5** (2.32 g, 66%) in two crops. Anal. Calcd for $\text{C}_{26}\text{H}_{30}\text{N}_2\text{CrBr}$: C, 62.16; H, 6.02; N, 5.58. Found: C, 62.52; H, 6.03; N, 5.60. UV-vis (Et_2O , λ_{max} , nm (ϵ , $\text{M}^{-1}\text{cm}^{-1}$)): 423 (7990), 582 (820).

Synthesis of $\text{CpCr}[(\text{XylNCMe})_2\text{CH}](\text{OTs})$ (2.6**).** Compound **2.3** (1.28 g, 2.79 mmol) and AgOTs (781 mg, 2.80 mmol, 1.00 equiv) were placed in a Schlenk flask followed by the addition of THF (60 mL). The mixture was stirred overnight at room temperature, filtered over Celite and the solvent was removed under reduced pressure. The residue was extracted with 32 mL of a hexanes/dichloromethane mixture (4:1), filtered over Celite and rinsed with hexanes (2×5 mL). The green (orange transmitted) filtrate was cooled to -20°C to yield black crystals of **2.6** (1.40 g, 84%) over several days in four crops. Anal. Calcd. for $\text{C}_{33}\text{H}_{37}\text{CrO}_3\text{N}_2\text{S}$: C, 66.76; H, 6.28; N, 4.72. Found: C, 66.50; H, 6.20; N, 4.34. UV-vis (Et_2O ; λ_{max} , nm (ϵ , $\text{M}^{-1}\text{cm}^{-1}$)): 411 (8140), 571 (548).

Synthesis of $\text{CpCr}[(\text{MesNCMe})_2\text{CH}](\text{OTs})$ (2.6a**).** The procedure described above for the preparation of **2.6** was followed with **2.3a** (997 mg, 2.05 mmol) and AgOTs (572 mg, 2.05 mmol, 1.00 equiv) in THF (50 mL). The reaction mixture was stirred overnight at room temperature. Upon workup, cooling to -20°C in 35 mL of hexanes/ CH_2Cl_2 (5:1) mixture provided black crystals of **2.6a** (940 mg, 74%) over several days in three crops. Anal. Calcd for $\text{C}_{35}\text{H}_{41}\text{N}_2\text{O}_3\text{SCr}$: C, 67.61; H, 6.65; N, 4.51. Found: C, 67.86; H, 6.94; N, 4.60. UV-vis (Et_2O ; λ_{max} , nm (ϵ , $\text{M}^{-1}\text{cm}^{-1}$)): 412 (8300), 570 (575).

Synthesis of $\text{CpCr}[(\text{DepNCMe})_2\text{CH}](\text{OTs})$ (2.6b**).** The procedure described above for the preparation of **2.6** was followed with **2.3b** (1.96 g, 3.82 mmol) and AgOTs (1.07 g, 3.82 mmol, 1.00 equiv) in THF (75 mL). The reaction mixture was stirred overnight at room temperature. Upon workup, cooling to -20°C in 45 mL of hexanes/ CH_2Cl_2 (4:1) mixture provided black crystals of **2.6a** (2.07 g, 84%) over several days in four crops. Anal. Calcd for $\text{C}_{37}\text{H}_{45}\text{N}_2\text{O}_3\text{SCr}$: C, 68.39; H, 6.99; N, 4.31. Found: C, 68.32; H, 7.30; N, 4.35. UV-vis (Et_2O ; λ_{max} , nm (ϵ , $\text{M}^{-1}\text{cm}^{-1}$)): 412 (8040), 576 (498).

Synthesis of $\text{CpCr}[(\text{XylNCMe})_2\text{CH}](\text{CH}_2\text{SiMe}_3)$ (**2.7**).

Method B. Compound **2.6** (202 mg, 0.340 mmol) was placed in a Schlenk flask followed by the addition of Et_2O (18 mL). $\text{Mg}(\text{CH}_2\text{SiMe}_3)_2 \cdot 1.05(1,4\text{-dioxane})$ (54.6 mg, 0.188 mmol, 0.55 equiv) in Et_2O (4 mL) was added dropwise to the Schlenk. The reaction was allowed to stir overnight at room temperature followed by removal of the solvent under reduced pressure, the residue was extracted with hexanes, filtered over Celite, and the solvent was again removed under reduced pressure. The violet solid was extracted with a minimum of hexanes (4 mL), filtered over Celite, and cooled to $-35\text{ }^\circ\text{C}$ to yield black crystals of **2.7** (150 mg, 86%) over several days in two crops. Anal. Calcd for $\text{C}_{30}\text{H}_{41}\text{N}_2\text{SiCr}$: C, 70.69; H, 8.11; N, 5.50. Found: C, 71.06; H, 8.11; N, 5.22. UV-vis (hexanes; λ_{max} , nm (ϵ , $\text{M}^{-1}\text{cm}^{-1}$)): 412 (6350), 568 (1180).

Method C. Compound **2.1** (102 mg, 0.241 mmol) was added to a Schlenk flask followed by the addition of THF (10 mL). $\text{Me}_3\text{SiCH}_2\text{I}$ (53.0 μL , 0.357 mmol, 1.5 equiv) was added to the solution and stirred for 10 min followed by the addition of Mn powder (133 mg, 2.42 mmol, 10 equiv). The reaction mixture was allowed to stir for 24 h at room temperature, at which point the reaction was determined to be complete by UV-vis spectroscopy. The reaction mixture was then allowed to stir for an additional 24 h before the solvent was removed under reduced pressure. The residue was extracted with hexanes (10 mL), filtered over Celite and rinsed with hexanes ($3 \times 5\text{ mL}$). The violet solution was concentrated to 3 mL and cooled to $-35\text{ }^\circ\text{C}$ to yield crystals of **2.7** (89 mg, 73%) over several days in two crops, purity confirmed by UV-vis spectroscopy.

Synthesis of $\text{CpCr}[(\text{MesNCMe})_2\text{CH}](\text{CH}_2\text{SiMe}_3)$ (2.7a**).** The procedure described above for the preparation of **2.7** (method **B**) was followed with **2.6a** (119 mg, 0.191 mmol) and $\text{Mg}(\text{CH}_2\text{SiMe}_3)_2 \cdot 1.05(1,4\text{-dioxane})$ (30.8 mg, 0.106 mmol, 0.56 equiv) in Et_2O (25 mL). The reaction mixture was allowed to stir overnight at room temperature, 1,4-dioxane (200 μL) was added and stirred for 1 h. Upon workup, cooling to $-35\text{ }^\circ\text{C}$ in hexanes (4 mL) provided black crystals of **2.7a** (51 mg, 50%) over several days in two crops. Anal. Calcd for $\text{C}_{32}\text{H}_{45}\text{N}_2\text{SiCr}$: C, 71.47; H, 8.43; N, 5.21. Found: C, 71.20; H, 8.05; N, 5.08. UV-vis (hexanes; λ_{max} , nm (ϵ , $\text{M}^{-1}\text{cm}^{-1}$)): 414 (6430), 568 (1080).

Synthesis of $\text{CpCr}[(\text{DepNCMe})_2\text{CH}](\text{CH}_2\text{SiMe}_3)$ (2.7b**).** The procedure described above for the preparation of **2.7** (method **B**) was followed with **2.6b** (195 mg, 0.300 mmol) and $\text{Mg}(\text{CH}_2\text{SiMe}_3)_2 \cdot 1.05(1,4\text{-dioxane})$ (48.5 mg, 0.167 mmol, 0.56 equiv) in Et_2O (30 mL). The reaction mixture was allowed to stir overnight at room temperature. Upon workup, cooling to $-35\text{ }^\circ\text{C}$ in hexanes (3 mL) provided black crystals of **2.7b** (116 mg, 68%) over several days in two

crops. Anal. Calcd for $C_{34}H_{49}N_2SiCr$: C, 72.17; H, 8.73; N, 4.95. Found: C, 72.06; H, 8.71; N, 5.06. UV-vis (hexanes; λ_{max} , nm (ϵ , $M^{-1}cm^{-1}$)): 414 (6310), 568 (1070).

Synthesis of $CpCr[(DppNCMe)_2CH](CH_2SiMe_3)$ (2.7c). The procedure described above for the preparation of **2.7** (method **B**) was followed with $CpCr[(DppNCMe)_2CH](OTf)$ (48.7 mg, 0.0712 mmol) and $Mg(CH_2SiMe_3)_2 \cdot 1.05(1,4\text{-dioxane})$ (11.5 mg, 0.0395 mmol, 0.56 equiv) in Et_2O (8 mL). The reaction mixture was allowed to stir for 1.5 h at room temperature. Upon workup, cooling to $-35\text{ }^\circ C$ in hexanes (2 mL) provided black crystals of **2.7c** (27.9 mg, 63%) over several days in two crops. Anal. Calcd for $C_{38}H_{57}N_2SiCr$: C, 73.38; H, 9.24; N, 4.50. Found: C, 74.96; H, 10.37; N, 4.63. UV-vis (hexanes; λ_{max} , nm (ϵ , $M^{-1}cm^{-1}$)): 416 (7080), 582 (1100).

Attempted synthesis of $CpCr[(XylNCMe)_2CH](CH_2CMe_2Ph)$. The procedure described above for the preparation of **2.7** (method **B**) was followed with **2.6** (249.4 mg, 0.4201 mmol) and $Mg(CH_2CMe_2Ph)_2 \cdot 1.85(1,4\text{-dioxane})$ (106.1 mg, 0.234 mmol, 0.56 equiv) in Et_2O (65 mL). The reaction mixture was allowed to stir for 3 days at room temperature. Upon workup, cooling to $-35\text{ }^\circ C$ in hexanes (3 mL) provided a small amount of crystals of $Cr[(XylNCMe)_2CH](C_6H_4CMe_2CH_2)$ (**2.8**), as characterized by X-ray crystallography. Anal. Calcd for $C_{31}H_{37}N_2Cr$: C, 76.04; H, 7.62; N, 5.72. Found: C, 75.64; H, 7.32; N, 5.58.

Attempted synthesis of $CpCr[(MesNCMe)_2CH](CH_2CMe_2Ph)$. The procedure described above for the preparation of **2.7** (method **B**) was followed with **2.6a** (129.0 mg, 0.2075 mmol) and $Mg(CH_2CMe_2Ph)_2 \cdot 1.85(1,4\text{-dioxane})$ (52.0 mg, 0.115 mmol, 0.55 equiv) in Et_2O (30 mL). The reaction mixture was allowed to stir for 1.5 h at room temperature. Upon workup, cooling to $-35\text{ }^\circ C$ in hexanes (3 mL) provided a small amount of crystals of $CpCr[(MesNCMe)_2CH]$ **2.1a**, as characterized by X-ray crystallography.

Synthesis of $CpCr[(XylNCMe)_2CH](CH_2CH_2Ph)$ (2.9). The procedure described above for the preparation of **2.2a** was followed with **2.3** (147 mg, 0.322 mmol) and $ClMgCH_2CH_2Ph$ (0.35 mL of 1.0 M solution in THF, 0.35 mmol, 1.1 equiv) in Et_2O (20 mL). The reaction mixture was allowed to stir for 6 days at room temperature, 1,4-dioxane (300 μL) was added and stirred for 0.5 h. Upon workup, the purple hexanes (2 mL) solution was cooled to $-35\text{ }^\circ C$ to yield crystals of **2.9** (69.8 mg, 41%) over several days in two crops. Anal. Calcd for $C_{34}H_{39}N_2Cr$: C, 77.39; H, 7.45; N, 5.31. Found: C, 77.20; H, 7.32; N, 5.60. UV-vis (hexanes; λ_{max} , nm (ϵ , $M^{-1}cm^{-1}$)): 420 (5320), 554 (1770).

Synthesis of $CpCr[(XylNCMe)_2CH](CH_2CHMe_2)$ (2.10). The procedure described above for the preparation of **2.2a** was followed with **2.3** (266 mg, 0.581 mmol) and $ClMgCH_2CHMe_2$

(0.32 mL of 2.0 M solution in Et₂O, 0.64 mmol, 1.1 equiv) in Et₂O (20 mL). The reaction mixture was allowed to stir overnight at room temperature in the dark, 1,4-dioxane (400 µL) was added and stirred for 0.5 h. Upon workup, the purple hexanes (15 mL) solution was cooled to -35 °C to yield crystals of **2.10** (179 mg, 64%) over several days in three crops. Anal. Calcd for C₃₀H₃₉N₂Cr: C, 75.12; H, 8.20; N, 5.84. Found: C, 74.87; H, 7.92; N, 5.86. UV-vis (hexanes; λ_{max}, nm (ε, M⁻¹cm⁻¹)): 396 (5510), 556 (1630).

Synthesis of CpCr[(DppNCMe)₂CH](CH₂CHMe₂) (2.10c). The procedure described above for the preparation of **2.7** (method **B**) was followed with CpCr[(DppNCMe)₂CH](OTf) (127 mg, 0.185 mmol) and Mg(CH₂CHMe₂)₂·0.618(1,4-dioxane) (20.1 mg, 0.104 mmol, 0.56 equiv) in Et₂O (12 mL). The reaction mixture was allowed to stir for 1 h at room temperature in the dark. Upon workup, the purple hexanes (2 mL) solution was cooled to -35 °C to yield crystals of **2.10c** (73.3 mg, 67%) over several days in three crops. Anal. Calcd for C₃₈H₅₅N₂Cr: C, 77.11; H, 9.37; N, 4.73. Found: C, 76.63; H, 10.45; N, 4.60. UV-vis (hexanes; λ_{max}, nm (ε, M⁻¹cm⁻¹)): 400 (5330), 562 (1530).

Synthesis of CpCr[(XylNCMe)₂CH](CH₂CMe₃) (2.11). The procedure described above for the preparation of **2.7** (method **B**) was followed with **2.6** (600 mg, 1.01 mmol) and Mg(CH₂CMe₃)₂·1.05(1,4-dioxane) (143 mg, 0.554 mmol, 0.55 equiv) in Et₂O (35 mL). The reaction mixture was allowed to stir for 1.5 h at room temperature. Upon workup, cooling to -35 °C in hexanes (15 mL) provided black crystals of **2.11** (335 mg, 67%) over several days in four crops. Anal. Calcd for C₃₁H₄₁N₂Cr: C, 75.42; H, 8.37; N, 5.67. Found: C, 75.27; H, 8.69; N, 5.66. UV-vis (hexanes; λ_{max}, nm (ε, M⁻¹cm⁻¹)): 404 (5170), 567 (1050).

Synthesis of CpCr[(MesNCMe)₂CH](CH₂CMe₃) (2.11a). The procedure described above for the preparation of **2.7** (method **B**) was followed with **2.6a** (302 mg, 0.486 mmol) and Mg(CH₂CMe₃)₂·1.26(1,4-dioxane) (75.2 mg, 0.271 mmol, 0.56 equiv) in Et₂O (30 mL). The reaction mixture was allowed to stir for 1.5 h at room temperature. Upon workup, the purple hexanes (4 mL) solution was cooled to -35 °C to yield crystals of **2.11a** (132 mg, 52%) over several days in four crops. Anal. Calcd for C₃₃H₄₅N₂Cr: C, 75.97; H, 8.69; N, 5.37. Found: C, 75.99; H, 9.00; N, 5.41. UV-vis (hexanes; λ_{max}, nm (ε, M⁻¹cm⁻¹)): 406 (5770), 568 (1150).

Synthesis of CpCr[(DepNCMe)₂CH](CH₂CMe₃) (2.11b). The procedure described above for the preparation of **2.7** (method **B**) was followed with **2.6b** (264 mg, 0.407 mmol) and Mg(CH₂CMe₃)₂·1.05(1,4-dioxane) (59.3 mg, 0.229 mmol, 0.56 equiv) in Et₂O (30 mL). The reaction mixture was allowed to stir for 1.5 h at room temperature. Upon workup, the purple hexanes (3 mL) solution was cooled to -35 °C to yield crystals of **2.11b** (102 mg, 46%) over

several days in two crops. Anal. Calcd for $C_{35}H_{49}N_2Cr$: C, 76.46; H, 8.98; N, 5.10. Found: C, 76.73; H, 9.23; N, 5.15. UV-vis (hexanes; λ_{max} , nm (ϵ , $M^{-1}cm^{-1}$)): 409 (5550), 568 (982).

Synthesis of $CpCr[(XylNCMe)_2CH](c-C_6H_{11})$ (2.12). The procedure described above for the preparation of **2.7** (method **B**) was followed with **2.6** (407 mg, 0.685 mmol) and $Mg(c-C_6H_{11})_2 \cdot 1.23(1,4\text{-dioxane})$ (107 mg, 0.374 mmol, 0.55 equiv) in cold ($-35\text{ }^{\circ}C$) Et_2O (30 mL). The reaction mixture was allowed to warm to room temperature while stirring for 1 h. Upon workup, the purple hexanes (3 mL) solution was cooled to $-35\text{ }^{\circ}C$ to yield crystals of **2.12** (73.8 mg, 21%). Anal. Calcd for $C_{32}H_{41}N_2Cr$: C, 76.01; H, 8.17; N, 5.54. Found: C, 75.66; H, 8.45; N, 5.72.

Synthesis of $CpCr[(XylNCMe)_2CH](CH_2CN)$ (2.13). Acetonitrile (28.0 μL , 0.536 mmol, 1.28 equiv) was added to a solution of $KN(SiMe_3)_2$ (95.4 mg, 0.478 mmol, 1.14 equiv) in 12 mL of a hexanes/toluene mixture (11:1) and the resulting reaction mixture was allowed to stir for 1 h at room temperature at which point it was transferred to a Schlenk flask containing **2.3** (191 mg, 0.418 mmol) dissolved in Et_2O (20 mL). The reaction mixture was allowed to stir for 3 days at room temperature. The volatiles were removed under reduced pressure, the residue was extracted with hexanes and Et_2O , filtered over Celite, and the solvent was again removed under reduced pressure. The solid was extracted with a minimum amount of Et_2O (9 mL), filtered over Celite, and the green (red transmitted) filtrate was cooled to $-35\text{ }^{\circ}C$ to yield crystals of **2.13** (60.7 mg, 31%) over several days in three crops. Anal. Calcd for $C_{28}H_{32}N_3Cr$: C, 72.70; H, 6.97; N, 9.08. Found: C, 72.40; H, 7.27; N, 8.68. UV-vis (hexanes; λ_{max} , nm (ϵ , $M^{-1}cm^{-1}$)): 420 (6610), 539 (914), 648 (610).

Synthesis of $CpCr[(XylNCMe)_2CH](CH_2Ph)$ (2.14). The procedure described above for the preparation of **2.2a** was followed with **2.3** (398.7 mg, 0.871 mmol) and $ClMgCH_2Ph$ (0.97 mL of 1.0 M solution in Et_2O , 0.97 mmol, 1.1 equiv) in Et_2O (25 mL) and toluene (1 mL). The reaction mixture was allowed to stir overnight at room temperature, 1,4-dioxane (400 μL) was added and stirred for 0.5 h. Upon workup, the green-blue hexanes (40 mL) solution was cooled to $-35\text{ }^{\circ}C$ to yield crystals of **2.14** (301 mg, 67%) over several days in two crops. Anal. Calcd for $C_{33}H_{37}N_2Cr$: C, 77.16; H, 7.26; N, 5.45. Found: C, 77.46; H, 7.46; N, 5.57. UV-vis (hexanes; λ_{max} , nm (ϵ , $M^{-1}cm^{-1}$)): 402 (6650), 577 (1120).

Synthesis of $CpCr[(MesNCMe)_2CH](CH_2Ph)$ (2.14a). The procedure described above for the preparation of **2.2a** was followed with **2.3a** (199.8 mg, 0.411 mmol) and $ClMgCH_2Ph$ (0.45 mL of 1.0 M solution in Et_2O , 0.45 mmol, 1.1 equiv) in Et_2O (25 mL). The reaction mixture was allowed to stir overnight at room temperature, 1,4-dioxane (400 μL) was added and stirred for 1

h. Upon workup, the green-blue hexanes solution was cooled to $-35\text{ }^{\circ}\text{C}$ to yield crystals of **2.14a** (145 mg, 65%) over several days in three crops. Anal. Calcd for $\text{C}_{35}\text{H}_{41}\text{N}_2\text{Cr}$: C, 77.60; H, 7.63; N, 5.17. Found: C, 77.96; H, 7.97; N, 5.29. UV-vis (hexanes; λ_{max} , nm (ϵ , $\text{M}^{-1}\text{cm}^{-1}$)): 400 (7060), 572 (1120).

Synthesis of $\text{CpCr}[(\text{DepNCMe})_2\text{CH}](\text{CH}_2\text{Ph})$ (2.14b). The procedure described above for the preparation of **2.2a** was followed with **2.3b** (232.8 mg, 0.453 mmol) and ClMgCH_2Ph (0.50 mL of 1.0 M solution in Et_2O , 0.50 mmol, 1.1 equiv) in Et_2O (30 mL). The reaction mixture was allowed to stir for 4 days at room temperature, 1,4-dioxane (500 μL) was added and stirred for 1 h. Upon workup, the green-blue hexanes solution was cooled to $-35\text{ }^{\circ}\text{C}$ to yield crystals of **2.14b** (135 mg, 52%) over several days in three crops. Anal. Calcd for $\text{C}_{37}\text{H}_{45}\text{N}_2\text{Cr}$: C, 78.00; H, 7.96; N, 4.92. Found: C, 78.32; H, 7.71; N, 4.82. UV-vis (hexanes; λ_{max} , nm (ϵ , $\text{M}^{-1}\text{cm}^{-1}$)): 404 (6350), 578 (1060).

Synthesis of $\text{CpCr}[(\text{DppNCMe})_2\text{CH}](\text{CH}_2\text{Ph})$ (2.14c). The procedure described above for the preparation of **2.2a** was followed with $\text{CpCr}[(2,6\text{-}^i\text{Pr}_2\text{C}_6\text{H}_3\text{NCMe})_2\text{CH}](\text{OTf})$ (47.2 mg, 0.0690 mmol) and ClMgCH_2Ph (0.08 mL of 1.0 M solution in Et_2O , 0.08 mmol, 1.2 equiv) in Et_2O (7 mL). The reaction mixture was allowed to stir for 1 h at room temperature, 1,4-dioxane (400 μL) was added and stirred for 20 min. Upon workup, the green-blue hexanes (1 mL) solution was cooled to $-35\text{ }^{\circ}\text{C}$ to yield crystals of **2.14c** (25.4 mg, 59%) over several days in three crops. Anal. Calcd for $\text{C}_{41}\text{H}_{53}\text{N}_2\text{Cr}$: C, 78.68; H, 8.54; N, 4.48. Found: C, 79.23; H, 9.45; N, 4.42. UV-vis (hexanes; λ_{max} , nm (ϵ , $\text{M}^{-1}\text{cm}^{-1}$)): 408 (6440), 582 (980).

Synthesis of $\text{CpCr}[(\text{XylNCMe})_2\text{CH}](\text{Ph})$ (2.15). The procedure described above for the preparation of **2.7** (method **B**) was followed with **2.6** (127.5 mg, 0.215 mmol) and $\text{Mg}(\text{Ph})_2 \cdot 2.74(1,4\text{-dioxane})$ (49.8 mg, 0.119 mmol, 0.55 equiv) in Et_2O (15 mL). The reaction mixture was allowed to stir for 1.5 h at room temperature. Upon workup, cooling the green (purple transmitted) solution in 10 mL of hexanes/ Et_2O (1.5:1) mixture to $-35\text{ }^{\circ}\text{C}$ provided crystals of **2.15** (48.0 mg, 45%) over several days in three crops. Anal. Calcd for $\text{C}_{32}\text{H}_{35}\text{N}_2\text{Cr}$: C, 76.93; H, 7.06; N, 5.61. Found: C, 74.76; H, 7.88; N, 5.66. UV-vis (hexanes; λ_{max} , nm (ϵ , $\text{M}^{-1}\text{cm}^{-1}$)): 436 (4650), 560 (1110).

Synthesis of $\text{CpCr}[(\text{XylNCMe})_2\text{CH}](\text{CH}=\text{CMe}_2)$ (2.16). The procedure described above for the preparation of **2.2a** was followed with **2.6** (54.9 mg, 0.0925 mmol) and $\text{BrMgCH}=\text{CMe}_2$ (0.20 mL of 0.5 M solution in THF, 0.10 mmol, 1.1 equiv) in Et_2O (15 mL). The reaction mixture was allowed to stir overnight at room temperature, 1,4-dioxane (100 μL) was added and stirred for 0.5 h. Upon workup, the red hexanes (2 mL) solution was cooled to $-35\text{ }^{\circ}\text{C}$ to yield

crystals of **2.16** (22.2 mg, 50%) over several days in three crops. Anal. Calcd for $C_{30}H_{37}N_2Cr$: C, 75.44; H, 7.81; N, 5.87. Found: C, 75.55; H, 8.92; N, 5.88. UV-vis (hexanes; λ_{max} , nm (ϵ , $M^{-1}cm^{-1}$)): 424 (5620), 549 (1480).

Synthesis of $CpCr[(XylNCMe)_2CH](C\equiv CH)$ (2.17). The procedure described above for the preparation of **2.2a** was followed with **2.3** (102.4 mg, 0.224 mmol) and $BrMgC\equiv CH$ (0.50 mL of 0.5 M solution in THF, 0.25 mmol, 1.1 equiv) in Et_2O (18 mL). The reaction mixture was allowed to stir overnight at room temperature, 1,4-dioxane (250 μ L) was added and stirred for 1 h. Upon workup, the orange-red hexanes (4 mL) solution was cooled to $-35\text{ }^{\circ}C$ to yield crystals of **2.17** (69.2 mg, 69%) over several days in two crops. Anal. Calcd for $C_{28}H_{31}N_2Cr$: C, 75.14; H, 6.98; N, 6.26. Found: C, 74.76; H, 7.80; N, 6.19. UV-vis (hexanes; λ_{max} , nm (ϵ , $M^{-1}cm^{-1}$)): 429 (5900), 535 (786).

Synthesis of $CpCr[(XylNCMe)_2CH](CH_2C_6H_4Me)$ (2.18). Compound **2.11** (54.9 mg, 0.111 mmol) was added to a solution of *p*-xylene (1.3 mL, 10.5 mmol, 95 equiv) in benzene (10 mL) over 3.5 h at room temperature. The reaction was allowed to stir for an additional 0.5 h, it was then cooled to $-35\text{ }^{\circ}C$ overnight followed by removal of the volatiles under reduced pressure. The solid was extracted with a minimum amount of hexanes, filtered over Celite, and the green-blue (purple transmitted) filtrate was cooled to $-35\text{ }^{\circ}C$ to yield crystals of **2.18** (32.1 mg, 55%) over several days in two crops. Anal. Calcd for $C_{34}H_{39}N_2Cr$: C, 77.39; H, 7.45; N, 5.31. Found: C, 77.05; H, 7.68; N, 5.54. UV-vis (hexanes; λ_{max} , nm (ϵ , $M^{-1}cm^{-1}$)): 400 (6560), 572 (1020).

Synthesis of $CpCr[(XylNCMe)_2CH](SPh)$ (2.19). A toluene (1 mL) solution of $PhSSPh$ (27.2 mg, 0.125 mmol, 0.52 equiv) was added to a toluene (5 mL) solution of compound **2.1** (102.2 mg, 0.2419 mmol). The reaction mixture was stirred for 6 h, concentrated under reduced pressure, filtered over Celite, and the green filtrate (4 mL) was cooled to $-35\text{ }^{\circ}C$ to yield black crystals of **2.19** (103.4 mg, 80%) over several days in two crops. Anal. Calcd for $C_{32}H_{35}N_2CrS$: C, 72.29; H, 6.63; N, 5.27. Found: C, 72.86; H, 6.81; N, 5.18. UV-vis (Et_2O ; λ_{max} , nm (ϵ , $M^{-1}cm^{-1}$)): 419 (6270), 670 (640).

Kinetics measurements of Me_3SiCH_2I activation. All kinetics measurements were performed according to the same experimental protocol. A typical experiment is described as a representative example with **2.1**. In a glovebox, **2.1** (13.0 mg, 0.0308 mmol) was placed in a 10 mL volumetric flask and filled to the mark with toluene. A 1.00 mL aliquot of this 3.08×10^{-3} M solution was transferred by pipette to a 25 mL volumetric flask followed by the addition of 7.5 μ L of Me_3SiCH_2I (added by microliter syringe) and the flask was filled to the mark with toluene and thoroughly mixed. An aliquot of the 1.23×10^{-4} M solution was transferred to an air-tight

UV-visible cell and transferred from the glovebox to the spectrophotometer, where the absorption at 427 nm was recorded every 0.3 min for 50 min. The resulting kinetic trace was fit

$$\frac{-d[\text{Cr} - \text{R}]}{dt} = \frac{k_1 k_2 [\text{Cr} - \text{R}][\text{PhSSPh}]}{k_{-1}[\text{Cr}(\text{II})] + k_2[\text{PhSSPh}]}$$

to a first-order decay curve to give the observed rate constant $k_{\text{obs}} = 2.00 \times 10^{-3} \text{ s}^{-1}$. The pseudo-first-order experiment was repeated four more times with varying excess concentrations of $\text{Me}_3\text{SiCH}_2\text{I}$. The second-order rate constant, $k_1 = 4.4(4) \times 10^{-1} \text{ M}^{-1}\text{s}^{-1}$, for the reaction was extracted from the slope of the straight line plot of k_{obs} vs $[\text{Me}_3\text{SiCH}_2\text{I}]$ ($R^2 = 0.9792$). The reactions with **2.1b** were performed in the same manner with $R^2 = 0.9845$.

Kinetics measurements of Cr(III)–R bond homolysis. All kinetics measurements were performed according to the same experimental protocol, with a representative example given below. In a glovebox, compound **2.14** (12.8 mg) was dissolved in 10 mL volumetric flask with hexanes ($2.49 \times 10^{-3} \text{ M}$) and used as a stock solution for all subsequent dilutions (the solution was stored at -35°C between experiments). 1.00 mL of this stock solution was pipetted to a 25 mL volumetric flask and PhSSPh (11.6 mg) was added and the flask was filled and thoroughly mixed. An aliquot of the solution was transferred to a UV-vis cell for air-sensitive samples and transferred from the glovebox to the spectrophotometer. The change in absorption at 560 nm was monitored over a period of 170 min at room temperature and the resulting data was fit to a first-order decay to give the observed rate constant $k_{\text{obs}} = 8.52 \times 10^{-4} \text{ s}^{-1}$. The experiment was repeated six times with increasing concentrations of PhSSPh where the observed rate constants were found to follow saturation kinetics, base on the following rate law: The data was then plotted as k_{obs}^{-1} vs $[\text{PhSSPh}]^{-1}$, shown in Figure 2.22, and the rate constant was extracted from the y-intercept of the linear fit; rate constant $k_1 = 3.2(5) \times 10^{-3} \text{ s}^{-1}$ for the Cr–C bond homolysis of compound **2.14**.

The rate constant determination was performed on the compounds with a minimum of five data points, with the exception of compounds **7** and **7a** due to the extended times required for the reactions to go to completion. As a result, the rate constants reported for these compounds are estimated based on their observed first-order rate constants with reaction of a large excess of PhSSPh, kinetic traces are shown in Figure 2.22.

General procedure for X-ray crystallography. X-ray diffraction data collection was performed by Dr. Brian O. Patrick or Anita Lam at UBC Vancouver. A single crystal of each compound was mounted on a glass fiber and measurements were made on a Bruker X8 APEX II diffractometer with graphite-monochromated Mo K α radiation. The data were collected at a

temperature of -100 ± 1 °C in a series of ϕ and ω scans in 0.50° oscillations. Data were collected and integrated using the Bruker SAINT software package⁶⁵ and were corrected for absorption effects using the multi-scan technique (SADABS)⁶⁶ (unless otherwise mentioned) and for Lorentz and polarization effects. All structures were solved by direct methods.⁶⁷ All non-hydrogen atoms were refined anisotropically (unless otherwise mentioned). All hydrogen atoms were placed in calculated positions but not refined. All refinements were performed using the SHELXTL crystallographic software package of Bruker-AXS.⁶⁸ The molecular drawings were generated by the use of ORTEP-3⁶⁹ and POV-Ray.

Structure details. Compounds **2.7c**, **2.8**, **2.10**, **2.10c**, **2.11**, and **2.16** crystallize with two independent molecules in the asymmetric unit. Compound **2.1a** crystallizes with one half-molecule residing on a two-fold axis of rotation. Additionally, the Cp ligand is disordered in four orientations. Two of the four orientations are symmetry-related to the other two as a result of the rotation axis. Refinement of the population of each of these fragments resulted in near equivalent values of 0.25. All non-hydrogen atoms in compound **2.1a**, except those of the Cp ligand, were refined anisotropically. The methyl hydrogens on C12 and C22 in complex **2.2a** were found to be disordered and were modeled in two orientations with 50% occupancy. The Cp ligand of compound **2.3** is disordered and was subsequently modeled in two orientations. Compound **2.3** also crystallizes with one disordered half-molecule of hexane in the asymmetric unit and was modeled in two orientations, with restraints employed to maintain similar geometries. All non-hydrogen atoms in compound **2.3**, except those of the disordered solvent atoms, were refined anisotropically. Compound **2.3a** crystallizes as a racemic twin, with both enantiomers present in the crystal. Compounds **2.3a** and **2.4** crystallize with unresolvable residual electron density, likely from disordered solvent in the lattice. The structures were refined without modeling any solvent molecules, then the PLATON/SQUEEZE⁷⁰ program was employed to search the cell for solvent accessible voids, and then to correct the X-ray diffraction data to eliminate any residual electron density found in those voids. The result from this procedure removed 127 residual electron density from the unit cell of **2.3a**, or approximately 16 electrons per asymmetric unit. This is less than one molecule of hexane or dichloromethane per asymmetric unit. The result from this procedure removed 41 residual electron density from the unit cell of **2.4**, or approximately 10 electrons per asymmetric unit. Since it is not possible to properly identify the solvent, the values for the formula weight, etc., reflect only those atoms found in the atom list; no assumptions were made as to the identity of the lattice solvent. In compound **2.3b**, one ethyl substituent is disordered and was modeled in two orientations with

roughly equivalent populations. Refinements converged with $R1 = 12.4\%$. The program ROTAX⁷¹ was used to look for possible non-merohedral twinning. The twin law corresponding to 180 degree twinning about the 0 1 1 reciprocal lattice direction was used to generate an HKLF5 format data set. Refinements using this data along with a refined batch scale factor, allowed to model to converge with $R1 = 5.8\%$. Compound **2.7b** crystallizes with one disordered ethyl group (C12 and C13) that was modeled in two orientations. Compound **2.14a** crystallizes as a racemic twin with the ratio of enantiomers determined to be 60:40 using the TWIN/BASF functions. Compound **2.14b** crystallizes on a mirror plane, with one half-molecule in the asymmetric unit. For compound **2.17**, data were corrected for absorption effects using the multi-scan technique (TWINABS)⁷². Compound **2.17** crystallizes as a two-component split crystal with the two components related by a 180° rotation about the (1 0 0) real axis. The data were integrated for both twin components, including both overlapping and non-overlapping reflections. The structure was solved by using non-overlapped data from the major twin component. Subsequent refinements were carried out using the HKLF 5 format data set containing complete data from component 1 and any overlapped reflections from component 2. The batch scale refinement showed a roughly 53:47 ratio between the major and minor twin components.

Chapter 3 Reactivity of $\text{CpCr}[(\text{ArNCMe})_2\text{CH}](\text{X})$ Complexes

The paramagnetic Cr(III) halide and pseudo-halide complexes $\text{CpCr}[(\text{ArNCMe})_2\text{CH}](\text{X})$, where $\text{X} = \text{Cl}$, Br , or OTs, are air-stable as crystalline solids that can be stored in air for years without any apparent decomposition, and even $\text{CpCr}[(\text{XylNCMe})_2\text{CH}](\text{R})$ alkyl complexes can be remarkably resistant to O_2 if protected from ambient light.⁴⁶ However, like most reduced metal complexes capable of single-electron oxidative addition of relatively strong carbon-halogen bonds,^{73,74} the Cr(II) compounds are highly air-sensitive. The utility of the $\text{CpCr}[(\text{XylNCMe})_2\text{CH}]$ system would be greatly enhanced if its tolerance to air and other impurities in substrates and solvents could be improved.

Herein, the problem of air-sensitivity was examined in the radical reactivity of $\text{CpCr}[(\text{ArNCMe})_2\text{CH}]$ using stoichiometric manganese as a reductant. The product of air oxidation of $\text{CpCr}[(\text{XylNCMe})_2\text{CH}]$ (**2.1**) is the Cr(III) μ -oxo complex **3.1**,^{75,76,77} which was previously characterized by X-ray crystallography from single-crystals isolated from a reaction mixture as a result of unintentional air exposure.⁷⁸ Although both the Cp and β -diketiminate ligands remain intact and Cr-bound in **3.1**, the Cr(III)–O bonds were expected to pose a significant obstacle to reforming the reactive Cr(II) complex **2.1** (Figure 3.1). Conversion of the μ -oxo product to other Cr(III) species more amenable to reduction to Cr(II) under catalytically relevant conditions is presented, including the independent synthesis, spectroscopic characterization, and structural elucidation of these Cr(III) species. The scope of manganese

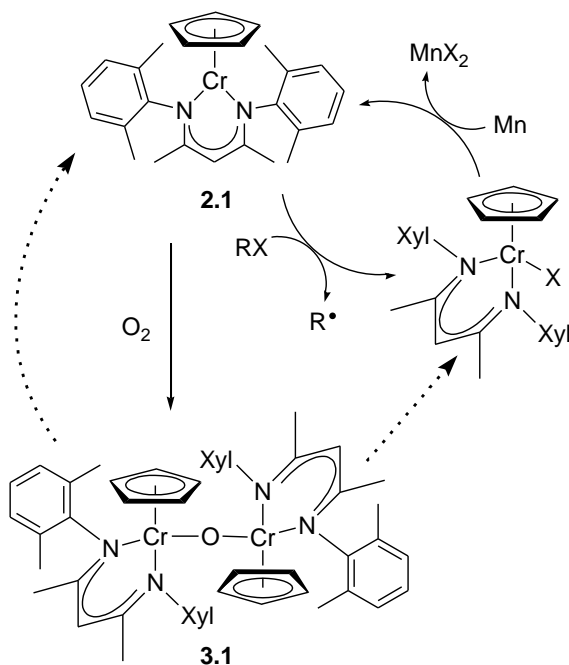


Figure 3.1. Proposed conversion of μ -oxo complex **3.1** back to the Cr(II) complex **2.1**.

reactivity with Cr(III) species is also discussed.

Chromium(III) compounds containing hydroxide, carboxylate, enolate, alkoxide, and fluoride ligands were prepared and reactivity studies were undertaken to establish methods for selectively breaking their strong Cr–O and Cr–F bonds. The β -diketiminato ligand was modified to discourage μ -oxo formation, leading to examination of the reactivity of a putative Cr(IV) oxo intermediate. Catalytic conditions for PPh_3 oxidation by oxygen atom transfer (OAT) with O_2 or air as oxygen atom sources, intra- and inter-molecular hydrogen atom transfer (HAT), and fluorine atom transfer is presented. The preparation and reactivity of a rare O-bound nitrosoarene complex is also discussed.

3.1 Synthesis of $\{\text{CpCr}[(\text{XylNCMe})_2\text{CH}]\}_2(\mu\text{-O})$

The Cr(III) μ -oxo complex $\{\text{CpCr}[(\text{XylNCMe})_2\text{CH}]\}_2(\mu\text{-O})$ (**3.1**) was prepared by reaction of the Cr(II) complex **2.1** with 0.5 equivalents of pyridine *N*-oxide under an inert atmosphere in hexanes (Figure 3.2, path A). Upon stirring overnight, the precipitate was isolated and dried to provide **3.1** as an analytically pure orange powder in high yield. Complex **3.1** exhibits a strong absorption band in the UV-vis spectrum with $\lambda_{\text{max}} = 362 \text{ nm}$ ($\epsilon = 20700 \text{ M}^{-1}\text{cm}^{-1}$) and a shoulder at 471 nm. The solution magnetic moment of $2.39 \mu_{\text{B}}$ for compound **3.1** is significantly lower than expected for two high-spin Cr(III) metal centres. Similar antiferromagnetic coupling was observed for the Cr(III) μ -oxo compound $[\{\text{Cr}(\text{NCS})(\text{TPyEA})\}_2\text{O}]$ ($\mu_{\text{eff}} = 1.63 \mu_{\text{B}}$ per Cr atom),^{75a} as well as the chromium porphyrin heterobimetallic compounds $(\text{py})(\text{TPP})\text{CrOFe}(\text{tmtaa})$ and $(\text{TPP})\text{CrOFe}(\text{Pc})$ ($\mu_{\text{eff}} = 3.51 \mu_{\text{B}}$ and $3.12 \mu_{\text{B}}$ per molecule, respectively).⁷⁹

Air exposure of a solution of the Cr(II) complex **2.1** resulted in a rapid colour change from green to orange with a UV-vis spectrum that matched that of the μ -oxo compound **3.1**. Attempts to determine the rate of reaction of O_2 with compound **2.1** were unsuccessful, as the reaction of a $9.8 \times 10^{-4} \text{ M}$ solution of **2.1** with 10 equivalents of dry O_2 reached completion prior to acquisition of the first spectrum ($< 5 \text{ sec}$). The UV-vis spectra shown in Figure 3.3, illustrating the conversion to compound **3.1**, were obtained by preparing a $1.10 \times 10^{-4} \text{ M}$ THF solution of the Cr(II) compound **2.1** in a glovebox, sealing the cell with a septum instead of a Hi-Vac Kontes valve, and obtaining spectra over a period of minutes as the imperfect seal slowly allowed air to contact the solution. The spectra shown in Figure 3.3 do not contain isosbestic points, suggesting that the conversion of compound **2.1** to **3.1** occurs through one or more intermediate species. This is consistent with the mechanism discussed below.

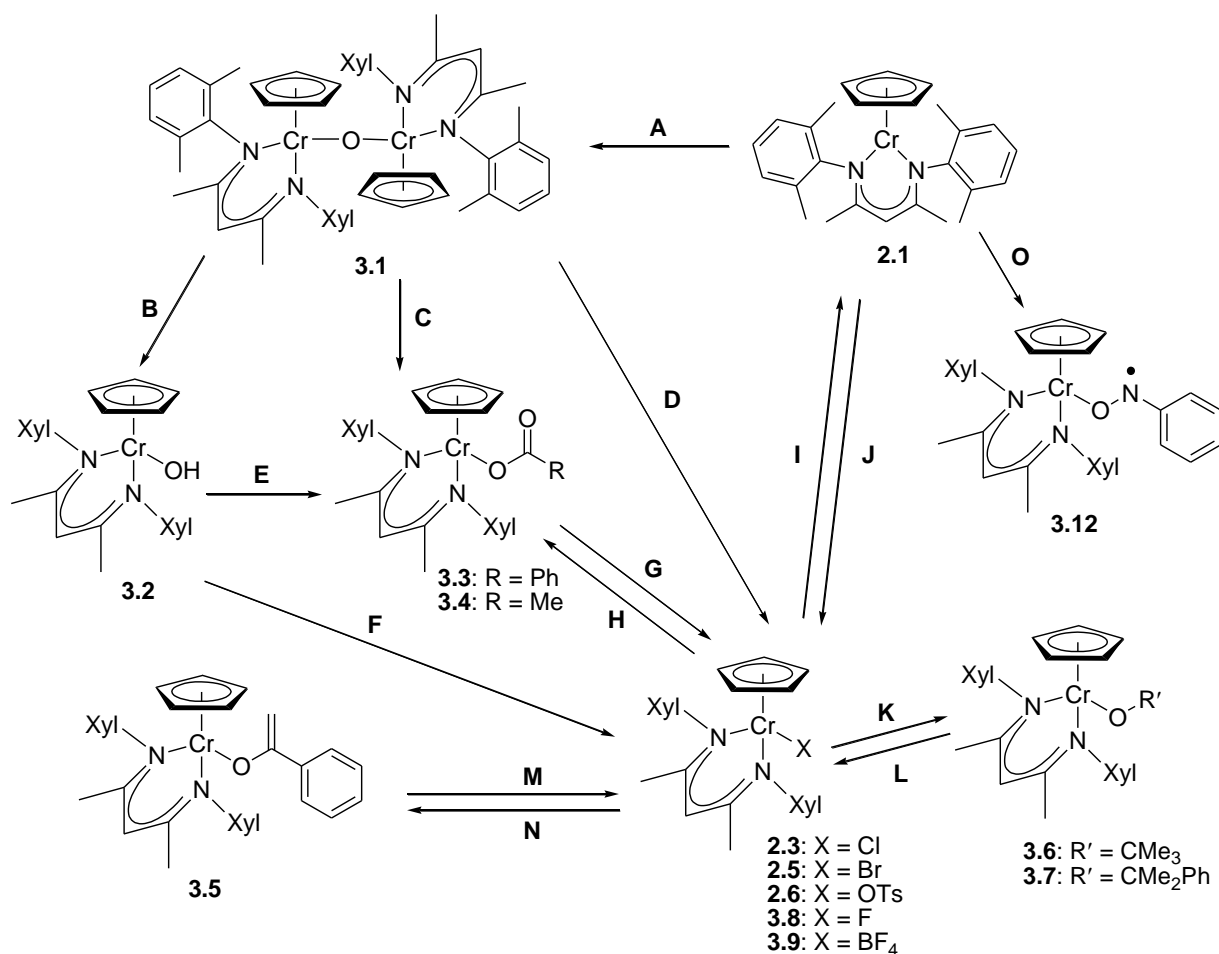
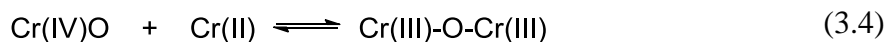
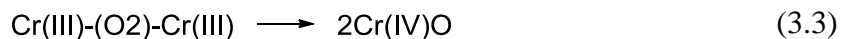
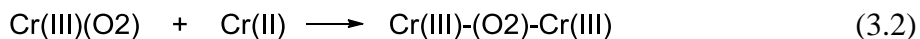
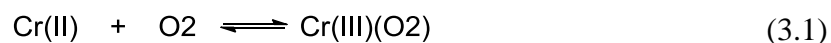


Figure 3.2. Interconversion of CpCr β-diketiminato complexes. A detailed description of reagents and reaction conditions for each reaction is given in the experimental section (3.13).

Previous work by Liston and West reported the formation of a Cr(III) μ-oxo porphyrin species from oxidation of Cr(II) porphyrins with oxygen.⁸⁰ They proposed that the first step involved the formation of a Cr(III) superoxo species (eq 3.1), which was subsequently trapped by another equivalent of Cr(II) porphyrin (eq 3.2). This intermediate then undergoes O–O bond cleavage forming two Cr(IV) oxo porphyrin compounds (eq 3.3), which react reversibly in solution with the Cr(II) porphyrin starting material to form a Cr(III) μ-oxo porphyrin complex (eq 3.4). Veige and co-workers also recently reported the formation of a Cr(IV) μ-oxo compound by a Cr(III)/Cr(V) redox couple analogous to the Cr(II)/Cr(IV) couple proposed by Liston and West.^{75f}



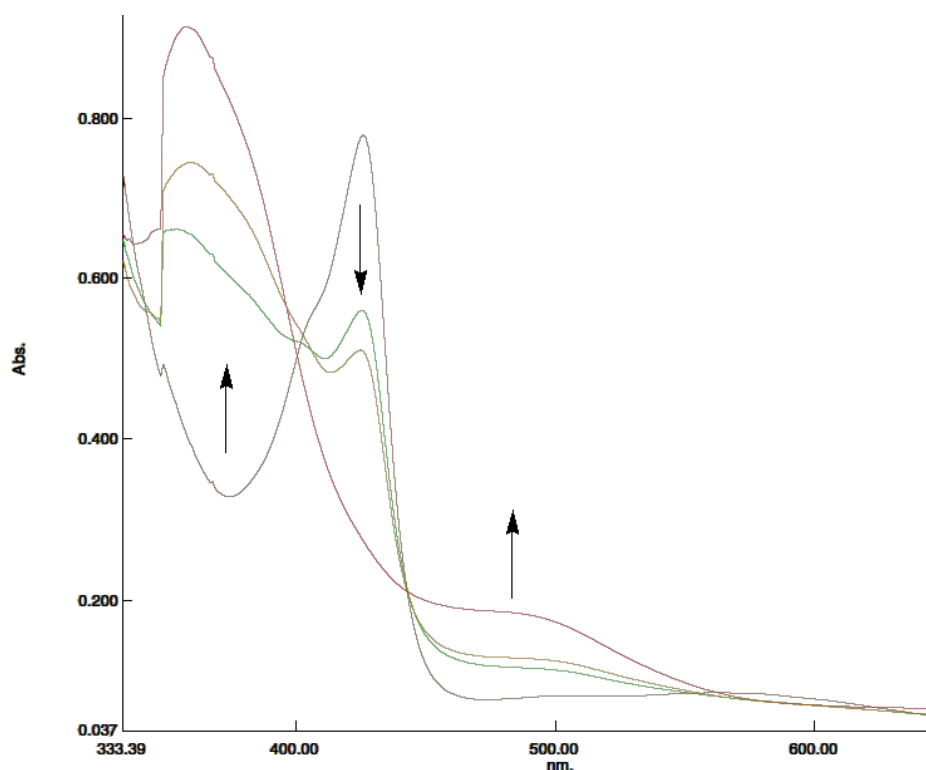


Figure 3.3. UV-vis spectra monitoring reaction of the Cr(II) compound **2.1** [1.10×10^{-4} M] with air.

Although compound **3.1** was the product of air oxidation of **2.1**, a subsequent colour change from orange to green was observed over several hours when solutions of **3.1** were subjected to air exposure. Therefore, the reaction of the Cr(II) compound **2.1** with pyridine *N*-oxide under air-free conditions provided a cleaner route for the isolation of μ -oxo compound **3.1**.

3.2 Reactivity of $\{\text{CpCr}[(\text{XylNCMe})_2\text{CH}]\}_2(\mu\text{-O})$

Attempts to further oxidize the Cr(III) μ -oxo compound **3.1** to a higher valent Cr oxo species were not successful. The reaction of the Cr(II) complex **2.1** with an excess of pyridine *N*-oxide did not effect the formation of **3.1** as the sole isolable product. In addition, **3.1** was unreactive toward a > 10 fold excess of pyridine *N*-oxide in a variety of solvents under an inert atmosphere over a two day period.

We found that atmospheric moisture was responsible for the air-sensitivity of complex **3.1**. Under an inert atmosphere, complex **3.1** reacted with a stoichiometric amount of degassed water to effect the colour change previously observed for the prolonged air exposure of **3.1** (Figure 3.2, path **B**). The UV-vis spectrum exhibits a strong absorption at 390 nm and two weaker absorptions at 506 nm and 611 nm. Characterization of this green species confirmed that the

water had protonated the μ -oxo ligand of **3.1** to produce two equivalents of a Cr(III) hydroxide compound $\text{Cr}[(\text{XylNCMe})_2\text{CH}](\text{OH})$ (**3.2**).

The μ -oxo complex **3.1** reacted cleanly with a variety of proton sources HX, where HX = $[\text{HNEt}_3]\text{Cl}$, $[\text{HLut}]\text{Br}$, $[\text{HCol}]\text{OTs}$, PhCO_2H (Lut = lutidine, 2,6-dimethylpyridine; Col = collidine, 2,4,6-trimethylpyridine), generating the monometallic Cr(III) complexes shown in Figure 3.2, paths **C** and **D**. The addition of two equivalents of acid in path **D** cleanly generated two equivalents of the corresponding Cr(III)–X complex, where X = Cl (**2.3**), Br (**2.5**), or OTs (**2.6**). Additionally, the reaction of **3.1** with two equivalents of benzoic acid yielded the Cr(III) benzoate complex $\text{Cr}[(\text{XylNCMe})_2\text{CH}](\text{O}_2\text{CPh})$ (**3.3**) in 66% isolated yield, shown in Figure 3.2, path **C**.

The clean conversion of the μ -oxo complex **3.1** to the Cr(III) halide and benzoate complexes (Figure 3.2, paths **C** and **D**) prompted further investigation. Reacting isolated Cr(III) hydroxide **3.2** with the HX sources under the same reaction conditions as complex **3.1** led to the clean formation of the Cr(III)–X compounds (Figure 3.2, paths **E** and **F**). This result suggested that the reaction of **3.1** with HX proceeded by an initial reaction of **3.1** with one equivalent of HX to form the Cr(III)–X product and a stoichiometric amount of the hydroxide species **3.2**, which then reacted with a second equivalent of HX to produce a second equivalent of Cr(III)–X and one equivalent of water (Figure 3.4). Notably, isolation of the Cr(III)–X compounds did not appear to be hindered by the stoichiometric amount of water presumably generated as the by-product of the reaction.

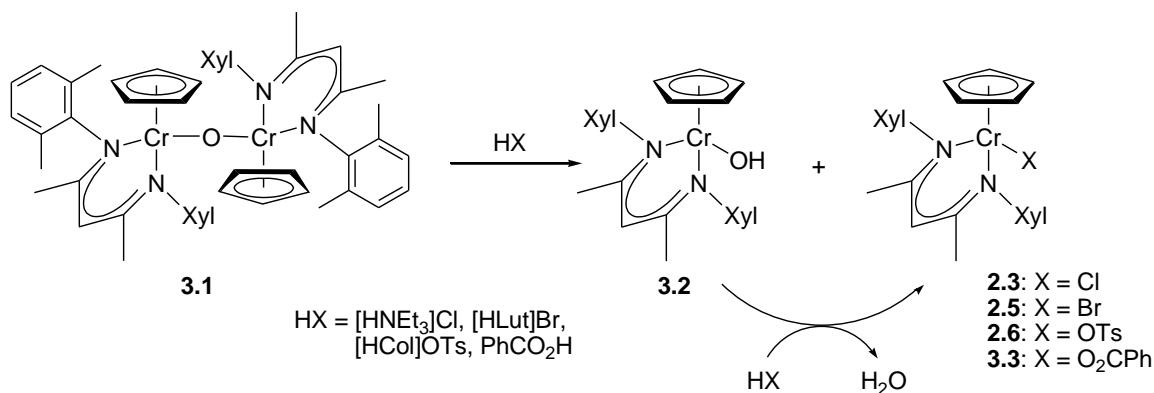
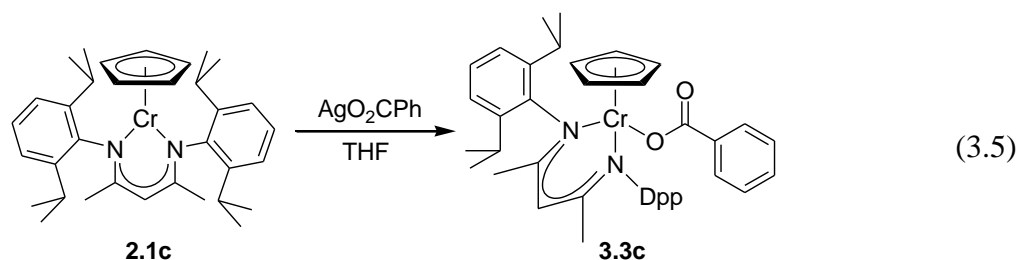


Figure 3.4. Conversion of μ -oxo compound **3.1** to Cr(III)–X species.

3.3 Synthesis of Cr(III) Benzoate and Acetate Complexes

The Cr(III) acetate complex CpCr[(XylNCMe)₂CH](O₂CMe) (**3.4**) was prepared by reaction of **2.3** with silver acetate (AgO₂CMe) in good yield (Figure 3.2, path **H**), analogous to the previously reported Cr(III) benzoate complex **3.3**.⁷⁸ The UV-vis spectrum of compound **3.4** displays a strong absorption band at 411 nm and two weaker bands at 508 and 588 nm.

A Cr(III) benzoate species was also prepared from the more sterically hindered Dpp substituted β -diketiminato ligand by single-electron oxidation of the Cr(II) precursor **2.1c** with one equivalent of AgO₂CPh (eq 3.5). The UV-vis spectrum of CpCr[(DppNCMe)₂CH](O₂CPh) (**3.3c**) is similar to the benzoate and acetate compounds **3.3** and **3.4**, respectively, with a strong absorption band at 416 nm and a weaker band at 584 nm.



3.4 Synthesis of a Cr(III) Enolate Complex

Acetophenone was deprotonated with $\text{KN}(\text{SiMe}_3)_2$,⁸¹ and the isolated potassium enolate was reacted with $\text{CpCr}[(\text{XylNCMe})_2\text{CH}](\text{I})$, Figure 3.2, path N. The product of the reaction could have formed either a Cr–C bonded ($\text{Cr}-\text{CH}_2\text{COPh}$) or a Cr–O bonded ($\text{Cr}-\text{OC}(=\text{CH}_2)\text{Ph}$) product. Crystallization provided a small amount of X-ray quality crystals of $\text{CpCr}[(\text{XylNCMe})_2\text{CH}][\text{OC}(=\text{CH}_2)\text{Ph}]$ (**3.5**), shown in Figure 3.5. Structural refinements of the X-ray data indicated that the crystal contained 10.1% of co-crystallized Cr(III) iodide starting material. However, the structure was of sufficient quality to confirm that the organic fragment

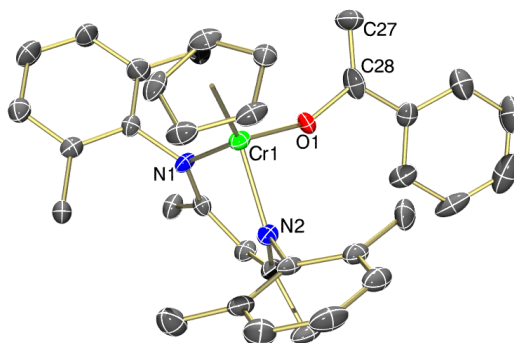


Figure 3.5. Thermal ellipsoid diagram (50%) of **3.5**. Compound **3.5** co-crystallizes with ~10% Cr(III) iodide starting material; the I atom of the co-crystallized starting material and all H atoms are omitted for clarity.

was in fact O-bound as an enolate. The large Cr–O–C bond angle of **3.5** (145.9(12) Å) is consistent with an O-bound enolate structure as opposed to a C-bound ligand, which would be expected to have a considerably smaller bond angle. The Cr–O bond length of 1.878(4) Å is also consistent with an O-bound ligand; even the shortest Cr–C bond length reported in Chapter 2 was significantly longer at 2.009(5) Å. In addition, the two hydrogen atoms bound to C27 were clearly visible during structural refinements of the crystallographic data for compound **3.5** and were consistent with sp² hybridization at the carbon atom. The UV-vis spectra of isolated **3.5** and the bulk recrystallization solution also suggested an O-bound enolate ligand due to the observed absorption bands at 407 and 607 nm and the absence of an absorption band between 530 and 560 nm characteristic of the Cr(III) hydrocarbyl compounds reported in Chapter 2.

The Cr(III) alkoxide compounds CpCr[(XylNCMe)₂CH](OR), where R = CMe₃ (**3.6**) or C(Me)₂Ph (**3.7**), were prepared by salt metathesis of the Cr(III) chloride compound **2.3** with the appropriate potassium alkoxide (Figure 3.2, path **K**). Both alkoxide compounds **3.6** and **3.7** have similar UV-vis spectra with absorption bands at 395, 490 and 730 nm. The solid-state molecular structure of **3.6** (Figure 3.6) displays a relatively large Cr–O–C bond angle of 151.8(2)°, to accommodate the large *tert*-butyl group of the alkoxide ligand. The Cr–N bond lengths for compound **3.6** (2.011(2) - 2.039(2) Å) are similar to the other Cr(III) compounds reported herein despite the sterically demanding alkoxide ligand, highlighting the importance of the flexibility of the Cr–O–C bond angle in accommodating the large *tert*-butyl group. The Cr–O bond length of **3.6** (1.867(2) Å) is similar to the octahedral Cr(III) alkoxide compounds [Cp'Cr(OAr)Cl]₂, where Cp' = C₅H₅ or C₅Me₅, and Ar = 2,6-*i*Pr₂C₆H₃) with Cr–O bond lengths of 1.869(2) and 1.8932(12) Å, respectively.⁸² Additionally, compound **3.6** displays very similar bonding parameters to those of **3.7**.

Figure 3.6. Thermal ellipsoid diagram (50%) of **3.6**. All H atoms are omitted for clarity.

3.6 Manganese Reactivity with Cr(III) Compounds

The oxophilicity of early first-row metals presents a challenge for catalyst design when these strong M–O bonds must be broken to reform reactive low-valent species. The reducing agents selected must also be compatible with the organic substrates, their functional groups, and the other reagents in the reaction mixture. A particularly effective strategy developed by Fürstner uses a multicomponent system with a first-row transition metal catalyst, stoichiometric reductant, and Me₃SiCl.⁸³ This system is useful with TiCl₃ for carbonyl coupling reactions, normally limited to stoichiometric transformations due to the strong Ti–O bonds formed, now rendered catalytic with Me₃SiCl providing the thermodynamic driving force to cleave the Ti–O bond, with the resulting Ti halide species being reduced with Zn powder.⁸⁴ This system was later extended to a chromium-catalyzed Nozaki-Hiyama-Kishi (NHK) reaction using Mn as the stoichiometric reductant of choice as it is inexpensive, exhibits very limited reactivity with typical organic halides and their functional groups, and the Mn halide by-products are only weakly Lewis acidic.¹³ In their development of asymmetric NHK catalysts, Cozzi and co-workers noted that Me₃SiCl activated the Mn, accelerating the reduction of CrCl₃ to Cr(II).¹⁴

Gansäuer and co-workers have also developed a similar system for epoxide ring-opening that uses catalytic Cp₂TiCl₂, Mn as the stoichiometric reductant, and [HCoI]Cl in place of chlorosilanes to cleave the Ti–O bond.⁸⁵ This strategy was also extended to chromium-catalyzed NHK reactions, replacing Me₃SiCl with [HCoI]Cl.⁸⁶ Kishi later reported the use of Cp₂ZrCl₂ as an effective transmetallating reagent for the chromium-catalyzed NHK reaction, providing increased substrate conversion compared to Me₃SiCl.⁸⁷

Although the Cr(III) iodide compound CpCr[(Xyl)NCMe)₂CH](I) was readily reduced to the Cr(II) compound **2.1** by commercial Mn powder (Figure 3.2, path I),⁴⁶ the corresponding chloride (**2.3**) and bromide (**2.5**) compounds required the use of Mn activated with substoichiometric amounts of PbCl₂ or PbBr₂.⁸⁸ Similarly, the Cr(III) hydroxide **3.2** and acetate **3.4** analogues were not reduced to compound **2.1** without the use of PbCl₂ activated Mn, while the alkoxide compound **3.7** did not react with activated Mn at room temperature over a 24 h period.

Somewhat analogous to the system used by Gansäuer,⁸⁵ the μ -oxo compound **3.1**, hydroxide **3.2**, and alkoxide **3.7** were all found to react with pyridinium halides to cleanly form the CpCr[(Xyl)NCMe)₂CH](X) halides (Figure 3.2, paths D, F, and L respectively), which in turn can be reduced to the Cr(II) compound **2.1** with activated Mn. Additionally, hydroxide **3.2** and alkoxide **3.7** both reacted with PhCO₂H in a similar reaction to form the benzoate compound **3.3**.

The use of a substoichiometric amount Me_3SiCl to activate Mn powder was successful, providing an alternative to lead halide salts for the reduction of the Cr(III) chloride (**2.3**) and bromide (**2.5**) complexes. The hydroxide compound **3.2** also reacted with Me_3SiCl to break the Cr–O bond, giving the chloride compound **2.3** (Figure 3.2, path **F**). Furthermore, the Cr(III) acetate compound **3.4** was readily converted to **2.3** by reaction with either Me_3SiCl or Cp_2ZrCl_2 , in the latter case generating a stoichiometric amount of $\text{Cp}_2\text{Zr}(\text{Cl})(\text{OAc})$ (Figure 3.2, path **G**).

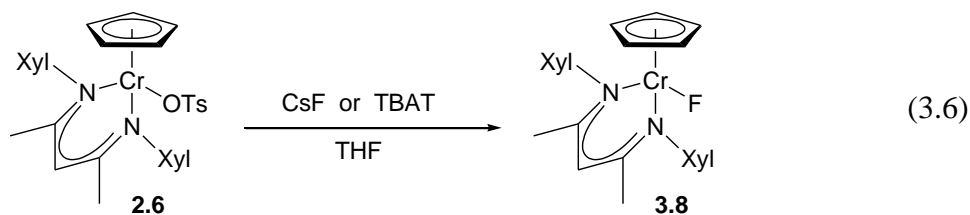
Interestingly, the alkoxide compound **3.7** reacted with Cp_2ZrCl_2 , as expected, to form compound **2.3** (Figure 3.2, path **L**) but **3.7** was completely unreactive toward Me_3SiCl (2 days at room temperature) under anhydrous conditions. However, an identical reaction conducted with the addition of 0.5 equivalents of H_2O led to complete conversion of alkoxide **3.7** to chloride **2.3**. It has previously been proposed by Wessjohann that Cr(III) alkoxides do not react directly with Me_3SiCl .⁸⁹ Additionally, Jacobsen reported that in the epoxide ring-opening reactions with Me_3SiN_3 catalyzed by Cr(III), the strict exclusion of water resulted in deactivation of the catalytic system while reactivation could be achieved with the addition of trace water, causing the formation of small amounts of HN_3 .⁹⁰ It was therefore proposed that HN_3 , and not Me_3SiN_3 , was in fact the active species for the key Cr(III)–OR bond cleavage step. This mechanism is consistent with the observed reactivity of the Cr(III) alkoxide compound **3.7** with Me_3SiCl in the presence of added water.

Treatment of the hydroxide compound **3.2**, acetate **3.4**, and enolate **3.5** with in situ generated MnI_2 resulted in transmetallation to form the Cr(III) iodide complex (Figure 3.2, paths **F**, **G**, and **M** respectively), which if conducted in the presence of excess Mn powder results in direct reduction to the Cr(II) compound **2.1**. The μ -oxo compound **3.1** was also found to react with MnX_2 , where $\text{X} = \text{Cl}$ or I , to form the appropriate Cr(III) halide species. Alternatively, the alkoxide compound **3.7** did not react with MnI_2 to form the Cr(III) iodide, potentially a contributing factor to the inability of activated Mn to reduce compound **3.7** since a Cr(III) alkoxide species is also expected to be stable with respect to Mn reduction due to the electron donating ability of the alkoxide ligand, consistent with Fürstner's original catalytic NHK mechanistic proposal.

3.7 Synthesis and Reactivity of a Cr(III) Fluoride Compound

The synthesis and structural characterization of Cr(III) fluoride compounds have been reported as a result of fluoride abstraction from perfluorinated counter ions by cationic Cr(III) species.^{91,92} A notable example was reported by Cotton and co-workers, where a Cr(II) species was oxidized with AgBF₄ followed by fluoride abstraction from the BF₄ counter ion.^{92a} In a rare example of the targeted synthesis of a Cr(III) fluoride complex by a method other than decomposition of a perfluoro anion, Jacobsen and co-workers reported the preparation of a chiral (Salen)Cr(III)(F) species by reaction of the (Salen)Cr(III)(BF₄) analogue with NaF.⁹³ Theopold reported the synthesis of a cationic half-sandwich Cp*Cr(Me)(THF)₂ species with PF₆⁻ counterion.⁹¹ The compound was catalytically active for the polymerization of ethylene but was short-lived in solution. One of the decomposition products was identified as the tetranuclear [Cp*₄Cr₄(μ-F)₅Cl₂][PF₆], which is formed as a result of halogen abstraction from the PF₆⁻ anion and dichloromethane solvent.

Unlike the synthesis of the Cr(III) chloride (**2.3**) and bromide (**2.5**) complexes, a Cr(III) fluoride analogue could not be prepared by reaction of the Cr(II) compound **2.1** with PbF₂. Treatment of compound **2.1** with AgF did, however, result in the oxidation of **2.1** to form the corresponding Cr(III) fluoride complex CpCr[(Xyl)NCMe)₂CH](F) (**3.8**), Figure 3.2, path **J**. Compound **3.8** was also readily prepared from reaction of the Cr(III) tosylate complex **2.6** with CsF (eq 3.6), although the reaction was much slower, requiring a reaction time of 8 days, compared to the overnight reaction with compound **2.1** and AgF. Alternatively, the synthesis of **3.8** was achieved from the tosylate complex **2.6** in an overnight reaction with tetrabutylammonium difluorotriphenylsilicate (Bu₄N[Ph₃SiF₂], TBAT); no reaction was observed with the Cr(III) chloride analogue **2.3** under identical reaction conditions.



The preparation of compound **3.8** by oxidation of compound **2.1** with AgF proved to be the more convenient synthetic protocol, providing superior yields and reduced reaction times. The solid-state molecular structure of compound **3.8**, shown in Figure 3.7, displays typical Cr–N bond lengths (2.026(1) Å average) and a Cr–F bond length of 1.859(1) Å, well within the range

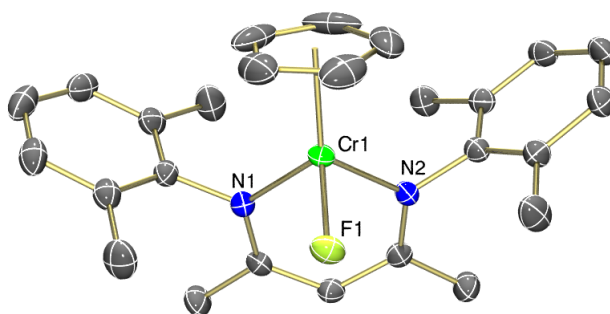


Figure 3.7. Thermal ellipsoid diagram (50%) of **3.8**. All H atoms are omitted for clarity.

of Cr(III) fluoride complexes containing a terminal Cr–F bond (1.802–1.930 Å).^{92,94} The UV-vis spectrum of **3.8** displays a strong absorption band at 402 nm and two weak bands at 506 and 608 nm. Interestingly, compound **3.8** displays an increased solubility in non-polar solvents compared to the Cr(III) chloride, bromide, and iodide analogues.

A toluene solution of compound **3.8** was treated with one equivalent of $\text{BF}_3 \cdot \text{Et}_2\text{O}$ (Figure 3.8), causing a rapid colour change to orange. Purification of the resulting Cr species by crystallization from a concentrated Et_2O solution provided $\text{CpCr}[(\text{Xyl})\text{NCMe}]_2\text{CH}(\text{BF}_4)$ (**3.9**). The UV-vis spectrum of **3.9** in Et_2O displays absorption bands at 403 and 579 nm. Dissolution of **3.9** in THF caused a colour change from orange to green with absorption bands at 403 and 604 nm. A comparison of the UV-vis spectra for compound **3.9** in Et_2O and THF is presented in Figure 3.9. The solvent dependence on the UV-vis spectrum of **3.9** indicated that the BF_4 ligand was interacting with the solvent. In fact, the UV-vis spectrum of **3.9** in THF is consistent with the formation of the Cr(III) fluoride species **3.8**, presumably due to a Lewis acid/base interaction

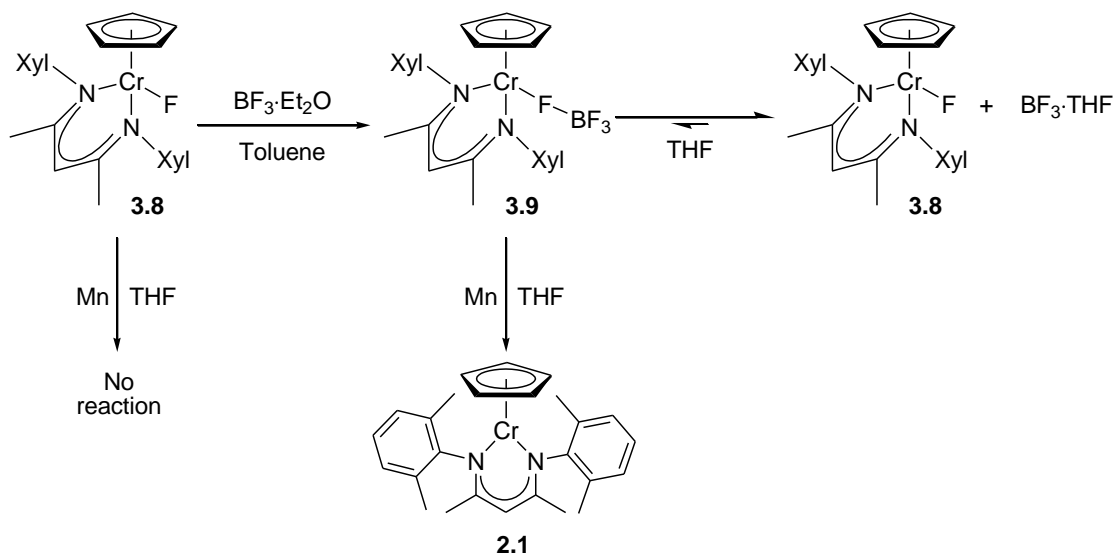


Figure 3.8. Reaction of the Cr(III)–F (**3.8**) and Cr(III)– BF_4 (**3.9**) complexes with Mn.

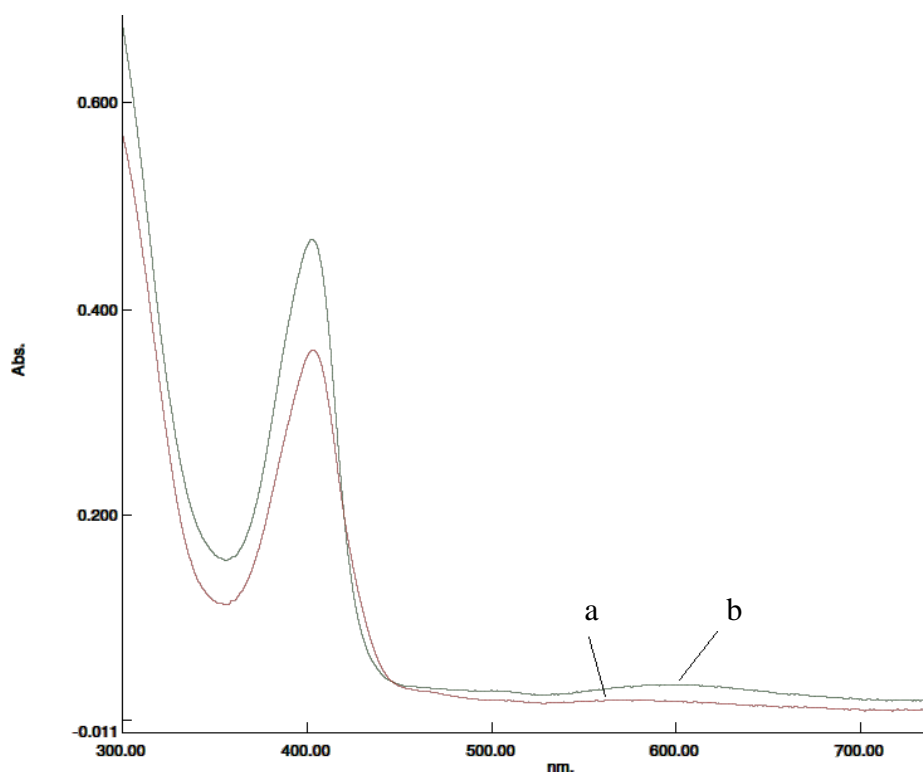


Figure 3.9. UV-vis spectra of the Cr(III)–BF₄ complex **3.9** [4.91×10^{-5} M] in (a) Et₂O and (b) THF/Et₂O (9:1).

between the BF₃ group and THF, forming a BF₃·THF adduct (Figure 3.8). This type of reactivity has been proposed as the mechanism by which a Cr(III) fluoride species was prepared by dissolving the Cr(III)–BF₄ adduct in acetonitrile, forming a BF₃·NCMe adduct.^{92b}

While the fluoride complex **3.8** does not react with Mn in THF, a THF solution of **3.9** (which displays absorption bands corresponding to Cr(III) fluoride **3.8**) does react with Mn, resulting in reduction of the Cr to the Cr(II) compound **2.1**. The difference in reactivity between **3.9** in THF and isolated **3.8** suggests that there may be an equilibrium between the Cr(III)–F (**3.8**) and Cr(III)–BF₄ (**3.9**) species in THF that lies mostly to the Cr(III)–F side, as shown in Figure 3.8, and the Cr(III)–BF₄ (**3.9**) species is present in low concentrations, to allow reduction of the Cr to the Cr(II) compound **2.1**.

The fluoride complex **3.8** reacted rapidly with Me₃SiCl, forming the Cr(III) chloride species **2.3** and the fluorosilane Me₃SiF, as shown in Figure 3.10. The formation of Me₃SiF was determined by ¹⁹F NMR analysis of the reaction mixture, which displayed a single peak at -158.4 ppm.⁹⁵ Fluoride abstraction from compound **3.8** was not achieved by reaction with R₃SiH compounds, where R = Et or Ph. Compound **3.8** did, however, react with (MeO)₃SiH to form the corresponding fluorosilane (MeO)₃SiF and the Cr(II) species **2.1**, as shown in Figure 3.10. A reaction was also observed upon treatment of compound **3.8** with an excess of PhSiH₃, forming

compound **2.1**. Interestingly, the major fluorosilane product was not that of the expected monofluorinated species $\text{PhSi}(\text{H})_2\text{F}$, but was in fact the trifluoro PhSiF_3 species. The reaction of compound **3.8** with $(\text{MeO})_3\text{SiH}$ reached completion after only 18 h, while the reaction with PhSiH_3 required significantly longer reaction times (138 h). The presence of electronegative atoms bound to the Si appears to greatly increase the rate of reaction,⁹⁶ as evidenced by the fast reaction with Me_3SiCl , and the reaction with $(\text{MeO})_3\text{SiH}$ compared to PhSiH_3 . This also explains the formation of PhSiF_3 from the reaction with PhSiH_3 : the formation of $\text{PhSi}(\text{H})_2\text{F}$ is slow, followed by further rapid reaction of this monofluorinated species with the remaining Cr(III) fluoride **3.8** to form a difluorinated species, and then finally the trifluorinated product observed in the reaction. This reaction presumably proceeds by formation of a 5 coordinate silicon intermediate, which would also be stabilized by an increased Lewis acidity of the Si atom as a result of increasing the number of F atoms bound to the Si.

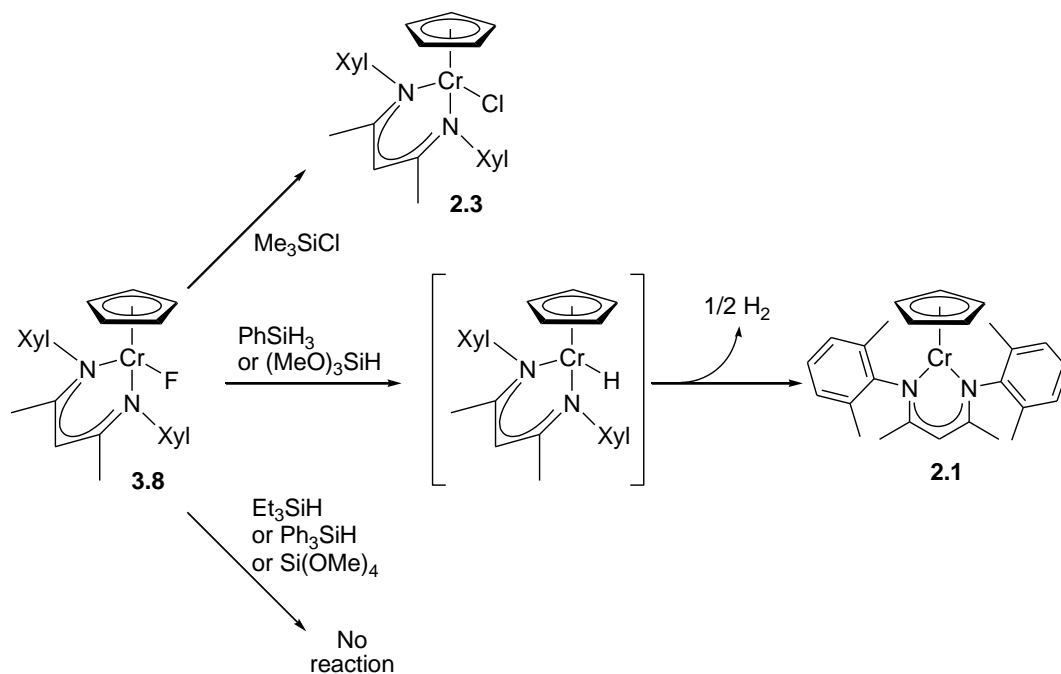


Figure 3.10. Reaction of the Cr(III) fluoride complex **3.8** with silanes.

Despite formation of the Cr(II) compound **2.1** from reaction of compound **3.8** with the trimethoxysilane (MeO)₃SiH, no reaction was observed with the tetra substituted silane Si(OMe)₄. This result was somewhat surprising considering a comparison of the potential Cr products of the two reactions. The formation of a Cr(III)–OMe complex would be highly energetically favourable compared to the formation of a Cr(III)–H species. This clearly indicates that the formation of strong Si–O and Si–F bonds are the determining factors governing the formation of reaction products.

With the formation of a Cr(III) hydride species being proposed as the intermediate in the reaction of the Cr(III) fluoride species with (MeO)₃SiH and PhSiH₃, characterization of a Cr(III) hydride species would provide further evidence to support this reaction sequence. Reaction of the Cr(III) tosylate species **2.6** with one equivalent of Na[HBET₃] led to the rapid formation of the Cr(II) compound **2.1**. Conducting the reaction at -35 °C also led to the formation of **2.1**. The reaction was complete within 15 min of addition of Na[HBET₃], with no intermediate Cr species observed in the reaction. This result suggested that the formation of a Cr(III) hydride intermediate leads to the rapid formation of Cr(II), presumably by an intermolecular reductive elimination of H₂ (Figure 3.11). Terminal, monomeric Cr(III) hydride species have previously been reported to be unstable with respect to elimination of H₂.⁹⁷ The larger Dpp N-aryl substituted analogue CpCr[(DppNCMe)₂CH](OTs) was also rapidly converted to the Cr(II) species **2.1c**, despite the presence to the large Dpp substituents, which did not prevent the bimolecular elimination of H₂.

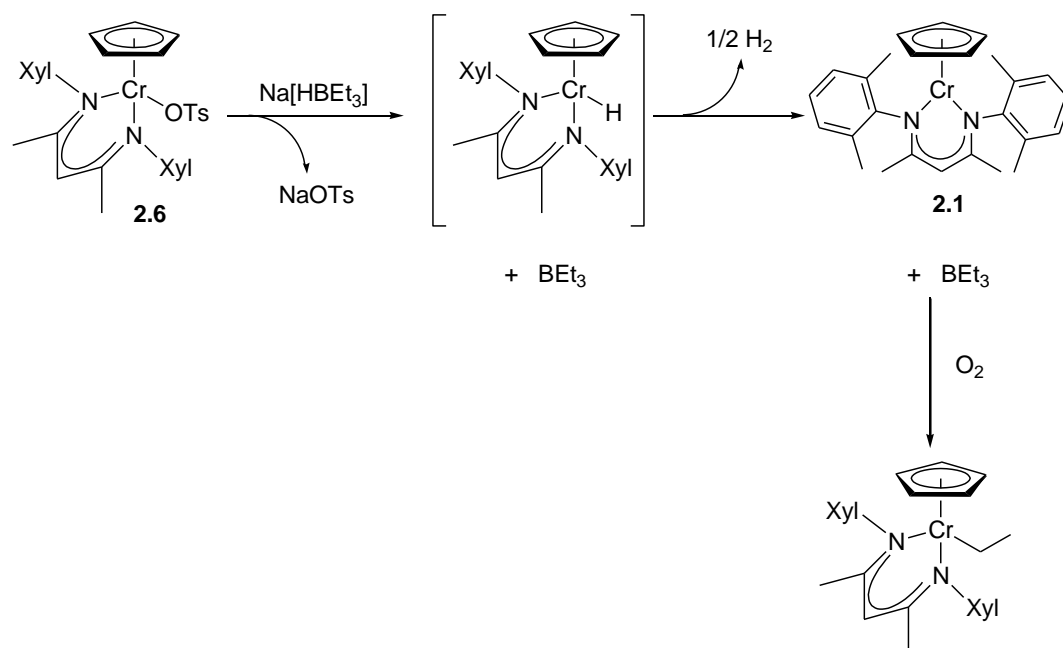


Figure 3.11. Reaction of the Cr(III) tosylate complex **2.6** with Na[HBET₃], and subsequent air exposure to form the Cr(III) ethyl species.

Upon air exposure of the reaction mixture obtained from **2.6** and Na[HB Et_3], the solution caused a rapid colour change, forming a purple solution, contrary to the previous observation that the Cr(II) compound **2.1** rapidly reacts with O $_2$ to form the μ -oxo species **3.1**. UV-vis analysis of the reaction mixture confirmed the formation of the Cr(III) ethyl complex CpCr[(XylNCMe) $_2$ CH](Et), as a result of the BEt $_3$ by-product reacting with O $_2$ to generate Et \cdot radicals, which were effectively trapped by the Cr(II) species **2.1** (Figure 3.11). Reaction of authentic **2.1** and BEt $_3$ with O $_2$ was presented in Chapter 2, as a method for preparing the Cr(III) ethyl complex.

The Cr(III) iodide complex CpCr[(XylNCMe) $_2$ CH](I) did not react directly with BEt $_3$, but the addition of O $_2$ resulted in the formation of CpCr[(XylNCMe) $_2$ CH](Et). Presumably, addition of O $_2$ to this reaction mixture leads to the formation of Et \cdot radicals, which perform an iodine atom abstraction from the Cr(III) iodide species to generate the Cr(II) complex **2.1** in solution, which is then able to rapidly trap the remaining ethyl radicals, forming the Cr(III) ethyl product, as shown in Figure 3.12. Surprisingly, the Cr(III) ethyl species did not form when the Cr(III) chloride (**2.3**) or bromide (**2.5**) complexes were subjected to the same reaction conditions. Compounds **2.3** and **2.5** remained completely unreacted in the presence of BEt $_3$ when subjected to air exposure. The difference in reactivity between the different halide compounds can be attributed to the differences in the Cr–X bonds, where X = I, Br, and Cl. The Cr–Cl and –Br bonds can be expected to have a larger barrier for halide abstraction compared to the Cr–I analogue, making halide atom abstraction from the Cr(III) iodide species much more facile compared to the chloride and bromide species. Therefore, the ethyl radicals are not able to

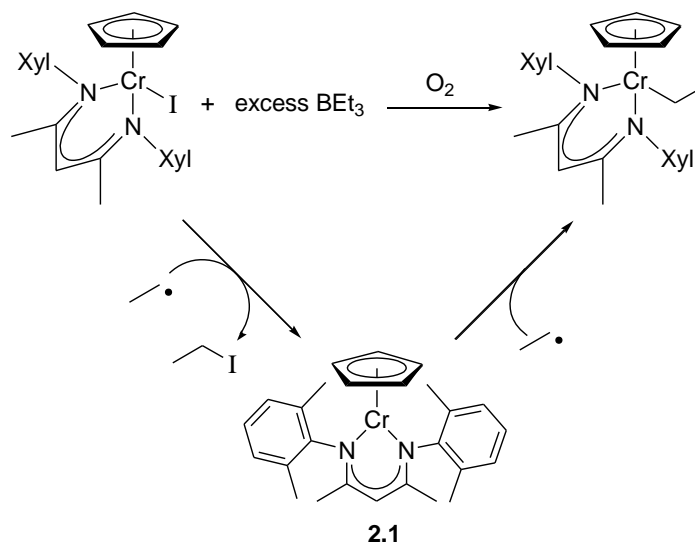


Figure 3.12. Reaction of CpCr[(XylNCMe) $_2$ CH](I) with BEt $_3$ and O $_2$.

effectively perform an atom abstraction from the chloride and bromide compounds under the given reaction conditions. Atom transfer reactions in the context of radical polymerization is discussed in Chapter 4.

The fluoride complex **3.8** was also subjected to reaction with BEt_3 and O_2 . Unlike the reaction observed upon addition of BF_3 to compound **3.8**, the addition of BEt_3 to compound **3.8** in non-coordinating solvent (hexanes) did not lead to formation of a $\text{Cr-F}\cdot\text{BEt}_3$ adduct. This difference in reactivity can be attributed to the reduced Lewis acidity of BEt_3 compared to that of BF_3 . However, upon addition of O_2 to the reaction mixture a rapid colour change was observed, from turquoise to purple, signifying the formation of the Cr(III) ethyl product.

^{19}F NMR analysis of the crude reaction mixture showed no evidence for the formation of $\text{CH}_3\text{CH}_2\text{F}$. Although this observation does not provide direct evidence to support a mechanism, it does suggest that formation of the Cr(III)-Et product is not formed by F atom transfer to the ethyl radical. It is therefore proposed that an intermediate boron species capable of F atom abstraction may be generated during the reaction. Two possible reaction pathways are shown in Figure 3.13. The first step in both pathways would involve the reaction between BEt_3 and O_2 , to generate $\text{Et}\cdot$ radicals and an intermediate boron species. The mechanism in pathway A is proposed to proceed by a direct reaction between a boron intermediate species and the fluoride compound **3.8** in a metathesis reaction, similar to the proposed reaction between compound **3.8** and silanes discussed above. Alternatively, the mechanism shown in pathway B would proceed by F atom abstraction from the Cr(III)-F compound to generate the Cr(II) compound **2.1**. The Cr(II) compound **2.1** would then trap an $\text{Et}\cdot$ radical to form the Cr(III)-Et product.

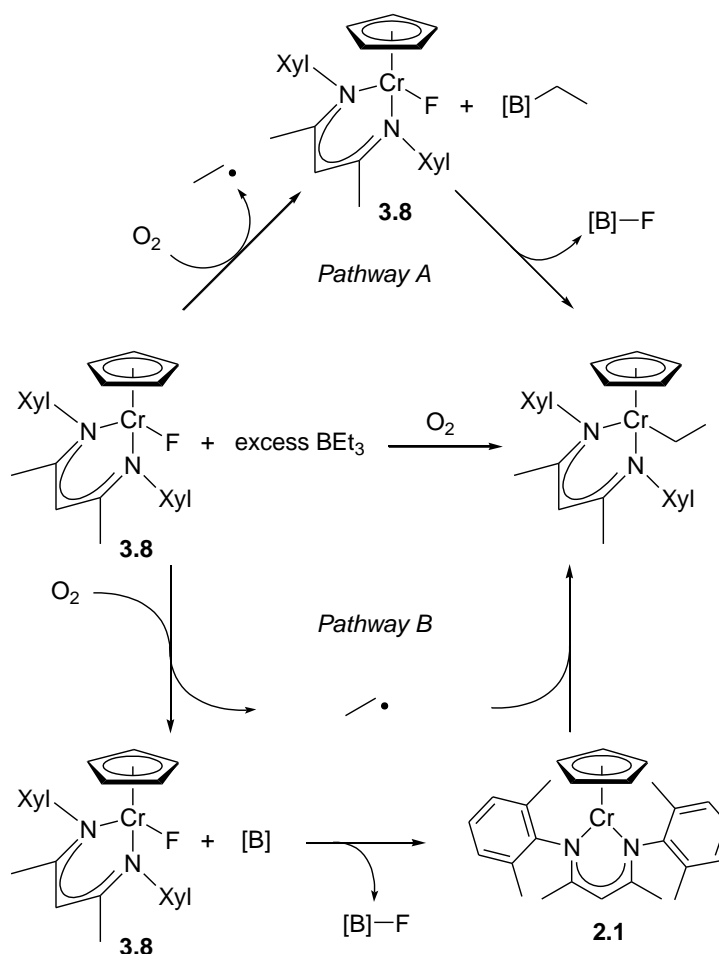


Figure 3.13. Reaction of Cr(III) fluoride complex **3.8** with BEt_3 and O_2 .

3.8 C–F Bond Formation with $CpCr[(Xyl)NCMe)_2CH](F)$.

The Cr(II) compound **2.1** reacted rapidly with chlorotriphenylmethane (Ph_3CCl) to form the Cr(III) chloride compound **2.3** and a $Ph_3C\cdot$ radical. The radical is extremely sterically protected by the presence of three phenyl groups and, as a result, compound **2.1** is not able to effectively trap the radical to form a Cr–C bond. The $Ph_3C\cdot$ radical is stable in solution and does not dimerize to form hexaphenylmethane due to steric limitations. The radical is also very stabilized by the three phenyl groups, forming a tertiary benzylic radical. The $Ph_3C\cdot$ radical does reversibly dimerize in solution, forming the compound commonly known as Gomberg's dimer, shown in Figure 3.14. The $Ph_3C\cdot$ radical is readily prepared from reaction of Ph_3CCl with Cu metal, and can be isolated as a white solid in the form of the dimer.⁹⁸ The dimer is stable in the solid state when stored under an inert atmosphere and protected from light.

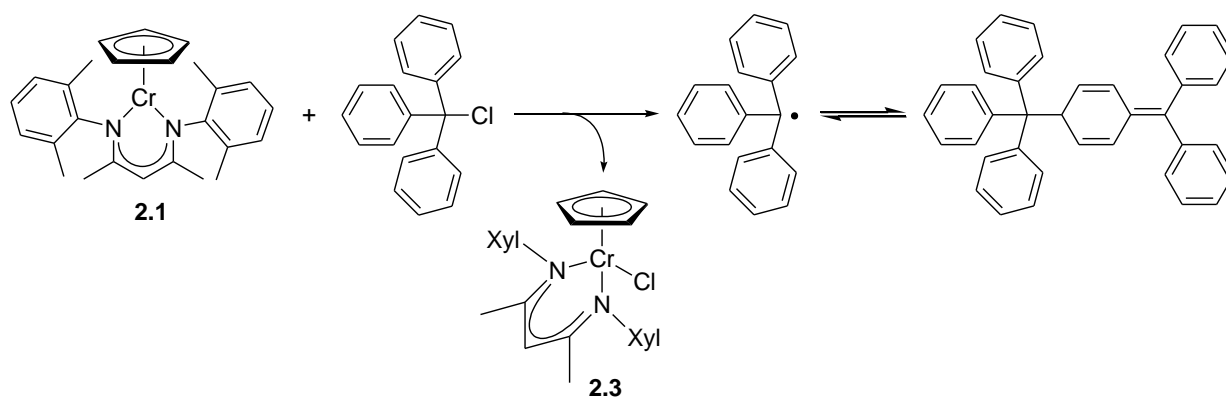


Figure 3.14. Reaction of the Cr(II) compound **2.1** with Ph_3CCl .

Upon mixing compound **2.1** and Ph_3CCl in THF, the solution became green (orange transmitted) and the crude reaction mixture displayed three absorption bands in the UV-vis spectrum. The bands at 419 and 577 nm corresponded to the Cr(III) chloride compound **2.3** and the third band at 514 nm was assigned to the $\text{Ph}_3\text{C}^\cdot$ radical. Notably, the $\text{Ph}_3\text{C}^\cdot$ radical has a reported $\epsilon = 661 \text{ M}^{-1}\text{cm}^{-1}$ (20 °C) at 516 nm⁹⁹ and therefore is easily distinguishable in the UV-vis spectrum as compound **2.3** does not absorb light in that region of the spectrum.

The fluoride compound **3.8** was reacted with Ph_3CCl and a substoichiometric amount of the Cr(II) compound **2.1**. Upon standing at room temperature the reaction slowly changed colour, the absorption bands in the UV-vis spectrum at 402, 505, and 607 nm corresponding to compound **3.8** were replaced by bands at 419 and 582 nm corresponding to the chloride compound **2.3**, and a peak appeared in the ^{19}F NMR spectrum at -126.9 ppm corresponding to Ph_3CF .¹⁰⁰ Heating the reaction mixture to 50 °C reduced the reaction time to 9 days (compared to 34 days at room temperature), with an ultimate conversion of 87% (Figure 3.15), as determined by integration in the ^{19}F NMR with an internal standard.

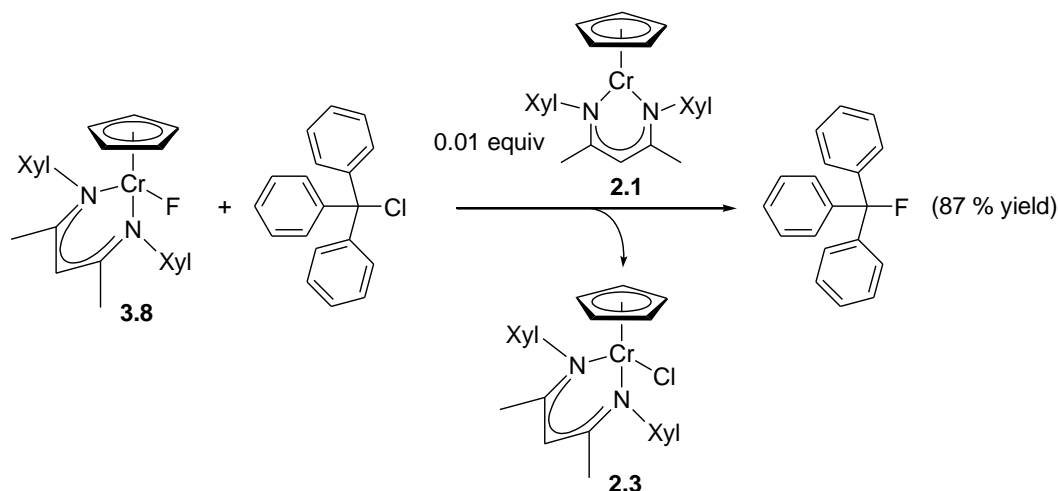


Figure 3.15. Conversion of Ph_3CCl to Ph_3CF with compound **3.8** as the F atom source.

The process proceeds by an initial reaction of the substoichiometric amount of compound **2.1** with Ph_3CCl to produce the chloride compound **2.3** and the $\text{Ph}_3\text{C}\cdot$ radical. The F atom abstraction from compound **3.8** generates the Cr(II) compound **2.1**, which then reacts with Ph_3CCl and the cycle continues, as shown in Figure 3.16. Although the Cr–F bond is stronger than the Cr–Cl bond, the combined bond strengths of Cr–F and $\text{Ph}_3\text{C–Cl}$ is less than that of $\text{Cr–Cl} + \text{Ph}_3\text{C–F}$, providing the thermodynamic driving force for the reaction.

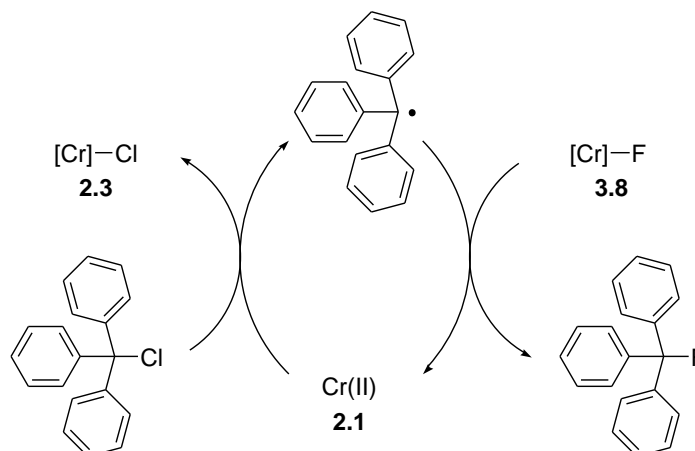


Figure 3.16. Proposed mechanism for C–F bond formation.

3.9 OAT Reactivity: PPh_3 Oxidation

The μ -oxo compound **3.1** rapidly reacted with Ph_3PI_2 causing a colour change from orange to green (Figure 3.17). The UV-vis spectrum of the reaction mixture was consistent with the formation of $\text{CpCr}[(\text{XylNCMe})_2\text{CH}](\text{I})$ and the ^{31}P NMR spectrum contained only one peak corresponding to OPPh_3 (~30 ppm).

The oxidation of PPh_3 was investigated to assess the stability of the cyclopentadienyl chromium β -diketiminate framework under catalytic oxidative conditions, and to compare the reactivity of μ -oxo **3.1** with other oxygen atom transfer (OAT) catalysts. Many of the examples of chromium catalyzed OAT involve a Cr(III)/Cr(V) redox couple where the Cr(III) must be sufficiently reducing to form a Cr(V) oxo, which then must be sufficiently oxidizing to react with organic substrates to achieve the oxo transfer.¹⁰¹ The Cr corrole system of Gray and co-workers is an example of the Cr(III)/Cr(V) oxo redox couple; the Cr(V) oxo reacts quickly with PPh_3 to generate OPPh_3 but the Cr(III) is slow to react with O_2 .^{76h} This system also suffers from product inhibition where the reduced Cr(III) corrole coordinates OPPh_3 , further reducing the rate of Cr(III) oxidation. Veige and co-workers adopted a tridentate pincer ligand which was found

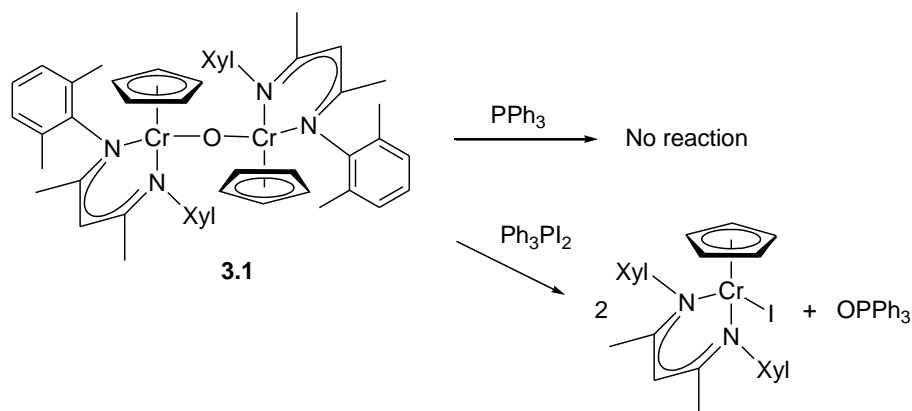


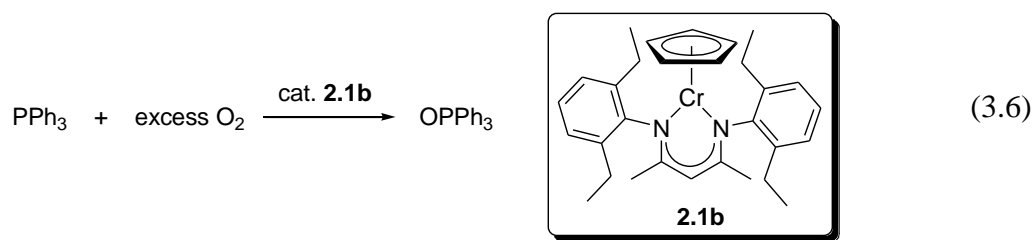
Figure 3.17. Formation of OPPh_3 from the μ -oxo complex **3.1**.

to increase the rate of Cr(III) oxidation by O_2 due to the open coordination site on the Cr centre created by moving from a tetra- to a tri-dentate ligand framework.^{76k}

Alternatively, using a Cr(II)/Cr(IV) oxo redox couple presents two potential advantages: the increased reactivity of the reduced Cr(II) toward oxidation with O_2 , and the expected higher reactivity of the Cr(IV) oxo species compared to a Cr(V) analogue. The latter observation was recently reported for the Cr corrole system where single-electron reduction of the Cr(V) oxo compound of Gray and co-workers to an anionic Cr(IV) oxo species was proposed to result in both an increased electrophilicity and an increase in the unpaired electron density of the oxygen atom.^{76j} Similarly, in situ generated aqueous CrO^{2+} reacted with PPh_3 to form OPPh_3 with a rate constant of $2.1(2) \times 10^3 \text{ M}^{-1} \text{ s}^{-1}$.¹⁰²

It was thought that a catalytic system could be achieved from a Cr(II) $\text{CpCr}[(\text{ArNCMe})_2\text{CH}]$ compound. As discussed above, the Cr(II) compound $\text{CpCr}[(\text{XylNCMe})_2\text{CH}]$ (**2.1**) reacted rapidly with O_2 to form the bimetallic Cr(III) μ -oxo compound **3.1**. Additionally, **2.1** does not readily coordinate OPPh_3 or other Lewis bases, avoiding the issue of product inhibition.^{75f,76h} Unfortunately, the μ -oxo compound **3.1** did not react with PPh_3 , presumably due to the highly stable nature of the μ -oxo core. The formation of **3.1** is thought to proceed through a terminal Cr(IV) oxo species: the monomeric $\text{CpCr}[(\text{XylNCMe})_2\text{CH}](\text{O})$ oxo intermediate would be expected to be much more reactive toward OAT reactions.

By replacing the 2,6-dimethylphenyl groups of the β -diketiminato ligand with slightly larger 2,6-diethylphenyl, the stability of the Cr(III) μ -oxo species should be reduced due to the increased bulk being directed at the already strained Cr–O–Cr core, leading to an increased likelihood of a Cr(IV) oxo. The Cr(II) compound $\text{CpCr}[(\text{DepNCMe})_2\text{CH}]$ (**2.1b**) was in fact found to catalyze the aerobic oxidation of PPh_3 to OPPh_3 (eq 3.6). Exposure of a solution of **2.1b** with a large excess of PPh_3 to one atmosphere of dry O_2 resulted in the formation of OPPh_3 with a maximum turnover number (TON; mol product/mol catalyst) of 20, based on isolated OPPh_3 . Air was also found to be an effective source of oxygen for this reaction as ^{31}P NMR analysis showed complete conversion of six equivalents of PPh_3 upon air exposure over a period of approximately 10 min. TONs were ultimately limited under the reaction conditions due to catalyst deactivation.



3.10 HAT Reactivity

As discussed above, the μ -oxo complex **3.1** did not react with excess pyridine *N*-oxide in THF. Alternatively, **3.1** was found to react with an excess of pyridine *N*-oxide in the presence of the hydrogen atom source γ -terpinene over a 2 day period at room temperature. Notably, complex **3.1** did not react with γ -terpinene in the absence of pyridine *N*-oxide, highlighting the need for an oxidant in the reaction. UV-vis analysis of the crude reaction mixture suggested that the product of the reaction was the Cr(III) hydroxide compound **3.2**. The solid-state molecular structure obtained from recrystallized **3.2** confirmed the intermolecular HAT, showing that the product of the reaction was the hydroxide complex **3.2** (Figure 3.18). The Cr–O bond length of 1.896(1) Å is slightly longer than the 1.814(2) Å reported for the cationic 5-coordinate Cr(III) hydroxide complex $[\text{Tp}^{\text{tBu,Me}}\text{Cr}(\text{OH})(\text{pz}'\text{H})]$, prepared from the Cr(IV) oxo precursor undergoing a hydrogen atom abstraction from substrates containing homolytic C–H bond dissociation energies (BDEs) < 92 kcal/mol.^{76g} Related hydrogen atom abstraction reactions of cyclohexadiene with well-defined Cr(V) oxo and Cr(III) superoxo complexes have recently been reported by Nam and co-workers.^{77b,c}

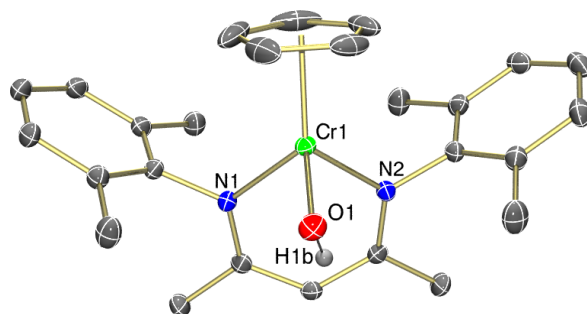


Figure 3.18. Thermal ellipsoid diagram (50%) of **3.2**. Disordered Cp and OH ligands were modeled in two orientations; in both cases only one is shown, and all H atoms, with the exception of the OH ligand, are omitted for clarity.

A possible mechanism for the observed HAT reactivity is shown in Figure 3.19. The lack of further oxidation of μ -oxo **3.1** with excess pyridine *N*-oxide suggests that the reaction of Cr(II) complex **2.1** with pyridine *N*-oxide may be reversible. The steric demands of the 2,6-dimethylphenyl substituted β -diketiminato ligand apparently aids in the reversible dissociation of μ -oxo **3.1**, analogous to the Cr porphyrin system described by Liston and West.⁸⁰ However, the proposed Cr(IV) oxo species generated upon Cr–O bond cleavage of **3.1** is rapidly trapped by the Cr(II) complex **2.1** in the absence of a substrate with weak C–H bonds. Similarly, the Cr(II) compound **2.1** does not react with γ -terpinene, so in the absence of oxidant, only a minute amount of Cr(III) hydroxide product **3.2** is presumably formed before the build up of complex **2.1** precludes further consumption of μ -oxo **3.1**. No further reaction of compound **3.2** was observed with the excess γ -terpinene.

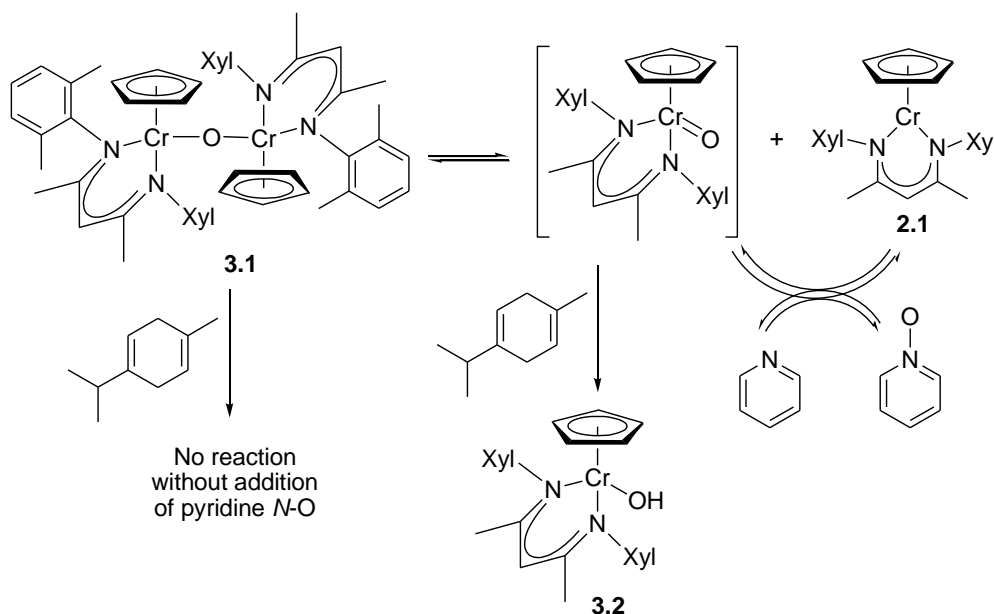


Figure 3.19. Proposed mechanism for the formation of the Cr(III) hydroxide **3.2** from the μ -oxo complex **3.1**.

The HAT reactivity ascribed to the putative chromium oxo species in Figure 3.19 is consistent with the expected strength of the O–H bond in **3.2**, the Cr(III) hydroxide product.¹⁰³ This rationale has been used to explain the radical reactivity of aqueous CrO^{2+} ,¹⁰⁴ as well as biologically relevant Cr(IV) and Cr(V) complexes.¹⁰⁵ Recent work with iron imido complexes has examined the role of N-based radical character in HAT reactivity.¹⁰⁶ We were therefore interested in isolating an analogue of the monomeric oxo intermediate in Figure 3.19 in order to evaluate the degree of oxo-based radical character¹⁰⁷ and its possible impact on reactivity.¹⁰⁸

Reaction of the bulkier 2,6-diethyl substituted Cr(II) compound **2.1b** with pyridine *N*-oxide or O_2 resulted in a rapid colour change to orange, consistent with Cr(III) μ -oxo formation, followed by a further colour change to green. The decrease in stability of the Cr(III) μ -oxo with increased steric bulk of the β -diketiminate ligand is consistent with the observed PPh_3 oxidation reactivity, suggesting a Cr(IV) oxo intermediate is the active OAT species in solution. The UV-vis spectrum of the green crude reaction mixture suggested formation of a Cr(III) hydroxide compound but no tractable products could be isolated from the reactions in variety of different solvents. Addition of the hydrogen atom source γ -terpinene to the reaction of the Cr(II) compound **2.1b** with pyridine *N*-oxide, analogous to the reaction of **2.1** to form hydroxide **3.2**, cleanly provided the Cr(III) hydroxide compound $\text{CpCr}[(\text{DepNCMe})_2\text{CH}](\text{OH})$ (**3.2b**), shown in Figure 3.20. Compound **3.2b** was more readily prepared compared to **3.2**, giving a higher yield with reduced reaction time, also consistent with the decreased stability of the bimetallic Cr(III) μ -oxo species when the larger β -diketiminate ligand framework is present.

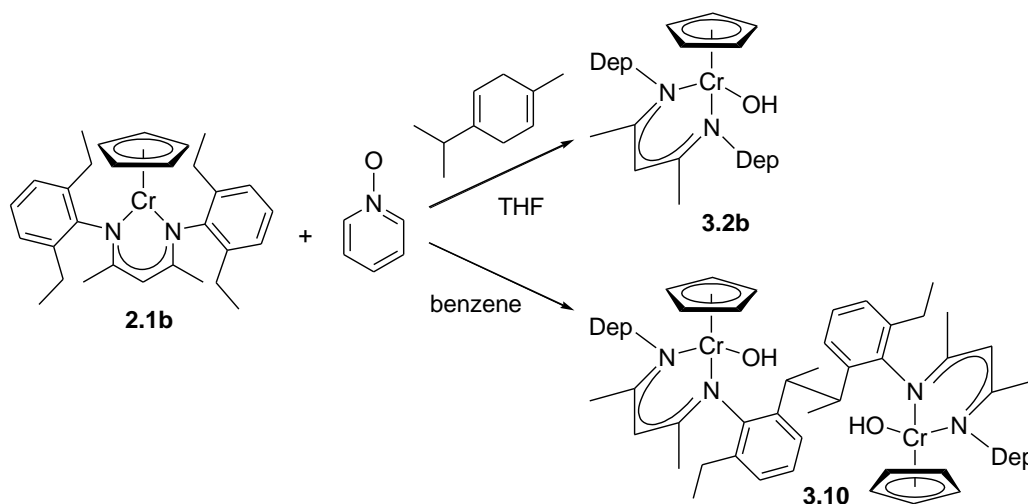


Figure 3.20. Reaction of the Cr(II) complex **2.1b** with pyridine *N*-oxide.

The formation of Cr(III) hydroxide species in the absence of γ -terpinene suggested that intermolecular HAT from solvent or even intramolecular HAT from the ligands was the route to the Cr(III) hydroxide formation. Compound **2.1b** was reacted with pyridine *N*-oxide in benzene to remove the possibility of solvent based HAT (Figure 3.20). The isolated product was characterized by X-ray crystallography as a Cr(III) hydroxide dimer, compound **3.10** (Figure 3.21). Compound **3.10** has similar bond lengths to the monometallic Cr(III) hydroxide **3.2** with Cr–O bond lengths of 1.8603(13) Å and 1.8665(13) Å and Cr–N bond lengths in the range of 2.0130(14) - 2.0295(15) Å.

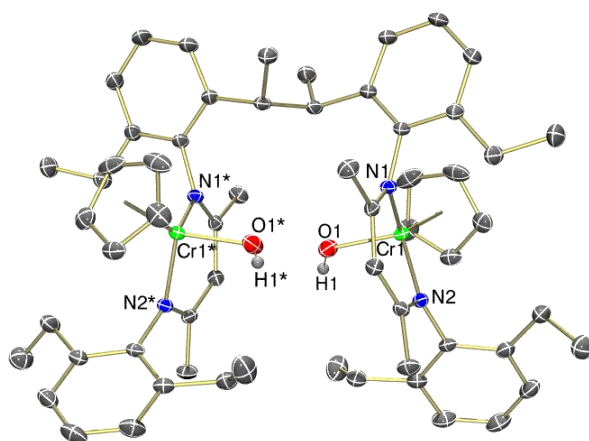


Figure 3.21. Thermal ellipsoid diagram (50%) of **3.10**. Compound **3.10** crystallizes with two independent molecules in the asymmetric unit, each residing on a two-fold axis of rotation; only one is shown, and all H atoms, with the exception of the OH ligand, are omitted for clarity.

In the absence of external hydrogen atom sources the Cr(IV) oxo intermediate underwent intramolecular HAT from the secondary benzylic groups of the β -diketiminate ligand followed by intermolecular radical C–C bond formation to generate the Cr(III) hydroxide dimer **3.10**. Examples of ligand based C–H activation of pyridinediimine backbone methyl groups resulting in intermolecular C–C coupling have been previously reported.¹⁰⁹ An example of intramolecular HAT from a β -diketiminate ligand was recently reported with an imido Fe(III) compound that results in intramolecular C–C bond formation.^{106b}

3.11 Synthesis of {CpCr[(HIPTNCMe)₂CH]}₂(μ -O)

Replacing the ortho substituents on the N-aryl groups of the β -diketiminate ligand with meta substituents removes the reactive benzylic C–H bonds in proximity to the Cr–O reactive site. The size of bulky substituents must be substantially increased when placed in meta positions if bimetallic μ -oxo formation is to be discouraged. Recently Piers used the

hexaisopropylterphenyl {HIPT, [3,5-(2,4,6-*i*Pr₃C₆H₂)₂C₆H₃]} substituents pioneered by Schrock¹¹⁰ to prevent unwanted C–H activation of the β -diketiminato ligand.¹¹¹

Preparation of the Cr(II) compound CpCr[(HIPTNCMe)₂CH] was achieved by the standard method of reacting CrCl₂ with one equivalent of NaCp followed by one equivalent of the deprotonated β -diketiminato ligand to form a solution that was green (magenta transmitted), similar to that of the Cr(II) compound **2.1**. The high solubility of the complex in hexanes precluded isolation by recrystallization. The CpCr[(HIPTNCMe)₂CH] compound reacted with pyridine *N*-oxide to form an orange solution with an absorption band at 371 nm and a shoulder absorption at 475 nm, similar to the μ -oxo compound **3.1** (Figure 3.22). The solid-state molecular structure obtained from the isolated orange crystalline material displayed the presence of the bimetallic Cr(III) μ -oxo core despite the introduction of the large meta substituents, shown in Figure 3.23. In addition, a thermal ellipsoid diagram displaying the full molecule is presented in appendix Figure A.1.

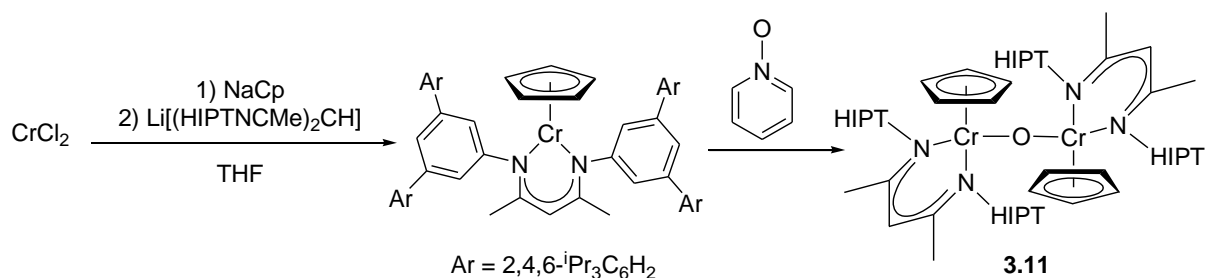


Figure 3.22. Synthesis of a HIPT substituted CpCr β -diketiminato complex and its reactivity with pyridine *N*-oxide.

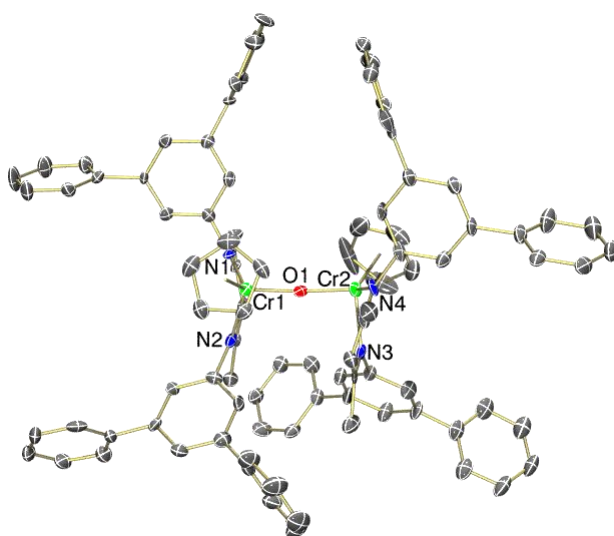


Figure 3.23. Thermal ellipsoid diagram (50%) of **3.11**. All H atoms and *iso*-propyl groups are omitted for clarity.

The specific bond lengths and angles for **3.11** are somewhat unreliable due to poor data quality, a trend previously observed in metal complexes bearing HIPT substituted ligands.^{110c,d} Compound **3.11** exhibits a Cr–O–Cr angle (174.3(2)°) that is essentially identical to the μ -oxo compound **3.1** (174.5(2)°). The Cr–O bond lengths (1.784(4) and 1.786(3) Å) in contrast are significantly shorter compared to **3.1** (1.834(3) Å). The Cr(III) μ -oxo complex [{Cr(NCS)(TPyEA)}₂O] exhibits a similar Cr–O–Cr bond angle of 176.5(6)° and Cr–O bond lengths of 1.82(1) and 1.81(1) Å.^{75a} The Cr–N bond lengths of compound **3.11** (2.022(4) – 2.037(4) Å) are slightly shorter compared to compound **3.1** (2.046(4) – 2.055(4) Å).⁷⁸ The solid-state molecular structure revealed a staggered type of arrangement for the Cp and β -diketimate ligands, where one half of the molecule is rotated approx 127° with respect to the other. The staggered geometry of the ligands is presumably a result of steric requirements in the molecule due to the large HIPT groups of the β -diketimate ligands. Compound **3.1** displays a similar twist of 143° in the solid state.⁷⁸

Additionally, preliminary reactivity studies of {CpCr[(HIPTNCMe)₂CH]}₂(μ -O) (**3.11**) suggested that the compound was actually less reactive compared to compound **3.1**. Unlike **3.1**, compound **3.11** did not react with H₂O, nor was there any reaction with excess pyridine *N*-oxide and γ -terpinene upon stirring for 10 days. The lack of protonolysis and HAT reactivity in combination with the shorter Cr–O bond lengths indicated that there was no significant increase in steric strain of the bimetallic μ -oxo species between the HIPT and Xylyl derivatives of the β -diketimate ligand.

3.12 Catalytic HAT

Attempts to render a catalytic HAT reaction based on a Cr(IV) oxo catalyst with O₂ as the oxidant, founded on the stoichiometric reactivity discussed above, proved challenging. When Mn was used as the stoichiometric reductant the catalyst turnovers were ultimately limited by one of two factors: either the Mn was deactivated by the presence of the oxidant and would no longer reduce the Cr(III) intermediates, as was the case with PbCl₂ activated Mn (Table 3.1, entries 2 and 4); or the oxidant was rapidly consumed by the activated Mn to form Mn oxides, as was the case with I₂ or Me₃SiCl activating agents (entries 1, 3, 5, and 6).¹¹² The best result for the Cr catalyzed conversion of γ -terpinene to *p*-cymene was limited to 4 turnovers of the catalyst, 2 equivalents of *p*-cymene per Cr (entries 7 and 8). The optimal reaction conditions were found with a catalytic amount of CpCr[(DepNCMe)₂CH](Cl) (**2.3b**), excess Zn as the stoichiometric reductant, and either Me₃SiCl or PbCl₂ as activating agents for the Zn.

As expected, the issues associated with using an air-sensitive reductant (in this case Mn) were overcome with the use of a more O₂ compatible metal, Zn. Unfortunately, catalyst turnover was limited with Zn due to decomposition of the Cr species under the reaction conditions in entries 7 and 8, an issue not previously encountered with the use of Mn as stoichiometric reductant. The addition of the Bronsted base triethylamine (NEt₃) was found to greatly improve the stability of the Cr species in situ, presumably as a means of sequestering Bronsted acids present in the reaction mixture.

Despite the initially promising results shown in entry 9, with 50% conversion after only 1.25 h, the high conversion observed in entry 10 (40%) under similar reaction conditions was achieved in the absence of Cr. The presence of Cr in entry 9 resulted in only a 10% improvement in the conversion of γ -terpinene to *p*-cymene, indicating that the role of Cr in this reaction may simply be stoichiometric in nature.

Table 3.1. HAT reactions for the conversion of γ -terpinene to *p*-cymene.

Entry	Cr Compound ^a	Reductant	Activators	Oxidant	Reaction Time	Conversion
1	10 mol % 2.1b	4 equiv Mn	5 mol % I ₂	O-py	Overnight	6%
2	10 mol % 2.1b	4 equiv Mn	2 mol % PbCl ₂	O-py	24 h	6%
3	10 mol % 2.3b	5 equiv Mn	5 equiv Me ₃ SiCl	O-py	3 days	4%
4	5 mol % 2.3b	2 equiv Mn	1 mol % PbCl ₂	O ₂ ^b	5 days	5%
5	9 mol % 2.3b	5 equiv Mn	5 equiv Me ₃ SiCl	O ₂	18 h	14%
6	20 mol % 2.3b	5 equiv Mn	5 equiv Me ₃ SiCl	O ₂ ^b	4 days	8%
7	11 mol % 2.3b	10 equiv Zn	6 equiv Me ₃ SiCl	O ₂	17 h	22%
8	12 mol % 2.3b	4 equiv Zn	2 mol % PbCl ₂	O ₂	48 h	25%
9	10 mol % 2.3b	5 equiv Zn	5 equiv Me ₃ SiCl, 5 equiv NEt ₃	O ₂	1.25 h	50%
10	-	5 equiv Zn	5 equiv Me ₃ SiCl, 5 equiv NEt ₃	O ₂	1.25 h	40%

^a The Cr(III)–Cl compound **2.3b** was pre-reduced in situ prior to addition of the oxidant. ^b O₂ was added stepwise in small aliquots throughout the reaction, to inhibit direct oxidation of Mn.

3.13 Synthesis and Reactivity of a Cr(III) Nitrosoarene Complex

Reaction of low-valent Cr β -diketiminate complex with nitrosobenzene was recently reported.¹¹³ The reaction product was characterized as a Cr(V) $[(\text{ArNCMe})_2\text{CH}](\text{O})(\text{NPh})$, where the $\text{PhN}=\text{O}$ bond had been broken to form an oxo and an imido ligand, resulting in a 4 electron oxidation of the metal centre. A similar Co(I) β -diketiminate species was also reported to break the $\text{PhN}=\text{O}$ bond, in that case forming a bimetallic species with a bridging μ -oxo and a μ -imido ligand.¹¹⁴

Nitrosoarenes exhibit a range of binding modes that varies widely depending on the coordination environment of the metal species, with both monometallic and multimetallic compounds known.¹¹⁵ Three coordination modes have been described for monometallic compounds where the $\text{N}=\text{O}$ bond remains intact (Figure 3.24). The most common binding mode is the κ^1 -N-bound moiety. The η^2 -ON-bound compounds are less common, and only rare examples of structurally characterized κ^1 -O-bound complexes have been reported for Mn, Fe, Zn, and Sn, all of which contain two nitrosoarene ligands coordinated to the metal centre.¹¹⁵

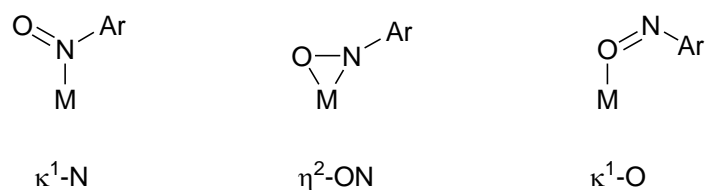


Figure 3.24. Nitrosoarene binding modes in transition metal compounds.

Reaction of the Cr(II) compound **2.1** with one equivalent of nitrosobenzene (PhNO) caused the solution to rapidly turn orange (Figure 3.2, path **O**). Recrystallization of the product provided X-ray quality crystals of a $\text{CpCr}[(\text{XylNCMe})_2\text{CH}](\text{ONPh})$ (**3.12**) compound and structural analysis was used to determine the binding mode of the PhNO ligand. A thermal ellipsoid diagram of compound **3.12** is shown in Figure 3.25, displaying a rare example of an O-bound nitrosoarene ligand. The PhNO ligand was modeled in two orientations due to disorder, a common motif observed in the other structurally characterized O-bound nitrosoarene transition metal complexes.¹¹⁵ The Cr–N bond lengths in compound **3.12** (2.003(2) and 2.006(2) Å) are typical for the CpCr β -diketiminate compounds reported herein. The Cr–O bond length of 1.864(2) Å is also typical of other Cr–O bonds for the CpCr β -diketiminate compounds. The PhNO ligand contains O–N bond lengths of 1.252(3) and 1.170(6) Å, N–C bond lengths of 1.393(5) and 1.415(11) Å, O–N–C bond angles of 113.4(4) and 120.5 (8) degrees, and Cr–O–N

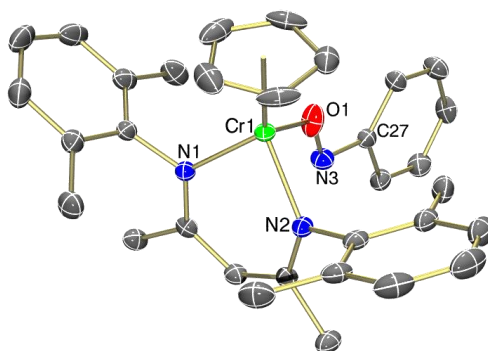


Figure 3.25. Thermal ellipsoid diagram (50%) of **3.12**. The disordered nitrosobenzene ligand was modeled in two orientations; only one is shown, and all H atoms are omitted for clarity.

angles of 129.2(2) and 147.5(3) degrees; note that two sets of bond lengths and angles are given as a result of the PhNO ligand being modeled in two orientations.

The UV-vis spectrum of compound **3.12** is unique amongst the CpCr β -diketiminato compounds having two strong absorption bands at 404 and 461 nm, possibly due to a different electronic structure of the compound compared to the other CpCr β -diketiminato compounds. The Cr(II) compound **2.1** does not bind Lewis bases to any appreciable extent, suggesting that the PhNO compound **3.12** is not a simple Lewis acid/base interaction between the Cr and O atoms. A more plausible description of the bonding interaction observed in compound **3.12** is therefore a formal single-electron reduction of the PhNO ligand as a result of electron transfer from the Cr. Compound **3.12** can be thought of as a Cr(III) compound with a (PhNO) $^{\cdot-}$ radical anion ligand. A recent report examined the redox noninnocence of κ^1 -N-bound nitrosoarene transition metal complexes by computational methods.¹¹⁶

Initial reactions conducted with compound **3.12** suggest that the complex does exhibit radical character on the N atom of the PhNO ligand. Reaction of compound **3.12** with an excess of the H atom sources C₅H₆, γ -terpinene, and Bu₃SnH all resulted in the colour of the reaction mixture changing from orange to green and the UV-vis spectrum of the crude reaction mixtures all contained absorption bands at 389 and 614 nm, and a shoulder at 500 nm, consistent with the formation of the hydroxide compound **3.2** (Figure 3.26). The reaction with γ -terpinene required a reaction time of 22 days at 50 °C to reach completion, while the reaction with C₅H₆ was complete after only 16 h at 50 °C. The reaction with Bu₃SnH did not require elevated temperatures to react and was complete after only 3 days at room temperature. The observed trend in reaction times is consistent with the differences in E–H bond strength, where E = Sn or C, of the three compounds (Bu₃SnH < C₅H₆ < γ -terpinene).

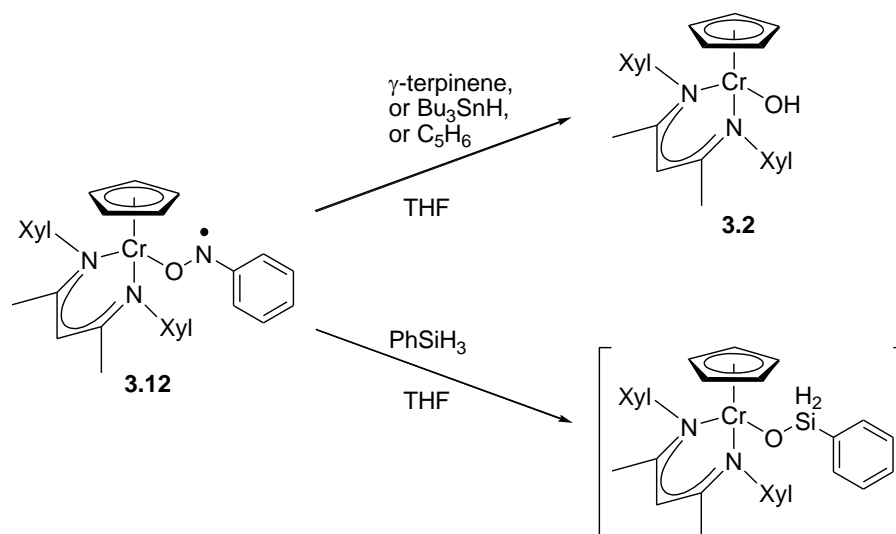


Figure 3.26. Reaction of nitrosobenzene compound **3.12** with H atom sources.

Alternatively, the use of PhSiH_3 led to a similar colour change but the UV-vis spectrum of the reaction mixture displayed absorption bands at 401 and 626 nm, and a shoulder at 500 nm. The identity of the resulting Cr species is tentatively assigned as a $\text{CpCr}[(\text{XylNCMe})_2\text{CH}][\text{OSi}(\text{H})_2\text{Ph}]$ compound, shown in Figure 3.26, based on the similarities of the UV-vis spectrum to the product obtained upon reaction of $\text{CpCr}[(\text{XylNCMe})_2\text{CH}](\text{OTs})$ (**2.6**) with $\text{Li}[\text{OSiMe}_3]$.

These reactions indicate cleavage of the N–O bond in the PhNO ligand of compound **3.12** as a result of H atom transfer to the PhNO ligand. Although the fate of the NPh group has not been identified in these reactions, one could postulate that an initial H atom transfer occurs at the N atom of the PhNO ligand followed by further reduction eventually leading to the formation of the hydroxide compound **3.12** and the aniline PhNH_2 . Characterization of the NPh containing products of the reactions will no doubt provide further insight into the reaction pathway.

3.14 Experimental Section

General considerations. Protocols were identical to those reported in section 2.13 using standard Schlenk and glovebox techniques unless otherwise indicated. Additionally, C_6D_6 was dried over sodium/benzophenone, purified by vacuum distillation, degassed by three freeze-vacuum-thaw cycles and stored under nitrogen prior to use. CDCl_3 was used as received or dried over P_2O_5 , purified by vacuum distillation, degassed by three freeze-vacuum-thaw cycles and stored under nitrogen prior to use.

Characterization. Protocols were identical to those reported in section 2.13. Additionally, ^{19}F and ^{31}P NMR spectra were recorded on a Varian Mercury Plus 400 spectrometer. ^{19}F NMR spectra were referenced to an internal standard PhCF_3 (-63.7 ppm in benzene) and ^{31}P NMR spectra were referenced to external PPh_3 (-4.9 ppm in benzene).

Materials. Protocols were identical to those reported in section 2.13. Additionally, benzoic acid, chlorotriphenylmethane, ethyl propionate, methyl propionate, 2-phenyl-2-propanol, nitrosobenzene, potassium *tert*-butoxide, pyridine *N*-oxide, triethylborane (1.0 M solution in hexanes), sodium triethylborohydride (1.0 M solution in THF), silver acetate, silver benzoate, silver fluoride, cesium fluoride, tetrabutylammonium difluorotriphenylsilicate, tributyltin hydride, chlorotrimethylsilane, phenylsilane, triethylsilane, trimethoxysilane, triphenylsilane, tetramethyl orthosilicate, and triphenylphosphine were purchased from Aldrich and used as received. Acetophenone and γ -terpinene were purchased from Aldrich, degassed by three freeze-vacuum-thaw cycles, and stored under nitrogen prior to use. $\text{K}[\text{OC}(\text{Me})_2\text{Ph}]$ was prepared by reacting $\text{HOC}(\text{Me})_2\text{Ph}$ with 1 equiv of $\text{KN}(\text{SiMe}_3)_2$ in hexanes/toluene (5:1) while stirring for 2 h. The product was isolated by vacuum filtration, rinsed with hexanes, dried under vacuum, and stored under nitrogen. $\text{K}[\text{OC}(=\text{CH}_2)\text{Ph}]$, $\text{K}[\text{OC}(=\text{CHMe})\text{OEt}]$, and $\text{K}[\text{OC}(=\text{CHMe})\text{OMe}]$ were prepared according to literature procedures outlining the preparation of similar potassium enolate compounds.⁸¹ Ph_3PI_2 was prepared according to the literature procedure.¹¹⁷ $\text{H}[(\text{HIPTNCMe})_2\text{CH}]$ was prepared with a slight modification to the literature procedure.¹¹¹

Synthesis of $\{\text{CpCr}[(\text{XylNCMe})_2\text{CH}]\}_2(\mu\text{-O})$ (3.1). $\text{CpCr}[(\text{XylNCMe})_2\text{CH}]$ (**2.1**) (495 mg, 1.17 mmol) was placed in a round bottom flask followed by the addition of 61.8 mg (0.65 mmol, 0.55 equiv) of pyridine *N*-oxide and approximately 10 mL of hexanes. After stirring overnight, the orange precipitate was isolated, rinsed with a small amount of Et_2O , and dried to produce an orange powder (408 mg, 81%). μ_{eff} (Evans, CDCl_3): 2.39 μ_{B} . Anal. Calcd. for $\text{C}_{52}\text{H}_{60}\text{N}_2\text{Cr}_2\text{O}$: C, 72.53; H, 7.02; N, 6.51. Found: C, 72.87; H, 6.87; N, 6.96. UV-vis (hexanes; λ_{max} , nm (ϵ , $\text{M}^{-1}\text{cm}^{-1}$)): 362 (20700), 471 (sh).

Synthesis of $\text{CpCr}[(\text{XylNCMe})_2\text{CH}](\text{OH})$ (3.2). Compound **2.1** (100 mg, 0.237 mmol) was placed in a Schlenk flask followed by the addition of THF, 200 μL (1.25 mmol, 5.25 equiv) of γ -terpinene, and 110 mg (1.16 mmol, 4.89 equiv) of pyridine *N*-oxide. The solution quickly turned orange and upon stirring for 2 days turned green, at which point the volatiles were removed under reduced pressure. The residue was extracted with hexanes, filtered over Celite, and the solvent was again removed under reduced pressure. The residue was extracted with a

minimum amount of hexanes (3 mL), filtered, and cooled to $-35\text{ }^{\circ}\text{C}$ to provide black crystals of **3.2** (36 mg, 35%) in three crops. Anal. Calcd. for $\text{C}_{26}\text{H}_{31}\text{N}_2\text{CrO}$: C, 71.05; H, 7.11; N, 6.37. Found: C, 70.94; H, 7.11; N, 6.50. UV-vis (hexanes; λ_{max} , nm (ϵ , $\text{M}^{-1}\text{cm}^{-1}$)): 387 (9280), 503 (730), 614 (730).

Synthesis of $\text{CpCr}[(\text{DepNCMe})_2\text{CH}](\text{OH})$ (3.2b**).** Compound **3.2b** was prepared in a similar manner to compound **3.2** with $\text{CpCr}[(\text{DepNCMe})_2\text{CH}]$ (**2.1b**) (94.1 mg, 0.197 mmol), γ -terpinene (300 μL , 1.86 mmol, 9.44 equiv), and pyridine *N*-oxide (36.9 mg, 0.388 mmol, 1.97 equiv). The reaction mixture was stirred overnight. Workup and cooling to $-35\text{ }^{\circ}\text{C}$ in hexanes (2 mL) provided 57.3 mg (59%) of **3.2b**. Anal. Calcd. for $\text{C}_{30}\text{H}_{39}\text{N}_2\text{CrO}$: C, 72.70; H, 7.93; N, 5.65. Found: C, 71.18; H, 7.99; N, 5.64. UV-vis (hexanes; λ_{max} , nm (ϵ , $\text{M}^{-1}\text{cm}^{-1}$)): 388 (10400), 503 (740), 614 (760).

Synthesis of $\text{CpCr}[(\text{XylNCMe})_2\text{CH}](\text{O}_2\text{CPh})$ (3.3**).** Compound **3.1** (119.5 mg, 0.139 mmol) and benzoic acid (34.4 mg, 0.282 mmol, 2.03 equiv) were placed in a Schlenk flask followed by the addition of THF (30 mL). The solution changed colour from orange to green and was stirred for 3 days, at which point the volatiles were removed under reduced pressure, the residue was extracted with approximately 5 mL of hexanes and 2 mL of CH_2Cl_2 , concentrated, and cooled to $-20\text{ }^{\circ}\text{C}$ to provide **3.3** (98.7 mg, 66%) in two crops with an identical UV-vis spectrum ($\lambda_{\text{max}} = 413, 503$ and 584 nm) to the product obtained by salt metathesis from **2.3** and AgO_2CPh . Elemental analysis data for **3.3** has been previously obtained.⁷⁸

Synthesis of $\text{CpCr}[(\text{DppNCMe})_2\text{CH}](\text{O}_2\text{CPh})$ (3.3c**).** Compound **2.1c** (198 mg, 0.370 mmol) and AgO_2CPh (85.7 mg, 0.374 mmol, 1.01 equiv) were placed in a Schlenk flask followed by the addition of THF (15 mL). After stirring overnight, the volatiles were removed under reduced pressure, the residue was extracted with hexanes, and filtered over Celite. The green solution was concentrated to a volume of approximately 2 mL and cooled to $-35\text{ }^{\circ}\text{C}$ to provide black crystals of **3.3c** (106 mg, 43%). Anal. Calcd. for $\text{C}_{35}\text{H}_{41}\text{N}_2\text{CrO}$: C, 75.08; H, 7.84; N, 4.27. Found: C, 74.98; H, 7.95; N, 4.21. UV-vis (hexanes; λ_{max} , nm (ϵ , $\text{M}^{-1}\text{cm}^{-1}$)): 416 (10200), 584 (830).

Synthesis of $\text{CpCr}[(\text{XylNCMe})_2\text{CH}](\text{O}_2\text{CMe})$ (3.4**).** Compound **2.3** (259 mg, 0.566 mmol) and AgO_2CMe (95.2 mg, 0.570 mmol, 1.01 equiv) were placed in a Schlenk flask followed by the addition of THF (20 mL). The mixture was stirred overnight at room temperature in the absence of light, the solvent was evacuated under reduced pressure, and the residue was extracted with 12 mL of a hexanes/dichloromethane mixture (3:1), filtered over Celite and rinsed with hexanes ($3 \times 3\text{ mL}$). The green filtrate was concentrated slightly and cooled to $-20\text{ }^{\circ}\text{C}$ to

provide black crystals of **3.4** (187 mg, 69%) over several days in three crops. Anal. Calcd. for $C_{28}H_{33}N_2O_2Cr$: C, 69.84; H, 6.91; N, 5.82. Found: C, 70.10; H, 6.91; N, 5.86. UV-vis (hexanes; λ_{max} , nm (ϵ , $M^{-1}cm^{-1}$)): 411 (9160), 508 (446), 588 (574).

Synthesis of $CpCr[(XylNCMe)_2CH][OC(=CH_2)Ph]$ (3.5**).** A toluene (1 mL) suspension of $K[OC(=CH_2)Ph]$ (16.9 mg, 0.107 mmol, 1.11 equiv) was reacted with $CpCr[(XylNCMe)_2CH](I)$ (52.9 mg, 0.0963 mmol) dissolved in toluene (4 mL) in a Schlenk flask overnight at room temperature. The solvent was evaporated under reduced pressure, the residue was extracted with hexanes (2 mL), filtered over Celite and cooled to $-35\text{ }^{\circ}C$ for 3 days to yield crystals of **3.5** (5.6 mg, 11%) suitable for X-ray crystallographic analysis. Due to the presence of co-crystallized iodide starting material, satisfactory elemental analysis for **5** was not obtained. UV-vis (hexanes; λ_{max} , nm (ϵ , $M^{-1}cm^{-1}$)): 407 (7600), 607 (500).

Synthesis of $CpCr[(XylNCMe)_2CH](OCMe_3)$ (3.6**).** Compound **2.3** (53.2 mg, 0.116 mmol) was placed in a Schlenk flask followed by the addition of Et_2O (7 mL), and KO^tBu (15.2 mg, 0.135 mmol, 1.17 equiv) suspended in Et_2O (3 mL). After stirring for 4 days, the volatiles were removed under reduced pressure, the residue was extracted with hexanes, and filtered over Celite. The solution was concentrated to a volume of approximately 0.5 mL and cooled to $-35\text{ }^{\circ}C$ to provide black crystals of **3.6** (24.0 mg, 42%) in two crops. Anal. Calcd. for $C_{30}H_{39}N_2CrO$: C, 72.70; H, 7.93; N, 5.65. Found: C, 71.16; H, 7.93; N, 5.58. UV-vis (hexanes; λ_{max} , nm (ϵ , $M^{-1}cm^{-1}$)): 393 (8620), 492 (880), 725 (550).

Synthesis of $CpCr[(XylNCMe)_2CH][OC(Me)_2Ph]$ (3.7**).** Compound **2.3** (59.8 mg, 0.131 mmol) was placed in a Schlenk flask followed by the addition of THF (7 mL). The addition of a 2 mL THF solution of $K[OC(Me)_2Ph]$ (23.2 mg, 0.133 mmol, 1.02 equiv) caused a rapid colour change from green to green-orange. After stirring for 5 days, the volatiles were removed under reduced pressure, the residue was extracted with hexanes, and filtered over Celite. The solution was concentrated to a volume of approximately 0.5 mL and cooled to $-35\text{ }^{\circ}C$ to provide black crystals of **3.7** (50.7 mg, 70%). Anal. Calcd. for $C_{35}H_{41}N_2CrO$: C, 75.38; H, 7.41; N, 5.02. Found: C, 73.81; H, 7.46; N, 5.04. UV-vis (hexanes; λ_{max} , nm (ϵ , $M^{-1}cm^{-1}$)): 395 (8920), 491 (640), 740 (450).

Synthesis of $CpCr[(XylNCMe)_2CH](F)$ (3.8**). Method A.** Compound **2.1** (259.6 mg, 0.614 mmol) and AgF (78.5 mg, 0.619 mmol, 1.01 equiv) were placed in a Schlenk flask, followed by the addition of THF (20 mL). Upon stirring overnight at room temperature, the solution became turquoise in colour, at which point the solvent was removed under reduced pressure, the residue extracted with Et_2O , filtered over Celite, and the solvent was again removed

under reduced pressure. The residue was extracted with a minimum of Et₂O (20 mL) and filtered over Celite. The resulting turquoise solution was cooled to -35 °C to provide black crystals of **3.8** (213 mg, 79%) in three crops. Anal. Calcd. for C₂₆H₃₀N₂CrF: C, 70.73; H, 6.85; N, 6.34. Found: C, 70.40; H, 6.86; N, 6.05. UV-vis (hexanes; λ_{max} , nm (ϵ , M⁻¹cm⁻¹)): 402 (10600), 506 (350), 608 (560).

Method B. Compound **2.6** (205.4 mg, 0.346 mmol) and CsF (59.0 mg, 0.388 mmol, 1.1 equiv) were placed in a Schlenk flask, followed by the addition of THF (18 mL). After stirring for 8 days, the solvent was removed under reduced pressure, the residue extracted with hexanes, filtered over Celite, and the solvent was again removed under reduced pressure. The residue was extracted with a minimum of hexanes (7 mL) and filtered over Celite. The resulting solution was cooled to -35 °C to provide **3.8** (101 mg, 66%) in two crops.

Method C. Compound **2.6** (22.4 mg, 0.038 mmol) and Bu₄N[Ph₃SiF₂] (22.3 mg, 0.041 mmol, 1.1 equiv) were placed in a 1 dram glass vial, followed by the addition of THF (1.5 mL). Upon stirring overnight the solution became turquoise in colour and the UV-vis spectrum of the crude reaction mixture matched that of isolated **3.8**.

Synthesis of CpCr[(XylNCMe)₂CH](BF₄) (3.9). Compound **3.8** (30.1 mg, 0.0682 mmol) was placed in a flask and dissolved in toluene (5 mL). The addition of BF₃·Et₂O (10 μ L, 0.0796 mmol, 1.2 equiv) caused a rapid colour change from green to orange. After stirring for 0.5 h, the volatiles were removed under reduced pressure, the residue extracted with Et₂O (5 mL), and filtered over Celite. The resulting orange solution was cooled to -35 °C to provide black crystals of **3.9** (15.1 mg, 44%) in two crops. Anal. Calcd. for C₂₆H₃₀N₂F₄BCr: C, 61.31; H, 5.94; N, 5.50. Found: C, 54.65; H, 5.75; N, 4.89. UV-vis (Et₂O; λ_{max} , nm (ϵ , M⁻¹cm⁻¹)): 403 (7300), 579 (410).

Synthesis of {CpCr[(DepNCMe)₂CH](OH)}₂ (3.10). CpCr[(DepNCMe)₂CH] (**2.1b**) (50.2 mg, 0.105 mmol) and pyridine *N*-oxide (10.7 mg, 0.113 mmol, 1.1 equiv) were placed in a round bottom flask followed by the addition of benzene (5 mL). The reaction mixture was stirred at room temperature overnight followed by removal of the solvent under reduced pressure. The residue was extracted with hexanes (1 mL), filtered over Celite, and cooled to -35 °C to provide a black microcrystalline solid (17.7 mg) in two crops. A third crop of crystals (4.4 mg, 8%) suitable for X-ray crystallography were isolated and identified as compound **3.10**. UV-vis (hexanes; λ_{max} , nm): 389, 503, 614.

Synthesis of {CpCr[(HIPTNCMe)₂CH]}₂O (3.11). H[(HIPTNCMe)₂CH] (136 mg, 0.129 mmol, 1.06 equiv) was placed in a Schlenk flask, dissolved in THF (5 mL), and cooled to

-35 °C. *n*-BuLi (0.09 mL of 1.6 M solution in hexanes, 0.14 mmol, 1.1 equiv) was added dropwise and the resulting yellow solution was allowed to warm to room temperature while stirring for 0.5 h. In a separate Schlenk flask, CrCl₂ (15.0 mg, 0.122 mmol) was suspended in THF (5 mL) followed by the addition of NaCp (0.7 mL of 2.0 M solution in THF, 0.14 mmol, 1.1 equiv), after stirring at room temperature for 0.5 h the Li[(HIPTNCMe)₂CH] prepared above was added. The resulting green (magenta transmitted) solution was stirred overnight followed by removal of the solvent under reduced pressure. The residue was extracted with hexanes and filtered over Celite followed by the addition of pyridine *N*-oxide (12.2 mg, 0.128 mmol, 1.05 equiv) causing the reaction mixture to turn orange over a period of 5 min. After stirring overnight at room temperature, the solvent was removed under reduced pressure, the residue extracted with hexanes, filtered over Celite, concentrated to a volume of approx. 0.5 mL and cooled to -35 °C to provide a small amount of orange crystalline material (4.5 mg) identified as compound **3.11** by X-ray crystallography. Due to the presence of co-crystallized unidentifiable solvent molecules, satisfactory elemental analysis for **3.11** was not obtained. UV-vis (hexanes; λ_{max} , nm): 371, 475 (sh).

Synthesis of CpCr[(XylNCMe)₂CH](ONPh) (3.12). Compound **2.1** (105.7 mg, 0.250 mmol) was placed in a Schlenk flask and dissolved in THF (10 mL). A THF (2 mL) solution of PhNO (27.5 mg, 0.257 mmol, 1.03 equiv) was added to the Schlenk flask dropwise at room temperature causing a rapid colour change to orange. After stirring overnight, the solvent was removed under reduced pressure, the residue extracted with hexanes (15 mL), and filtered over Celite. The resulting orange solution was cooled to -35 °C to provide black crystals of **3.12** (83.5 mg, 63%). μ_{eff} (Evans, C₆D₆): 2.77 μ_{B} . Anal. Calcd. for C₃₂H₃₅N₃CrO: C, 72.57; H, 6.66; N, 7.93. Found: C, 72.34; H, 6.82; N, 8.23. UV-vis (hexanes; λ_{max} , nm (ϵ , M⁻¹cm⁻¹)): 404 (10100), 461 (7620).

Experimental details for reactions presented in Figure 3.2:

Path A. The synthesis of compound **3.1**, by reacting compound **2.1** with pyridine *N*-oxide, is described above. Alternatively, air exposure of a 1.10×10^{-4} M solution of compound **2.1** in THF rapidly converts to an orange solution with a UV-vis spectrum that is identical to that of authentic **3.1**.

Path B. The synthesis of compound **3.2**, by reacting compound **2.1** with pyridine *N*-oxide and γ -terpinene, is described above. Alternatively, compound **3.2** was prepared by the addition of N₂ sparged H₂O (6.0 μ L, 0.33 mmol, 2.1 equiv) to a THF solution (30 mL) of compound **3.1** (135 mg, 0.157 mmol). Upon stirring overnight at room temperature the solution turned green in

colour at which point the volatiles were removed under reduced pressure. The residue was extracted with hexanes (30 mL), filtered over Celite, and the solution was concentrated and then cooled to $-25\text{ }^{\circ}\text{C}$ to provide a green powder of **3.2** (71 mg, 52%) in two crops with an identical UV-vis spectrum to the product obtained from the reaction of **2.1** with pyridine *N*-oxide and γ -terpinene. X-ray quality crystals of **3.2** could not be obtained by this method.

Path C. The synthesis of compound **3.3**, by reacting compound **3.1** with benzoic acid, is described above.

Path D (X = Cl). Method 1. Compound **3.1** (51.3 mg, 0.060 mmol) and $[\text{HNEt}_3]\text{Cl}$ (16.6 mg, 0.12 mmol, 2.0 equiv) were placed in a Schlenk flask followed by the addition of THF (15 mL). The solution changed colour from orange to green upon stirring for 5 minutes and was stirred overnight at room temperature to ensure the reaction had gone to completion. The UV-vis spectrum of the crude reaction mixture was identical to that of authentic **2.3**. The volatiles were removed under reduced pressure, the residue extracted with Et_2O , filtered over Celite, and the solvent was again removed under reduced pressure. The residue was extracted with a minimum of toluene and then cooled to $-35\text{ }^{\circ}\text{C}$ to provide black crystals of **2.3** (10 mg, 19%).

Method 2. Compound **3.1** (4.6 mg, 0.005 mmol) and MnCl_2 (9.4 mg, 0.075 mmol) were placed in a vial followed by the addition of THF (1 mL). Upon stirring overnight at room temperature, the UV-vis spectrum of the crude reaction mixture confirmed the formation of compound **2.3**.

Path D (X = Br). Compound **3.1** (12.9 mg, 0.015 mmol) and $[\text{HLut}]\text{Br}$ (8.5 mg, 0.045 mmol) were placed in a Schlenk flask followed by the addition of THF (2 mL). The solution changed colour from orange to green upon stirring for 10 minutes and was stirred for 3 days at room temperature to ensure the reaction had gone to completion. The clean conversion to **2.5** was confirmed by UV-vis analysis of the crude reaction mixture.

Path D (X = I). Mn powder (10 mg, 0.18 mmol) and I_2 (4.4 mg, 0.017 mmol) were placed in a 4 mL vial followed by the addition of THF (0.5 mL). The mixture was stirred for 1 h before being filtered over Celite (to remove unreacted Mn powder) into a THF solution (1 mL) of compound **3.1** (4.9 mg, 0.006 mmol). The reaction mixture turned from orange to green upon stirring for 5 days. The clean conversion to $\text{CpCr}[(\text{XylNCMe})_2\text{CH}](\text{I})$ was confirmed by UV-vis analysis of the crude reaction mixture.

Path D (X = OTs). The procedure described above for the preparation of **2.3** (method 1) was followed with compound **3.1** (59.5 mg, 0.069 mmol) and [HCol]OTs (42.6 mg, 0.15 mmol, 2.1 equiv) in THF (15 mL). Upon stirring overnight the UV-vis spectrum of the crude reaction mixture was identical to that of authentic **2.6**.

Path E (R = Ph). Compound **3.2** (33.6 mg, 0.076 mmol) and benzoic acid (13.1 mg, 0.11 mmol, 1.4 equiv) were placed in a Schlenk flask followed by the addition of Et₂O (5 mL). Upon stirring for 5 days, the UV-vis spectrum of the solution was identical to that of authentic **3.3**.

Path F (X = Cl). [HNEt₃]Cl (0.6 mg, 0.004 mmol) was placed in a vial followed by the addition of a THF solution (1 mL) of compound **3.2** (2.0 mg, 0.004 mmol). The reaction mixture changed colour from green to orange to transmitted light over a period of 5 minutes and was stirred overnight at room temperature to ensure the reaction had gone to completion. The clean conversion to compound **2.3** was confirmed by UV-vis analysis of the crude reaction mixture.

Path F (X = Br). [HLut]Br (1.1 mg, 0.006 mmol) was placed in a vial followed by the addition of a THF solution (1 mL) of compound **3.2** (2.0 mg, 0.004 mmol). The reaction mixture changed colour from green to orange to transmitted light over a period of 5 minutes and was stirred overnight at room temperature to ensure the reaction had gone to completion. The clean conversion to compound **2.5** was confirmed by UV-vis analysis of the crude reaction mixture.

Path F (X = I). Mn powder (8 mg, 0.15 mmol) and I₂ (4.4 mg, 0.017 mmol) were placed in a vial followed by the addition of THF (0.5 mL). The mixture was stirred for 1 h before being filtered over Celite (to remove unreacted Mn powder) into a THF solution (1 mL) of compound **3.2** (5.2 mg, 0.012 mmol). The reaction mixture rapidly changed colour from green to orange to transmitted light and was stirred overnight at room temperature to ensure the reaction had gone to completion. The clean conversion to CpCr[(XylNCMe)₂CH](I) was confirmed by UV-vis analysis of the crude reaction mixture.

Path F (X = OTs). [HCol]OTs (2.1 mg, 0.007 mmol) was placed in a vial followed by the addition of a THF solution (1 mL) of compound **3.2** (2.0 mg, 0.004 mmol). The reaction mixture changed colour from green to orange to transmitted light over a period of 5 minutes and was stirred overnight at room temperature to ensure the reaction had gone to completion. The clean conversion to compound **2.6** was confirmed by UV-vis analysis of the crude reaction mixture.

Path G (R = Me, X = Cl). Method 1. Compound **3.4** (4.2 mg, 0.009 mmol) was dissolved in THF (1 mL) followed by the addition of Me₃SiCl (10 μ L of a 1.0 M solution in THF, 0.01 mmol). Upon stirring overnight at room temperature, UV-vis analysis of the crude reaction mixture confirmed the formation of compound **2.3**.

Method 2. Compound **3.4** (10.0 mg, 0.021 mmol) and Cp_2ZrCl_2 (8.1 mg, 0.028 mmol) were dissolved in C_6D_6 (1 mL). The formation of $\text{Cp}_2\text{Zr}(\text{Cl})(\text{OAc})$ was determined by comparison of the ^1H NMR spectrum of the reaction mixture with literature values.¹¹⁸

Path G (R = Me, X = I). Mn powder (13.7 mg, 0.25 mmol) and I_2 (2.3 mg, 0.009 mmol) were placed in a 4 mL vial followed by the addition of THF (1 mL). The mixture was stirred until it became colourless before being filtered over Celite (to remove unreacted Mn powder) into a THF solution (1 mL) of compound **3.4** (4.2 mg, 0.009 mmol). The reaction mixture rapidly turned darker orange in colour to transmitted light and was stirred overnight at room temperature to ensure the reaction had gone to completion. The clean conversion to $\text{CpCr}[(\text{XylNCMe})_2\text{CH}](\text{I})$ was confirmed by UV-vis analysis of the crude reaction mixture.

Path G (R = Me, X = OTs). Compound **3.4** (11.5 mg, 0.024 mmol) and $[\text{HCol}]\text{OTs}$ were placed in a Schlenk flask followed by the addition of THF (4 mL). Upon stirring for 0.75 h, UV-vis analysis of the crude reaction mixture confirmed the formation of **2.6**.

Path H (R = Ph). The synthesis of compound **3.3** was achieved according to the literature procedure, by reacting compound **2.3** with AgO_2CPh .⁷⁸

Path H (R = Me). The synthesis of compound **3.4**, by reacting the Cr(III) chloride compound **2.3** with AgOAc , is described above.

Path I (X = Cl). Compound **2.3** (26 mg, 0.057 mmol), Mn (165 mg, 3.0 mmol, 53 equiv), and PbCl_2 (2 mg, 0.007 mmol, 0.1 equiv) were placed in a Schlenk flask, followed by the addition of THF (4 mL). Upon stirring overnight at room temperature, the solution changed colour from orange to magenta to transmitted light signifying reduction to compound **2.1**. In the absence of PbCl_2 , no reaction was observed over the same time period; determined by UV-vis analysis of the crude reaction mixture.

Path I (X = Br). Compound **2.5** (31.7 mg, 0.063 mmol) and Mn (162 mg, 2.95 mmol, 47 equiv) were placed in a Schlenk flask, followed by the addition of THF (2 mL). The Schlenk flask was then immersed in an oil bath preheated to 35 °C. Upon stirring for 15 h no reaction was observed, at which point the flask was removed from heat and PbBr_2 (~5 mg) was added to the reaction mixture. Upon stirring for 1 h at room temperature, the solution changed colour from orange to magenta to transmitted light signifying reduction to compound **2.1**.

Path I (X = BF_4). Compound **3.9** (5.0 mg, 0.0098 mmol) and Mn powder (7.1 mg, 0.13 mmol, 13 equiv) were placed in a vial, followed by the addition of THF (1 mL). Upon stirring overnight at room temperature, the solution was green (red transmitted) and stirring for an additional 5 days resulted in a further colour change to green (magenta transmitted). The clean

conversion to compound **2.1** was confirmed by UV-vis analysis of the crude reaction mixture. The Cr(III) fluoride compound **3.9** did not react with Mn under the same reaction conditions.

Path J (X = Br). The synthesis of compound **2.5**, by reacting the Cr(II) compound **2.1** with one half equiv of PbBr₂, is described in Chapter 2.

Path J (X = I). The synthesis of CpCr[(XylNCMe)₂CH](I) was achieved according to the literature procedure, by reacting the Cr(II) compound **2.1** with one half equiv of I₂.³⁵

Path K. The synthesis of compounds **3.6** and **3.7**, by reacting the Cr(III) chloride compound **2.3** with the appropriate potassium alkoxide, is described above.

Path L (R' = CMe₂Ph, X = Cl). Method 1. [HNEt₃]Cl (0.9 mg, 0.007 mmol) was placed in a vial followed by the addition of a hexanes solution (1 mL) of compound **3.7** (1.5 mg, 0.003 mmol) and THF (0.5 mL). Upon stirring overnight, the clean conversion to compound **2.3** was confirmed by UV-vis analysis of the crude reaction mixture.

Method 2. Cp₂ZrCl₂ (1.6 mg, 0.006 mmol) was placed in a vial followed by the addition of a hexanes solution (1 mL) of compound **7** (1.5 mg, 0.003 mmol) and THF (0.5 mL). Upon stirring overnight, the clean conversion to compound **2.3** was confirmed by UV-vis analysis of the crude reaction mixture.

Method 3. Compound **3.7** (5.1 mg, 0.009 mmol) was placed in a vial followed by the addition of THF (1.5 mL), Me₃SiCl (11.5 μ L, 0.091 mmol), and H₂O (50 μ L of 0.089 M solution in THF, 0.0044 mmol). Upon stirring for 48 h, the clean conversion to compound **2.3** was confirmed by UV-vis analysis of the crude reaction mixture. Without the addition of H₂O, under otherwise identical conditions, no reaction was observed over the same time period.

Path M. Mn powder (3.5 mg, 0.06 mmol) and I₂ (5.2 mg, 0.02 mmol) were placed in a vial, followed by the addition of THF (1 mL). The mixture was stirred for 1 h before being filtered over Celite (to remove unreacted Mn powder) into a THF solution (1 mL) of compound **3.5** (5.0 mg, 0.009 mmol). Upon stirring for 1 h, the reaction mixture changed colour from green to orange to transmitted light and was stirred overnight at room temperature to ensure the reaction had gone to completion. The clean conversion to CpCr[(XylNCMe)₂CH](I) was confirmed by UV-vis analysis of the crude reaction mixture.

Path N. The synthesis of compound **3.5**, by reacting CpCr[(XylNCMe)₂CH](I) with K[OC(=CH₂)Ph], is described above.

Path O. The synthesis of compound **3.12**, by reacting the Cr(II) compound **2.1** with ONPh, is described above.

Cr(III) fluoride (**3.8**) reactions with silanes:

Me₃SiCl. Compound **3.8** (12.3 mg, 0.028 mmol) was dissolved in a 1.63×10^{-2} M PhCF₃ solution of benzene (~1 mL), followed by the addition of Me₃SiCl (250 μ L of 1.0 M solution in THF, 0.25 mmol, 9.0 equiv). Upon addition of the Me₃SiCl, the solution rapidly changed colour from turquoise to green (orange transmitted) and ¹⁹F NMR analysis of the crude reaction mixture displayed a peak at -158.4 ppm (Me₃SiF).⁹⁵

Et₃SiH. Compound **3.8** (13.3 mg, 0.030 mmol) was dissolved in a 1.63×10^{-2} M PhCF₃ solution of benzene (1 mL), followed by the addition of Et₃SiH (100 μ L, 0.63 mmol, 21 equiv). The reaction mixture was placed in a J. Young tube and heated in a 60 °C oil bath for 41 h. The ¹⁹F NMR spectrum contained only one peak corresponding to the internal reference PhCF₃.

Ph₃SiH. Compound **3.8** (11.7 mg, 0.027 mmol) and Ph₃SiH (206 mg, 0.79 mmol, 30 equiv) were dissolved in a 1.63×10^{-2} M PhCF₃ solution of benzene (1 mL). The reaction mixture was placed in a J. Young tube and heated in a 65 °C oil bath for 190 h. The ¹⁹F NMR spectrum contained only one peak corresponding to the internal reference PhCF₃.

PhSiH₃. Compound **3.8** (13.8 mg, 0.031 mmol) was dissolved in a 1.63×10^{-2} M PhCF₃ solution of benzene (1 mL), followed by the addition of PhSiH₃ (42 μ L, 0.34 mmol, 11 equiv). The reaction mixture was placed in a J. Young tube and heated in a 60 °C oil bath. ¹⁹F NMR spectra of the reaction were obtained periodically to monitor the progress of the reaction over a period of 138 h, during which time the solution changed colour from turquoise to green (magenta transmitted). The final spectrum contained a major peak at -141.9 ppm (s, PhSiF₃)¹¹⁹ and a minor peak at -138.0 ppm (s).

(MeO)₃SiH. Compound **3.8** (15.1 mg, 0.034 mmol) was dissolved in a 1.63×10^{-2} M PhCF₃ solution of benzene (1 mL), followed by the addition of (MeO)₃SiH (40 μ L, 0.31 mmol, 9.2 equiv). The reaction mixture was placed in a J. Young tube and heated in a 65 °C oil bath for 18 h. The clean conversion to the Cr(II) compound **2.1** was confirmed by UV-vis analysis of the crude reaction mixture. ¹⁹F NMR analysis of the crude reaction mixture contained a major peak at -158 ppm (s, (MeO)₃SiF)¹¹⁹ and an unidentified minor product at -138.3 ppm (d).

Si(OMe)₄. Compound **3.8** (14.0 mg, 0.032 mmol) was dissolved in a 1.63×10^{-2} M PhCF₃ solution of benzene (1 mL), followed by the addition of Si(OMe)₄ (40 μ L, 0.27 mmol, 8.6 equiv). The reaction mixture was placed in a J. Young tube and heated in a 60 °C oil bath for 65 h. The ¹⁹F NMR spectrum contained only one peak corresponding to the internal reference PhCF₃.

Reduction of CpCr[(XylNCMe)₂CH](OTs) (2.6) with Na[HBET₃]. Compound **2.6** (24.8 mg, 0.042 mmol) was dissolved in THF (10 mL) and cooled to -35 °C. Addition of Na[HBET₃] (0.045 mL of a 1.0 M solution in THF, 0.045 mmol, 1.1 equiv) caused a colour change from green (orange transmitted) to green (magenta transmitted) over a period of 15 min while stirring. The clean conversion to the Cr(II) compound **2.1** was confirmed by UV-vis analysis of the crude reaction mixture.

Reaction of CpCr[(XylNCMe)₂CH](I) with Et• radicals. Compound CpCr[(XylNCMe)₂CH](I) (11.0 mg, 0.020 mmol) was dissolved in hexanes (3 mL), followed by the addition of BEt₃ (0.22 mL of a 1.0 M solution in hexanes, 0.22 mmol, 11 equiv). Air (4 mL, 0.036 mmol O₂, 1.8 equiv O₂) was bubbled through the solution while stirring, causing a rapid colour change from green (orange incident) to purple. UV-vis analysis of the crude reaction mixture confirmed the formation of CpCr[(XylNCMe)₂CH](Et). Under identical reaction conditions, no reaction was observed with the Cr(III) chloride (**2.3**) and bromide (**2.5**) compounds.

Reaction of 3.8 with Et• radicals. Compound **3.8** (10.1 mg, 0.23 mmol) was dissolved in hexanes (3 mL), followed by the addition of BEt₃ (0.22 mL of a 1.0 M solution in hexanes, 0.22 mmol, 9.6 equiv). Air (4 mL, 0.036 mmol O₂, 1.8 equiv O₂) was bubbled through the solution while stirring, causing a rapid colour change from turquoise to purple.

Reaction of compound 2.1 with Ph₃CCl. Compound **2.1** (29.9 mg, 0.071 mmol) and Ph₃CCl (10.1 mg, 0.036 mmol, 0.51 equiv) were dissolved in THF (8 mL). The green (red transmitted) solution was stirred at room temperature overnight, followed by the addition of an additional 11.4 mg of Ph₃CCl (0.041 mmol, 0.58 equiv), which caused a rapid colour change to green (orange transmitted). The UV-vis spectrum of the crude reaction mixture contained 3 absorption bands: 419 nm and 577 nm (compound **2.3**), and 514 nm (Ph₃C• radical).⁹⁹

Synthesis of Ph₃CF. Compound **3.8** (15.2 mg, 0.0344 mmol), Ph₃CCl (11.9 mg, 0.0427 mmol, 1.2 equiv), and compound **2.1** (0.2 mg, 0.0005 mmol, 0.01 equiv) were dissolved in a 1.63 × 10⁻² M PhCF₃ solution of benzene (1 mL). The reaction mixture was placed in a J. Young tube and heated in a 50 °C oil bath. ¹⁹F NMR spectra of the reaction were obtained periodically to monitor the progress of the reaction over a period of 9 days, during which time the solution changed colour from turquoise to green (orange transmitted). The final spectrum contained a singlet at -126.9 ppm corresponding to Ph₃CF (87% yield).¹⁰⁰ The UV-vis spectrum of the crude reaction mixture contained absorption bands at 419 and 582 nm, corresponding to compound **2.3**.

Under identical reaction conditions, no reaction was observed with organic halides $\text{Me}_3\text{CH}_2\text{I}$, $c\text{-C}_6\text{H}_{11}\text{Cl}$, $c\text{-C}_6\text{H}_{11}\text{I}$, or $\text{PhC}(\text{Me})\text{Br}$.

PPh₃ reactions:

Ph₃PI₂ reaction. Compound **3.1** (12.2 mg, 0.014 mmol) was dissolved in CDCl_3 (0.75 mL) followed by the addition of Ph_3PI_2 (7.3 mg, 0.014 mmol, 1.0 equiv) causing a rapid colour change from orange to green. The ^{31}P NMR spectrum displayed a single peak at ~30 ppm corresponding to OPPh_3 . The clean conversion to $\text{CpCr}[(\text{XylNCMe})_2\text{CH}](\text{I})$ was confirmed by UV-vis analysis of the crude reaction mixture.

PPh₃ oxidation with O₂. Compound **2.1b** (17.9 mg, 0.0374 mmol) and PPh_3 (537 mg, 2.05 mmol, 55 equiv) were placed in a 25 mL Schlenk flask followed by the addition of hexanes (8 mL). The reaction mixture was frozen by submersing the reaction vessel in liquid N_2 and the headspace was evacuated under reduced pressure followed by the addition of O_2 (1 atm). The reaction mixture was allowed to warm to room temperature while stirring. The reaction was allowed to stir for 20 h at which point the precipitate was collected and rinsed with hexanes to afford OPPh_3 (169.5 mg, 20 TON) as determined by comparison with the literature ^1H and ^{31}P NMR spectra.

PPh₃ oxidation with air. Compound **2.1b** (5.0 mg, 0.010 mmol) and PPh_3 (17.0 mg, 0.065 mmol, 6.5 equiv) were dissolved in C_6D_6 (0.5 mL). A ^{31}P NMR spectrum was acquired using a J. Young tube after which the reaction mixture was exposed to air and the progress of the reaction was monitored by ^{31}P NMR until complete conversion to OPPh_3 was observed (~10 minutes) with the growth of a single peak at 27 ppm.

Catalytic HAT reactions: general procedure for product isolation. Upon completion, the reactions were concentrated under reduced pressure, diluted with hexanes/EtOAc (5%), filtered over Celite and concentrated under reduced pressure. The residual green liquid was subjected to silical gel chromatography with hexanes/EtOAc (5%) as eluent to remove the Cr, providing a colourless liquid composed of a mixture of the starting material γ -terpinene and the desired product *p*-cymene. Conversion was determined by comparison of the relative integration values in the ^1H NMR spectrum.

Table 3.1, entry 1. Mn powder (228 mg, 4.15 mmol, 4.15 equiv) and I_2 (12.2 mg, 0.048 mmol, 0.05 equiv) were placed in a Schlenk flask followed by the addition of THF (4 mL). The reaction mixture was allowed to stir at room temperature for 0.5 h followed by the addition of compound **2.1b** (47.1 mg, 0.098 mmol, 0.01 equiv), γ -terpinene (160 μL , 1.00 mmol), and pyridine *N*-oxide (195 mg, 2.05 mmol, 2 equiv). The reaction mixture was allowed to stir

overnight resulting in the formation of a large amount of pale green precipitate, consistent with the formation of Mn oxides. Typical workup provided a colourless liquid composed of a mixture of γ -terpinene and *p*-cymene (6% conversion).

Table 3.1, entry 1 control experiment. Mn powder (71 mg, 1.3 mmol) and pyridine *N*-oxide (54 mg, 0.57 mmol) were placed in a Schlenk flask followed by the addition of THF (1 mL). No reaction was observed upon stirring overnight at room temperature. The addition of I₂ (9.1 mg, 0.04 mmol) resulted in the formation of a large amount of pale green precipitate within 5 minutes.

Table 3.1, entry 2. Mn powder (209 mg, 3.80 mmol, 3.70 equiv) and PbCl₂ (5.0 mg, 0.018 mmol, 0.02 equiv) were placed in a Schlenk flask followed by the addition of THF (4 mL), compound **2.1b** (46.8 mg, 0.098 mmol, 0.01 equiv), γ -terpinene (165 μ L, 1.03 mmol), and pyridine *N*-oxide (193 mg, 2.02 mmol, 2 equiv). The reaction mixture was allowed to stir for 24 h (no pale green precipitate was observed) followed by the typical workup to provide a colourless liquid composed of a mixture of γ -terpinene and *p*-cymene (6% conversion).

Table 3.1, entry 3. Mn powder (116 mg, 2.11 mmol, 4.8 equiv) and compound **2.3b** (22.3 mg, 0.043 mmol, 0.10 equiv) were placed in a Schlenk flask followed by the addition of THF (3 mL), and Me₃SiCl (275 μ L, 2.17 mmol, 5.0 equiv). The reaction was allowed to stir overnight resulting in a colour change of the solution from orange to magenta to transmitted light, signifying the reduction of compound **2.3b** to the Cr(II) compound **2.1b**. γ -Terpinene (70 μ L, 0.44 mmol), and a THF solution (1 mL) of pyridine *N*-oxide (91.9 mg, 0.97 mmol, 2.2 equiv) were added and the reaction was allowed to stir for 3 days resulting in the formation of a large amount of pale green precipitate. Typical workup provided a colourless liquid composed of a mixture of γ -terpinene and *p*-cymene (4% conversion).

Table 3.1, entry 4. Compound **2.3b** (27.1 mg, 0.053 mmol, 0.05 equiv), PbCl₂ (4.0 mg, 0.014 mmol, 0.01 equiv), Mn powder (122 mg, 2.22 mmol, 2.2 equiv), THF (3 mL), and γ -terpinene (165 μ L, 1.03 mmol) were added to a Schlenk flask. Upon stirring overnight the solution changed colour from orange to magenta to transmitted light. Seven aliquots of O₂ (0.56 mL, 0.025 mmol) were periodically bubbled through the reaction mixture over a period of 5 days. Typical workup provided a colourless liquid composed of a mixture of γ -terpinene and *p*-cymene (5% conversion).

Table 3.1, entry 5. Compound **2.3b** (20.7 mg, 0.040 mmol, 0.09 equiv), Mn powder (114 mg, 2.08 mmol, 4.8 equiv), THF (3.5 mL), Me₃SiCl (275 μ L, 2.17 mmol, 5.0 equiv) and γ -terpinene (70 μ L, 0.44 mmol) were added to a Schlenk flask. Upon stirring for 4.5 h the solution

changed colour from orange to magenta to transmitted light at which point the headspace of the Schlenk was flushed with O₂ (1 atm) and the reaction was allowed to stir for 18 h. Typical workup provided a colourless liquid composed of a mixture of γ -terpinene and *p*-cymene (14% conversion).

Table 3.1, entry 6. Compound **2.3b** (46.2 mg, 0.090 mmol, 0.21 equiv), Mn powder (128 mg, 2.33 mmol, 5.4 equiv), THF (3 mL), Me₃SiCl (275 μ L, 2.17 mmol, 5.0 equiv), and γ -terpinene (70 μ L, 0.44 mmol) were added to a Schlenk flask. Upon stirring for 1.5 h the solution changed colour from orange to magenta to transmitted light at which point ten aliquots of O₂ (1.00 mL, 0.045 mmol) were periodically bubbled through the reaction mixture over a period of 4 days. Typical workup provided a colourless liquid composed of a mixture of γ -terpinene and *p*-cymene (8% conversion).

Table 3.1, entry 7. Compound **2.3b** (45.2 mg, 0.088 mmol, 0.11 equiv), Zn powder (543 mg, 8.30 mmol, 10 equiv), THF (3.5 mL), Me₃SiCl (615 μ L, 4.86 mmol, 6.0 equiv) and γ -terpinene (130 μ L, 0.81 mmol) were added to a Schlenk flask. Upon stirring for 5 minutes the solution changed colour from orange to magenta to transmitted light at which point the headspace of the Schlenk was flushed with O₂ (1 atm) and the reaction was allowed to stir for 17 h. Typical workup provided a colourless liquid composed of a mixture of γ -terpinene and *p*-cymene (22% conversion).

Table 3.1, entry 8. Compound **2.3b** (50.4 mg, 0.098 mmol, 0.12 equiv), Zn powder (227 mg, 3.47 mmol, 4.3 equiv), PbCl₂ (5.0 mg, 0.018 mmol, 0.02 equiv), THF (4 mL), and γ -terpinene (130 μ L, 0.81 mmol) were added to a Schlenk flask. Upon stirring for 2 h the solution changed colour from orange to magenta to transmitted light at which point the reaction was cooled in liquid N₂ and the headspace was evacuated under reduced pressure followed by the addition of O₂ (1 atm). The reaction was allowed to warm to room temperature and stirred for 48 h. Typical workup provided a colourless liquid composed of a mixture of γ -terpinene and *p*-cymene (25% conversion).

Table 3.1, entry 9. Compound **2.3b** (22.9 mg, 0.045 mmol, 0.10 equiv), Zn powder (144 mg, 2.20 mmol, 5.0 equiv), THF (3 mL), Me₃SiCl (275 μ L, 2.17 mmol, 5.0 equiv), NEt₃ (300 μ L, 2.15 mmol, 5.0 equiv), and γ -terpinene (70 μ L, 0.44 mmol) were added to a Schlenk flask. Upon stirring for 15 minutes the solution changed colour from orange to magenta to transmitted light at which point the headspace of the Schlenk was flushed with O₂ (1 atm) and the reaction was allowed to stir for 1.25 h. Typical workup provided a colourless liquid composed of a mixture of γ -terpinene and *p*-cymene (50% conversion).

Table 3.1, entry 10. Zn powder (145 mg, 2.22 mmol, 5.1 equiv), THF (3 mL), Me₃SiCl (275 μ L, 2.17 mmol, 5.0 equiv), NEt₃ (300 μ L, 2.15 mmol, 5.0 equiv), and γ -terpinene (70 μ L, 0.44 mmol) were added to a Schlenk flask. The headspace of the Schlenk was flushed with O₂ (1 atm) and the reaction was allowed to stir for 1.25 h. Typical workup provided a colourless liquid composed of a mixture of γ -terpinene and *p*-cymene (40% conversion). The high conversion observed in this reaction was achieved without a Cr catalyst and the presence of Cr in entry 9 resulted in only a 10% improvement in the conversion of γ -terpinene to *p*-cymene.

Reaction of compound 3.12 with H atom sources:

γ -Terpinene. Compound **3.12** (5.0 mg, 0.0094 mmol) was dissolved in THF (3 mL) followed by the addition of γ -terpinene (16 μ L, 0.10 mmol, 11 equiv). The reaction mixture was placed in a Teflon stoppered thick-walled glass reaction vessel that was immersed in an oil bath preheated at 50 °C. Upon stirring for 22 days, the UV-vis spectrum of the reaction mixture displayed absorption bands at 389 and 614 nm, and a shoulder at 500 nm.

C₅H₆. Compound **3.12** (4.7 mg, 0.0089 mmol) was dissolved in THF (3 mL) followed by the addition of C₅H₆ (16 μ L, 0.19 mmol, 21 equiv). The reaction mixture was placed in a Teflon stoppered thick-walled glass reaction vessel that was immersed in an oil bath preheated at 50 °C. Upon stirring for 16 h, the UV-vis spectrum of the reaction mixture was identical to that of the reaction between compound **3.12** and γ -terpinene described above.

Bu₃SnH. Compound **3.12** (2.3 mg, 0.0043 mmol) was dissolved in THF (2 mL) followed by the addition of Bu₃SnH (24 μ L, 0.091 mmol, 21 equiv). Upon stirring at room temperature for 3 days, the UV-vis spectrum of the reaction mixture was identical to that of the reaction between compound **3.12** and γ -terpinene described above.

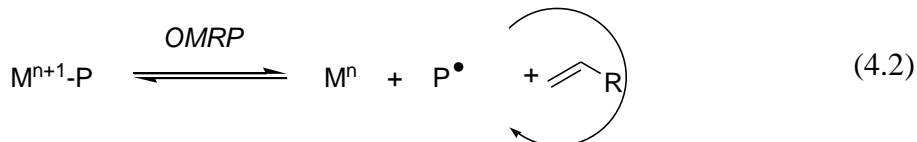
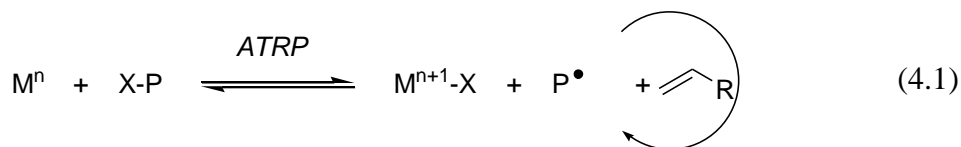
PhSiH₃. Compound **3.12** (2.3 mg, 0.0043 mmol) was dissolved in THF (2 mL) followed by the addition of PhSiH₃ (12 μ L, 0.097 mmol, 22 equiv). The reaction mixture was placed in a Teflon stoppered thick-walled glass reaction vessel and stirred for 3 days at room temperature, at which point the reaction vessel was immersed in an oil bath preheated at 50 °C. Upon stirring for an additional 2 days, the solution had turned green and was stirred for an additional 2 days to ensure the reaction had gone to completion. The UV-vis spectrum of the reaction mixture displayed absorption bands at 401 and 626 nm.

General procedure for X-ray crystallography. Protocols were identical to those reported in section 2.13.

Structure details. The Cp and hydroxide ligands of compound **3.2** are disordered and were subsequently modeled in two orientations. For compounds **3.4** and **3.5**, data were corrected for absorption effects using the multi-scan technique (TWINABS).⁷² Compound **3.4** and compound **3.5** both crystallize as a two-component split crystal with the two components related by a 51° rotation about the (0 0 1) real axis for **3.4** and a 33° rotation about the (1 0 0) real axis for **3.5**. The data were integrated for both twin components, including both overlapping and non-overlapping reflections. The structures were both solved by using non-overlapped data from the major twin component. Subsequent refinements were carried out using the HKLF 5 format data set, containing complete data from component 2 and any overlapped reflections from component 1 for **3.4**, and complete data from component 1 and any overlapped reflection from component 2 for **3.5**. The batch scale refinement showed a roughly 53:47 ratio between the major and minor twin components for **3.4**, and a roughly 82:18 ratio between the major and minor twin components for **3.5**. Additionally, structural refinements indicated that compound **3.5** co-crystallizes with 10.1% CpCr[(XylNCMe)₂CH](I) starting material in the crystal lattice. Compound **3.10** crystallizes with two independent molecules in the asymmetric unit, each residing on a two-fold axis of rotation. Compound **3.11** crystallizes with unresolvable residual electron density, likely from disordered solvent in the lattice. The structure was refined without modeling any solvent molecules, then the PLATON/SQUEEZE⁷⁰ program was employed to search the cell for solvent accessible voids, and then to correct the X-ray diffraction data to eliminate any residual electron density found in those voids. The result from this procedure removed 840 residual electron density from the unit cell, or approximately 210 electrons per asymmetric unit. Since it is not possible to properly identify the solvent, the values for the formula weight, etc, reflect only those atoms found in the atom list. The nitrosobenzene ligand of compound **3.12** is disordered and was subsequently modeled in two orientations. All non-hydrogen atoms in compound **3.12**, except C27B, were refined anisotropically.

Chapter 4 Controlled Radical Polymerization of Vinyl Acetate

There is a delicate balance that must be achieved in metal-mediated CRP in order to obtain polymers with desirable properties.²⁹ In the case of ATRP, changing the redox potential of the metal centre will affect the BDE of metal–halide species, thereby causing a shift in the ATRP equilibrium (eq 4.1). If the equilibrium lies too far to the side of the $M^{n+1}X$ species then the polymerization process is uncontrolled. On the contrary, if the metal complex is mostly in the reduced state then the polymer chains remain largely capped and no polymerization is achieved. Steric effects play a larger role in OMRP systems, where the growing polymer radical intermediates bind directly to the metal centre (eq 4.2). In this case, strong M–C bonds may cause the equilibrium to lie too far to the side of the dormant polymer chains, where polymer chain growth can not occur at any appreciable rate. If the M–C bonds are too weak then the metal complex is not able to control the polymerization process. In the case of copper systems, the M–C bonds are too weak to control the growth by OMRP and therefore ATRP conditions are the only way to provide controlled chain growth.¹²⁰ Interestingly, many of the reported systems actually control chain growth by both ATRP and OMRP processes, if M–X bonds are available.¹²¹



Despite the recent advancements in CRP, controlling the polymerization of vinyl acetate (VAc) remains challenging due to the high-energy radical intermediates present during the polymerization process compared to other monomers.¹²² The OMRP of VAc with cobalt has provided the best results, recently achieving M_w/M_n values below 1.1, despite the complexities of the Co(II)/Co(III) redox couple, which exhibit a range of termination and chain transfer steps that are dependent on the spin state of the Co species and the degree of solvent coordination.¹²³ The use of CpCr β -diketiminates would provide a potentially simplified system for studying the polymerization of VAc due to the high-spin nature of the compounds and the lack of solvent

coordination. Indeed, collaboration between the Smith and Poli research groups resulted in the development of a Cr based system for the polymerization of vinyl acetate, making use of the Cr(II) compounds **2.1** – **2.1c**.³⁴ Compound CpCr[(XylNCMe)₂CH] (**2.1**) was found to control the polymerization of VAc with the use of the radical azo initiator 2,2'-azobis(4-methoxy-2,4-dimethylvaleronitrile) (V-70) to initiate the reaction (VAc/V-70/**2.1** = 500:0.8:1) upon heating to 50 °C for 4 h and then 90 °C for an additional 4 h, providing 11% conversion of the monomer. Unfortunately, further heating for 66 h at 90 °C did not lead to further polymer growth. Characterization of the poly(vinyl acetate) (PVAc) by size exclusion chromatography (SEC) revealed an $M_w/M_n = 1.81$ and a number average molecular weight $M_n = 11500$ compared to the theoretical value $M_{n(th)} = 4730$. The discrepancy between the observed and expected M_n values is indicative of low initiator efficiency.

The more sterically hindered CpCr[(DppNCMe)₂CH] (**2.1c**), under identical reaction conditions as **2.1**, led to an increased conversion of 34% after 84 h. While the M_w/M_n decreased throughout the reaction reaching a value of 1.21 for the final sample, the M_n was again much greater than expected (54800 vs 14600).⁵⁴ Interestingly, compound **2.1c** provided much higher conversions (70%) when conducted under milder reaction conditions (30 °C) after only 46 h.³⁴ The increased monomer conversion at lower temperatures suggested that a thermally accessible mechanism was only operational at higher temperatures, leading to lower monomer conversion, likely a result of a deactivation process.

The work presented herein focuses on the issues of poor initiator efficiency and thermal deactivation. The well-defined Cr(III) hydrocarbyl compounds presented in Chapter 2 were tested as polymerization initiators for OMRP of VAc. The Cr containing product of thermal deactivation was isolated and structurally characterized. Additionally, ATRP and reverse ATRP conditions were established for the polymerization of VAc. Stoichiometric reactions were also conducted with various polymerization initiators and model substrates to address low initiator efficiencies, and to probe the interplay between OMRP and ATRP for this system.

4.1 A Single-Component Chromium Reagent for OMRP

In light of the kinetics studies presented in Chapter 2, two compounds were identified as potential single-component OMRP mediators. Both the Cr(III) neopentyl (**2.11**) and benzyl (**2.14**) compounds exhibit appreciable rates of Cr–C bond homolysis at room temperature with similar rate constants of $3.6(3) \times 10^{-3}$ and $3.2(5) \times 10^{-3} \text{ s}^{-1}$, respectively, and yet can be readily synthesized and isolated as stable crystalline compounds on a preparative scale. The reaction

half-lives for the Cr–C bond cleavage are 3.2 and 3.6 min, respectively. By comparison, the reaction half-life of the azo initiator V-70 of 36 min¹²⁴ under the previously reported reaction conditions (50 °C)⁵⁴ is an order of magnitude longer than compounds **2.11** and **2.14**. Short initiation periods are the key to ensuring that polymer chains of uniform molecular weight are generated at the beginning of the polymerization process to minimize molecular weight distributions.¹²⁵ Organometallic initiators in general provide an advantage over two-component systems that use a separate radical initiator and transition metal mediating species. The nature of an organometallic initiator dictates that the radical is generated simultaneously with the transition metal trapping species, in the same location and in equal amounts, as shown in Figure 4.1. Therefore, the OMRP equilibrium is established from the very beginning of the reaction and the radical initiator and transition metal trapping species are generated in exactly a 1:1 ratio, while two component initiator/trap systems require induction periods before reaching equilibrium.³⁰ Although single-component organometallic initiator/trap systems present a clear advantage over two component systems they remain under explored, with only two previously reported examples of organocobalt systems, both of which operate at elevated temperatures (50–60 °C) for the production of poly(methyl acrylate) (PMA).¹²⁶

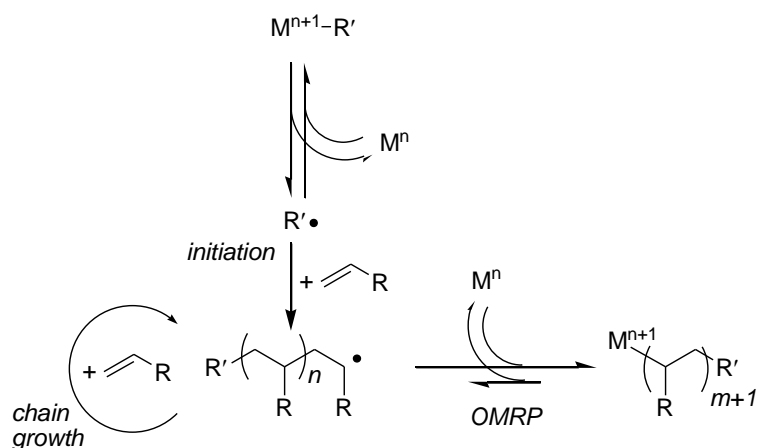


Figure 4.1. Initiation and controlled polymerization with a single-component organometallic species

The Cr(III) neopentyl compound **2.11** was found to effectively initiate the polymerization of VAc at room temperature. In the presence of 1200 equivalents of monomer, compound **2.11** produced PVAc up to 14% monomer conversion after 400 h ($M_n = 16200$ vs $M_{n(th)} = 15100$, $M_w/M_n = 1.46$). There is no visible induction period for the polymerization (Figure 4.2a) indicating fast initiation, consistent with the observed Cr–C bond homolysis of compound **2.11**. In contrast to the results obtained with V-70 initiator, the PVAc obtained from **2.11** displays

good agreement between the observed and theoretical molecular weight values (Figure 4.2b), indicating high initiator efficiency. However, the rate of conversion slowed over time, as can be seen in Figure 4.2a, suggesting that deactivation of the growing polymer chains occurs slowly under the reaction conditions, which also leads to broad molecular weight distributions.

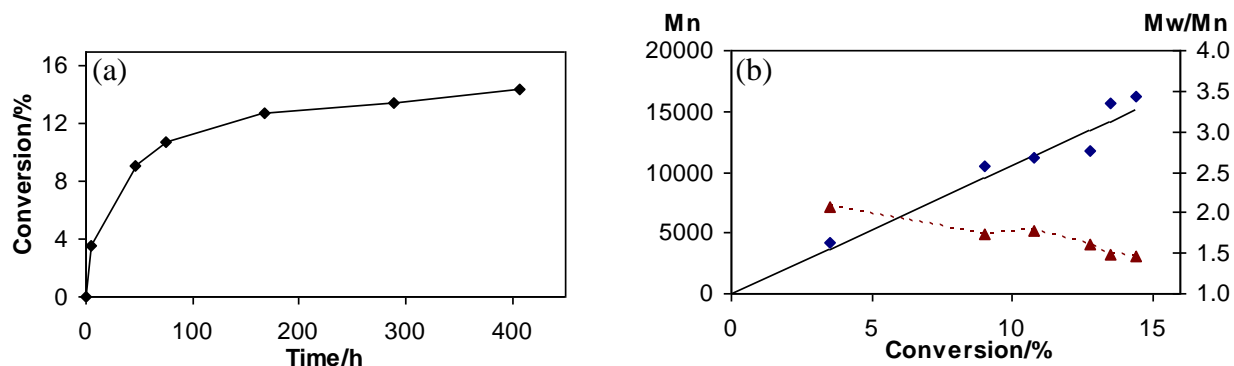


Figure 4.2. (a) Conversion as a function of time for the VAc polymerization initiated by compound **2.11**. Conditions: VAc/**2.11** = 1200:1. T = room temp. (b) Variation of the M_n (diamonds) and M_w/M_n (triangles) as a function of conversion, the solid line represents $M_{n(th)}$.

Despite the similarities between the Cr–C bond homolysis rate constants for the Cr(III) neopentyl (**2.11**) and benzyl (**2.14**) compounds, **2.14** was not an efficient radical initiator for OMRP of VAc due to stabilization of the benzyl radical compared to the much more reactive neopentyl radical. While the rate constant for methyl radicals reacting with VAc is $1.4 \times 10^4 \text{ M}^{-1}\text{s}^{-1}$, the benzyl radical is 3 orders of magnitude less at $14 \text{ M}^{-1}\text{s}^{-1}$,¹²⁷ owing to the poor initiation of VAc with compound **2.14**. To demonstrate the importance of Cr–C bond homolysis for initiation and control of the polymerization process, the Cr(III) methyl (**2.2**) and phenyl (**2.15**) compounds were also tested as initiators for VAc polymerization.

As expected, the Cr(III) phenyl compound **2.15**, it did not initiate polymerization of VAc, even at elevated temperatures (55 °C for 48 h). When the Cr(III) methyl analogue **2.2** was subjected to polymerization reaction conditions by dissolving 16.1 mg of **2.2** in 4 mL of VAc, only 9% monomer conversion was observed after 48 h at room temperature. The PVAc had both high M_n (83900 compared to $M_{n(th)} = 9140$) and high $M_w/M_n = 3.4$. The broad molecular weight distribution and large disparity between expected and observed molecular weights is consistent with the slow release of Me· radicals into solution, which rapidly react with the VAc monomer. In addition, absorption bands in the UV-vis spectrum of the reaction mixture were identifiable as those of compound **2.2**, even after the 48 h reaction time, indicating that most of the Cr(III) methyl compound remained unreacted. When the experiment was repeated with the exclusion of

light, no PVAc was produced, a result of the established photosensitivity of the Cr(III) hydrocarbyl compounds with respect to Cr–C bond homolysis. These results clearly support that the fast rate of Cr–C bond homolysis in compound **2.11**, to generate highly reactive neopentyl radicals and one equivalent of the corresponding Cr(II) species **2.1**, is the reason that compound **2.11** is able to function effectively as a single-component OMRP reagent for the polymerization of VAc.

UV-visible spectroscopic analysis of the polymerization reaction of VAc with compound **2.11** revealed significant changes in the spectrum after 10 min, displaying absorption bands at 422 and 556 nm (Figure 4.3b), indicating that compound **2.11** had initiated the polymerization. The peaks observed in the UV-vis spectrum were presumably Cr-capped dormant polymer chains of the form $\text{CpCr}[(\text{XylNCMe})_2\text{CH}](\text{PVAc})$. After 400 h of polymerization the high energy absorption band had shifted to 412 nm, while the 556 nm band had decreased slightly in intensity (Figure 4.3c), in conjunction with the observed decrease in rate of polymerization. The polymerization reaction mixture was then heated to 70 °C for 3.5 h to produce a colour change

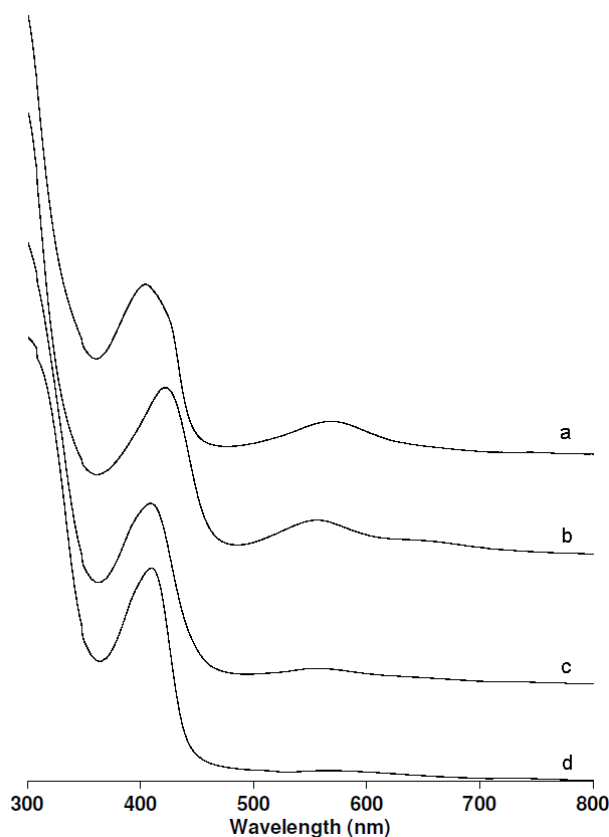


Figure 4.3. Evolution of the UV-vis properties during the VAc polymerization controlled by compound **2.11** (conditions as shown in Figure 4.2). (a) Initial spectrum of compound **2.11**; (b) after 10 min of polymerization; (c) after 400 h of polymerization; (d) after warming to 70 °C (spectrum of the decomposition product).

from purple to green (orange transmitted), with the higher energy absorption band increasing in intensity and the low energy band (556 nm) being replaced by a much less intense band at 575 nm (Figure 4.3d). The results of the thermal decomposition suggested there was still Cr-capped PVAc after 400 h, despite the significant decrease in the rate of polymerization.

Perhaps the most striking difference between the single-component polymerization process with compound **2.11** and the two component azo initiated (**2.1**/V-70) polymerization experiments is the difference in monomer conversion. The V-70 system reached a plateau of 11% conversion after only 4 h at 50 °C and did not lead to further conversion at elevated temperatures,⁵⁴ while the single-component system, although slow, showed continued growth over the entire 400 h polymerization process. This demonstrates that initiation and reversible trapping of the growing polymer chain can be achieved at room temperature, but at elevated temperatures there is a deactivation process that leads to rapid deactivation of growing polymer chains.

Extension of the polymerization protocol established with compound **2.11** to styrene led to the formation of polymers with large molecular weight distributions, signifying uncontrolled radical polymerization. Both the steric and electronic properties of radical polystyrene (PS) chains prevent the Cr(II) from effectively controlling the polymerization process. The highly stable secondary-benzylic radicals of the growing PS chains remain in high concentrations during polymerization, as shown by the equilibrium in Figure 4.4, leading to free radical

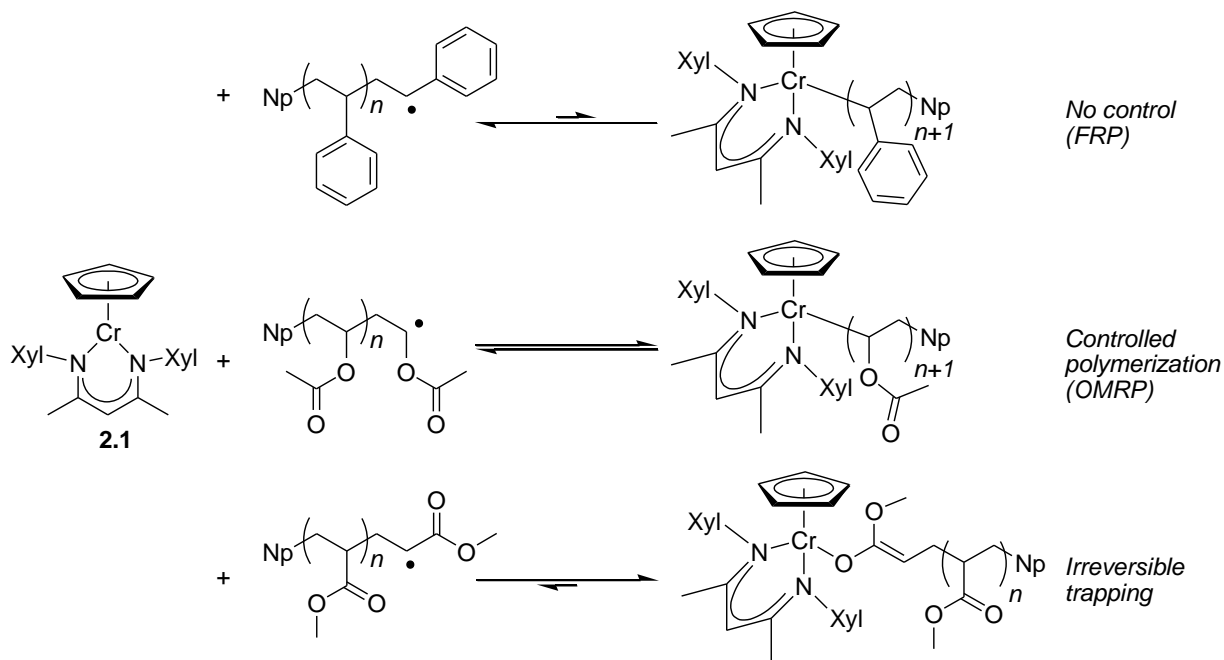


Figure 4.4. Comparison of the radical polymerization of styrene, VAc, and MA using compound **2.11** as initiator.

polymerization (FRP) conditions, despite the presence of the Cr(II).

Compound **2.11** was also ineffective at moderating the radical polymerization of methyl acrylate (MA). Upon radical initiation of MA by compound **2.11**, the short chains are irreversibly trapped by the Cr(II), presumably forming an O-bound Cr(III) enolate complex (discussed in section 4.5). Interestingly, this process also resulted in uncontrolled polymerization due to the highly reactive nature of the MA monomer, which will polymerize upon standing at room temperature without addition of external initiator.

4.2 Identification of the Deactivated Complex, and Mechanistic Implications

From the UV-vis analysis discussed above, compound **2.11** reacted in neat vinyl acetate to initiate polymerization causing a change in the UV-vis spectrum, and subsequent heating produced a further change in the spectrum to an unknown Cr species. To determine the identity of the Cr, the unreacted monomer was removed from the reaction mixture under reduced pressure, followed by extraction of the Cr species from the PVAc with diethyl ether. The highly coloured extracts signified that the Cr was not covalently bound to the insoluble polymeric material. The deeply coloured nature of the extracts also suggested that the Cp and/or β -diketiminato ligands remained bound to the Cr. Upon cooling the green (orange transmitted) solution at $-35\text{ }^{\circ}\text{C}$, X-ray quality crystals were obtained. Structural analysis identified the material as the Cr(III) acetate complex $\text{CpCr}[(\text{XylNCMe})_2\text{CH}](\text{O}_2\text{CMe})$ (**3.4**), as shown in Figure 4.5, corresponding to a 23% isolated yield based on Cr. Compound **3.4** was independently synthesized by reaction of the Cr(III) chloride precursor **2.3** with AgO_2CMe (Chapter 3), with UV-vis analysis confirming that **3.4** was the major decomposition product formed in the heated polymerization reaction.

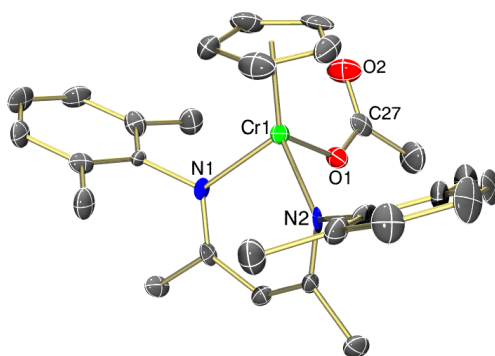


Figure 4.5. Thermal ellipsoid diagram (50%) of **3.4**. All H atoms are omitted for clarity.

Somewhat surprisingly, compound **3.4** displays a Cr–O bond length that does not differ significantly from that of the benzoate compounds **3.3** or **3.3c** (see Table 4.1). Conversely, the Cr–N bonds of **3.3c** appear to lengthen slightly compared to **3.3** and **3.4**, as a means of alleviating steric strain in the molecule, a feature also observed with the μ -oxo compound **3.1**. The Cr–O–C angle in the two benzoate compounds is ~ 4 degrees larger than the acetate analogue, owing to the increased steric requirements of the benzoate ligand.

Table 4.1. Selected bond lengths (Å) and bond angles (deg) for complexes **3.3**, **3.3c**, and **3.4**.

	3.3	3.3c	3.4
Cr–N(1)	2.0079(14)	2.0233(18)	2.010(5)
Cr–N(2)	2.0125(14)	2.0359(19)	2.004(6)
Cr–O(1)	1.9355(12)	1.9309(15)	1.952(5)
O(1)–C	1.286(2)	1.299(3)	1.278(9)
O(2)–C	1.221(2)	1.227(3)	1.230(9)
O(1)–C–O(2)	125.69(16)	126.0(2)	124.9(7)
O(1)–C–C	113.82(14)	113.3(2)	115.2(7)
O(2)–C–C	120.49(15)	120.7(2)	119.9(7)
Cr–O(1)–C	138.26(11)	137.99(15)	133.6(5)

To further study the mechanism of formation of the acetate compound **3.4** during polymerization, the Cr(II) compound **2.1** was stirred with commercially obtained PVAc while heating to 50 °C for 24 h, during which time no reaction was observed. Compound **2.1** was also treated with VAc under similar conditions. In both cases the UV-vis spectrum of the reaction mixtures indicated the presence of unreacted **2.1**, thereby precluding the formation of the acetate compound **3.4** by a simple oxidative addition from alkyl or vinyl acetate species. These results suggested a more complicated mechanism for the formation of compound **3.4**. The proposed mechanism for the formation of **3.4** is that of 2,1-insertion (head-to-head) of the VAc monomer during chain growth, leading to β -acetate elimination, as shown in Figure 4.6. Head-to-head insertion is well documented for the radical polymerization of vinyl acetate, a result of the high

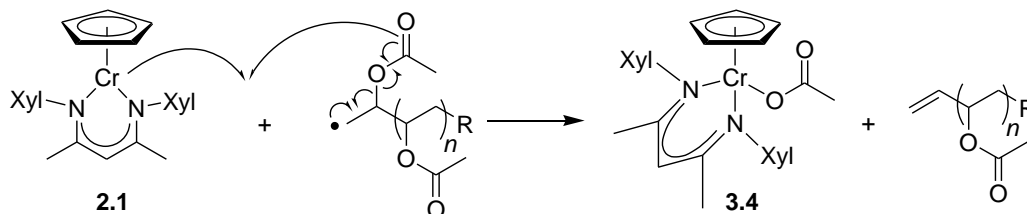


Figure 4.6. Proposed mechanism for the β -acetate transfer deactivation process.

energy radical intermediates having poor regioselectivity for radical addition to monomers.^{122,128}

Normal 1,2-insertion during polymerization results in formation of polymer chains with a secondary radical, while the 2,1-insertion forms a primary radical, as shown in Figure 4.7. Based on the significant degree of steric discrimination observed for the Cr(III) hydrocarbyl compounds in Chapter 2, it is expected that the primary radical species would form a much stronger Cr–C bond compared to the secondary radical species. In other words, as the 2,1-insertion products are formed during polymerization, the Cr trapping will lead to stable Cr-capped dormant polymer chains, causing a decrease in the rate of polymerization. This is consistent with the observed decrease in rate of polymerization throughout the course of the reaction shown in Figure 4.2a.

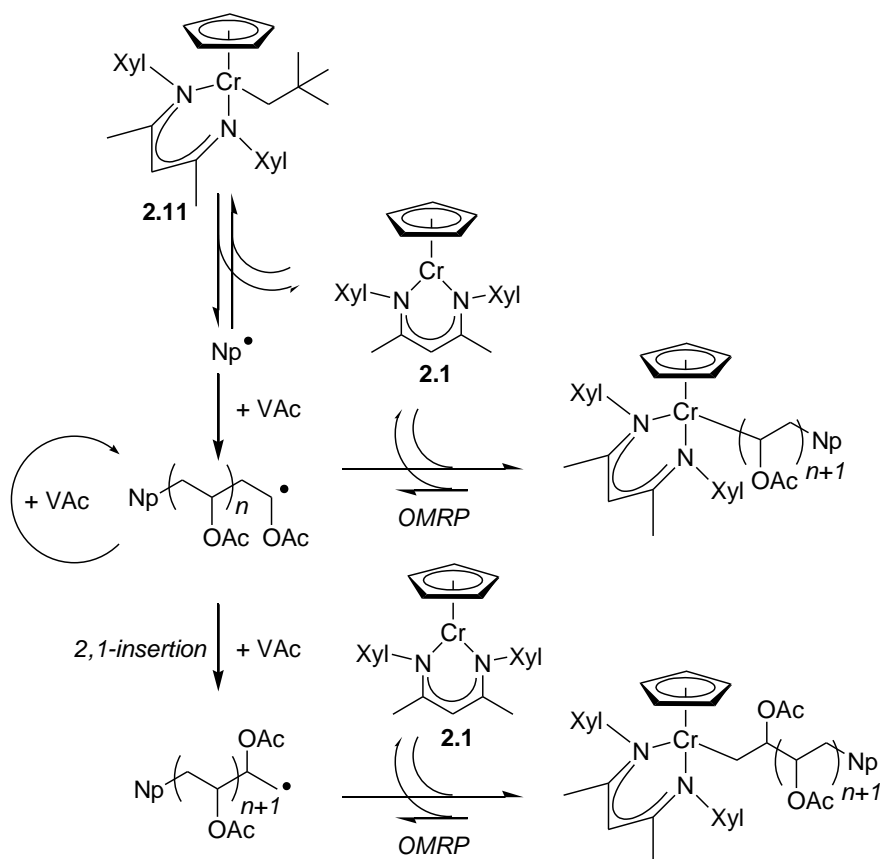


Figure 4.7. Proposed mechanism for the OMRP of VAc with compound **2.11**.

β -Acetate elimination has been observed previously as a decomposition mode with Ni and Pd catalysts in the copolymerization of ethylene and VAc.¹²⁹ However, formation of the acetate compound **3.4** from the Cr-capped dormant chains is not likely to proceed by the classical β -acetate elimination mechanism observed in other systems. The classical mechanism involves coordination of the pendant acetate group to the metal centre, which requires an open coordination site. Although the Cr centre is coordinatively unsaturated (15 electrons), the high-

spin state (3 unpaired electrons) of the Cr dictates that the three metal-based orbitals available for bonding are half-occupied. As such, formation of a 17 electron intermediate would require energetically unfavourable electron-pairing at the metal centre.¹³⁰ An alternative mechanism involving β -acetate abstraction from the radical chain species, shown in Figure 4.6, is therefore proposed. Homolytic bond cleavage leading to β -atom transfer has also been observed for a (R)Co(porphyrin) system, where the planar 4-coordinate porphyrin precludes the availability of a vacant site *cis* to the R group required for migration of the β -atom.¹³¹ Formation of the Cr-capped dormant PVAc chains proposed in Figure 4.7, as a result of the head-to-head insertion, are only reactivated upon heating, leading to rapid β -acetate transfer to form the acetate compound **3.4** (Figure 4.6). Unfortunately, characterization of PVAc isolated from polymerization of VAc in the presence of **2.11** at elevated temperature did not provide additional evidence to support the proposed mechanism; no vinyl chain end resonances were observable in the ¹³C NMR spectrum.

4.3 ATRP of Vinyl Acetate

Polymerizations of VAc were carried out under ATRP conditions (eq 4.1) using compounds **2.1** and **2.1c**, with a chloro initiator. The initiator MeCH(Cl)COOMe (In-Cl) was chosen due to its relatively weak C–Cl bond, thus ensuring rapid initiator consumption by the Cr(II) species. The reactions were carried out with 0.5 equivalents of In-Cl per Cr. The monomer consumption was initially rapid and then gradually slowed throughout the course of the reactions. After 400 h of polymerization, compound **2.1** provided 19% monomer conversion (Figure 4.8a) with relatively high M_n (34300 compared to $M_{n(th)} = 15100$) and $M_w/M_n = 1.75$ (Figure 4.8b). Compound **2.1c** gave higher conversion (34%), seen in Figure 4.8a, but the process was much less controlled, giving a final molecular weight distribution of 2.44 (Figure 4.8c). By comparison, the same polymerization reactions, when conducted at 50 °C, resulted in low conversions of only 5.4% and 7% for compounds **2.1** and **2.1c**, respectively, and very low initiator efficiencies were observed.¹³² Increasing the amount of initiator to one equivalent resulted in higher conversions of 16% and 26% for **2.1** and **2.1c**, respectively, but the system continued to suffer from poor initiator efficiencies.¹³² Similar to the reported OMRP of VAc at 50 °C, the reactions conducted under ATRP conditions reached maximum conversion after 4 h, suggesting the same acetate transfer deactivation mechanism is operative under both ATRP and OMRP conditions. The large disparities between observed and expected molecular weights were again indicative of poor initiator efficiency.

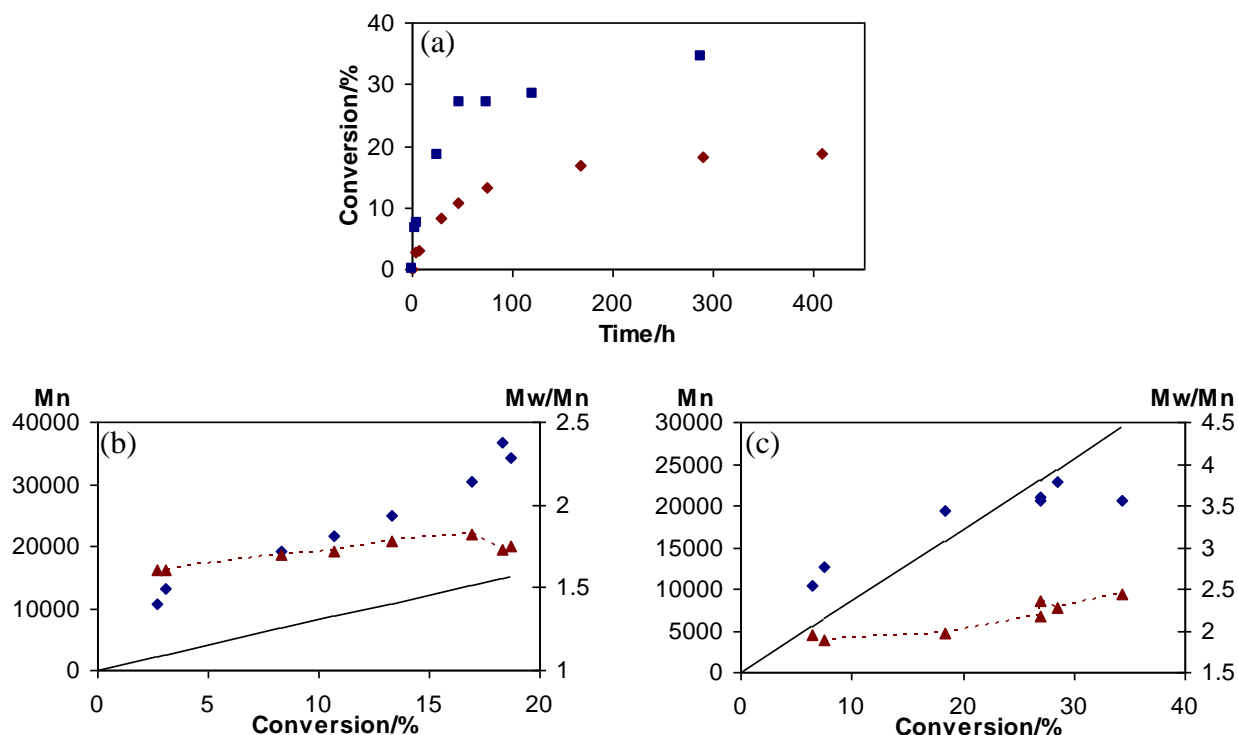


Figure 4.8. (a) Conversion as a function of time for the VAc polymerization initiated by MeCH(Cl)COOMe (In-Cl) in the presence of compound **2.1** (diamonds) or **2.1c** (squares). Conditions: VAc/Cr(II)/In-Cl = 500:0.5:1. T = room temp. Variation of the M_n (diamonds) and M_w/M_n (triangles) as a function of conversion for compound **2.1** (b) and **2.1c** (c), the solid line represents $M_{n(th)}$.

4.4 Reverse ATRP of Vinyl Acetate

Polymerizations of VAc were also carried out under reverse ATRP conditions. Under reverse ATRP conditions the Cr(III) chloride species was used as starting material, with the azo initiator V-70 added as a radical source. Under these reaction conditions there is initially no Cr(II) present in the solution, thereby precluding the involvement of an OMRP mechanism, at least until the chloride ligand has been abstracted from the Cr(III) chloride species by growing polymer chains. In the presence of 0.5 and 1.5 equivalents of V-70 initiator, compound **2.3c** controlled the polymerization of VAc, although the monomer conversions were again low, reaching maximum conversions of 32% and 50%, respectively, with deactivation occurring within the first 8 to 20 h of the polymerization process (Figure 4.9a). These reactions were conducted at 50 °C and the resulting polymers displayed similar characteristics to those obtained by the ATRP method, with low initiator efficiencies and M_w/M_n in the range of 1.6 – 1.9 (Figure 4.9b and c). Interestingly, under reverse ATRP conditions compounds **2.3** and **2.3c** provided essentially identical monomer conversions.¹³²

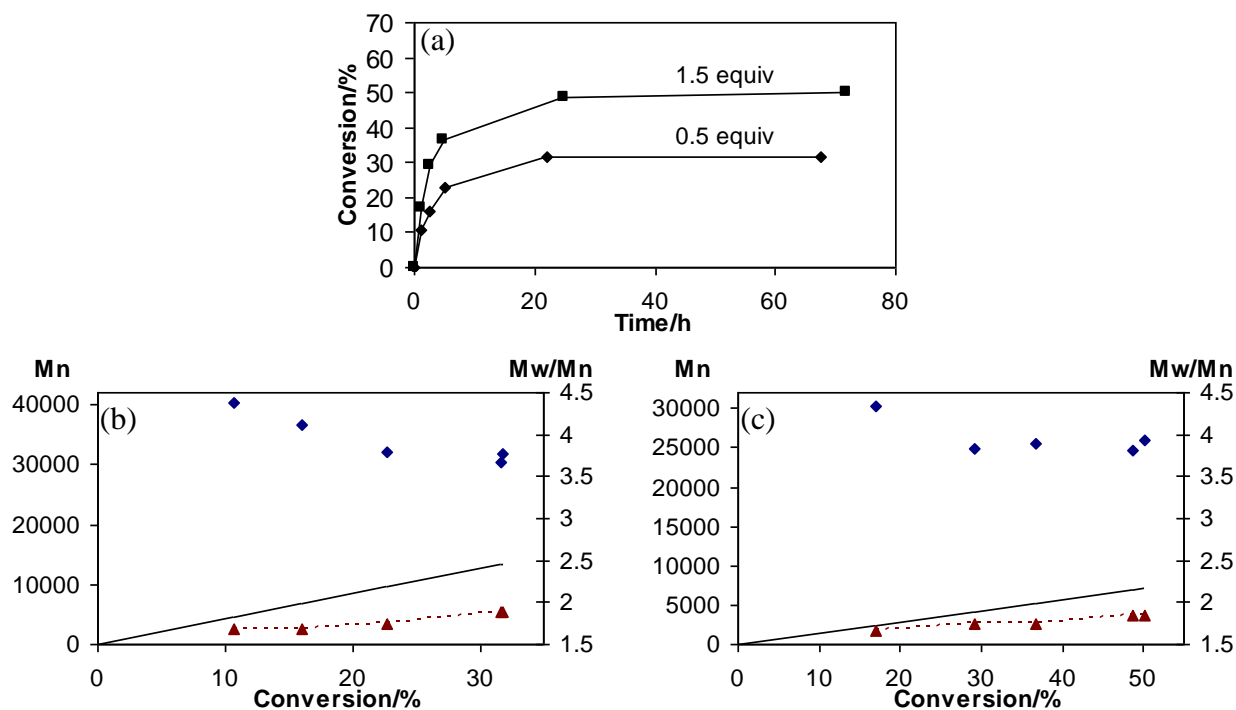


Figure 4.9. (a) Conversion as a function of time for the VAc polymerization initiated by V-70 in the presence of compound **2.3c**. Conditions: VAc/Cr/V-70 = 500:1:(0.5-1.5). $T = 50^\circ\text{C}$. Variation of the M_n (diamonds) and M_w/M_n (triangles) as a function of conversion for 0.5 equivalents V-70 (b) and 1.5 equivalents V-70 (c), the solid line represents $M_{n(th)}$.

The Cr(III) acetate complex **3.4** was also subjected to reverse ATRP conditions to determine whether the acetate group could act as the transfer agent, similar to the chloride group in standard reverse ATRP conditions. Indeed complex **3.4** controlled the polymerization of VAc initiated by V-70. A reaction using 0.5 equivalents of V-70 led to slightly higher monomer conversion (47%), shown in Figure 4.10a, compared to the chloride analogue **2.3** (31%) under identical conditions. The M_w/M_n was slightly higher, reaching a final value of 2.2 (Figure 4.10b), and again the conversion reached a plateau due to radical deactivation within the first 20 h.

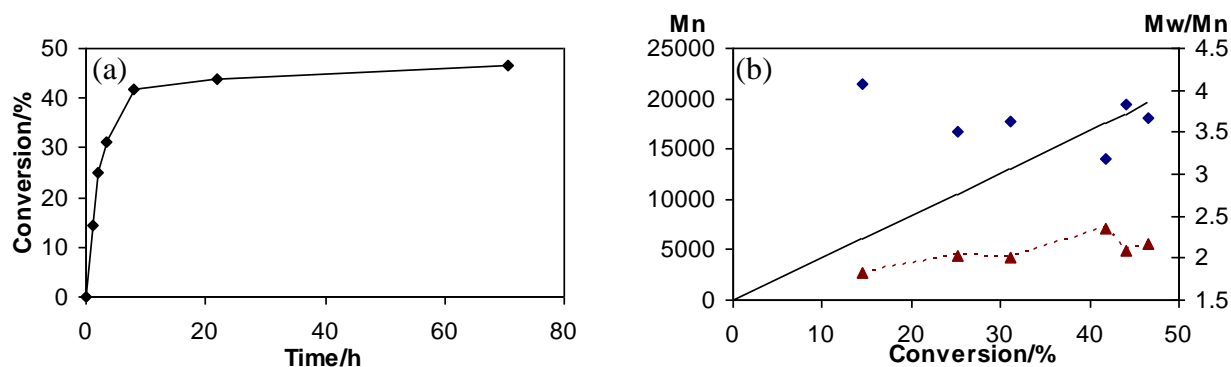


Figure 4.10. (a) Conversion as a function of time for the VAc polymerization initiated by V-70 in the presence of compound **3.4**. Conditions: VAc/Cr/V-70 = 500:1:0.5. $T = 50^\circ\text{C}$. (b) Variation of the M_n (diamonds) and M_w/M_n (triangles) as a function of conversion, the solid line represents $M_{n(\text{th})}$.

4.5 Stoichiometric Reactions with $\text{CpCr}[(\text{XylNCMe})_2\text{CH}]$

Spectroscopic analysis of the VAc polymerization reaction at room temperature in the presence of the Cr(II) compound **2.1** and 0.5 equivalents of the ATRP initiator In-Cl showed rapid consumption of the initiator. After 10 min, the absorption bands of **2.1** at 427 and 573 nm had been replaced by two new absorption bands at 420 and 581 nm. The same reaction in THF solvent (no VAc present) produced identical absorption bands within the same time period. Complex **2.1** also reacted rapidly with phenacyl chloride (PhCOCH_2Cl), showing complete conversion upon mixing at room temperature. The rapid reactions observed between compound **2.1** and the two halide compounds, In-Cl and PhCOCH_2Cl , are consistent with their relatively weak C–Cl bonds due to the presence of $\alpha\text{-C(O)R}$ substituents. Chlorine abstraction from these substrates would lead to formation of 0.5 equivalents of the Cr(III) choride complex **2.3** and a MeCHCOOMe or PhCOCH_2 radical, which will react rapidly with the remaining Cr(II) to form a Cr(III) species. The resulting Cr(III) species could form either a Cr–C bonded (Cr– $\text{CH}(\text{Me})\text{COOMe}$ and Cr– CH_2COPh) or a Cr–O bonded (Cr– $\text{OC}(=\text{CHMe})\text{OMe}$ and Cr– $\text{OC}(=\text{CH}_2)\text{Ph}$) product. The UV-vis spectra of the reaction products lacked the distinctive absorption band between 530 – 560 nm characteristic of Cr(III) hydrocarbyl compounds, suggesting formation of the O-bound enolate species shown in Figure 4.11.

The independent synthesis and characterization of the Cr(III) enolate complex $\text{CpCr}[(\text{XylNCMe})_2\text{CH}][\text{OC}(=\text{CH}_2)\text{Ph}]$ (**3.5**) was presented in Chapter 3, confirming the formation of an O-bound enolate species. In a similar reaction, methyl propionate was deprotonated with $\text{KN}(\text{SiMe}_3)_2$, and the isolated potassium enolate was reacted with $\text{CpCr}[(\text{XylNCMe})_2\text{CH}](\text{I})$. Despite repeated attempts, X-ray quality crystals of the resulting

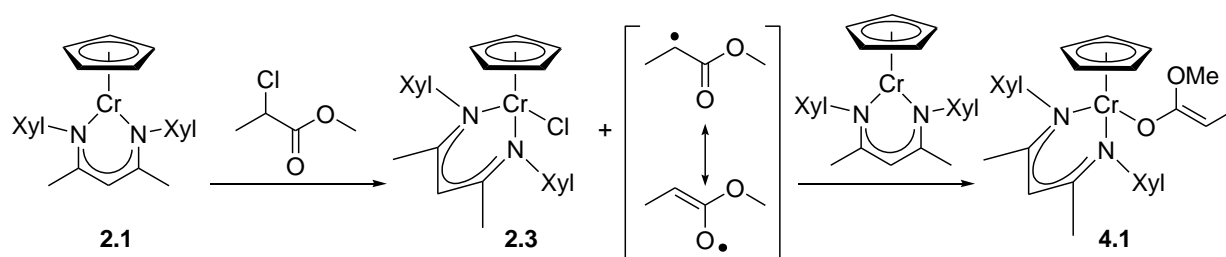


Figure 4.11. Reaction of the Cr(II) compound **2.1** with 0.5 equivalents of MeCH(Cl)COOMe.

enolate complex CpCr[(XylNCMe)₂CH][OC(=CHMe)OMe] (**4.1**) could not be isolated, but the structure has been tentatively assigned as an O-bound enolate based on the similarities with compound **3.5**: the UV-vis spectrum of the product contained absorption bands at 397 and 635 nm, similar to compound **3.5**, consistent with an O-bound product.

Deprotonation of ethyl propionate and subsequent reaction with CpCr[(XylNCMe)₂CH](I), on the other hand, led to the isolation of a small amount of X-ray quality crystals. Structural analysis of the isolated material revealed the formation of an unanticipated product CpCr[(XylNCMe)₂CH][OC(Et)=C(Me)COOEt] (**4.2**), shown in Figure 4.12. Formation of the OC(Et)=C(Me)COOEt moiety likely arose as a by-product during the deprotonation protocol as a result of the formed product K[OC(=CHMe)OEt] reacting with the starting material in a substitution reaction. Regardless of the nature of the isolated enolate complex, this structure confirms the bonding mode of the complex as an O-bound enolate. With a Cr–O bond length of 1.916(2) Å, a C(29)–C(30) double bond of 1.375(5) Å, and a Cr–O–C bond angle of 161.8(2) degrees, compound **4.2** displays similar bonding parameters to the Cr(III) enolate complex **3.5**.

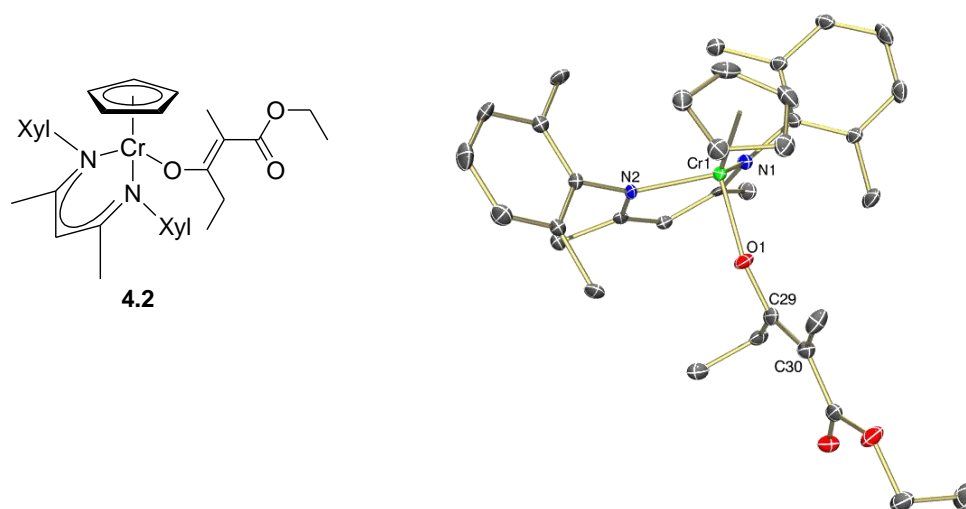


Figure 4.12. Thermal ellipsoid diagram (50%) of the Cr(III) enolate complex **4.2**. Complex **4.2** crystallizes with two independent molecules in the asymmetric unit; only one is shown, and all H atoms are omitted for clarity.

Isolated Cr(III) enolate compound **4.1** did not initiate the polymerization of VAc at room temperature after 2 days, followed by heating to 50 °C for an additional 21 h. This result indicates that the Cr(III) enolate complex **4.1** does not undergo Cr–O bond homolysis to generate the MeCHCOOMe radical. Therefore, the ability of Cr(II) to efficiently trap the enolate radicals generated during the initiation process under ATRP conditions, combined with the irreversible formation of the Cr(III) enolate product, accounts for the low initiator efficiencies observed for the polymerization reactions of VAc carried out with compounds **2.3** and **2.3c** under ATRP conditions. In addition, these results also support the inability of compound **2.3** to effectively control the polymerization of methyl acrylate, due to irreversible trapping of the growing polymer chains, as shown in Figure 4.4.

In contrast to the fast reactions observed between compound **2.1** and the organic halides described above, **2.1** reacted much more slowly with organic compounds that contained stronger C–Cl bonds. Compound **2.1** reacted with a stoichiometric amount of either 1-chloroethyl acetate (MeCH(Cl)OAc) or chloromethyl pivalate (^tBuCOOCH₂Cl) over a 24 h period at room temperature, while no reaction was observed with neopentyl chloride at room temperature or at 50 °C over the same time period. The reactions were monitored by UV-vis spectroscopy, clearly showing the formation of the Cr(III) chloride compound **2.3** and a Cr(III) alkyl product (due to the appearance of a broad absorption band at ~550 nm). In the case of the 1-chloroethyl acetate reaction, the absorption band at 558 nm decreased in intensity over extended reaction times, indicative of Cr–C bond homolysis leading to decomposition of the putative Cr(III) alkyl species CpCr[(XylNCMe)₂CH][CH(Me)OAc]. The reaction of **2.1** with chloromethyl pivalate maintained the strong absorption band at 546 nm after 4 days, indicative of the greater stability of the Cr(III) compound CpCr[(XylNCMe)₂CH](CH₂OOC^tBu) with a primary alkyl ligand compared to the formation of the secondary alkyl ligand CH(Me)OAc. These results are also in agreement with the proposed deactivation mechanism under OMRP conditions of VAc, where the 2,1-insertion leads to formation of a primary alkyl radical, which forms a much stronger Cr–C bond compared to the secondary radicals formed during a normal 1,2-insertion (Figure 4.7).

1-Chloroethyl acetate was chosen as a model substrate to further investigate the ATRP mechanism discussed above. The relatively slow stoichiometric reaction between the Cr(II) compound **2.1** and 1-chloroethyl acetate, suggested that chloride atom abstraction from the dormant chloride capped PVAc chains under ATRP conditions would also be slow. Given the

observation that reversible Cr–C bond homolysis is relatively rapid under the same reaction conditions, it is therefore proposed that OMRP is the dominant control mechanism, even under ATRP conditions, for the polymerization of VAc using the CpCr β -diketiminate system. Initiation by standard ATRP or reverse ATRP conditions inevitably leads to control by the OMRP mechanism, as shown in Figure 4.13. These results represented the first reported case of a system where the OMRP mechanism was dominant. A vanadium system that preferentially operates under an OMRP mechanism has since been reported.¹³³

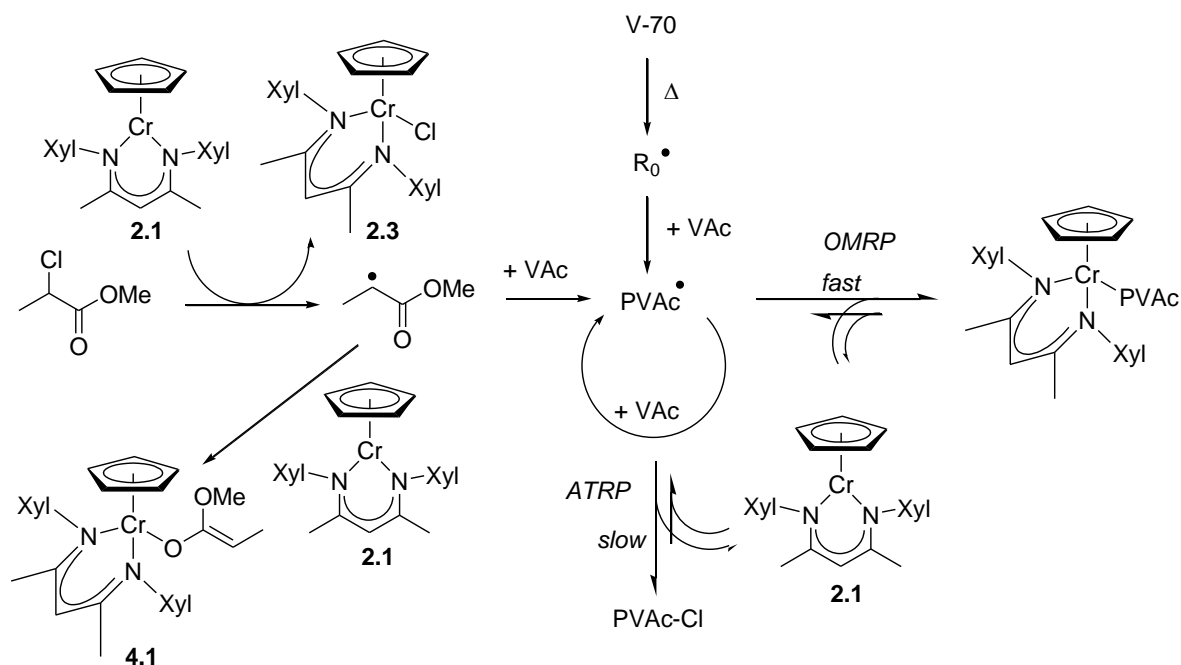


Figure 4.13. Proposed mechanism of ATRP and reverse ATRP for the polymerization of VAc using CpCr β -diketiminate complexes as polymerization mediators.

In the absence of VAc monomer, the Cr(II) compound **2.1** reacted with the azo initiator V-70 causing a colour change from green (magenta transmitted) to red transmitted, although no product was isolated from the reaction. Using a similar azo compound 2,2'-azobisisobutyronitrile (AIBN) a similar reaction was observed, causing a colour change from magenta transmitted to orange. The reaction of compound **2.1** with AIBN required heating to elevated temperatures (80 °C) to induce thermolytic decomposition of the AIBN, producing NCCMe_2 radicals that were trapped by compound **2.1** (Figure 4.14). Isolation of the Cr(III) compound $\text{CpCr}[(\text{XylNCMe})_2\text{CH}](\text{NCCMe}_2)$ (**4.3**) again underscores the ability of the Cr(II) compound **2.1** to effectively trap organic radicals. Similar to the enolate complexes described above, compound **2.1** could form either a Cr–C bond or a Cr–N bond when trapping the

NCCMe₂ radical. Based on the highly sensitive nature of the Cr(III) hydrocarbyl compounds to steric modification, it is therefore proposed that compound **4.3** would form an N-bound Cr(III) ketenimine species as opposed to a C-bound species with the Cr atom bound to a tertiary C atom. This N-bound complex **4.3** is the opposite binding mode to that observed for the Cr(III) cyanomethyl complex **2.13**, which forms a C-bound product through a primary C atom.

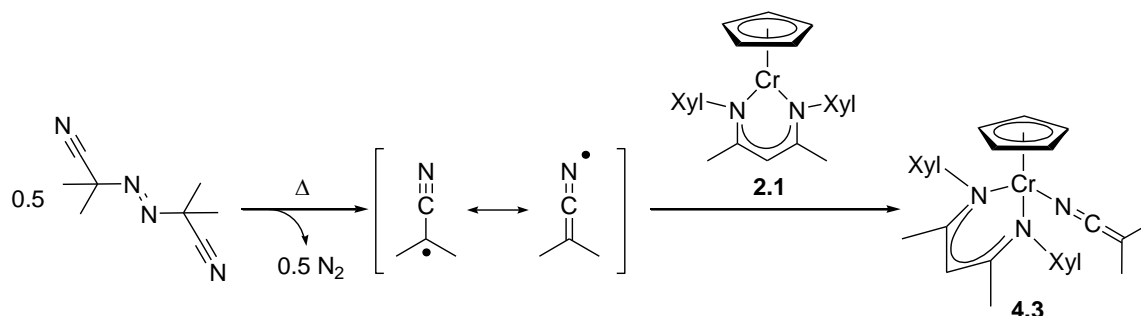


Figure 4.14. Reaction of the Cr(II) compound **2.1** with AIBN.

4.6 Experimental Section

General Considerations. Protocols were identical to those reported in section 2.13 using standard Schlenk and glovebox techniques unless otherwise indicated.

Characterization. Protocols were identical to those reported in section 2.13. Additionally, size exclusion chromatography (SEC) of poly(vinyl acetate) was carried out in filtered THF (flow rate: 1 mL/min) at 30 °C on a Polymer Laboratories PL-GPC 50 Plus (two PLgel mixed-C columns in series) equipped with a PL-AS RT autosampler and PL-RI detector. The isolated polymer samples were dissolved in THF and the polymer solutions were filtered (pore size = 0.45 μm) before chromatographic analysis. The columns were calibrated against linear polystyrene standards (Polymer Laboratories).

Materials. Protocols were identical to those reported in section 2.13. Additionally, 2,2'-azobisisobutyronitrile, ethyl propionate, methyl propionate, and PVAc (typical M_w = 113000) were purchased from Aldrich and used as received. 2,2'-Azobis(4-methoxy-2,4-dimethylvaleronitrile) (V-70, 96%) was purchased from Wako and used as received. Cyclohexyl chloride, methyl 2-chloropropionate, chloromethyl pivalate, and neopentyl chloride were purchased from Aldrich, degassed by three freeze-vacuum-thaw cycles, and stored under nitrogen prior to use. Vinyl acetate (99+%, Aldrich) and methyl acrylate were passed through a column of neutral alumina to remove stabilizer, dried over calcium hydride, purified by vacuum distillation, degassed by three freeze-vacuum-thaw cycles, and stored under nitrogen at -35 °C.

Compounds 1-chloroethyl acetate,¹³⁴ **2.1c**,³² and **2.3c**³² were prepared according to literature procedures. K[OC(=CHMe)OMe] and K[OC(=CHMe)OEt] were prepared according to literature procedures outlining the preparation of similar potassium enolate compounds.⁸¹

OMRP procedure for polymerization of VAc with compound 2.11. Compound **2.11** (17.5 mg, 0.035 mmol) was placed in a Schlenk flask followed by the addition of VAc (4.0 mL, 43 mmol, 1200 equiv). The reaction mixture was stirred at room temperature. At the desired time, a sample was removed from the Schlenk flask for analysis. The monomer conversion was determined gravimetrically after removal of the unconverted monomer under reduced pressure, and the resulting residue was used for SEC characterization.

OMRP procedure for characterization of compound 3.4. Compound **2.11** (35.8 mg, 0.0725 mmol) was placed in a Schlenk flask followed by the addition of VAc (4 mL, 43 mmol, 600 equiv). The reaction mixture was stirred at room temperature for 13 days, followed by heating at 60 °C overnight. The volatiles were removed under reduced pressure, the residue extracted with Et₂O, filtered over Celite, and concentrated under reduced pressure. After cooling the green (orange transmitted) solution (~1 mL) at -35 °C for 3 days, the solution was decanted to remove a small amount of polymer precipitate and the solution was again cooled for 2 weeks to provide X-ray quality crystals of compound **3.4** (7.9 mg, 23%).

OMRP control reactions: Compound 2.1 + VAc. Compound **2.1** (29 mg, 0.070 mmol) was placed in a Teflon stoppered thick-walled glass reaction vessel followed by the addition of VAc (2 mL, 21 mmol, 300 equiv). The reaction vessel was immersed in a water bath preheated at 65 °C, and stirred overnight. The UV-vis spectrum of the reaction mixture displayed absorption bands at 426 and 567 nm, corresponding to unreacted **2.1**.

Compound 2.1 + PVAc. Commercially obtained PVAc (117 mg, typical $M_w = 113000$) was dissolved in THF (4 mL) followed by the addition of compound **2.1** (37.8 mg, 0.089 mmol). The reaction mixture divided into two fractions and one was stirred at room temperature while the other fraction was placed in a Teflon stoppered thick-walled glass reaction vessel that was immersed in an oil bath preheated at 50 °C. Upon stirring for 24 h, the UV-vis spectra of both fractions displayed absorption bands at 426 and 567 nm, corresponding to unreacted **2.1**.

OMRP procedure for polymerization of VAc with compound 2.2. Compound **2.2** (16.1 mg, 0.035 mmol) was placed in a Schlenk flask followed by the addition of VAc (4.0 mL, 43 mmol, 1250 equiv). After stirring for 48 h at room temperature, the reaction mixture displayed absorption bands in the UV-vis spectrum at 418 and 546 nm, corresponding to unreacted **2.2**. A sample was removed from the Schlenk flask for analysis. The monomer conversion (9.0%) was

determined gravimetrically after removal of the unconverted monomer under reduced pressure, and the resulting residue was used for SEC characterization: $M_n = 83900$, $M_{n(th)} = 9140$, $M_w/M_n = 3.36$. Under otherwise identical conditions, when this reaction was repeated with the exclusion of ambient laboratory light, no PVAc was produced.

OMRP procedure for polymerization of VAc with compound 2.15. Compound **2.15** (9.4 mg, 0.019 mmol) was placed in a Schlenk flask followed by the addition of VAc (4.0 mL, 43 mmol, 2300 equiv). After stirring for 4 days at room temperature, the reaction mixture was heated at 55 °C for another 3 days. The UV-vis spectrum of the reaction mixture displayed absorption bands at 436 and 561 nm, corresponding to unreacted **2.15**.

OMRP procedure for polymerization of styrene with compound 2.11. Compound **2.11** (14.3 mg, 0.029 mmol) was placed in a Schlenk flask followed by the addition of styrene (4 mL, 35 mmol, 1200 equiv). After stirring at room temperature for 7 days, a sample was removed from the Schlenk flask for analysis. The unconverted monomer was removed under reduced pressure, and the resulting residue was used for SEC characterization, which revealed a bimodal molecular weight distribution. High molecular weight chains: $M_n = 251000$, $M_w/M_n = 1.55$; low molecular weight chains: $M_n = 5730$, $M_w/M_n = 1.52$.

OMRP procedure for polymerization of MA with compound 2.11. Compound **2.11** (5.4 mg, 0.011 mmol) was placed in a Schlenk flask followed by the addition of MA (4.0 mL, 44 mmol, 4000 equiv). The solution changed colour from purple to green over a period of 5 min while stirring at room temperature. After 17 h, a sample was removed from the Schlenk flask for analysis. The monomer conversion (25%) was determined gravimetrically after removal of the unconverted monomer under reduced pressure, and the resulting residue was used for SEC characterization: $M_n = 21500$, $M_{n(th)} = 89060$, $M_w/M_n = 16.0$.

ATRP procedure with compound 2.1. Compound **2.1** (40.5 mg, 0.0959 mmol) was placed in a Schlenk flask followed by the addition of VAc (4.0 mL, 43 mmol, 500 equiv) and methyl 2-chloropropionate (5 μ L, 0.46 mmol, 0.5 equiv). The reaction mixture was stirred at room temperature. At the desired time, a sample was removed from the Schlenk flask for analysis. The monomer conversion was determined gravimetrically after removal of the unconverted monomer under reduced pressure, and the resulting residue was used for SEC characterization.

ATRP procedure with compound 2.1c. The ATRP procedure described above was followed with compound **2.1c** (47.1 mg, 0.0881 mmol), methyl 2-chloropropionate (4.7 μ L, 0.044 mmol, 0.5 equiv) and VAc (4.0 mL, 43 mmol, 500 equiv)

Reverse ATRP procedure with compound 2.3c: Run 1 (0.5 equiv of initiator).

Compound **2.3c** (49.4 mg, 0.087 mmol) and V-70 (13.7 mg, 0.044 mmol, 0.5 equiv) were placed in a Teflon stoppered thick-walled glass reaction vessel followed by the addition of VAc (4.0 mL, 43 mmol, 1200 equiv). The reaction vessel was immersed in an oil bath preheated at 50 °C, and stirred. At the desired time, the reaction vessel was rapidly cooled to room temperature by immersion into iced water before sample withdrawal. The monomer conversion was determined gravimetrically after removal of the unconverted monomer under reduced pressure, and the resulting residue was used for SEC characterization.

Run 2 (1.5 equiv of initiator). The reverse ATRP procedure described above was followed with compound **2.3c** (49.3 mg, 0.087 mmol), V-70 (40.4 mg, 0.13 mmol, 1.5 equiv), and VAc (4.0 mL, 43 mmol, 500 equiv).

Reverse ATRP procedure with compound 3.4. The reverse ATRP procedure described above was followed with compound **3.4** (43.0 mg, 0.089 mmol), V-70 (13.7 mg, 0.044 mmol, 0.5 equiv), and VAc (4.0 mL, 43 mmol, 500 equiv).

Radical polymerization of VAc with a Cr(III) enolate compound. Compounds CpCr[(XylNCMe)₂CH](I) (151 mg, 0.275 mmol) and K[OC(=CHMe)OMe] (42.3 mg, 0.335 mmol, 1.22 equiv) were placed in a Schlenk flask followed by the addition of toluene (15 mL). The mixture was stirred overnight at room temperature at which point the solvent was evaporated under reduced pressure. The residue was extracted with hexanes (10 mL) and filtered over Celite. The resulting green solution (UV-vis: λ_{max} = 397 nm, 635 nm) was cooled to -35 °C to yield 25.1 mg (18%) of compound CpCr[(XylNCMe)₂CH][OC(=CHMe)OMe] (**4.1**). This batch was then dissolved in VAc (2 mL). Stirring at room temperature for 54 h and then warming to 50°C for 21.5 h did not result in any polymerization process.

Attempted synthesis of CpCr[(XylNCMe)₂CH][OC(=CHMe)OEt]. Compounds CpCr[(XylNCMe)₂CH](I) (76.5 mg, 0.139 mmol) and K[OC(=CHMe)OEt] (24.9 mg, 0.178 mmol, 1.28 equiv) were placed in a flask followed by the addition of toluene (4 mL). Upon stirring for 6 h at room temperature, the solvent was evaporated under reduced pressure. The residue was extracted with hexanes (2 mL) and filtered over Celite. The resulting green solution (UV-vis: λ_{max} = 399 nm, 628 nm) was cooled to -35 °C to yield 3 small X-ray quality crystals. The isolated material was identified by single-crystal X-ray diffraction as CpCr[(XylNCMe)₂CH][OC(Et)=C(Me)COOEt] (**4.2**).

Synthesis of CpCr[(XylNCMe)₂CH](NCCMe₂) (4.3). Compound **2.1** (99.2 mg, 0.235 mmol) was placed in a Schlenk flask, followed by the addition of hexanes (25 mL) and an AIBN (19.9 mg, 0.121 mmol, 0.52 equiv) solution in hexanes (2 mL). No reaction was observed after stirring at room temperature for 5 days. An additional 5 – 10 mg of AIBN was placed in the reaction mixture, followed by heating at 80 °C for 2 days, at which point the solution became orange to transmitted light. The volatiles were evaporated under reduced pressure, the residue extracted with hexanes (10 mL), filtered over Celite, and the solvent was again evaporated under reduced pressure. The residue was extracted with a minimum of hexanes (1.5 mL), filtered over Celite, and the green (orange transmitted) solution was cooled to -35 °C overnight to yield 14.1 mg of **4.3** (12%). Anal. Calcd. for C₃₀H₃₆N₃Cr: C, 73.44; H, 7.40; N, 8.56. Found: C, 73.20; H, 7.41; N, 8.34.

Reactions of 2.1 with organic halides:

Methyl 2-chloropropionate. Compound **2.1** (42.3 mg, 0.100 mmol) was placed in a flask and dissolved in THF (15 mL), followed by the addition of MeCH(Cl)COOMe (5.4 µL, 0.050 mmol, 0.50 equiv). Upon stirring for 1 h at room temperature, the solution changed colour from green (magenta transmitted) to orange transmitted with absorption bands in the UV-vis spectrum at 420 and 581 nm.

1-Chloroethyl acetate. Compound **2.1** (16.8 mg, 0.040 mmol) and MeCH(Cl)OAc (6.2 mg, 0.051 mmol, 1.3 equiv) were placed in a 1 dram glass vial followed by the addition of toluene (2 mL). Upon stirring at room temperature overnight, the UV-vis spectrum contained absorption bands at 421 and 558 nm. Upon standing overnight, the same UV-vis sample contained bands at 417 and 567 nm.

Chloromethyl pivalate. Compound **2.1** (10.9 mg, 0.026 mmol) was placed in a 1 dram glass vial and dissolved in toluene (2 mL), followed by the addition of ^tBuCOOCH₂Cl (3 µL, 0.021 mmol, 0.80 equiv). Upon stirring at room temperature for 4 days, the UV-vis spectrum contained absorption bands at 421 and 546 nm.

Neopentyl chloride. Compound **2.1** (11.9 mg, 0.028 mmol) was placed in a 1 dram glass vial and dissolved in toluene (2 mL), followed by the addition of Me₃CCH₂Cl (2 µL, 0.016 mmol, 0.58 equiv). Upon stirring at room temperature for 24 h, the UV-vis spectrum contained absorption bands at 427 and 574 nm corresponding to unreacted Cr(II) starting material **2.1**. The reaction mixture was then transferred to a Teflon stoppered thick-walled glass reaction vessel that was immersed in an oil bath preheated at 50 °C, and stirred for an additional 24 h. The UV-vis spectrum of the reaction mixture was identical before and after heating.

General procedure for X-ray crystallography. Protocols were identical to those reported in section 2.13.

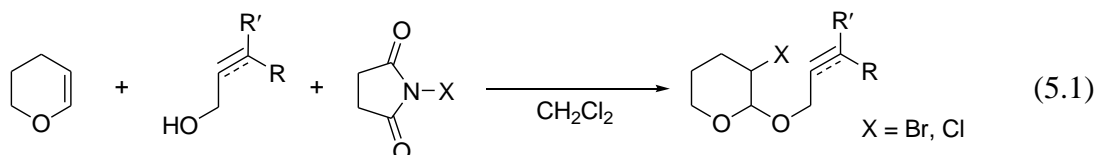
Structure details. Compound **4.3** crystallizes with two independent molecules in the asymmetric unit.

Chapter 5 Carbon-based Radicals for C–C and C–P Bond Formation

The results presented in this chapter are somewhat complementary to that of Chapter 4, with a focus on the use of C-based radicals for the synthesis of discrete organic molecules. Both intra- and intermolecular C–C bond forming reaction were targeted. In particular, the radical cyclization of bromoacetals proceeded smoothly with low chromium-catalyst loadings. Chloroacetals were also cyclized, although typically resulting in lower yields. Initial results examining the addition of alkyl radicals to substituted olefins are also presented. A series of small scale stoichiometric reactions were conducted to evaluate the reactivity of Cr(III) hydrocarbyl compounds towards methyl acrylate and other similar substituted enones, with the goal of developing a protocol that would be catalytic in Cr. Initial results are also presented for the Cr-catalyzed radical alkylation of $\text{Ph}_2\text{P}-\text{PPh}_2$ for the production of tertiary phosphines.

5.1 Radical Cyclization of Haloacetals

The radical cyclization of haloacetals, termed the Ueno-Stork reaction,¹³⁵ is considered a benchmark reaction when establishing new methods for radical-based C–C bond formation.¹³⁶ The starting materials are easily prepared on a large scale from the appropriate enol ether, allyl or propargyl alcohol, and *N*-halosuccinimide.¹³⁷ Synthesis of the haloacetal substrates reported herein is outlined in eq 5.1.



The iodo acetals are considerably less stable compared to the bromo and chloro analogues, and must be stored at low temperatures to prevent decomposition.¹³⁷ The radical cyclization of haloacetals was first reported using stoichiometric organotin hydride reagents.¹³⁵ These reagents are typically only effective at mediating cyclization of the iodo and bromo substrates and, in addition, the organotin by-products exhibit high toxicity in the environment. Subsequent developments in the field of transition metal-catalyzed reactions are also typically limited to cyclization of the iodo and bromo substrates.^{21,22,137,138} Oshima and co-workers have reported the use of zirconocene-based reagents that catalyze the cyclization of bromoacetals and can be used stoichiometrically for the cyclization of chloroacetals.¹³⁹ The decreased reactivity of chloroacetals compared to the bromo and iodo derivatives is a direct result of the increased carbon-halogen bond strength of the C–Cl bond compared to the C–Br and –I bonds.

The synthesis of $\text{CpCr}[(\text{XylNCMe})_2\text{CH}](\text{CH}_2\text{SiMe}_3)$ (**2.7**) in high yield from the Cr(II) compound **2.1** by oxidative addition of $\text{Me}_3\text{SiCH}_2\text{I}$ was presented in Chapter 2, using an excess of Mn powder to selectively reduce the Cr(III) iodide product back to the reactive Cr(II) species. A similar reaction with compound **2.1** and the bromoacetal **5.1a** resulted in formation of the Cr(III) alkyl complex **5.2**, as shown in Figure 5.2. The solid-state molecular structure of **5.2** is shown in Figure 5.1. Single-crystals of **5.2** contain a co-crystallized mixture of one of the diastereomeric pairs of the cyclized ligand. The Cr–N bond lengths (2.0391(13) and 2.0317(13) Å) are typical of CpCr β -diketiminato alkyl compounds. The Cr–C bond length of compound **5.2** (2.1223(16) Å) and Cr–C–C bond angle ($127.3(6)^\circ$ average) are comparable to the structurally similar isobutyl compound **2.10** (Cr–C = 2.123(5) Å average and Cr–C–C = $126.6(4)^\circ$ average). The UV-vis spectrum of compound **5.2** displays typical absorption bands at 413 and 556 nm.

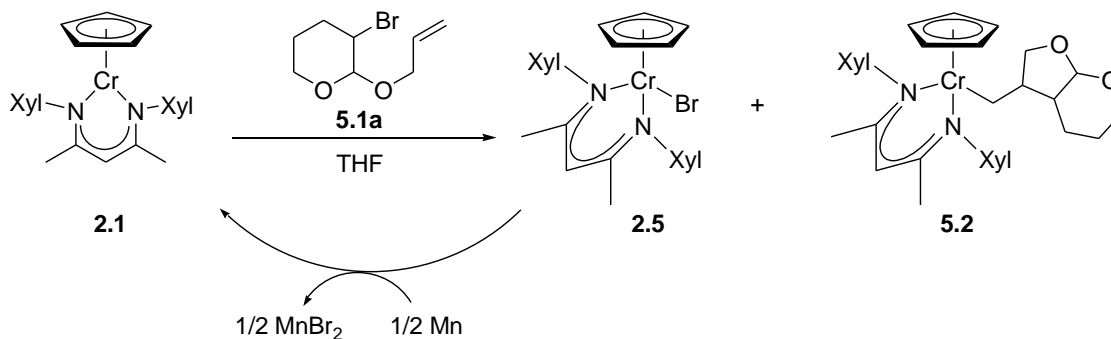


Figure 5.2. Oxidative addition of **5.1a** with the Cr(II) compound **2.1**.

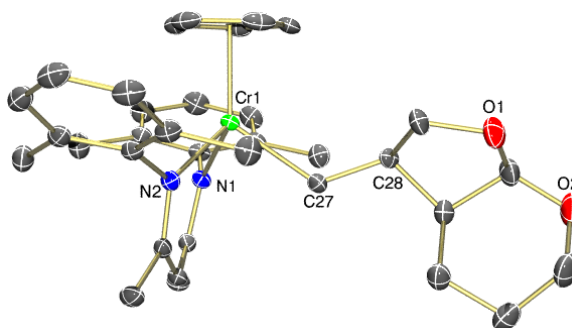


Figure 5.1. Thermal ellipsoid diagram (50%) of compound **5.2**. The cyclized ligand crystallizes as a mixture of one of the diastereomeric pairs; only one enantiomer is shown, and all H atoms are omitted for clarity.

The synthesis and stability of compound **5.2** is consistent with the established trends in steric limitations of the CpCr β -diketiminato system. A large difference in the rate constant for Cr–C bond homolysis is observed between the isobutyl complex **2.10** and the neopentyl complex **2.11** (Figure 5.3a). Similar steric discrimination was also observed for the OMRP of vinyl acetate in Chapter 4, where the Cr(II) compound **2.1** effectively controlled the polymerization of VAc until a 2,1-insertion of monomer occurred, generating a primary radical that formed a much more stable Cr-capped dormant polymer chain (Figure 5.3b). A similar mechanism is observed when the bromoacetal **5.1a** reacts with compound **2.1** to form a secondary radical. The remaining Cr(II) in the reaction mixture is not able to irreversibly trap the secondary radical, which then undergoes a rapid intramolecular radical cyclization reaction. The resulting primary alkyl radical of the cyclized product is then trapped by the Cr(II) to form the Cr(III) complex **5.2** (Figure 5.3c).

Figure 5.3. Steric hindrance and Cr–R bond homolysis in Cr(III) alkyl complexes.

In Chapter 2, Cr–C bond homolysis of the Cr(III) hydrocarbyl compounds was readily induced under photolytic conditions, and the Cr(III) alkyl compound **5.2** is no exception. Upon stirring a mixture of compound **5.2** with one equivalent of PhSSPh under an inert atmosphere on the laboratory windowsill, the solution changed colour from purple to green over a period of 2 days. The Cr had converted to the Cr(III)–SPh compound **2.19** and upon chromatographic purification of the reaction mixture the thioether compound **5.3** was identified by ^1H NMR. The light-induced Cr–C bond homolysis generates the bicyclic organic radical and compound **2.1**, which both react with PhSSPh to form the thioether **5.3** and the Cr(III)–SPh compound **2.19**, respectively (Figure 5.4).

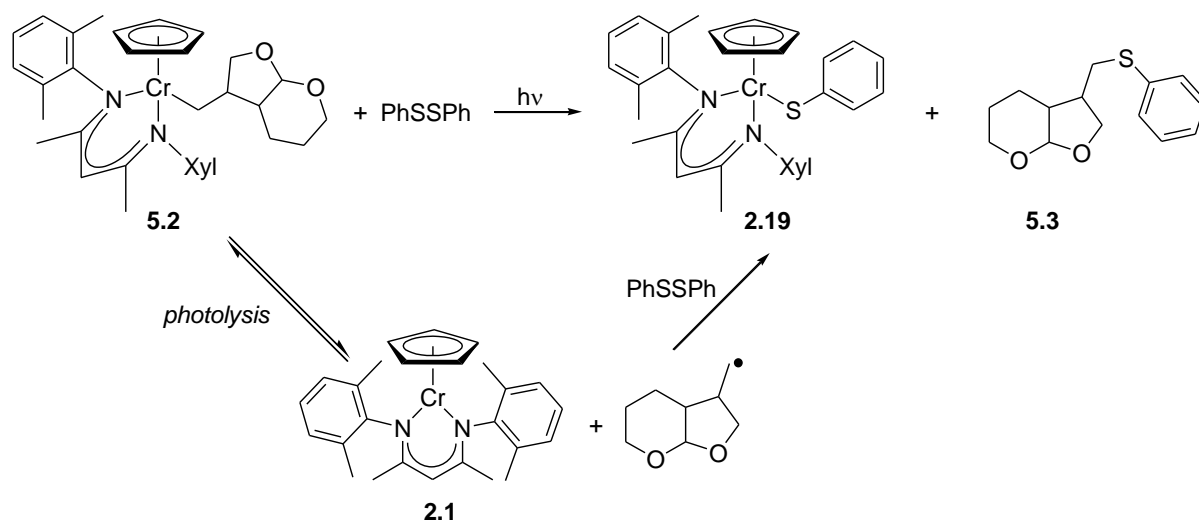
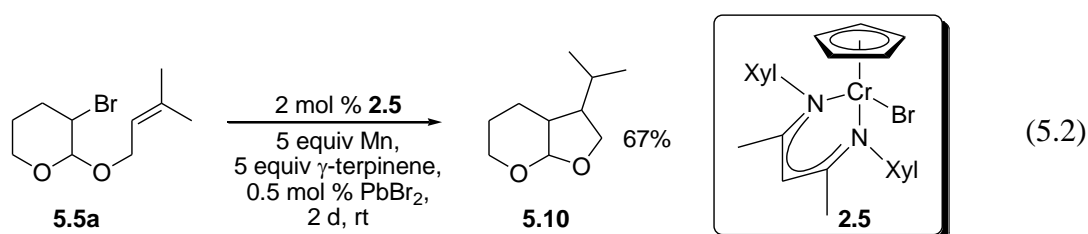


Figure 5.4. Photolysis of the Cr(III) alkyl compound **5.2**.

The addition of R groups (eq 5.1) to the haloacetals by using substituted allyl alcohols as starting materials significantly decreases the ability of the Cr(II) to trap the cyclized products. The radical cyclization of bromoacetals was rendered catalytic in chromium with the use of Mn powder, γ -terpinene as hydrogen atom donor,^{103c,140} and a substoichiometric amount of PbBr_2 , with only 2 mol % of the bromide complex **2.5**. As discussed in Chapter 3, substoichiometric amounts of lead(II) halides can be used to activate Mn powder.⁸⁸ The cyclization of bromoacetal **5.5a** under the reaction conditions shown in eq 5.2, with 1 mmol of **5.5a**, 2 mol % of the Cr(III) bromide compound **2.5** at room temperature, provided the cyclized product **5.10** in 67% isolated yield. In a control experiment, performing the cyclization of **5.5a** in the absence of chromium catalyst **2.5** under otherwise identical reaction conditions, no cyclized product was obtained.



Increasing the reaction temperature to 50 °C allowed for a reduced reaction time of 38.5 h (compared to 2 days at room temperature) and a significant increase in yield (85%) of the cyclized product **5.10**, shown in Table 5.1, entry 5. Under these standard conditions, the cyclized product **5.9** was also obtained in high yield (Table 5.1, entry 2). The cyclization of compound **5.6a** provided the desired product **5.11** (Table 5.1, entry 7) in a lower yield compared to the other bromoacetals. The secondary benzylic radical intermediate generated upon cyclization of **5.6a** does not react efficiently the H atom donor γ -terpinene, leading to unwanted side reactions and a lower yield of the desired product **5.11**.^{140a,141} The propargyl substituted bromoacetal **5.7a** was also successfully cyclized to form the desired product **5.12** (Table 5.1, entry 9). The use of 8 equivalents of γ -terpinene as opposed to the standard 4 equivalents was found improve the yield of compound **5.12**. The increased concentration of H atom donor (γ -terpinene) in this reaction presumably inhibits unwanted side reactions of the highly reactive alkenyl radical intermediate. The observed diastereomeric ratios of the cyclized products **5.9**–**5.11** and the E/Z ratio of compound **5.12** were consistent with previously reported values.

Table 5.1. Chromium-catalyzed radical cyclization of bromo and chloro acetals.^a

X = Cl (**2.3**),
Br (**2.5**)

Entry	Substrate ^b	X	Product	Isolated Yield ^c
1		Br (5.1a)		Recovered starting material ^d
2		Br (5.4a)		93% (82/12)
3		Cl (5.4b)		56% (93/7)
4		Cl (5.4b)		70% (80/20) ^e
5		Br (5.5a)		85% (65/35) ^f
6		Cl (5.5b)		57% (61/39) ^g
7		Br (5.6a)		28% (79/21) ^g
8		Cl (5.6b)		29% (83/17)
9		Br (5.7a)		77% (E/Z = 42/58) ^h
10		Cl (5.7b)		47% (E/Z = 43/57)

^a When X = Br: **2.3** (2 mol %), PbBr₂ (≤ 1 mol %), 38.5 h at 50 °C; X = Cl: **2.5** (20 mol %), PbCl₂ (≤ 1 mol %), 88 h at 70 °C. ^b Substrate (1 mmol). ^c Isolated yields. Diastereomeric ratios are in parentheses. ^d Isolated 73% unreacted **5.1a**. ^e Ten day reaction time. ^f Mn (5 equiv) and γ-terpinene (5 equiv) were used. ^g Mn (4 equiv) was used. ^h γ-Terpinene (8 equiv) was used.

The development of catalysts capable of selectively activating the strong C–Cl bonds of organic chlorides remains challenging in organometallic chemistry.^{138e,139,142} The ability of the Cr(II) compound **2.1** to activate C–Cl bonds was explored in Chapter 4 in the context of controlled radical polymerization. Compound **2.1** reacted rapidly with stabilized organic chloride substrates but the reduction of unactivated C–Cl bonds was much slower. Nevertheless, cyclization of chloroacetal substrates was also investigated using the chloride compound **2.3**. Gratifyingly, our system was also capable of catalyzing the radical cyclization of chloroacetal substrates. Compounds **5.4b** – **5.7b** were cyclized under standard conditions with a catalyst loading of 20 mol % **2.3** at 70 °C. With a reaction time of 88 h, yields for the cyclization of the chloroacetals were in the range of 29–57%, with a similar trend in yields as with the bromoacetals. Compounds **5.9** and **5.10** were isolated in the highest yields (56 and 57%,

respectively), shown in Table 5.1, entries 3 and 6, while compound **5.12** was only slightly lower at 47% (Table 5.1, entry 10), and, as expected, compound **5.11** was isolated in only 29% yield (Table 5.1, entry 8).

The proposed mechanism of the catalytic conversion of haloacetals with CpCr β -diketiminate complexes is shown in Figure 5.5. The Cr cycles between Cr(III) halide and Cr(II) species during the reaction, with Mn powder to reduce the Cr(III) halide to Cr(II). The haloacetal substrate is reduced by the Cr(II) to form the Cr(III) halide species and the organic radical intermediate, which rapidly undergoes an intramolecular C–C bond forming step followed by H atom abstraction from γ -terpinene to provide the reduced cyclized product and 0.5 equivalents of the by-product *p*-cymene.

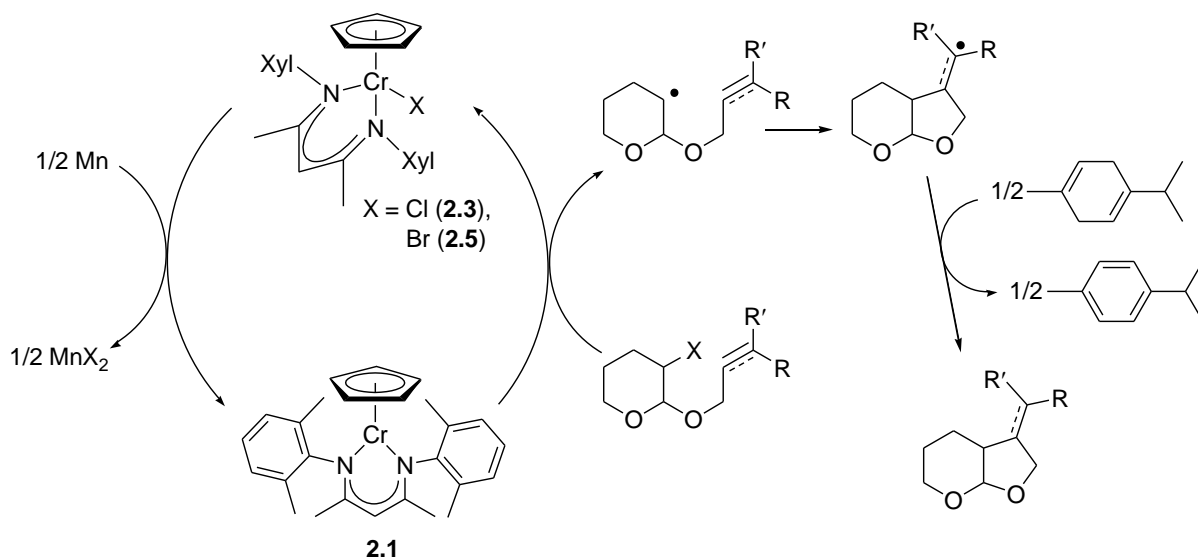
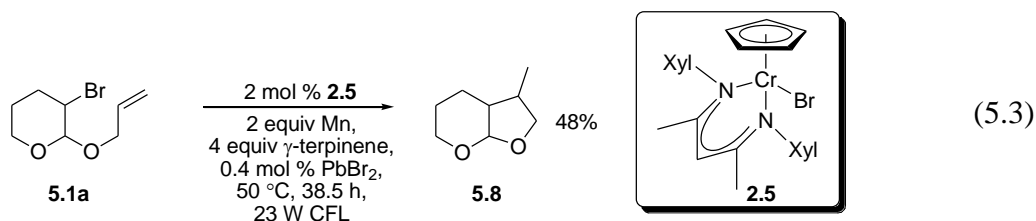


Figure 5.5. Proposed mechanism for the chromium-catalyzed radical cyclization of haloacetals.

The overall lower yields obtained with the chloroacetals compared to the bromoacetals is attributed to the reduced activity of compound **2.1** towards reduction of the chloro substrates. Under the catalytic conditions established for cyclization of the bromoacetals, the resting state of the Cr catalyst was the Cr(III) bromide species **2.5**. The fast step in the reaction involved oxidative addition of the bromoacetal to compound **2.1** to generate compound **2.5** and the organic radical, while the rate determining step in the catalytic cycle was reduction of the Cr(III) bromide **2.5** back to Cr(II). On the contrary, the catalytic conditions established for cyclization of the chloroacetals showed an opposite trend in the relative rates of reaction: the reduction of the Cr(III) chloride **2.3** back to Cr(II) was faster than oxidative addition of the chloroacetal with compound **2.1**. Indeed, increasing the reaction time to 10 days for the cyclization of chloroacetal **5.4b** (Table 5.1, entry 4) led to an increased yield of the cyclized product **5.9** (70%). To the best

of the author's knowledge, this represents the first catalytic Ueno–Stork reaction of chloroacetals.

As expected, subjecting the sterically unhindered bromoacetal **5.1a** to the standard catalytic reaction condition did not lead to high turnover, as compound **5.1a** (73%) was recovered from the reaction mixture uncyclized (Table 5.1, entry 1). Keeping in mind the observed photolysis of the Cr(III) alkyl complex **5.2** discussed above, the bromoacetal **5.1a** was subjected to catalytic cyclization conditions under the light of a 23 W household compact fluorescent bulb. The cyclized product **5.8** was obtained in 48% yield (eq 5.3). This result demonstrates that the Cr–C bond can be sufficiently labilized under mild photolytic conditions to achieve modest catalyst turnover for these cyclization reactions.



5.2 Chromium Catalyst Regeneration in Haloacetal Cyclization

The active catalyst species in the haloacetal cyclization reaction, compound **2.1**, is extremely air-sensitive forming the Cr(III) μ -oxo compound **3.1** in the presence of oxygen. As a result, the haloacetal cyclizations must be performed with the strict exclusion of oxygen. Based on the stoichiometric reactions presented in Chapter 3, the μ -oxo compound **3.1** has now been employed as a catalyst precursor and conditions that allow for compound **3.1** to be converted back to the active catalyst under catalytically relevant reaction conditions have been developed.

In a control experiment, the direct use of compound **3.1** as a catalyst precursor under the standard reaction conditions led to <40% conversion of compound **5.4a** (Table 5.2, entry 1), and no substrate conversion was observed with 1 mol% of **3.1** if the PbBr_2 additive was replaced with 3 mol % of lutidinium bromide, [HLut]Br, despite the established reaction of **3.1** with [HLut]Br to form the Cr(III) bromide **2.5** (Chapter 3). However, the μ -oxo compound **3.1** was readily reduced to **2.1** if two equivalents of [HLut]Br and an excess of Mn were added before the haloacetal and γ -terpinene. Subsequent addition of the desired bromo substrate **5.4a** under standard reaction conditions resulted in an 83% isolated yield of **5.9** (Table 5.2, entry 2); only a 10% decrease in yield compared to the standard conditions using the Cr(III) bromide catalyst **2.5**

(Table 5.1, entry 2). Table 5.2, entry 3 shows the optimized reaction conditions with only 1 mol % of the μ -oxo **3.1** providing 90% isolated yield of the desired cyclized product.

Table 5.2. Optimization experiments to reduce the air-sensitivity of haloacetal cyclizations.^a

Reaction scheme: **5.4a** $\xrightarrow[\text{50 } ^\circ\text{C, 38.5 h, 4 equiv } \gamma\text{-terpinene, 2 equiv Mn}]{\text{cat. Cr(III)-X}}$ **5.9**

Entry	Cr Catalyst	Additives	Yield ^b
1	1 mol % 3.1	1 mol % PbBr ₂	<40%
2	1 mol % 3.1	3 mol % [HLut]Br	83% (82/18) ^c
3	1 mol % 3.1	3 mol % [HLut]Br, 1 mol % PbBr ₂	90% (82/18)
4	2 mol % 2.5	10 mol % Me ₃ SiCl	87% (82/18) ^d
5	2 mol % 2.5	10 mol % Me ₃ SiCl	92% (80/20) ^e

^a Substrate (1 mmol). ^b Isolated yields. Diastereomeric ratios are in parentheses.

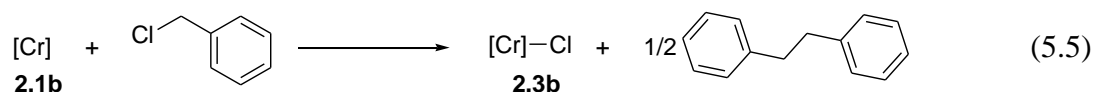
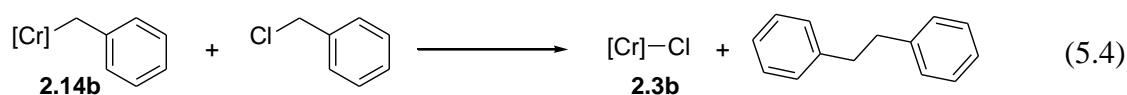
^c Compound **3.1** mixed with 3 mol % [HLut]Br and Mn (2 equiv) for 4 h prior to addition of substrate. No reaction is observed without pre-mixing step. ^d 24 h

reaction time. ^e Reagents were mixed under air prior to reaction for 22 h at 65 °C.

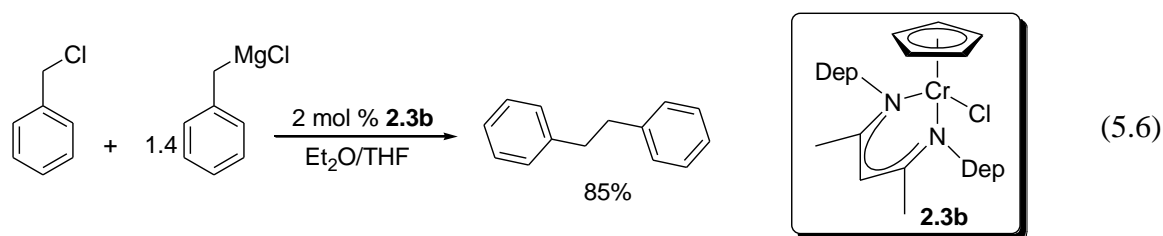
It was also determined that a substoichiometric amount of Me₃SiCl could be used to activate the Mn in place of the PbBr₂ under the standard reaction conditions, with only a slight decrease in yield (Table 5.2, entry 4). Most notable is the result in Table 5.2, entry 5 where the reaction vessel was charged with the reagents and solvent under ambient atmosphere, after which the headspace of the reaction vessel was purged with N₂ before being sealed. The reaction was heated to 65 °C for 22 h to afford a 92% isolated yield upon workup. The success of the reaction can be attributed to the fact that Me₃SiCl-activated Mn reacts rapidly with O₂ to form Mn oxides, the same reason the Mn was not effective for the HAT reactions presented in Chapter 3. The activated Mn scrubbed the reaction of trace oxygen before the Cr(III) bromide catalyst **2.5** was reduced to the air-sensitive Cr(II) state (**2.1**), thereby alleviating the need to meticulously exclude trace oxygen from the haloacetal cyclization reactions.

5.3 C–C Bond Formation with Benzyl Radicals

The radical trapping agent PhSSPh, used in Chapter 2, reacted with both the Cr(II) and the C-based radicals that formed upon Cr–C bond homolysis. Another strategy described above makes use of an H atom donor such as γ -terpinene to react selectively with the organic radical, leaving the Cr(II) intact. Yet another possibility in exploring Cr–C bond homolysis is to use a substrate that selectively reacts with the Cr(II) but not with the organic radical. The Cr(III) benzyl compounds **2.14**–**2.14c** undergo rapid Cr–C bond homolysis in solution but, due to the highly stabilized nature of the benzyl radical, the compounds are not efficient radical initiators for controlled radical polymerization. The compounds are also stable with respect to bibenzyl formation, despite the rapid bimolecular coupling of benzyl radicals in solution. The inherent stability of the Cr(III) benzyl compounds is due to the presence of very small amounts of Cr(II) in solution, which prevents bibenzyl formation by keeping $[\text{PhCH}_2\cdot]$ low. As a result, a different approach was taken to examine the radical chemistry of the Cr(III) benzyl compounds. The addition of PhCH₂Cl consumes the Cr(II) by forming the Cr(III) chloride, thereby shutting down the persistent radical effect of the Cr(II). Stoichiometric reactions performed by Caitlyn Liberto are shown in eq 5.4 and 5.5.¹⁴³ In eq 5.4, reaction of the Cr(III) benzyl compound **2.14b** with one equivalent of benzyl chloride (PhCH₂Cl) formed the Cr(III) chloride complex **2.3b** and bibenzyl. Reaction of the Cr(II) compound **2.1b** with one equivalent of PhCH₂Cl resulted in the same product formation (eq 5.5).



In both eq 5.4 and 5.5 salt metathesis of **2.3b** to form **2.14b** or reduction of the chloride species **2.3b** to Cr(II) would reform the Cr starting materials of each reaction, respectively, and an excess of PhCH₂Cl should then render the reactions catalytic in Cr. Both approaches were examined under catalytic reaction conditions. Optimized reaction conditions of the salt metathesis method are shown in eq 5.6. Using 2 mol % of the Cr(III) chloride compound **2.3b**, PhCH₂Cl, and a slight excess of a benzyl Grignard reagent (ClMgCH₂Ph), the coupled product bibenzyl was isolated from the reaction mixture in 85% yield. In the proposed mechanism shown in Figure 5.6, the chloride compound **2.3b** first reacts with the Grignard reagent to form the



Cr(III) benzyl species **2.14b**, which rapidly undergoes homolysis to generate the benzyl radical and one equivalent of Cr(II). The Cr(II) compound **2.1b** is then capable of reducing the PhCH_2Cl to reform the chloride species **2.3b**, which generates another equivalent of $\text{PhCH}_2\cdot$ radical. The effective concentration of Cr(II) in the reaction mixture is minimized by the presence of PhCH_2Cl , which limits the ability of the Cr(II) to effectively trap the benzyl radicals, thereby leading to bibenzyl formation.

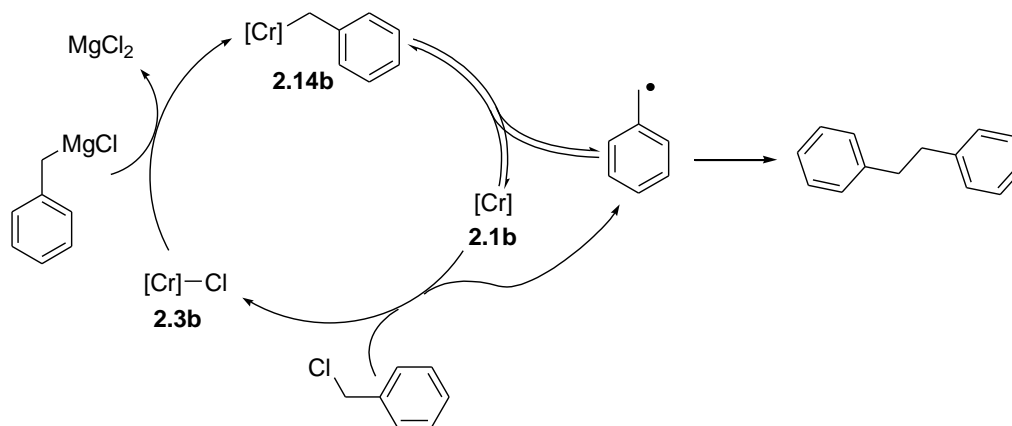


Figure 5.6. Proposed catalytic cycle for the chromium-catalyzed synthesis of bibenzyl from PhCH_2Cl and ClMgCH_2Ph .

The second method for bibenzyl formation involved the use of activated Mn to reduce the Cr(III) chloride compound **2.3b** to Cr(II), which then reduces PhCH_2Cl . The reaction shown in eq 5.7 formed bibenzyl in 94% isolated yield with 5 mol % Cr catalyst (**2.3b**). The mechanism for bibenzyl formation in this reaction is similar to the one proposed in Figure 5.6, with the main difference being that the Cr(III) chloride species **2.3b** is reduced to Cr(II) by Mn, as opposed to a salt metathesis reaction. The effective concentration of Cr(II) is again minimized by the presence of PhCH_2Cl in the reaction, which allows for the formation of bibenzyl due to inefficient radical trapping by the Cr(II), as shown in Figure 5.7.

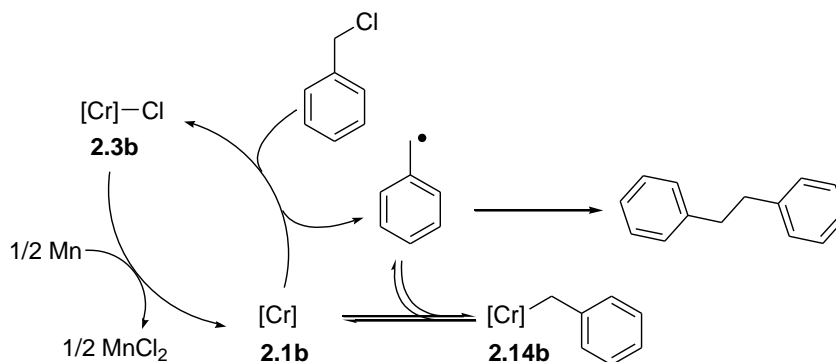
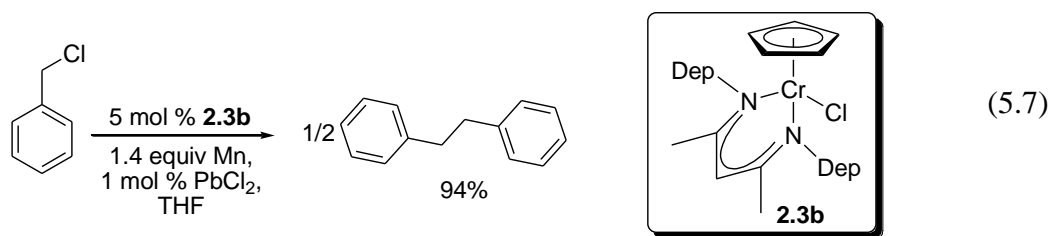
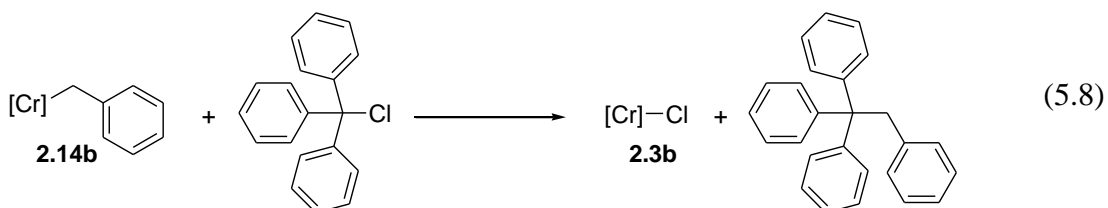
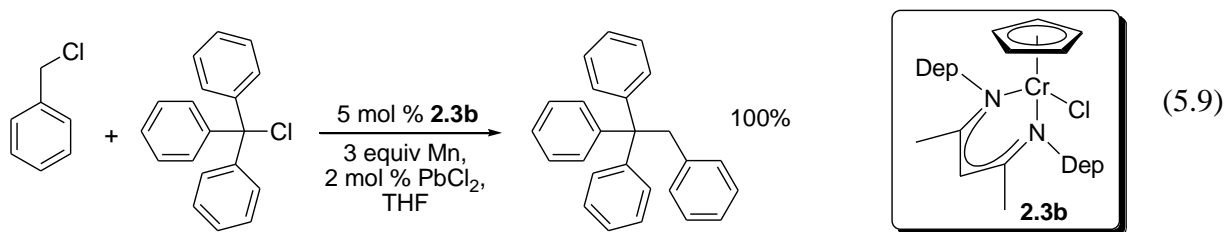


Figure 5.7. Proposed catalytic cycle for the chromium-catalyzed synthesis of bibenzyl from PhCH_2Cl with Mn as a reducing agent.

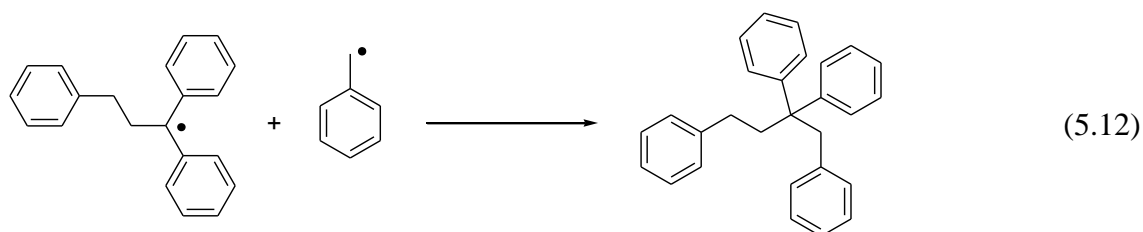
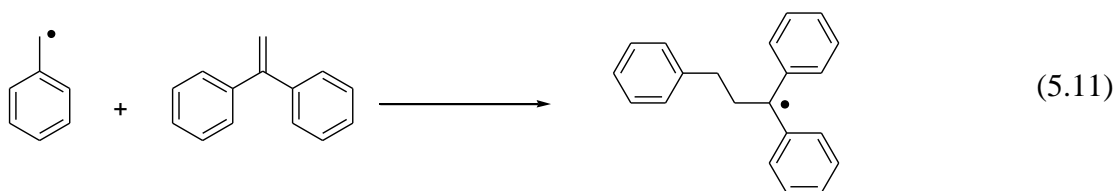
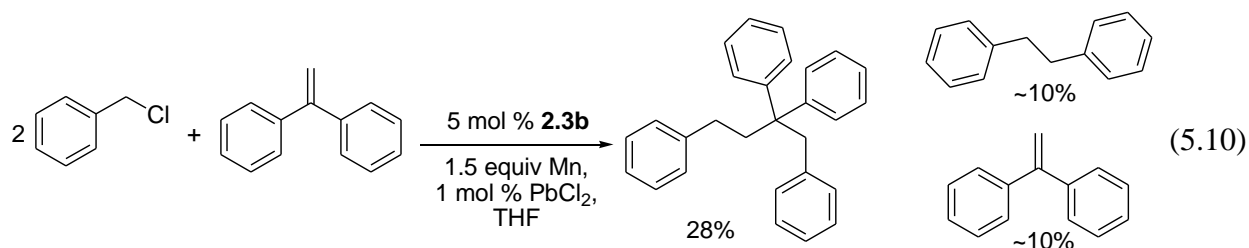
Stoichiometric reactions involving coupling of $\text{PhCH}_2\cdot$ and $\text{Ph}_3\text{C}\cdot$ radicals were examined with the Cr(III) benzyl complex **2.14b**.¹⁴³ Reaction of compound **2.14b** with one equivalent of Ph_3CCl resulted in formation of the Cr(III) chloride species **2.3b** and the heterocoupled organic product $\text{Ph}_3\text{CCH}_2\text{Ph}$, as shown in eq 5.8.¹⁴³ Similar to the bibenzyl formation discussed above, the synthesis of $\text{Ph}_3\text{CCH}_2\text{Ph}$ was rendered catalytic with the use of activated Mn to reduce the chloride compound **2.3b** to Cr(II). Eq 5.9 displays the synthesis of $\text{Ph}_3\text{CCH}_2\text{Ph}$ from PhCH_2Cl and Ph_3CCl using a catalytic amount of compound **2.3b**. Due to the weaker C–Cl bond in Ph_3CCl , it will be reduced by Cr(II) more rapidly than the PhCH_2Cl substrate under the reaction conditions, which would lead to a build up in the concentration of stable $\text{Ph}_3\text{C}\cdot$ radicals in the reaction mixture, followed by reduction of PhCH_2Cl by the Cr(II) to generate $\text{PhCH}_2\cdot$ radicals, which would be readily trapped by the preformed $\text{Ph}_3\text{C}\cdot$ radicals to selectively form the desired heterocoupled product. No bibenzyl was detected under the reaction conditions outlined in eq 5.9.





5.4 Addition of Alkyl Radicals to Substituted Olefins

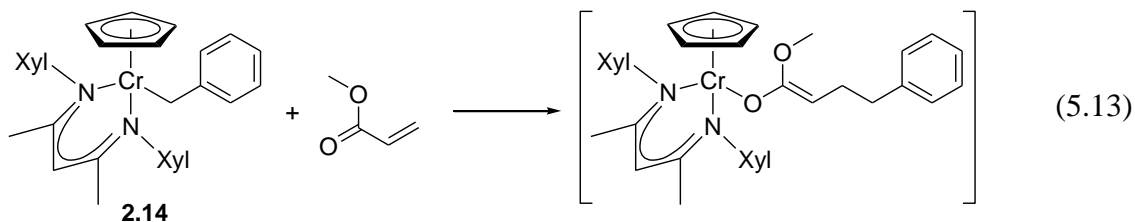
The rates of reaction between benzyl radicals and substituted olefins ($\text{CH}_2=\text{CX}_2$) vary greatly depending on the X substituents of the olefin.¹²⁷ Although the rate of reaction between benzyl radicals and vinyl acetate is slow, other olefins are much more prone to radical addition by benzyl radicals.¹²⁷ 1,1-Diphenylethylene ($\text{Ph}_2\text{C}=\text{CH}_2$) is used as a radical scavenger when probing reactions for the presence of radical intermediates.¹⁴⁴ Under catalytic reaction conditions similar to those outlined in eq 5.7 for the coupling of benzyl radicals, addition of $\text{Ph}_2\text{C}=\text{CH}_2$ significantly reduced the amount of bibenzyl produced in the reaction. The major product of this reaction is shown in eq 5.10, the result of two benzyl radicals adding to the double bond of the $\text{Ph}_2\text{C}=\text{CH}_2$ substrate. Only a small amount of bibenzyl and unreacted $\text{Ph}_2\text{C}=\text{CH}_2$ were isolated from the reaction. Presumably, the reaction product $[\text{PhCH}_2\text{C}(\text{Ph})_2\text{CH}_2\text{CH}_2\text{Ph}]$ is formed by an initial reaction of a $\text{PhCH}_2\cdot$ radical with $\text{Ph}_2\text{C}=\text{CH}_2$ to



form the tertiary radical intermediate shown in eq 5.11. This radical intermediate species then reacts with a second equivalent of benzyl radical, as shown in eq 5.12, to form the observed product.

As discussed in Chapter 4, the Cr(III) neopentyl compound **2.11** reacted rapidly with methyl acrylate but was unable to control the polymerization of that monomer due to irreversible binding of the resulting enolate radical to Cr(II), forming a Cr(III) enolate species. Although the Cr was not an effective control agent for the radical polymerization of methyl acrylate, the effective trapping of enolate radicals by the Cr(II) compound **2.1** represented a potentially useful tool from a synthetic organic perspective.

Treatment of the Cr(III) benzyl compound **2.14** with 12 equivalents of methyl acrylate resulted in the reaction mixture becoming green upon stirring overnight. The UV-vis spectrum of the reaction mixture contained absorption bands at 401 and 586 nm, similar to the other Cr(III) enolate compounds presented in Chapters 3 and 4. In contrast, no reaction was observed with the Cr(III)–CH₂SiMe₃ compound **2.7** under similar reaction conditions. As discussed in Chapter 2, compound **2.7** does not undergo Cr–C bond homolysis, suggesting that the observed reaction between compound **2.14** and methyl acrylate (eq 5.13) proceeds by a radical mechanism as a result of Cr–C bond homolysis, and not due to a simple conjugate addition of the olefin to the organometallic complex. Similarly, the Cr(III) neopentyl compound **2.11** also reacted with



methyl acrylate in solution to produce a green mixture with absorption bands at 406 and 607 nm. In an attempt to generate the neopentyl compound **2.11** in situ, in the presence of methyl acrylate, a reductive recycle reaction was conducted with the Cr(II) compound **2.1**, one equivalent of Me₃CCH₂I, and 5 equivalents of methyl acrylate and Mn. The reaction mixture was initially the green (magenta transmitted) colour of the Cr(II). Upon stirring for 1 h, the solution became orange transmitted and after stirring overnight the solution unexpectedly changed back to the initial colour of the Cr(II) compound **2.1**. Based on observations in Chapter 3, the Cr(III) enolate species that would be generated under the reaction conditions could undergo transmetallation with the resulting MnI₂ to form the Cr(III) iodide species, which would be reduced by the Mn powder back to Cr(II). The reactions shown in Figure 5.8 suggested that

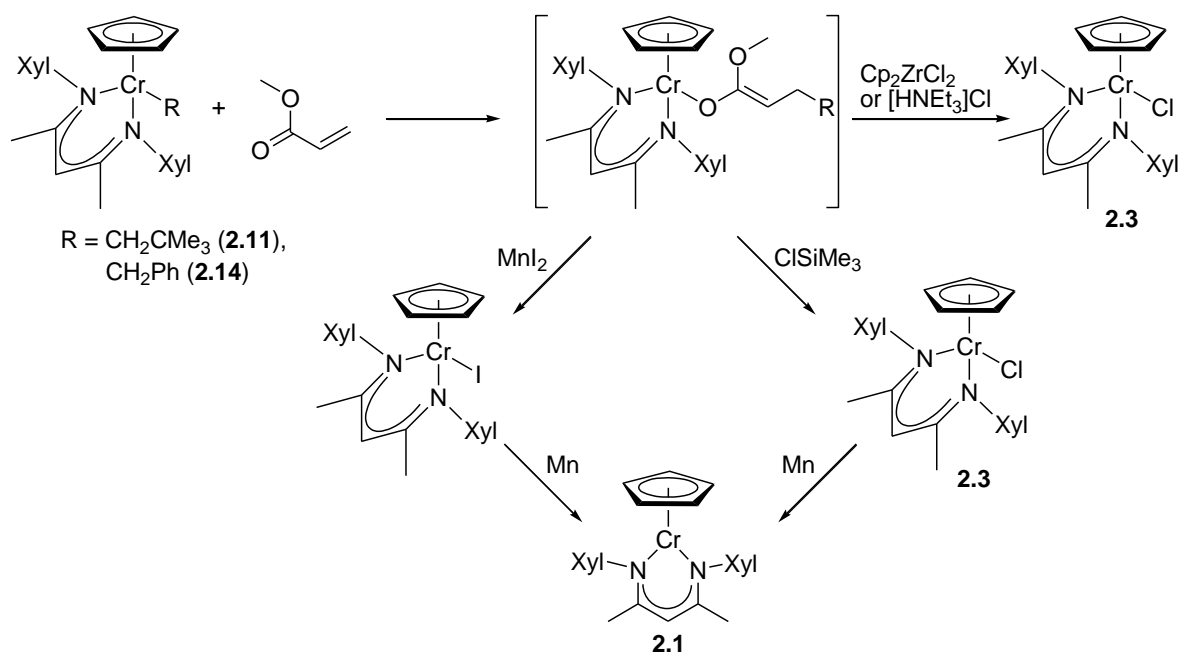


Figure 5.8. Conversion of Cr(III) enolate species to Cr(III) halides and reduction to Cr(II).

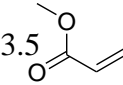
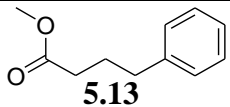
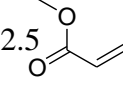
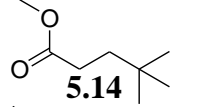
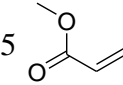
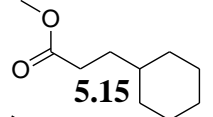
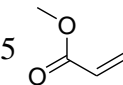
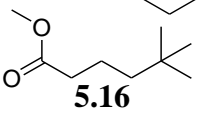
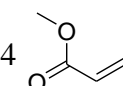
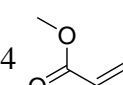
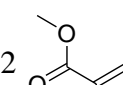
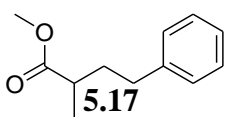
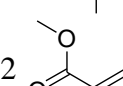
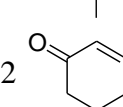
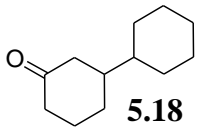
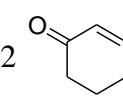
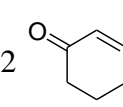
this was indeed the case since the in situ generated Cr(III) enolate compounds shown in Figure 5.8 reacted with MnI_2 to form the Cr(III) iodide species, which was then reduced with Mn . Transmetalation was also observed with Cp_2ZrCl_2 to form the chloride compound **2.3**. Protonolysis of the Cr(III) enolates with $[\text{HNEt}_3]\text{Cl}$ also provided the chloride compound **2.3**. Reaction of the Cr(III) enolates with ClSiMe_3 also generated compound **2.3**, which, when performed in the presence of Mn , resulted in reduction of the Cr to compound **2.1** (Figure 5.8).

The reactions shown in Figure 5.8 represent a variety synthetic methods capable of converting the Cr(III) enolates to Cr(III) halides and reduction to Cr(II). Similar to the catalytic reactions presented above for bibenzyl formation, establishing conditions by which the Cr(II) compound is converted back to the Cr(III) hydrocarbyl species remains as the final step in a potential catalytic cycle. As such, addition of an organic halide to Cr(II) would provide the final step to complete the catalytic cycle. Table 5.3 lists a series of initial reactions exploring the addition of alkyl radicals to enones under catalytic conditions.

In entry 1, methyl acrylate was treated with benzyl radicals that were generated in situ by reduction of PhCH_2Cl with Cr(II). Activated Mn was used as a stoichiometric reductant for the Cr(III) halide. The Cr(II) present in the reaction mixture would be able to trap the enolate radical generated upon addition of the $\text{PhCH}_2\cdot$ radical to methyl acrylate. The Mn(II) halide formed throughout the course of the reaction would be capable of reacting with the Cr(III) enolate intermediate to presumably form a Mn enolate species and the Cr(III) halide. The

desired product **5.13** was isolated in low yield from the reaction. Benzyl radicals are typically much less reactive compared to other less stabilized C-based radicals.¹²⁷ Indeed, the use of more reactive radicals did lead to an increase in yield. The use of Me₃CBr and Me₃CCH₂Br in entries 2 and 4, respectively, provided moderate increases in yield compared to PhCH₂Cl.

Table 5.3. Addition of alkyl radicals to enones.

Entry	R-X	Enone	[Cr]	Additives	Time	Product	Yield
1	PhCH ₂ Cl	3.5 	0.10 (2.3)	2 Mn, 0.02 PbCl ₂	7 d	 5.13	16%
2	Me ₃ CBr	2.5 	0.07 (2.5)	5 Mn, 0.01 PbBr ₂	5 d	 5.14	24%
3	<i>c</i> -C ₆ H ₁₁ Br	5 	0.11 (2.5)	5 Mn, 0.01 PbBr ₂	3 d	 5.15	<10%
4	Me ₃ CCH ₂ Br	5 	0.06 (2.5)	3 Mn, 0.01 PbBr ₂	7 d	 5.16	33%
5	PhCH ₂ Cl	4 	0.10 (2.3)	2 Mn, 2 Me ₃ SiCl	4 d	5.13	11%
6	Me ₃ CCH ₂ I	4 	0.20 (2.1)	3 Mn, Cp ₂ ZrCl ₂	2 d	5.16	<10%
7	PhCH ₂ Cl	2 	0.09 (2.3)	2 Mn, 0.03 PbCl ₂ , 2 Me ₃ SiCl	3 d	 5.17	28%
8	PhCH ₂ Cl	2 	0.09 (2.3)	2 Mn, 0.03 PbCl ₂ , Cp ₂ ZrCl ₂	4 d	5.17	9%
9	<i>c</i> -C ₆ H ₁₁ Br	2 	0.10 (2.5)	2 Mn, 1.5 Me ₃ SiCl	2 d	 5.18	25%
10	<i>c</i> -C ₆ H ₁₁ Br	2 	0.10 (2.5)	2.5 Mn, 1.3 Pr ₃ SiCl	1 d	5.18	<20%
11	<i>c</i> -C ₆ H ₁₁ Br	2 	0.10 (2.5)	2 Mn, 0.01 PbCl ₂ , Cp ₂ ZrCl ₂	2 d	5.18	0%

The stability of a potential Mn enolate species under the reaction conditions was unknown and, therefore, the other reactions in Figure 5.8 for the abstraction of an enolate ligand from Cr(III) were tested under catalytic reaction conditions. The use of Me₃SiCl to abstract the enolate moiety from a Cr(III) intermediate in entry 5 showed no improvement in yield compared

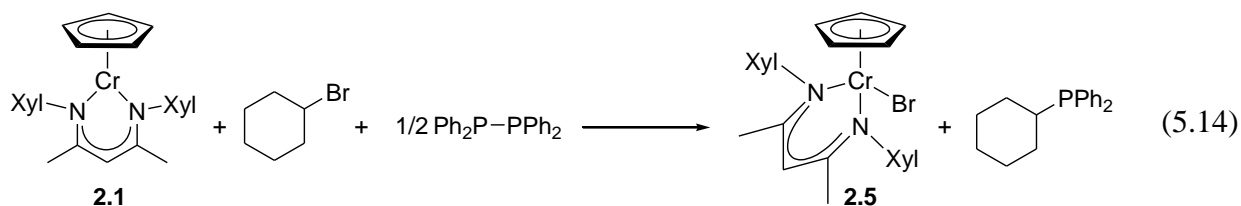
to the Mn(II) halide method. The use of Cp_2ZrCl_2 initially appeared promising based on the fast reactions observed with Cr(III) enolate species, but under catalytic conditions the yields were inferior compared to the other methods, as shown in entries 6, 8, and 11. In the reactions described in entries 6 and 8 it was discovered that the acrylates were polymerizing under the reaction conditions. In fact, zirconocene enolates have been used as catalysts for the coordination polymerization of methyl methacrylate, as well as other polar vinyl monomers.¹²⁸ Although the Cp_2ZrCl_2 appears to be an efficient stoichiometric transmetallation reagent with the Cr(III) enolates, and has received extensive use by Kishi and co-workers with Cr(III) alkoxides,^{15,16,87} the resulting zirconocene enolates are incompatible with the enone substrates under catalytic conditions.

The use of methyl methacrylate instead of methyl acrylate provided a higher yield upon reaction with PhCH_2Cl , as shown in entry 7. The substrate 2-cyclohexen-1-one ($\text{C}_6\text{H}_8\text{O}$) was also subjected to reaction with cyclohexyl radicals in entries 9–11. The best yield was obtained with Me_3SiCl , entry 9. Recent work by Weix and co-workers reported improved yields for the synthesis of silyl enol ethers by conjugate addition of alkyl halides to $\text{C}_6\text{H}_8\text{O}$ with the use of R_3SiCl , where $\text{R} = \text{Et}$ or Pr , as opposed to Me_3SiCl .¹⁴⁵ The use of Pr_3SiCl instead of Me_3SiCl did not provide an increased yield of compound **5.18** under the conditions outlined in entry 10.

5.5 Chromium Catalyzed C–P Bond Formation

Phosphine complexes are ubiquitous in transition metal-catalyzed cross-coupling reactions for organic synthesis.¹⁴⁶ Preparation of commercially available phosphines often involves the use of harsh reagents and reaction conditions.¹⁴⁷ An alternative method for the preparation of organophosphorus complexes involves the formation of organic radical intermediates. Phosphorus containing compounds with P–P bonds can act as efficient trapping agents for organic radicals.¹⁴⁸ The use of white phosphorus (P_4) as a radical trap for the synthesis of PR_3 , where $\text{R} = \text{Ph}$, Ph_3Sn , Me_3Si , and $c\text{-C}_6\text{H}_{11}$, was achieved with the use of stoichiometric Ti(III) reagents to generate the $\text{R}\cdot$ radicals by single-electron reduction of the R-halide reagents.¹⁴⁹ The production of ArPPh_2 , where Ar is a substituted aryl, by reaction of $\text{Ar}\cdot$ radicals with $\text{Ph}_2\text{P–PPh}_2$ provides a radical route for heterosubstituted phosphines.¹⁴⁸ Although $\text{Ph}_2\text{P–PPh}_2$ is also an efficient trap for alkyl radicals, providing RPPH_2 products, where R is an alkyl group, few examples exist of the high yield synthesis of such compounds by a radical mechanism.^{148,150}

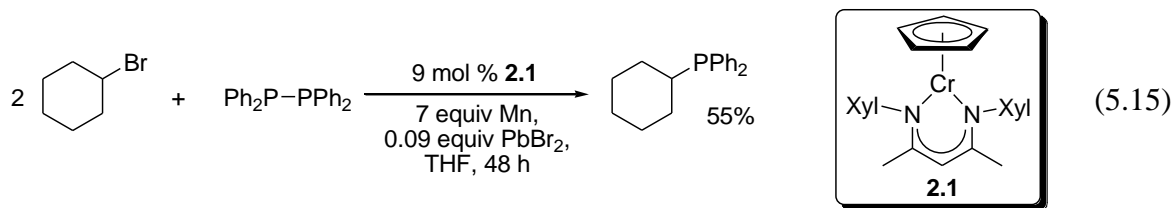
A stoichiometric reaction of the Cr(II) compound **2.1** with one equivalent of *c*-C₆H₁₁Br in the presence of 0.5 equivalents of Ph₂P–PPh₂ provided *c*-C₆H₁₁PPh₂ as the only P containing product of the reaction, with only a small amount of unreacted Ph₂P–PPh₂ remaining, eq 5.14. The same reaction was setup using a catalytic amount of compound **2.1** and activated Mn to reduce the Cr(III) halide formed as a result of alkyl halide reduction. Somewhat surprisingly, ³¹P NMR analysis of the reaction showed only one peak corresponding to unreacted Ph₂P–PPh₂, even though the formation of a precipitate (presumably Mn(II) halide) was observed during the reaction.



A series of control experiments were conducted to examine the possibility of unwanted side reactions inhibiting this reaction under catalytic conditions. The Cr(II) compound **2.1** did not react with Ph₂P–PPh₂ in THF overnight. Additionally, no reaction was observed between PbBr₂ activated Mn and Ph₂P–PPh₂, and no reaction was observed upon addition of *c*-C₆H₁₁Br. This result demonstrated that the precipitate was only formed in the presence of Cr under the catalytic conditions, suggesting that the *c*-C₆H₁₁Br was reacting with the Cr(II) to form the Cr(III) bromide, and that the Cr(III) bromide was being reduced by Mn to form the MnBr₂ insoluble precipitate, and yet the desired product was not observed by NMR. Suspicions arose as to the formation of a Mn(II) halide phosphine adduct in the reaction mixture,¹⁵¹ and that the Mn phosphine complex may not be soluble in C₆D₆ used for NMR analysis upon completion of the reaction.

Manganese(II) chloride was recently used to abstract phenanthroline from molybdenum complexes, which forms a stable Mn phenanthroline complex.¹⁵² Under catalytic reaction conditions, the addition of bipyridine at the end of the Ph₂P–PPh₂ alkylation reaction resulted in a large amount of precipitate being formed, and the NMR spectrum of the reaction mixture contained a large peak corresponding to the desired product *c*-C₆H₁₁PPh₂. Interestingly, the yield of the reaction was significantly reduced when bipyridine was present during the reaction, and was therefore added only after the reaction was complete. The reaction shown in eq 5.15 was conducted with 9 mol % Cr leading to 55% yield of *c*-C₆H₁₁PPh₂. A small amount of an unidentified compound with a ³¹P NMR signal at -8.4 ppm was also detected. The amount of

this unidentified product appears to be concentration dependent, as the amount of unwanted product is reduced when the reaction is performed with higher concentrations of substrates.



Since $\text{Ph}_2\text{P-PPh}_2$ is typically prepared from the commercially available Ph_2PCl , the use of Ph_2PCl directly in these reactions is synthetically desirable by removing the need to prepare the diphosphine substrate. Ongoing research in the Smith group has resulted in the direct use of Ph_2PCl under similar reaction conditions to those presented herein for the synthesis of *c*- $\text{C}_6\text{H}_{11}\text{PPh}_2$, and further studies are currently underway to optimize the reaction conditions and expand the scope of alkyl halides.

5.6 Experimental Section

General considerations. Protocols were identical to those reported in sections 2.13 and 3.14 using standard Schlenk and glovebox techniques unless otherwise indicated.

Characterization. Protocols were identical to those reported in sections 2.13 and 3.14. Additionally, high resolution mass spectrometry was performed with a Waters Micromass LCT Premier Time of Flight mass spectrometer.

Materials. Protocols were identical to those reported in sections 2.13 and 3.14. Additionally, allyl alcohol, 2-butyne-1-ol, cinnamyl alcohol, 3-methyl-2-buten-1-ol, *trans*-2-hexen-1-ol, 3,4-dihydro-2*H*-pyran, *N*-chlorosuccinimide, *N*-bromosuccinimide, and chlorotripropylsilane were purchased from Aldrich and used as received. 2-Cyclohexen-1-one, benzyl chloride, cyclohexyl bromide, neopentyl bromide, neopentyl iodide, and *tert*-butyl bromide were purchased from Aldrich, degassed by three freeze-vacuum-thaw cycles, and stored under nitrogen prior to use. Methyl methacrylate was passed through a column of neutral alumina to remove stabilizer, dried over calcium hydride, purified by vacuum distillation, degassed by three freeze-vacuum-thaw cycles, and stored under nitrogen at $-35\text{ }^\circ\text{C}$. Compounds **5.1a**,¹⁵³ **5.4a**,¹⁵⁴ **5.5a**,¹⁵⁴ **5.5b**,^{139c} **5.6a**,^{139c} **5.7**,¹⁵⁵ **5.8**,¹⁵⁴ **5.10**,¹⁵⁴ **5.11**,^{139c} and **5.12**¹⁵⁶ have been previously characterized in the literature.

Synthesis of $\text{CpCr}[(\text{XylNCMe})_2\text{CH}](\text{C}_8\text{H}_{13}\text{O}_2)$ (5.2**).** Compound **2.1** (206 mg, 0.488 mmol) and Mn powder (257 mg, 4.69 mmol, 9.60 equiv) were placed in a Schlenk flask with

THF (10 mL). Compound **5.1a** (122 mg, 0.551 mmol, 1.13 equiv) was transferred to the Schlenk with THF (1 mL) and the reaction mixture was stirred for 23 h at room temperature. The solvent was removed under reduced pressure, the residue was extracted with hexanes (35 mL), filtered through Celite, and the solvent was again removed under reduced pressure. The purple residue was extracted with hexanes (10 mL), filtered through Celite and cooled to -35 °C to yield crystals of **5.2** (129 mg, 47%) in four crops. Anal. Calcd for C₃₄H₄₃N₂O₂Cr: C, 72.44; H, 7.69; N, 4.97. Found: C, 72.30; H, 8.39; N, 4.79. UV-vis (hexanes, λ_{max} , nm(ϵ , M⁻¹cm⁻¹)): 413 (5470), 556 (1730).

General Procedure for the Preparation of Haloacetals. The haloacetal compounds were prepared according to a related literature procedure.¹³⁷ *N*-bromosuccinimide or *N*-chlorosuccinimide (1 equiv) was placed in a two-neck flask with a nitrogen inlet valve and a stopper, and the head-space was evacuated and back-filled three times. The flask was cooled in an ice-bath at which point CH₂Cl₂ (4 mL) and the appropriate alcohol (1.3 - 1.7 equiv) were added followed by the dropwise addition of 3,4-dihydro-2*H*-pyran (1 equiv). The reaction mixture was stirred for 1 h in the ice-bath and then stirred for an additional 1 to 18 h at room temperature. The reaction was then diluted with Et₂O (50 mL) and filtered onto ice-water (100 mL). The aqueous layer was washed with Et₂O (3 × 50 mL). The combined organic layer was dried (MgSO₄), filtered and the solvent was removed under reduced pressure. The product was purified by silica column chromatography (hexanes/Et₂O or hexanes/EtOAc) and degassed by three freeze-vacuum-thaw cycles and stored under nitrogen prior to use.

Some alcohols were used as the limiting reagent with an excess (1.5 equiv) of 3,4-dihydro-2*H*-pyran.

Preparation of 2-allyloxy-3-chlorotetrahydropyran (5.1b, mixture of stereoisomers, 65/35). The procedure reported above was followed with *N*-chlorosuccinimide (2.68 g, 20.0 mmol, 1.00 equiv), allyl alcohol (2.00 mL, 29.3 mmol, 1.47 equiv) and 3,4-dihydro-2*H*-pyran (1.81 mL, 20.0 mmol, 1.00 equiv) with CH₂Cl₂ (4 mL). The reaction was stirred in an ice bath for 1 h and for an additional 4 h at room temperature. Purification by silica column chromatography (hexanes/EtOAc 4:1) afforded **5.1b** (1.18 g, 34% yield) as a colourless oil. ¹H NMR (400.1 MHz, CDCl₃) δ 1.46-1.57 (m, 1H), 1.70-2.03 (m, 2H), 2.11-2.23 (m, 0.35H), 2.28-2.37 (m, 0.65H), 3.48-3.61 (m, 1H), 3.77-3.94 (m, 2H), 3.97-4.12 (m, 1H), 4.23-4.30 (m, 1H), 4.59 (d, *J* = 4.0 Hz, 0.65H), 4.78 (d, *J* = 2.9 Hz, 0.35H), 5.17-5.24 (m, 1H), 5.29-5.41 (m, 1H), 5.87-6.01 (m, 1H). HRMS *m/z* calcd for C₈H₁₃O₂Cl+Na: 199.0502, found 199.0782 [*M*⁺+Na].

Preparation of 3-chloro-2-[(*E*)-2-hexenyloxy]tetrahydropyran (5.4b, mixture of stereoisomers, 66/34). The procedure reported above was followed with *N*-chlorosuccinimide (2.67 g, 20.0 mmol, 1.13 equiv), *trans*-2-hexen-1-ol (3.50 mL, 29.5 mmol, 1.66 equiv) and 3,4-dihydro-2*H*-pyran (1.61 mL, 17.8 mmol, 1.00 equiv) with CH₂Cl₂ (4 mL). The reaction was stirred in an ice bath for 1 h and for an additional 18 h at room temperature. Purification by silica column chromatography (hexanes/EtOAc 4:1) afforded **5.4b** (2.02 g, 52% yield) as a colourless oil. ¹H NMR (400.1 MHz, CDCl₃) δ 0.90 (t, *J* = 7.4 Hz, 3H), 1.34-1.57 (m, 3H), 1.68-2.08 (m, 4H), 2.09-2.23 (m, 0.34H), 2.26-2.37 (m, 0.66H), 3.45-3.61 (m, 1H), 3.76-3.94 (m, 2H), 3.95-4.06 (m, 1H), 4.16-4.25 (m, 1H), 4.58 (d, *J* = 4.0 Hz, 0.66H), 4.77 (d, *J* = 2.8 Hz, 0.34H), 5.50-5.63 (m, 1H), 5.67-5.81 (m, 1H). HRMS *m/z* calcd for C₁₁H₁₉O₂Cl+Na: 241.0971, found 241.1251 [*M*⁺+Na].

Preparation of 3-chloro-2-(3-phenyl-2-propenyloxy)tetrahydropyran (5.6b, mixture of stereoisomers, 60/40). The procedure reported above was followed with *N*-chlorosuccinimide (2.68 g, 20.0 mmol, 1.01 equiv), cinnamyl alcohol (2.67 g, 19.9 mmol, 1.00 equiv) and 3,4-dihydro-2*H*-pyran (2.70 mL, 29.8 mmol, 1.50 equiv) with CH₂Cl₂ (4 mL). The reaction was stirred in an ice bath for 1 h and for an additional 4 h at room temperature. Purification by silica column chromatography (hexanes/EtOAc 4:1) afforded **5.6b** (1.70 g, 34% yield) as a colourless oil. ¹H NMR (400.1 MHz, CDCl₃) δ 1.53 (m, 1H), 1.69-2.07 (m, 2H), 2.12-2.26 (m, 0.40H), 2.28-2.40 (m, 0.60H), 3.50-3.64 (m, 1H), 3.79-4.16 (m, 2H), 4.18-4.30 (m, 1H), 4.43 (dd, *J* = 5.7, 12.7 Hz, 1H), 4.65 (d, *J* = 4.1 Hz, 0.60H), 4.84 (d, *J* = 2.9 Hz, 0.40H), 6.25-6.37 (m, 1H), 6.58-6.74 (m, 1H), 7.20-7.44 (m, 5H). HRMS *m/z* calcd for C₁₄H₁₇O₂Cl+Na: 275.0815, found 275.0905 [*M*⁺+Na].

Preparation of 3-bromo-2-(2-propynyloxy)tetrahydropyran (5.7a). The procedure reported above was followed with *N*-bromosuccinimide (4.16 g, 23.4 mmol, 1.17 equiv), 2-butyne-1-ol (1.50 mL, 20.1 mmol, 1.00 equiv) and 3,4-dihydro-2*H*-pyran (2.70 mL, 29.8 mmol, 1.49 equiv) with CH₂Cl₂ (4 mL). The reaction was stirred in an ice bath for 1 h and for an additional 1 h at room temperature. Purification by silica column chromatography (hexanes/EtOAc 4:1) afforded **5.7a** (2.49 g, 53% yield) as a colourless oil. ¹H NMR (400.1 MHz, CDCl₃) δ 1.40-1.59 (m, 1H), 1.86 (t, *J* = 2.4 Hz, 3H), 1.90-2.07 (m, 2H), 2.33-2.44 (m, 1H), 3.52-3.65 (m, 1H), 3.79-3.93 (m, 1H), 3.99-4.16 (m, 1H), 4.17-4.35 (m, 2H), 4.84 (d, *J* = 3.8 Hz, 1H). HRMS *m/z* calcd for C₉H₁₃O₂Br+Na: 254.9997, found 255.0149 [*M*⁺+Na].

Preparation of 3-chloro-2-(2-propynyloxy)tetrahydropyran (5.7b, mixture of stereoisomers, 70/30). The procedure reported above was followed with *N*-chlorosuccinimide (2.67 g, 20.0 mmol, 1.00 equiv), 2-butyne-1-ol (1.50 mL, 20.1 mmol, 1.00 equiv) and 3,4-dihydro-2*H*-pyran (2.70 mL, 29.8 mmol, 1.49 equiv) with CH₂Cl₂ (4 mL). The reaction was stirred in an ice bath for 1 h and for an additional 16 h at room temperature. Purification by silica column chromatography (hexanes/EtOAc 4:1) afforded **5.7b** (1.19 g, 32% yield) as a colourless oil. ¹H NMR (400.1 MHz, CDCl₃) δ 1.43-1.53 (m, 1H), 1.70-1.90 (m, 4H), 1.94-2.07 (m, 1H), 2.09-2.36 (m, 1H), 3.49-3.63 (m, 1H), 3.75-3.96 (m, 1.70H), 3.97-4.16 (m, 0.30H), 4.17-4.37 (m, 2H), 4.77 (d, *J* = 3.5 Hz, 0.70H), 4.94 (d, *J* = 2.8 Hz, 0.30H). HRMS *m/z* calcd for C₉H₁₃O₂Cl+Na: 211.0502, found 211.0676 [*M*⁺+Na].

Photolysis of compound 5.2. Compound **5.2** (27.4 mg, 0.0486 mmol) was placed in a Schlenk flask followed by the addition of hexanes (2 mL) and PhSSPh (10.8 mg, 0.0495 mmol, 1.02 equiv). The reaction mixture was stirred at room temperature overnight in a glovebox, during which time no colour change was observed. The flask was then removed from the glovebox and placed on the laboratory windowsill. Upon stirring for 2 days, the reaction mixture turned green, at which point the solvent was removed under reduced pressure, the residue extracted with hexanes (2 mL), and the solvent was again removed under reduced pressure. Purification by silica column chromatography (hexanes/EtOAc 10:1) afforded **5.3**. ¹H NMR (400.1 MHz, CDCl₃) δ 1.41-1.65 (m, 3 H), 1.72-1.84 (m, 1H), 2.03-2.15 (m, 1H), 2.53-2.66 (m, 1H), 2.91 (dd, *J* = 8.0, 12.6 Hz, 1H), 3.02 (dd, *J* = 7.6, 12.6 Hz, 1H), 3.59-3.68 (m, 2H), 4.03 (dd, *J* = 6.0, 10.4 Hz, 1H), 5.24 (d, *J* = 3.7 Hz, 1H), 7.16-7.38 (m, 5H).

General procedure for the radical cyclization of haloacetals. Cyclization of the bromoacetal substrates was performed with the Cr(III) bromide compound **2.5** and PbBr₂, while cyclization of the chloroacetal substrates was achieved with the Cr(III) chloride compound **2.3** and PbCl₂. In a glovebox, the appropriate Cr(III) halide (**2.5** or **2.3**) (2 or 20 mol %, respectively), Mn powder (2 equiv) and PbX₂ (X = Br or Cl, respectively) (< 1 mol %) were placed in a Teflon stoppered thick-walled glass reaction vessel with THF (3 mL). γ-Terpinene (4 equiv) was then introduced into the reaction vessel followed by the addition of haloacetal (1 mmol, 1 equiv) in THF (1 mL). The reaction vessel was then sealed, removed from the glovebox and placed in an oil bath. The bromo substrates were stirred for 38.5 h at 50 °C and the chloro substrates for 88 h at 70 °C, at which point the solvent was removed under reduced pressure. The residue was extracted with hexanes (4 mL), filtered through Celite, and purified by silica column chromatography (hexanes/EtOAc) to yield compounds **5.8** – **5.12** as clear

liquids. Product identification was performed using ^1H NMR for comparison with the literature values.

Attempted cyclization of bromoacetal 5.5a without chromium. The cyclization procedure described above was followed with PbBr_2 (2.0 mg, 0.0054 mmol, 0.5 mol %), Mn powder (273 mg 4.97 mmol, 4.93 equiv), γ -terpinene (800 μL , 4.98 mmol, 4.93 equiv) and **5.5a** (252 mg, 1.01 mmol). The reaction was stirred for 2 days at room temperature. No cyclized product was isolated upon workup and purification by silica column chromatography (hexanes/EtOAc 8:1). The same reaction conducted at room temperature with 2 mol % of compound **2.5** produced the cyclized product **5.10** [114 mg, 67% (diastereomer ratio 71/29)].

Attempted cyclization of bromoacetal 5.1a (Table 5.1, entry 1). The cyclization procedure described above was followed with **2.5** (10.2 mg, 0.0203 mmol, 2 mol %), PbBr_2 (1.8 mg, 0.0049 mmol, 0.5 mol %), Mn powder (139 mg 2.54 mmol, 2.54 equiv), γ -terpinene (640 μL , 3.98 mmol, 3.98 equiv) and **5.1a** (221 mg, 1.00 mmol). During the 38.5 h reaction time the reaction vessel was kept in a 50 $^\circ\text{C}$ oil bath in the dark. Workup and purification by silica column chromatography (hexanes/EtOAc 10:1) afforded unreacted starting material **5.1a** (162 mg, 73%) as a clear oil. No cyclized product was isolated from the reaction.

Cyclization of bromoacetal 5.4a (Table 5.1, entry 2). The cyclization procedure described above was followed with **2.5** (10.5 mg, 0.0209 mmol, 2 mol %), PbBr_2 (3.0 mg, 0.0082 mmol, 0.8 mol %), Mn powder (114 mg 2.07 mmol, 2.04 equiv), γ -terpinene (640 μL , 3.98 mmol, 3.93 equiv) and **5.4a** (266 mg, 1.01 mmol). The reaction was stirred in an oil bath at 50 $^\circ\text{C}$ for 38.5 h. Workup and purification by silica column chromatography (hexanes/EtOAc 4:1) afforded **5.9** [173 mg, 93% (diastereomer ratio 82/18)] as a clear oil. ^1H NMR (400.1 MHz, CDCl_3) δ 0.89 (t, $J = 7.1$ Hz, 3H), 1.14-1.46 (m, 7H), 1.49-1.75 (m, 3H), 1.79-1.99 (m, 1H), 2.21-2.37 (m, 1H), 3.41 (ddd, $J = 2.4, 11.5, 1.5$ Hz, 0.18H), 3.53 (dd, $J = 8.2, 8.2$ Hz, 0.18H), 3.60-3.67 (m, 1.64H), 3.70-3.78 (m, 0.82H), 3.84-3.91 (m, 0.18H), 3.94 (dd, $J = 8.0, 8.0$ Hz, 0.82H), 4.28 (dd, $J = 8.2, 8.2$ Hz, 0.18H), 4.99 (d, $J = 3.6$ Hz, 0.18H), 5.28 (d, $J = 3.7$ Hz, 0.82H).

Cyclization of chloroacetal 5.4b (Table 5.1, entry 3). The cyclization procedure described above was followed with **2.3** (89.9 mg, 0.196 mmol, 20 mol %), PbCl_2 (1.8 mg, 0.0065 mmol, 0.6 mol %), Mn powder (114 mg 2.07 mmol, 2.06 equiv), γ -terpinene (640 μL , 3.98 mmol, 3.96 equiv) and **5.4b** (220 mg, 1.01 mmol). The reaction was stirred in an oil bath at 70 $^\circ\text{C}$ for 88 h. Workup and purification by silica column chromatography (hexanes/EtOAc 4:1) afforded **5.9**

[104 mg, 56% (diastereomer ratio 93/7)] as a yellow oil with a different diastereomer ratio but otherwise identical ^1H NMR spectrum as **5.9** obtained from the cyclization of **5.4a**.

Cyclization of chloroacetal 5.4b (Table 5.1, entry 4). The cyclization procedure described above was followed with **2.3** (91.1 mg, 0.199 mmol, 20 mol %), PbCl_2 (3.0 mg, 0.011 mmol, 1 mol %), Mn powder (126 mg 2.29 mmol, 2.27 equiv), γ -terpinene (640 μL , 3.98 mmol, 3.94 equiv) and **5.4b** (221 mg, 1.01 mmol). The reaction was stirred in an oil bath at 70 $^\circ\text{C}$ for 10 days. Workup and purification by silica column chromatography (hexanes/EtOAc 10:1) afforded **5.9** [131 mg, 70% (diastereomer ratio 80/20)] as a yellow oil with a different diastereomer ratio but otherwise identical ^1H NMR spectrum as **5.9** obtained from the cyclization of **5.4a**.

Cyclization of bromoacetal 5.5a (Table 5.1, entry 5). The cyclization procedure described above was followed with **2.5** (10.1 mg, 0.0201 mmol, 2 mol %), PbBr_2 (2.0 mg, 0.0054 mmol, 0.5 mol %), Mn powder (272 mg 4.94 mmol, 4.92 equiv), γ -terpinene (800 μL , 4.98 mmol, 4.96 equiv) and **5.5a** (251 mg, 1.01 mmol). The reaction was stirred in an oil bath at 50 $^\circ\text{C}$ for 38.5 h. Workup and purification by silica column chromatography (hexanes/EtOAc 3:1) afforded **5.10** [146 mg, 85% (diastereomer ratio 65/35)] as a clear oil. ^1H NMR (400.1 MHz, CDCl_3) δ 0.80 (d, $J = 6.6$ Hz, 1.95H), 0.87 (d, $J = 6.7$ Hz, 1.05H), 0.93 (d, $J = 6.5$ Hz, 1.95H), 0.95 (d, $J = 6.8$ Hz, 1.05H), 1.28-1.46 (m, 1H), 1.50-2.00 (m, 5.65H), 2.02-2.19 (m, 0.35H), 3.42 (ddd, 2.5, 10.9, 11.5 Hz, 0.35H), 3.62-3.79 (m, 2.30H), 3.84-3.91 (m, 0.35H), 3.94 (dd, $J = 7.9$, 7.9 Hz, 0.65H), 4.18 (dd, $J = 8.6$, 8.6 Hz, 0.35H), 4.99 (d, $J = 3.6$ Hz, 0.35 H), 5.29 (d, $J = 3.3$ Hz, 0.65 H).

Cyclization of chloroacetal 5.5b (Table 5.1, entry 6). The cyclization procedure described above was followed with **2.3** (91.5 mg, 0.200 mmol, 20 mol %), PbCl_2 (2.3 mg, 0.0083 mmol, 0.8 mol %), Mn powder (227 mg 4.13 mmol, 4.05 equiv), γ -terpinene (645 μL , 4.02 mmol, 3.93 equiv) and **5.5b** (209 mg, 1.02 mmol). The reaction was stirred in an oil bath at 70 $^\circ\text{C}$ for 88 h. Workup and purification by silica column chromatography (hexanes/EtOAc 4:1) afforded **5.10** [98.4 mg, 57% (diastereomer ratio 61/39)] as a clear oil with a different diastereomer ratio but otherwise identical ^1H NMR spectrum as **5.10** obtained from the cyclization of **5.5a**.

Cyclization of bromoacetal 5.6a (Table 5.1, entry 7). The cyclization procedure described above was followed with **2.5** (10.3 mg, 0.0205 mmol, 2 mol %), PbBr_2 (1.9 mg, 0.0052 mmol, 0.5 mol %), Mn powder (210 mg 3.83 mmol, 3.79 equiv), γ -terpinene (640 μL , 3.98 mmol, 3.94 equiv) and **5.6a** (300 mg, 1.01 mmol). The reaction was stirred in an oil bath at 50 $^\circ\text{C}$ for 38.5 h. Workup and purification by silica column chromatography (hexanes/EtOAc 4:1) afforded **5.11** [60.8 mg, 28% (diastereomer ratio 79/21)] as a colourless oil. ^1H NMR (400.1 MHz, CDCl_3) δ

1.27-2.03 (m, 5H), 2.52-2.90 (m, 3H), 3.36-3.47 (m, 0.21H), 3.60-3.69 (m, 1H), 3.73-3.82 (m, 1.58H), 3.84-3.92 (m, 1H), 4.17 (dd, $J = 8.2, 8.2$ Hz, 0.21H), 5.03 (d, $J = 3.6$ Hz, 0.21H), 5.28 (d, $J = 3.7$ Hz, 0.79 H), 7.12-7.32 (m, 5H).

Cyclization of chloroacetal 5.6b (Table 5.1, entry 8). The cyclization procedure described above was followed with **2.3** (91.5 mg, 0.200 mmol, 20 mol %), PbCl_2 (2.0 mg, 0.0072 mmol, 0.7 mol %), Mn powder (122 mg 2.22 mmol, 2.25 equiv), γ -terpinene (640 μL , 3.98 mmol, 4.04 equiv) and **5.6b** (249 mg, 0.987 mmol). The reaction was stirred in an oil bath at 70 °C for 88 h. Workup and purification by silica column chromatography (hexanes/EtOAc 10:1) afforded **5.11** [61.5 mg, 29% (diastereomer ratio 83/17)] as a yellow oil with a different diastereomer ratio but otherwise identical ^1H NMR spectrum as **5.11** obtained from the cyclization of **5.6a**.

Cyclization of bromoacetal 5.7a (Table 5.1, entry 9). The cyclization procedure described above was followed with **2.5** (10.9 mg, 0.0217 mmol, 2 mol %), PbBr_2 (3.0 mg, 0.0082 mmol, 0.8 mol %), Mn powder (114 mg 2.07 mmol, 2.07 equiv), γ -terpinene (1.30 mL, 8.09 mmol, 8.12 equiv) and **5.7a** (232 mg, 0.997 mmol). The reaction was stirred in an oil bath at 50 °C for 38.5 h. Workup and purification by silica column chromatography (hexanes/EtOAc 10:1) afforded **5.12** [118 mg, 77% (*E/Z* ratio 42/58)] as a colourless oil. ^1H NMR (400.1 MHz, CDCl_3) δ 1.22-1.34 (m, 0.58 H), 1.47-2.04 (m, 6.42H), 2.55-2.72 (m, 1H), 3.44 (dt, $J = 2.3, 11.4$ Hz, 0.58H), 3.62-3.74 (m, 0.42H), 3.80-3.91 (m, 1H), 4.23 (d, $J = 12.4$ Hz, 0.42H), 4.46 (d, $J = 11.4$ Hz, 0.58H), 4.53 (d, $J = 12.4$ Hz, 0.42H), 4.61 (d, $J = 12.9$ Hz, 0.58H), 5.13 (d, $J = 3.8$ Hz, 0.58H), 5.19 (d, $J = 4.0$ Hz, 0.42H), 5.23-5.36 (m, 1H).

Cyclization of chloroacetal 5.7b (Table 5.1, entry 10). The cyclization procedure described above was followed with **2.3** (92.0 mg, 0.201 mmol, 20 mol %), PbCl_2 (3.0 mg, 0.011 mmol, 1 mol %), Mn powder (116 mg 2.11 mmol, 2.10 equiv), γ -terpinene (640 μL , 3.98 mmol, 3.96 equiv) and **5.7b** (190 mg, 1.01 mmol). The reaction was stirred in an oil bath at 70 °C for 88 h. Workup and purification by silica column chromatography (hexanes/EtOAc 10:1) afforded **5.12** [72 mg, 47% (*E/Z* ratio 43/57)] as a colourless oil with a different isomer ratio but otherwise identical ^1H NMR spectrum as **5.12** obtained from the cyclization of **5.7a**.

Cyclization of bromoacetal 5.1a under photolytic conditions. The cyclization procedure described above was followed with **2.5** (11.3 mg, 0.0225 mmol, 2 mol %), PbBr_2 (1.6 mg, 0.0044 mmol, 0.4 mol %), Mn powder (133 mg 2.41 mmol, 2.41 equiv), γ -terpinene (640 μL , 3.98 mmol, 3.98 equiv) and **5.1a** (222 mg, 1.00 mmol). During the 38.5 h reaction time in a 50 °C oil bath the reaction vessel was placed 10 cm from a 23 Watt household compact fluorescent light bulb. Workup and purification by silica column chromatography (hexanes/EtOAc 10:1)

afforded **5.8** [68 mg, 48% (diastereomer ratio 83/17)] as a colourless oil. ¹H NMR (400.1 MHz, CDCl₃) δ 0.97 (d, *J* = 6.9 Hz, 2.49 H), 1.02 (d, *J* = 6.6 Hz, 0.51H), 1.31-1.72 (m, 4H), 1.79-1.96 (m, 1H), 2.33-2.51 (m, 1H), 3.37-3.49 (m, 0.34H), 3.58-3.66 (m, 1.66H), 3.71-3.79 (m, 0.83H), 3.83-3.91 (m, 0.17H), 3.94 (dd, *J* = 8.0, 8.0 Hz, 0.83H), 4.27 (dd, *J* = 8.2, 8.2 Hz, 0.17H), 5.00 (d, *J* = 3.6 Hz, 0.17H), 5.28 (d, *J* = 3.8 Hz, 0.83H).

Cyclization of 5.4a with pre-catalyst 3.1 (Table 5.2, entry 1). The cyclization procedure described above was followed with compound **3.1** (8.4 mg, 0.010 mmol, 1 mol %), PbBr₂ (2.1 mg, 0.006 mmol, 1 mol %), Mn powder (112 mg, 2.03 mmol, 2.0 equiv), γ-terpinene (640 μL, 3.98 mmol, 3.9 equiv), and **5.4a** (265.7 mg, 1.01 mmol). The reaction was stirred in a 50 °C oil bath for 38.5 h. Workup and purification by silica column chromatography (hexanes/EtOAc 5:1) provided a mixture of starting material **5.4a** and the desired product **5.9** (<40% conversion).

Cyclization of 5.4a with pre-catalyst 3.1 (Table 5.2, entry 2). The cyclization procedure described above was followed with compound **3.1** (10.6 mg, 0.012 mmol, 1 mol %), Mn powder (124 mg, 2.26 mmol, 2.2 equiv), [HLut]Br (6.8 mg, 0.036 mmol, 3.6 mol %) and THF (3 mL) were added to a Teflon stoppered thick-walled glass reaction vessel. Upon stirring for 4 h the solution change colour from orange to green, at which point γ-terpinene (640 μL, 3.98 mmol, 4.0 equiv) and **5.4a** (265.2 mg, 1.01 mmol) were added to the reaction mixture. The reaction was stirred in a 50 °C oil bath for 38.5 h. Workup and purification by silica column chromatography (hexanes/EtOAc 5:1) afforded **5.9** [154 mg, 83 % (diastereomer ratio 82/18)] as a clear liquid.

Cyclization of 5.4a with pre-catalyst 3.1 (Table 5.2, entry 3). The cyclization procedure described above was followed with compound **3.1** (9.0 mg, 0.010 mmol, 1 mol %), Mn powder (119 mg, 2.17 mmol, 2.2 equiv), PbBr₂ (3.7 mg, 0.010 mmol, 1 mol %), [HLut]Br (5.7 mg, 0.030 mmol, 3 mol %), γ-terpinene (640 μL, 3.98 mmol, 4.0 equiv), and **5.4a** (261.5 mg, 0.99 mmol). The reaction was stirred in a 50 °C oil bath for 38.5 h. Workup and purification by silica column chromatography (hexanes/EtOAc 5:1) afforded **5.9** [164 mg, 90 % (diastereomer ratio 82/18)] as a clear liquid.

Cyclization of 5.4a with Me₃SiCl as Mn activator (Table 5.2, entry 4). The cyclization procedure described above was followed with compound **2.5** (10.4 mg, 0.021 mmol, 2 mol %), Mn powder (139 mg, 2.53 mmol, 2.5 equiv), Me₃SiCl (12.7 μL, 0.10 mmol, 10 mol %), γ-terpinene (640 μL, 3.98 mmol, 3.9 equiv), and **5.4a** (268.8 mg, 1.02 mmol). The reaction was stirred in a 50 °C oil bath for 24 h. Workup and purification by silica column chromatography (hexanes/EtOAc 5:1) afforded **5.9** [165 mg, 87 % (diastereomer ratio 82/18)] as a clear liquid.

Cyclization of 5.4a setup under ambient atmosphere (Table 5.2, entry 5). Under ambient atmosphere **2.5** (10.2 mg, 0.020 mmol, 2 mol %), Mn powder (114 mg, 2.08 mmol, 2.1 equiv), γ -terpinene (640 μ L, 3.98 mmol, 4.0 equiv), a solution (4 mL dry THF) of **5.4a** (262 mg, 1.00 mmol), and Me₃SiCl (12.5 μ L, 0.099 mmol, 10 mol %) were added to a Teflon stoppered thick-walled glass reaction vessel. The headspace of the reaction vessel was flushed with dry N₂ and then sealed and allowed to stir in a 65 °C oil bath for 22 h. Workup and purification by silica column chromatography (hexanes/EtOAc 5:1) afforded **5.9** [169 mg, 92 % (diastereomer ratio 80/20)] as a clear liquid.

Synthesis of bibenzyl: Method A. Compound **2.3b** (9.3 mg, 0.018 mmol, 2 mol %) was dissolved in Et₂O (5 mL) followed by addition of an Et₂O (1 mL) solution of PhCH₂Cl (127 mg, 1.00 mmol) and ClMgCH₂Ph (1.40 mL of 1.0 M solution in Et₂O, 1.4 mmol, 1.4 equiv). Upon stirring for 16 h at room temperature, THF (1 mL) was added to the reaction mixture causing the rapid formation of a large amount of ionic precipitate. After stirring for an additional 48 h, the reaction was concentrated under reduced pressure, diluted with hexanes/MeO^tBu (40:1), filtered over Celite, concentrated, and purified by silica column chromatography (hexanes/ MeO^tBu 40:1) to afford bibenzyl (155 mg, 85%) as a white crystalline solid. ¹H NMR (400.1 MHz, CDCl₃) δ 2.93 (s, 4H), 7.17-7.31 (m, 10H).

Method B. Compound **2.3b** (49.0 mg, 0.095 mmol, 5 mol %), PbCl₂ (6.0 mg, 0.022 mmol, 1 mol %), and Mn powder (154 mg 2.80 mmol, 1.4 equiv) were placed in a Schlenk flask, followed by the addition of THF (4.5 mL) and PhCH₂Cl (230 μ L, 2.00 mmol). The reaction was stirred in an oil bath at 50 °C for 63 h during which time a large amount of white precipitate formed. The reaction mixture was concentrated under reduced pressure, diluted with hexanes/MeO^tBu (40:1), filtered over Celite, concentrated, and purified by silica column chromatography (hexanes/ MeO^tBu 40:1) to afford bibenzyl (171 mg, 94%) as a white crystalline solid with an identical ¹H NMR spectrum to the product obtained by method A.

Synthesis of Ph₃CCH₂Ph. Compound **2.3b** (25.0 mg, 0.049 mmol, 5 mol %), PbCl₂ (4.6 mg, 0.017 mmol, 2 mol %), Mn powder (162 mg 2.95 mmol, 3.0 equiv), and Ph₃CCl (281 mg, 1.01 mmol, 1.01 equiv) were placed in a Schlenk flask, followed by the addition of THF (7.5 mL) and a THF (1 mL) solution of PhCH₂Cl (127 mg, 1.00 mmol). Upon stirring for 23 h at room temperature, a large amount of white precipitate formed. The reaction mixture was concentrated under reduced pressure, diluted with hexanes/MeO^tBu (40:1), filtered over Celite, concentrated, and purified by silica column chromatography (hexanes/ MeO^tBu 20:1) to afford Ph₃CCH₂Ph (338 mg, 100%) as a pale yellow solid. The product was identified by comparison of the ¹H

NMR spectrum with literature values.¹⁵⁷ ¹H NMR (400.1 MHz, CDCl₃) δ 3.95 (s, 2H, CH₂), 6.63 (d, 2H, *o*-CH₂Ph), 6.98 (t, 2H, *m*-CH₂Ph), 7.04-7.29 (m, 16H).

Synthesis of PhCH₂C(Ph)₂CH₂CH₂Ph. Compound **2.3b** (49.5 mg, 0.096 mmol, 5 mol %), PbCl₂ (4.0 mg, 0.014 mmol, 1 mol %), and Mn powder (161 mg 2.93 mmol, 1.5 equiv) were placed in a Schlenk flask, followed by the addition of THF (4.5 mL), PhCH₂Cl (230 μL, 2.00 mmol), and Ph₂C=CH₂ (175 μL, 0.991 mmol, 0.50 equiv). The reaction was stirred in an oil bath at 50 °C for 63 h during which time a large amount of white precipitate formed. The reaction mixture was concentrated under reduced pressure, diluted with hexanes/MeO^tBu (40:1), filtered over Celite, concentrated, and purified by silica column chromatography (hexanes/ MeO^tBu 40:1) to afford PhCH₂C(Ph)₂CH₂CH₂Ph (99 mg, 28%) as a white solid. ¹H NMR (400.1 MHz, CDCl₃) δ 2.31-2.36 (m, 2H), 2.49-2.53 (m, 2H), 3.60 (s, 2H), 6.68 (d, 2H), 7.13-7.42 (m, 18H). Bibenzyl (~10%) and Ph₂C=CH₂ (~10%) were also isolated in a separate fraction.

Reaction of benzyl compound 2.14 with methyl acrylate. Compound **2.14** (14.0 mg, 0.027 mmol) was placed in a flask followed by the addition of hexanes (4 mL) and methyl acrylate (30 μL, 0.33 mmol, 12 equiv). Upon stirring overnight at room temperature, the solution became green (yellow transmitted) in colour with absorption bands at 401 and 586 nm.

Reaction of neopentyl compound 2.11 with methyl acrylate. Compound **2.6** (655 mg, 1.10 mmol) was placed in a Schlenk flask followed by the addition of Et₂O (30 mL) and an Et₂O (5 mL) solution of Mg(CH₂CMe₃)₂·1.05(1,4-dioxane) (162 mg, 0.626 mmol, 0.57 equiv). Upon stirring at room temperature for 2 h, the volatiles were removed under reduced pressure, the residue extracted with hexanes (30 mL), and filtered over Celite. Methyl acrylate (395 μL, 4.38 mmol, 4.0 equiv) was added to the purple solution and upon stirring at room temperature for 48 h, the solution gradually became green with a final UV-Vis spectrum displaying absorption bands at 406 and 607 nm. The volatiles were removed under reduced pressure to remove unreacted methyl acrylate and the residue was extracted with hexanes (7.5 mL) and used in subsequent reactions without further purification.

Reaction of in situ generated Cr(III) enolates with various substrates:

MnI₂. Mn powder (35.9 mg, 0.65 mmol, 3.0 equiv) and I₂ (5.7 mg, 0.023 mmol, 0.1 equiv) were placed in a 4 mL vial followed by the addition of THF (0.5 mL). The mixture was stirred at room temperature until it became colourless (2 h) before addition of the Cr(III) enolate solution (1.5 mL, 0.221 mmol) generated above from reaction of **2.11** with methyl acrylate. Upon stirring for 5 min, the solution changed colour to green (orange transmitted) and after stirring overnight underwent a further colour change to green (magenta transmitted). UV-vis

analysis of the crude reaction mixture ($\lambda_{\text{max}} = 426$ and 567 nm) confirmed the formation of compound **2.1**.

ClSiMe₃. The Cr(III) enolate solution (1.5 mL, 0.221 mmol) generated above from reaction of **2.11** with methyl acrylate was placed in a 4 mL vial followed by the addition of Me₃SiCl (300 μ L of a 1.0 M solution in THF, 0.300 mmol, 1.4 equiv). Upon stirring for 10 min, the solution changed colour to green (orange transmitted) at which point the reaction mixture was transferred to a another vial containing Mn powder (25.9 mg, 0.47 mmol, 2 equiv) and Me₃SiCl (200 μ L of a 1.0 M solution in THF, 0.200 mmol, 0.9 equiv) in THF (0.5 mL). Upon stirring overnight, the mixture underwent a further colour change to green (magenta transmitted). UV-vis analysis of the crude reaction mixture ($\lambda_{\text{max}} = 426$ and 566 nm) confirmed the formation of compound **2.1**.

Cp₂ZrCl₂. Cp₂ZrCl₂ (67.0 mg, 0.229 mmol, 1.0 equiv) was dissolved in THF (1 mL) followed by the addition of the Cr(III) enolate solution (1.5 mL, 0.221 mmol) generated above from reaction of **2.11** with methyl acrylate. Upon stirring for 5 min, the solution became green (orange transmitted) in colour and was allowed to stir overnight to ensure the reaction had gone to completion (no further colour change was observed). UV-vis analysis of the crude reaction mixture confirmed the formation of compound **2.3**. Under similar reaction conditions, the Cr(III) enolate generated above from reaction of **2.14** with methyl acrylate was also converted to compound **2.3**.

[HNEt₃]Cl. [HNEt₃]Cl (32.8 mg, 0.237 mmol, 1.1 equiv) was dissolved in THF (1 mL) followed by the addition of the Cr(III) enolate solution (1.5 mL, 0.221 mmol) generated above from reaction of **2.11** with methyl acrylate. The solution rapidly became green (orange transmitted) in colour and was allowed to stir overnight to ensure the reaction had gone to completion (no further colour change was observed). UV-vis analysis of the crude reaction mixture confirmed the formation of compound **2.3**.

Addition of alkyl radicals to enones:

Table 5.3, entry 1. Compound **2.3** (44.1 mg, 0.096 mmol, 0.096 equiv), Mn powder (113 mg, 2.05 mmol, 2.0 equiv), and PbCl₂ (5.8 mg, 0.021 mmol, 0.02 equiv) were placed in a Schlenk flask, followed by the addition of THF (7 mL). The mixture was stirred at room temperature until **2.3** was reduced to Cr(II) (**2.1**), at which point methyl acrylate (350 μ L, 3.66 mmol, 3.7 equiv) and PhCH₂Cl (115 μ L, 1.00 mmol) were added to the flask. After stirring for 7 days, the mixture was concentrated under reduced pressure and redissolved in THF (5 mL), followed by the addition of saturated aqueous [NH₄]Cl. The aqueous layer was washed with Et₂O (3 \times 25 mL). The combined organic layer was rinsed with saturated aqueous NaHCO₃ (20

mL), dried (MgSO₄), filtered, and the solvent was removed under reduced pressure. The product was purified by silica column chromatography (hexanes/EtOAc 15:1) to afford **5.13** (28 mg, 16%) as a pale yellow liquid. ¹H NMR (400.1 MHz, CDCl₃) δ 1.93-2.00 (m, 2H), 2.34 (t, 2H), 2.66 (t, 2H), 3.67 (s, 3H), 7.17-7.30 (m, 5H). A small amount of bibenzyl was also isolated in a separate fraction.

Table 5.3, entry 2. Compound **2.5** (36.8 mg, 0.073 mmol, 0.07 equiv), Mn powder (286 mg, 5.21 mmol, 5.1 equiv), and PbBr₂ (2.8 mg, 0.0076 mmol, 0.01 equiv) were placed in a Schlenk flask, followed by the addition of THF (4 mL), methyl acrylate (225 μL, 2.50 mmol, 2.5 equiv), and Me₃CBr (115 μL, 1.02 mmol). After stirring for 5 days, the reaction mixture was diluted with Et₂O (10 mL) followed by the slow addition of 1 M HCl (10 mL) while stirring. The mixture was diluted with Et₂O (50 mL), rinsed with 1 M HCl (25 mL) and brine (25 mL), dried (MgSO₄), filtered, and the solvent was removed under reduced pressure. Vacuum distillation of the residue afforded **5.14** (35 mg, 24%) as a colourless liquid. ¹H NMR (400.1 MHz, CDCl₃) δ 0.89 (s, 9H), 1.53-1.57 (m, 2H), 2.26-2.31 (m, 2H), 3.67 (s, 3H).

Table 5.3, entry 3. Compound **2.5** (31.7 mg, 0.063 mmol, 0.11 equiv), Mn powder (162 mg, 2.95 mmol, 5 equiv), and PbBr₂ (3 mg, 0.0082 mmol, 0.01 equiv) were placed in a Schlenk flask, followed by the addition of THF (2 mL). Upon stirring for 1 h, compound **2.5** was reduced to Cr(II) (**2.1**) followed by the addition of methyl acrylate (265 μL, 2.94 mmol, 4.9 equiv) with THF (1 mL) and *c*-C₆H₁₁Br (73 μL, 0.60 mmol). After stirring for 3 days, the reaction mixture was diluted with Et₂O (10 mL) followed by the slow addition of 1 M HCl (10 mL) while stirring. The mixture was diluted with Et₂O (50 mL), rinsed with 1 M HCl (25 mL) and brine (25 mL), dried (MgSO₄), filtered, and the solvent was removed under reduced pressure. The residue was extracted with hexanes/EtOAc (10:1), filtered through silica, and the solvent was removed under reduced pressure. Vacuum distillation of the residue afforded a small amount of **5.15** as a colourless liquid. ¹H NMR (400.1 MHz, CDCl₃) δ 0.75-0.89 (m, 2H), 1.17-1.24 (m, 4H), 1.49-1.55 (m, 2H), 1.60-1.71 (m, 5H), 1.67-1.71 (m, 2H), 3.66 (s, 3H).

Table 5.3, entry 4. Compound **2.5** (29.1 mg, 0.058 mmol, 0.06 equiv), Mn powder (172 mg, 3.12 mmol, 3.1 equiv), and PbBr₂ (2.6 mg, 0.0071 mmol, 0.01 equiv) were placed in a Schlenk flask, followed by the addition of THF (5 mL), methyl acrylate (450 μL, 4.99 mmol, 5.0 equiv), and Me₃CCH₂Br (126 μL, 1.00 mmol). After stirring for 7 days, the solution was decanted and the solid Mn was rinsed with THF (2 × 3 mL). Saturated aqueous [NH₄]Cl (20 mL) was added to the combined rinsings. The aqueous layer was washed with Et₂O (3 × 20 mL). The combined organic rinsings were washed with saturated aqueous NaHCO₃ (20 mL),

dried (MgSO_4), filtered, and the solvent was removed under reduced pressure. The product was purified by silica column chromatography (hexanes/EtOAc 10:1) to afford **5.16** (53 mg, 33%) as a pale yellow liquid. ^1H NMR (400.1 MHz, CDCl_3) δ 0.88 (s, 9H), 1.16-1.21 (m, 2H), 1.57-1.62 (m, 2H), 2.28 (t, 2H), 3.67 (s, 3H).

Table 5.3, entry 5. Compound **2.3** (47.3 mg, 0.103 mmol, 0.10 equiv) and Mn powder (103 mg, 1.88 mmol, 1.9 equiv) were placed in a Schlenk flask, followed by the addition of THF (5 mL), Me_3SiCl (250 μL , 1.98 mmol, 2.0 equiv), methyl acrylate (360 μL , 3.99 mmol, 4.0 equiv), and PhCH_2Cl (115 μL , 1.00 mmol). After stirring for 4 days, H_2O (10 mL) was added and the aqueous layer was rinsed with EtOAc (3×25 mL). The combined organic rinsings were washed with brine (20 mL) and the solvent was removed under reduced pressure. The residue was extracted with THF (15 mL) to which was added $[\text{Bu}_4\text{N}]\text{F}$ (1.2 mL of a 1.0 M solution in THF) while stirring. After stirring for 20 min, the mixture was poured onto H_2O (20 mL), and the aqueous layer was rinsed with Et_2O (3×50 mL). The combined organic rinsings were washed with H_2O (50 mL) and brine (50 mL), dried (MgSO_4), filtered, and the solvent was removed under reduced pressure. The product was purified by silica column chromatography (hexanes/EtOAc 15:1) to afford **5.13** (19 mg, 11%) as a pale yellow liquid.

Table 5.3, entry 6. Compound **2.1** (42.5 mg, 0.101 mmol, 0.20 equiv), Cp_2ZrCl_2 (147 mg, 0.50 mmol, 1.0 equiv), and Mn powder (71 mg, 1.3 mmol, 2.6 equiv) were placed in a Schlenk flask, followed by the addition of THF (5 mL), methyl acrylate (180 μL , 2.00 mmol, 4.0 equiv), and $\text{Me}_3\text{CCH}_2\text{I}$ (66 μL , 0.50 mmol). After stirring for 2 days, the mixture was diluted with EtOAc (15 mL), stirred with Florisil (150 mg) for 2 h, filtered over Celite, and the solvent was removed under reduced pressure. The residue was extracted with hexanes/EtOAc (15:1), filtered over Celite, and the solvent was removed under reduced pressure to provide a small amount of yellow liquid, which contained a mixture of **5.16** and other unidentified products (^1H NMR).

Table 5.3, entry 7. Compound **2.3** (40.8 mg, 0.089 mmol, 0.09 equiv), Mn powder (106 mg, 1.92 mmol, 1.9 equiv), and PbCl_2 (7.2 mg, 0.026 mmol, 0.03 equiv) were placed in a Schlenk flask, followed by the addition of THF (3 mL) and DMF (0.3 mL). The mixture was stirred at room temperature until **2.3** was reduced to Cr(II) (**2.1**), at which point methyl methacrylate (215 μL , 2.01 mmol, 2.0 equiv), Me_3SiCl (250 μL , 1.98 mmol, 2.0 equiv), and PhCH_2Cl (115 μL , 1.00 mmol) were added to the flask. After stirring for 3 days, the mixture was filtered through silica and rinsed with Et_2O (100 mL). The solvent was removed under reduced pressure, the residue extracted with hexanes and the product was purified by silica column chromatography (hexanes/EtOAc (1 to 3.5%)) to afford **5.17** (53 mg, 28%) as a

colourless liquid. ^1H NMR (400.1 MHz, CDCl_3) δ 1.18 (d, 3H), 1.70-1.77 (m, 1H), 1.98-2.07 (m, 1H), 2.44-2.53 (m, 1H), 2.62 (t, 2H), 3.68 (s, 3H), 7.17-7.21 (m, 3H), 7.26-7.30 (m, 2H).

Table 5.3, entry 8. Compound **2.3** (40.6 mg, 0.089 mmol, 0.09 equiv), Cp_2ZrCl_2 (300 mg, 1.03 mmol, 1.0 equiv), Mn powder (109 mg, 1.98 mmol, 2.0 equiv), and PbCl_2 (7.7 mg, 0.028 mmol, 0.03 equiv) were placed in a Schlenk flask, followed by the addition of THF (4 mL), methyl methacrylate (215 μL , 2.01 mmol, 2.0 equiv), and PhCH_2Cl (115 μL , 1.00 mmol). After stirring for 4 days, the mixture was diluted with Et_2O (5 mL), filtered over Celite, and the solvent was removed under reduced pressure. The residue was extracted with hexanes/ EtOAc (1:1) and stirred with 3 M HCl (50 mL). The aqueous layer was washed with hexanes/ EtOAc (1:1) and the combined organic rinsings were dried (MgSO_4), filtered, and the solvent was removed under reduced pressure. The product was purified by silica column chromatography (hexanes/ EtOAc (3.5%)) to afford **5.17** (16 mg, 9%) as a colourless liquid.

Table 5.3, entry 9. Compound **2.5** (53.0 mg, 0.106 mmol, 0.10 equiv) and Mn powder (131 mg, 2.38 mmol, 2.3 equiv) were placed in a Schlenk flask, followed by the addition of THF (5 mL), Me_3SiCl (190 μL , 1.50 mmol, 1.5 equiv), 2-cyclohexen-1-one (190 μL , 1.97 mmol, 1.9 equiv), and *c*- $\text{C}_6\text{H}_{11}\text{Br}$ (125 μL , 1.02 mmol). After stirring for 2 days, the mixture was filtered through silica and rinsed with Et_2O (100 mL). The solvent was removed under reduced pressure and the residue was stirred with 2 M HCl (2 mL) at 40 $^\circ\text{C}$ for 8 h. The aqueous layer was washed with Et_2O (3×10 mL), dried (MgSO_4), filtered, and the solvent was removed under reduced pressure. The product was purified by silica column chromatography (hexanes/ EtOAc (5%)) to afford **5.18** (45 mg, 25%) as a pale yellow liquid. ^1H NMR (400.1 MHz, CDCl_3) δ 0.91-1.02 (m, 2H), 1.08-1.26 (m, 4H), 1.32-1.42 (m, 1H), 1.52-1.76 (m, 7H), 1.82-1.89 (m, 1H), 2.01-2.11 (m, 2H), 2.18-2.27 (m, 1H), 2.30-2.40 (m, 2H). Under similar reaction conditions, using PbBr_2 activated Mn and Cp_2ZrCl_2 instead of Me_3SiCl , no product was isolated from the reaction (Table 5.3, entry 11).

Table 5.3, entry 10. Compound **2.5** (50.0 mg, 0.10 mmol, 0.10 equiv) and Mn powder (141 mg, 2.57 mmol, 2.6 equiv) were placed in a Schlenk flask, followed by the addition of THF (3 mL), Pr_3SiCl (285 μL , 1.30 mmol, 1.3 equiv). Upon stirring overnight, compound **2.5** was reduced to Cr(II) (**2.1**), as indicated by the change in colour to green (magenta transmitted). 2-Cyclohexen-1-one (193 μL , 2.00 mmol, 2.0 equiv) and *c*- $\text{C}_6\text{H}_{11}\text{Br}$ (122 μL , 1.00 mmol) were then added to the mixture, which was allowed to stir for an additional 24 h. The reaction mixture was diluted with hexanes, filtered over Celite, and the solvent was removed under reduced pressure. The resulting residue was stirred with 2 M HCl (2 mL) at 40 $^\circ\text{C}$ for 8 h. The aqueous

layer was washed with Et₂O (3 × 6 mL), dried (MgSO₄), filtered, and the solvent was removed under reduced pressure. The product was purified by silica column chromatography (hexanes/EtOAc (5%)) to afford 43 mg of a pale yellow liquid that contained a mixture of compound **5.18** and an unidentified compound with Pr₃Si signals in the ¹H NMR spectrum. The Pr₃Si signals were not due to the silyl enol ether species that is present prior to deprotection.

Synthesis of *c*-C₆H₁₁PPh₂:

Stoichiometric in compound 2.1. Compound **2.1** (15.3 mg, 0.0362 mmol, 2.1 equiv) and Ph₂P–PPh₂ (6.4 mg, 0.017 mmol) were placed in a vial with C₆D₆ (1 mL) and stirred at room temperature overnight. No reaction occurred between the reagents overnight (determined by UV-vis). *c*-C₆H₁₁Br (4.5 μL, 0.037 mmol, 2.1 equiv) was added to the mixture. After stirring for 4 days, the mixture was analyzed by UV-vis (λ_{max} = 424 and 583 nm), showing complete conversion to the bromide compound **2.5**. ³¹P NMR of the reaction mixture displayed a major peak at -3.4 ppm (s, *c*-C₆H₁₁PPh₂) and a minor peak at -14.4 ppm (s, Ph₂P–PPh₂).¹⁴⁹

Catalytic in compound 2.1. Mn powder (11.3 mg, 0.206 mmol, 6.7 equiv), PbBr₂ (1.0 mg, 0.0027 mmol, 0.09 equiv), and Ph₂P–PPh₂ (11.4 mg, 0.0308 mmol) were placed in a Schlenk flask, followed by the addition of compound **2.1** (1.0 mL of a 2.75 × 10⁻³ M solution in THF, 0.00275 mmol, 0.09 equiv) and *c*-C₆H₁₁Br (7.5 μL, 0.061 mmol, 2.0 equiv). Upon stirring for 48 h, bipyridine (19.3 mg, 0.124 mmol, 4.0 equiv) was added and the mixture was stirred for an additional 10 min. The solvent was removed under reduced pressure, the residue extracted with benzene, and filtered over Celite into an NMR tube. PPh₃ standard (200 μL of a 0.270 M solution in benzene) was added to the tube prior to NMR analysis. *c*-C₆H₁₁PPh₂ was present in 55% yield, determined by comparison of relative integration values obtained after determination of the *T*₁ relaxation. An unidentified product with a peak at -8.4 ppm was also present (~7% based on relative integration values).

General procedure for X-ray crystallography. Protocols were identical to those reported in section 2.13.

Structure details. Compound **5.2** crystallizes as a mixture of one of the diastereomeric pairs of the cyclized ligand and was subsequently modeled in two orientations.

Chapter 6 Synthesis and Reductive Elimination from CpCr Aryl Complexes

In Chapters 4 and 5, C–C and C–P bond formation was achieved using free radical intermediates. In contrast, the results presented in this chapter will focus on C–C bond formation at the metal centre. A common mode of C–C bond formation with transition metal compounds involves reductive elimination of two ligands from the metal.¹ An example of this type of reactivity using Cr is alkyne trimerization.¹⁵⁸ As shown in Figure 6.1, the first steps in alkyne trimerization involve coordination of two alkynes to the metal centre, followed by oxidative coupling of the two alkynes to form a Cr(III) chromacyclopentadienyl species. This is followed by insertion of a third alkyne and, finally, reductive elimination from the Cr(III) metal centre to form the arene product and a Cr(I) species.

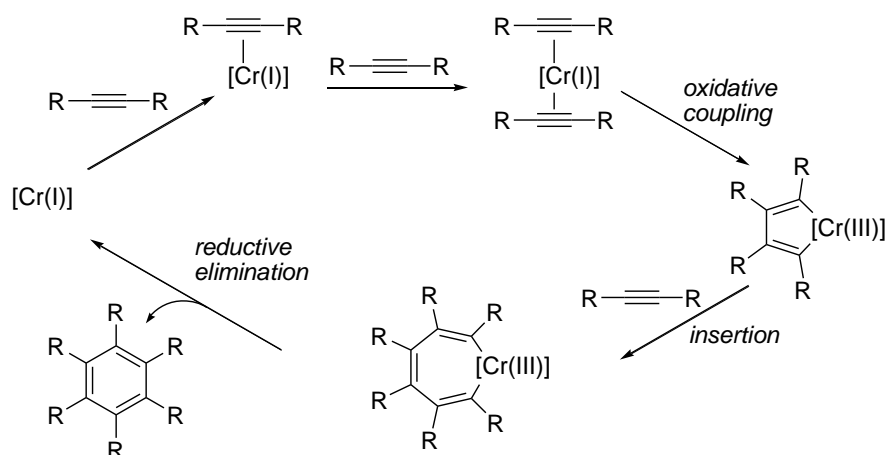
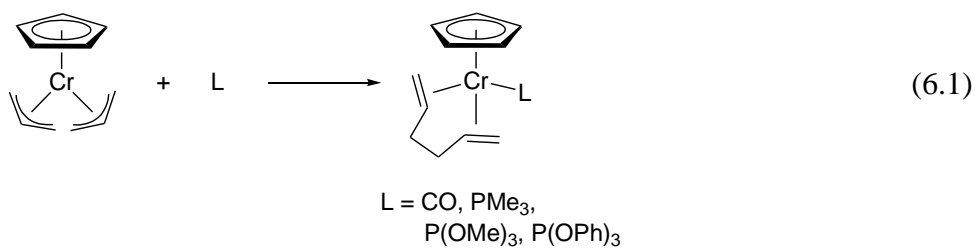


Figure 6.1. Chromium-catalyzed alkyne trimerization.

Reductive elimination has also been observed in the half-sandwich CpCr bis(η^3 -allyl) complex shown in eq 6.1.¹⁵⁹ Similar to the alkyne trimerization, reductive elimination of the allyl compound proceeds through a Cr(III)/Cr(I) redox couple to form a new C–C bond. These examples involve homocoupling of organic substrates, where multiple equivalents of the same substrate are used to form the product.



In the interest of studying C–C bond formation at a Cr metal centre, the β -diketiminate must be replaced with another ligand that will form a reactive Cr–C bond. The preparation of a Cr(II) compound $\text{CpCr}(\text{C}_6\text{H}_4\text{CH}_2\text{NMe}_2)$ (**6.1**) was reported by Jonas when studying metallocene ligand substitution.¹⁶⁰ This complex is structurally similar to the CpCr β -diketiminate compounds in that it contains an η^5 -Cp and a bidentate monoanionic ligand. Chromium(III) aryl compounds are also well-known for insertion and reductive elimination reactions to form biaryl products.¹⁶¹ Due to the similarities between the β -diketiminate and $\text{CpCr}(\text{C}_6\text{H}_4\text{CH}_2\text{NMe}_2)$ compounds, many of the synthetic protocols developed for the β -diketiminate system should be readily transferable for the preparation of mixed aryl and alkyl-aryl Cr(III) compounds.

While the examples described above represent homocoupling of organic substrates, heterocoupling with organochromium compounds has been comparatively under studied, likely due to the similarities between homocoupling and alkene polymerization.¹⁶² Herein, the Cr(II) compound $\text{CpCr}(\text{C}_6\text{H}_4\text{CH}_2\text{NMe}_2)$ (**6.1**) is examined as a potential precursor for heterocoupling reactions. The single-electron oxidation of compound **6.1** was used to prepare compounds of the form $\text{CpCr}(\text{C}_6\text{H}_4\text{CH}_2\text{NMe}_2)(\text{X})$, and various reaction conditions were examined with an eye towards inducing reductive elimination in these Cr(III) compounds. Alkyne insertion reactivity of these compounds is also presented. $\text{CpCr}(\text{C}_6\text{H}_4\text{CH}_2\text{NMe}_2)(\text{R})$ compounds, where R = alkyl and aryl, were prepared and tested under various condition for reductive elimination, with initial results indicating that oxidatively induced reductive elimination from a Cr(IV) intermediate species occurs under relatively mild reaction conditions.

6.1 Synthesis of $\text{CpCr}(\text{C}_6\text{H}_4\text{CH}_2\text{NMe}_2)$

The preparation of $\text{CpCr}(\text{C}_6\text{H}_4\text{CH}_2\text{NMe}_2)$ (**6.1**) was reported in a review article examining metallocene ligand substitution.¹⁶⁰ Compound **6.1** was prepared by reaction of chromocene (Cp_2Cr) with $\text{Li}[\text{C}_6\text{H}_4\text{CH}_2\text{NMe}_2]$ in THF at 60 °C in 70–80% yield, as shown in Figure 6.2. In the same issue of *Angewandte Chemie* the solid-state molecular structure of **6.1** was also reported in a separate review.¹⁶³ Compound **6.1** was also reported to reversibly bind ethylene, and to react with diphenylacetylene ($\text{PhC}\equiv\text{CPh}$).¹⁶⁰ Upon treatment with H^+ , the organic fragment was obtained, as shown in Figure 6.2. Although the organometallic species formed upon treatment of **6.1** with $\text{PhC}\equiv\text{CPh}$ was not directly observed, compound **6.2** was proposed as the intermediate species, the formation of which arose upon insertion of $\text{PhC}\equiv\text{CPh}$ into the Cr–C bond of the deprotonated *N,N*-dimethylbenzylamine ligand.

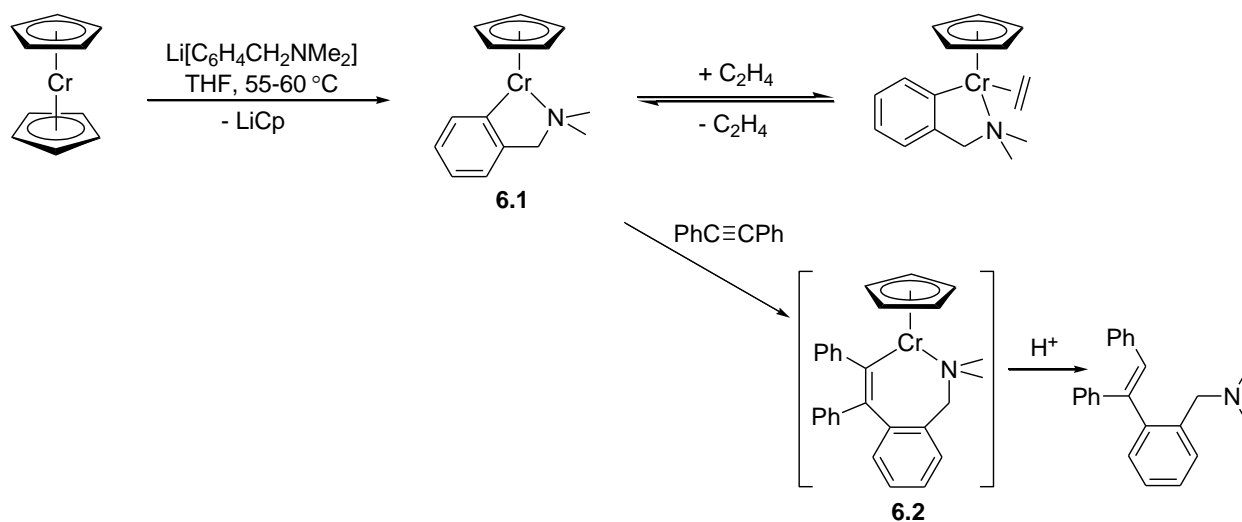


Figure 6.2. Previously reported synthesis and reactivity of $\text{CpCr}(\text{C}_6\text{H}_4\text{CH}_2\text{NMe}_2)$ (**6.1**).

A more facile synthesis of compound **6.1** is now reported directly from CrCl_2 . Compound **6.1** was prepared by sequential addition of NaCp and $\text{Li}[\text{C}_6\text{H}_4\text{CH}_2\text{NMe}_2]$ to a suspension of CrCl_2 in THF. Since the only characterization data previously available for compound **6.1** was the crystal structure, the isolated material prepared according to the reaction shown in Figure 6.3 was fully characterized to confirm the identity of the product as that of compound **6.1**. The solid-state molecular structure of **6.1**, shown in Figure 6.3, is very similar to the previously reported complex,¹⁶³ with a Cr–N bond length of 2.110(2) Å and Cr–C(1) bond length of 2.056(2) Å. The UV-vis spectrum of compound **6.1** contains two strong absorption bands at 325 and 374 nm and a weaker absorption at 467 nm. The metal centre of **6.1** is clearly much more exposed compared to the sterically hindered $\text{CpCr}(\text{II})$ β -diketiminates analogues. Given the lack of steric protection in **6.1**, it is notable that the complex does not undergo ligand redistribution¹⁶⁴ to form Cp_2Cr and $\text{Cr}(\text{C}_6\text{H}_4\text{CH}_2\text{NMe}_2)_2$.¹⁶⁵

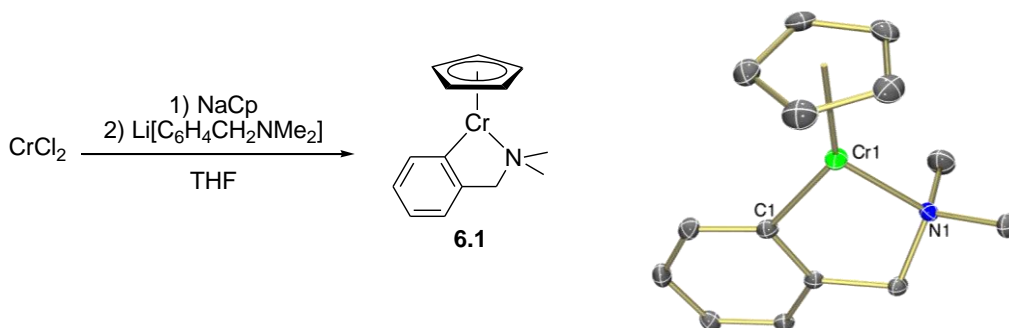


Figure 6.3. Synthesis of compound $\text{CpCr}(\text{C}_6\text{H}_4\text{CH}_2\text{NMe}_2)$ (**6.1**). Thermal ellipsoid diagram (50%) of **6.1** with all H atoms omitted for clarity.

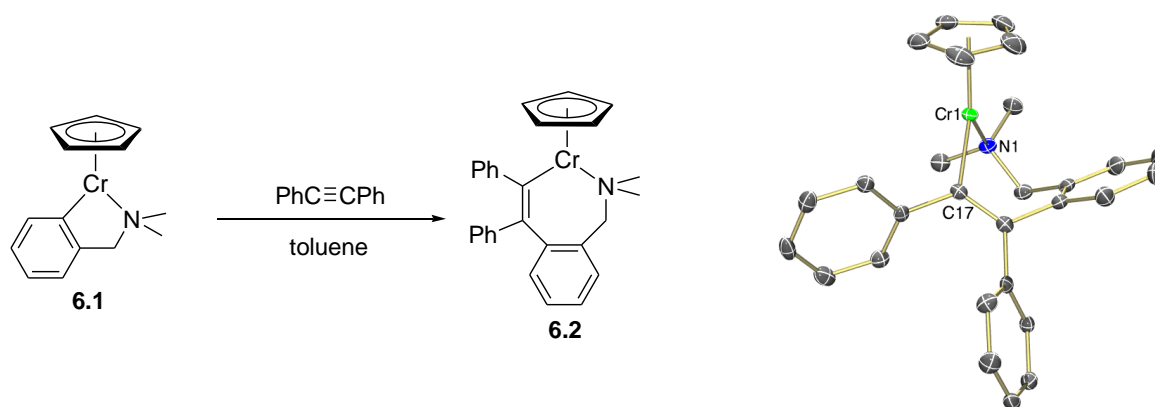


Figure 6.4. Synthesis of compound $\text{CpCr}[\text{C}(\text{Ph})\text{C}(\text{Ph})\text{C}_6\text{H}_4\text{CH}_2\text{NMe}_2]$ (**6.2**). Thermal ellipsoid diagram (50%) of **6.2** with all H atoms omitted for clarity.

Treatment of compound **6.1** with one equivalent of $\text{PhC}\equiv\text{CPh}$ caused a rapid colour change from orange to burgundy. Recrystallization of the resulting product provided compound $\text{CpCr}[\text{C}(\text{Ph})\text{C}(\text{Ph})\text{C}_6\text{H}_4\text{CH}_2\text{NMe}_2]$ (**6.2**) in high yield. The solid-state molecular structure of **6.2**, shown in Figure 6.4, confirmed the structure proposed by Jonas.¹⁶⁰ The Cr–N bond length (2.134(3) Å) of compound **6.2** is slightly longer than that of **6.1** and the Cr–C(17) bond length of 2.088(3) Å is also slightly longer compared to the Cr–C bond of compound **6.1**. The N–Cr–C(17) bond angle of the chelating ligand (94.27(8)°) is also significantly larger compared to the angle in compound **6.1** (83.32(6)°) due to the larger ring size of the metallacycle. The UV-vis spectrum of **6.2** displays an absorption band at 509 nm. Despite the expanded chelate ring size of compound **6.2** compared to **6.1**, as a result of $\text{PhC}\equiv\text{CPh}$ insertion, the material is stable at room temperature in solution for days, and solid samples of the compound stored under an inert atmosphere have shown no signs of decomposition after 2 years.

The utility of compound **6.1** as a protonolysis precursor has been previously examined in the Smith laboratory for the synthesis of $\text{CpCr}(\text{LX})$ compounds, where LX is a bidentate monoanionic ligand.¹⁶⁶ Compound **6.2** was treated with *N,N*-dimethylbenzylamine in the attempted conversion of **6.2** back to **6.1** by protonolysis. No reaction occurred upon stirring at room temperature for 4 days.

6.2 Single-Electron Oxidation of $\text{CpCr}(\text{C}_6\text{H}_4\text{CH}_2\text{NMe}_2)$

The synthesis of Cr(III) compounds of the form $\text{CpCr}(\text{C}_6\text{H}_4\text{CH}_2\text{NMe}_2)(\text{X})$ was targeted in order to examine their stability with respect to reductive coupling, and to prepare synthetic precursors that could be used to prepare $\text{CpCr}(\text{C}_6\text{H}_4\text{CH}_2\text{NMe}_2)(\text{R})$ compounds, where R = alkyl or aryl. Compound **6.1** reacted cleanly with 0.5 equivalents of I_2 to provide the Cr(III) iodide

compound **6.3**, as shown in Figure 6.5. The UV-vis spectrum of compound **6.3** displays absorption bands at 512 and 696 nm, and two shoulder bands at 378 and 430 nm.

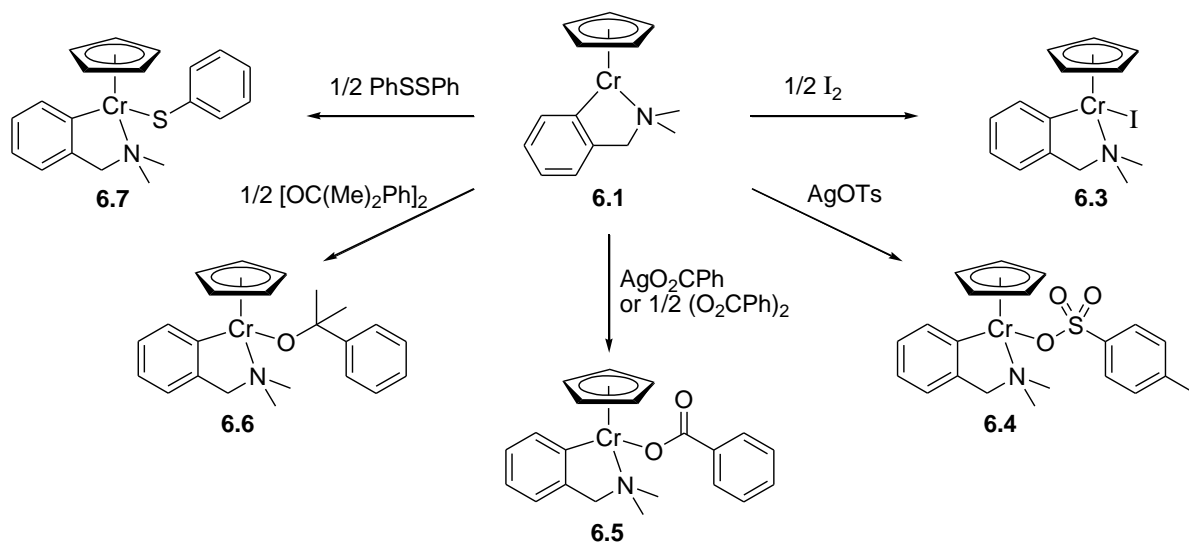


Figure 6.5. Synthesis of Cr(III) $\text{CpCr}(\text{C}_6\text{H}_4\text{CH}_2\text{NMe}_2)(\text{X})$ compounds by single-electron oxidation of $\text{CpCr}(\text{C}_6\text{H}_4\text{CH}_2\text{NMe}_2)$ (**6.1**).

The oxidation of compound **6.1** with the appropriate silver reagents provided $\text{CpCr}(\text{C}_6\text{H}_4\text{CH}_2\text{NMe}_2)(\text{OTs})$ (**6.4**) and $\text{CpCr}(\text{C}_6\text{H}_4\text{CH}_2\text{NMe}_2)(\text{O}_2\text{CPh})$ (**6.5**). The benzoate compound **6.5** was also readily prepared by reaction of compound **6.1** with 0.5 equivalents of benzoyl peroxide. The UV-vis spectra of compounds **6.4** and **6.5** were similar to the iodide compound **6.3**, with absorption bands at 365, 418, and 499 nm for **6.4**, and 414 and 504 nm for **6.5**. The band at ~ 415 nm has a smaller extinction coefficient compared to the 500 nm band for all three compounds (**6.3** – **6.5**). These two absorption bands appear to be characteristic of $\text{CpCr}(\text{C}_6\text{H}_4\text{CH}_2\text{NMe}_2)(\text{X})$ compounds, where X = halide or pseudo-halide.

Compound **6.1** reacted with dicumyl peroxide to form the Cr(III) alkoxide compound $\text{CpCr}(\text{C}_6\text{H}_4\text{CH}_2\text{NMe}_2)[\text{OC}(\text{Me})_2\text{Ph}]$ (**6.6**). The solid-state molecular structure of compound **6.6** is shown in Figure 6.6a. The Cr–N (2.135(2) Å) and Cr–C(1) (2.051(3) Å) bond lengths in compound **6.6** are similar to those of compounds **6.1** and **6.2**. The Cr–O bond length (1.828(2) Å) of the alkoxide ligand is slightly shorter than that of the CpCr β -diketiminato compounds **3.6** and **3.7**, but the Cr–O–C angle ($140.2(2)^\circ$) is approximately 10 degrees smaller compared to that of compounds **3.6** and **3.7**, presumably a result of the decreased steric bulk of the benzylamine ligand of **6.6** compared to the larger β -diketiminato ligand. Compound **6.6** contains a distorted three-legged piano stool geometry with the O–Cr–N bond angle ($87.25(7)^\circ$) being significantly smaller compared to the O–Cr–C(1) bond angle of $99.66(8)^\circ$.

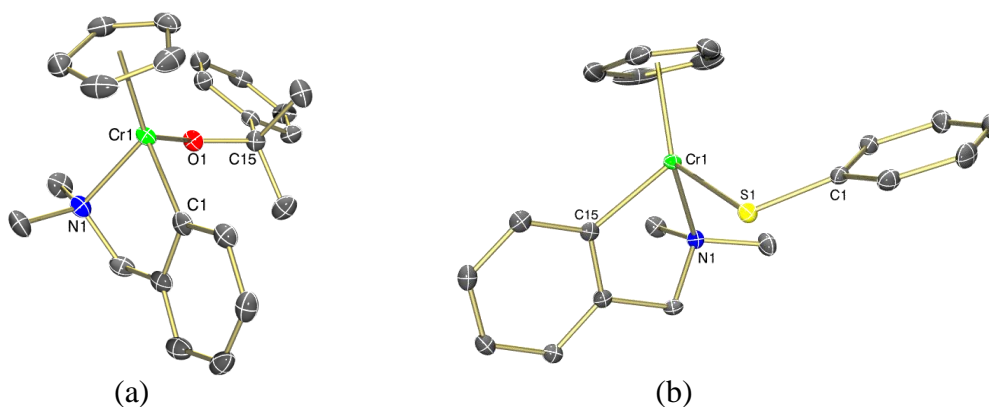


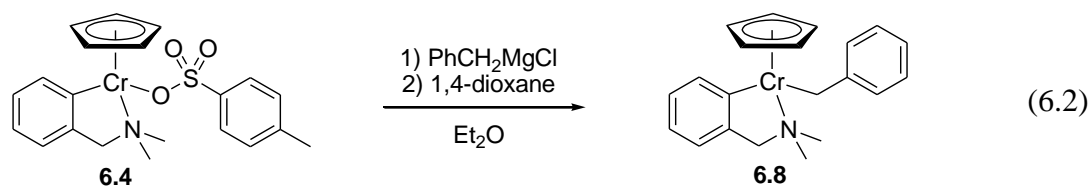
Figure 6.6. Thermal ellipsoid diagrams (50%) of the Cr(III) alkoxide compound **6.6** (a) and the Cr(III)–SPh compound **6.7** (b). All H atoms are omitted for clarity.

The Cr(II) compound **6.1** also reacted very rapidly with PhSSPh, forming the Cr(III) complex $\text{CpCr}(\text{C}_6\text{H}_4\text{CH}_2\text{NMe}_2)(\text{SPh})$ (**6.7**). Figure 6.6b displays the solid-state molecular structure of **6.7**. The Cr–S bond length of 2.3479(5) Å and Cr–S–C(15) bond angle of 113.05(6)° are similar to the CpCr β -diketiminato analogue **2.19**. The structure of **6.7** is similar to the alkoxide compound **6.6** with Cr–N and Cr–C(1) bond lengths of 2.131(2) and 2.050(2) Å, respectively. The major difference in compound **6.7** is that the three-legged piano stool geometry is not distorted like that of compound **6.6**. The S–Cr–N and S–Cr–C(1) bond angles are very similar to one another. In fact, the S–Cr–N angle (94.93(5)°) is actually slightly larger than the S–Cr–C(1) angle (92.05(5)°), the opposite trend in bond angle size compared to the alkoxide **6.6**.

The UV-vis spectrum of the alkoxide **6.6** displays absorption bands at 432 and 579 nm. The Cr(III)–SPh complex **6.7** has an absorption band at 533 nm and two shoulder bands at 341 and 400 nm. The UV-vis spectra of **6.6** and **6.7** contain distinctive absorption bands that allow for easy distinction from the Cr(II) starting material and the Cr(III) halide analogues, providing a useful characterization technique for these paramagnetic complexes when analyzing reaction products.

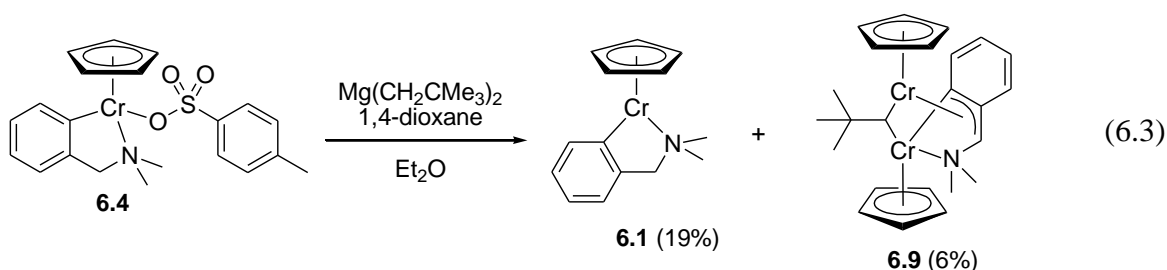
6.3 Synthesis of $\text{CpCr}(\text{C}_6\text{H}_4\text{CH}_2\text{NMe}_2)(\text{R})$ Complexes

Given the high yielding synthesis of the tosylate compound **6.4**, this complex was chosen as a precursor for testing salt metathesis reactions in the synthesis of $\text{CpCr}(\text{C}_6\text{H}_4\text{CH}_2\text{NMe}_2)(\text{R})$ compounds, where R = alkyl or aryl. A Cr(III) benzyl compound was prepared by reaction of compound **6.4** with ClMgCH_2Ph to provide compound $\text{CpCr}(\text{C}_6\text{H}_4\text{CH}_2\text{NMe}_2)(\text{CH}_2\text{Ph})$ (**6.8**) in



high yield (eq 6.2). Solutions of compound **6.8** are red, with an absorption band at 575 nm and a shoulder at 390 nm.

Synthesis of a Cr(III) neopentyl complex was also attempted by reaction of compound **6.4** with the dialkyl Grignard reagent $\text{Mg}(\text{CH}_2\text{CMe}_3)_2$ (eq 6.3). Upon workup, a first fraction of black crystals was isolated, followed by the isolation of a second small fraction of black crystals. Characterization of the first fraction (X-ray and UV-vis) identified the material as the Cr(II) compound **6.1** (19% yield), while the remaining solution contained a significantly different UV-vis spectrum with an absorption band at 535 nm and a shoulder at 400 nm. X-ray diffraction of a single-crystal isolated from the second fraction identified the material as an unexpected bimetallic compound $(\text{CpCr})_2(\mu\text{-CHCMe}_3)(\mu\text{-}\eta^3\text{:}\kappa^2\text{-C}_6\text{H}_4\text{CHNMe}_2)$ (**6.9**) in 6% yield. The structure of **6.9**, shown in Figure 6.7, contains two CpCr groups with a bridging alkylidene and a bridging benzylamine ligand. The Cr–Cr distance in **6.9** of 2.6416(5) Å and the Cr–C(10) bond lengths of 2.036(2) and 2.054(2) Å are similar to other Cr μ -alkylidene compounds.¹⁶⁷ The Cr(2)–C(3) (2.118(2) Å), Cr(2)–C(4) (2.206(2) Å), and Cr(2)–C(9) (2.185(2) Å) bond lengths are all relatively short, indicating an η^3 -benzyl interaction.¹⁶⁸ The Cr(1)–N bond length of 2.128(2) Å and Cr(1)–C(9) bond length of 2.028(2) Å are similar to the other CpCr benzylamine compounds reported herein. The benzylamine ligand is coordinated κ^2 -N,C to Cr(1) and is bound in an η^3 -benzyl bonding interaction to Cr(2). The geometry at the two metal atoms can be described as three-legged piano stool Cr(III) metal centres.



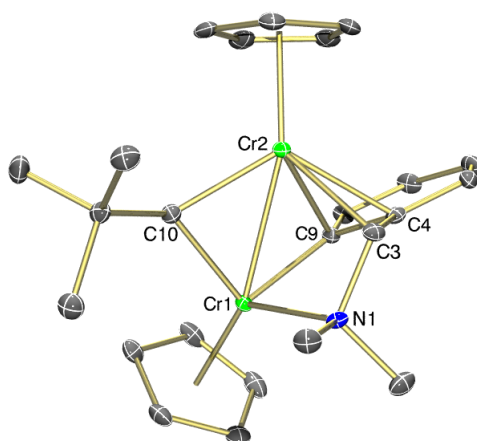


Figure 6.7. Thermal ellipsoid diagram (50%) of **6.9**. All H atoms are omitted for clarity.

Reaction of the tosylate compound **6.4** with $\text{Mg}(\text{C}_6\text{H}_4\text{Me})_2$ caused a rapid colour change to purple. Recrystallization from hexanes provided compound **6.10** in good yield, shown in Figure 6.8. The Cr–N (2.131(1) Å) and Cr–C(1) (2.040(1) Å) bond lengths are similar to the other CpCr(III) benzylamine complexes. The three-legged piano stool geometry of **6.10** is distorted slightly, with C(15)–Cr–C(1) and C(15)–Cr–N bond angles of $97.58(6)^\circ$ and $93.84(5)^\circ$, although to a lesser extent than the alkoxide compound **6.6**. The Cr–C(15) bond length of 2.075(1) Å is slightly shorter compared to the sterically crowded $\text{CpCr}[(\text{XylNCMe})_2\text{CH}](\text{Ph})$ complex **2.15**. The UV-vis spectrum of **6.10** displays two strong absorption bands at 378 and 393 nm and a weaker band at 538 nm.

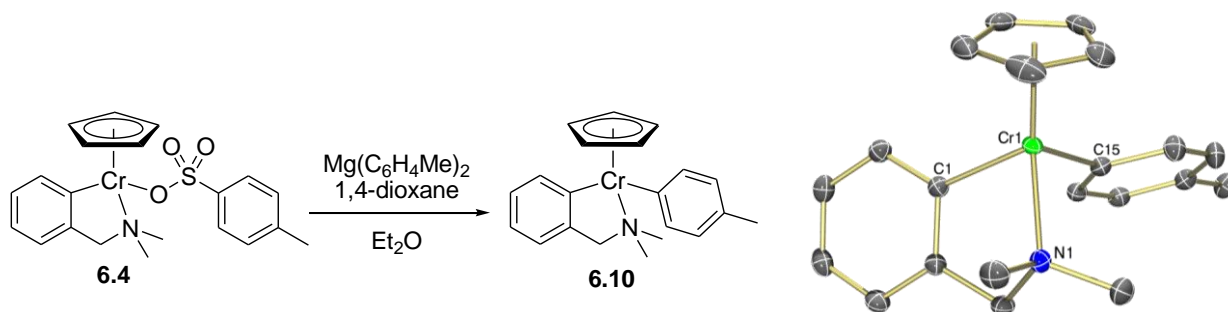


Figure 6.8. Synthesis of compound $\text{CpCr}(\text{C}_6\text{H}_4\text{CH}_2\text{NMe}_2)(\text{C}_6\text{H}_4\text{Me})$ (**6.10**). Thermal ellipsoid diagram (50%) of **6.10** with all H atoms omitted for clarity.

6.4 Comparison of $\text{CpCr}(\text{C}_6\text{H}_4\text{CH}_2\text{NMe}_2)$ with $\text{CpCr}[\text{C}(\text{Ph})\text{C}(\text{Ph})\text{C}_6\text{H}_4\text{CH}_2\text{NMe}_2]$

The single-electron oxidation of the Cr(II) compound **6.2** was examined for comparison to that of compound **6.1**. Treatment of **6.2** with 0.5 equivalents of I_2 provided the iodide complex $\text{CpCr}[\text{C}(\text{Ph})\text{C}(\text{Ph})\text{C}_6\text{H}_4\text{CH}_2\text{NMe}_2](\text{I})$ (**6.11**) in high yield (Figure 6.9). Compound **6.11** has a strong absorption band at 555 nm and a weaker absorption at 725 nm, which is significantly different from the spectrum of the Cr(III) iodide compound **6.3**. The solid-state molecular structure of compound **6.11**, shown in Figure 6.10, contains Cr–C(17) (2.097(5) Å) and Cr–N (2.194(4) Å) bond lengths that are the longest of the compounds reported in this chapter. The Cr–I bond length of 2.6877(9) Å is similar to the CpCr β -diketiminato Cr(III) iodide complexes. Similar to the alkoxide (**6.6**) and aryl (**6.10**) compounds, **6.11** has a slightly distorted geometry with I–Cr–N and I–Cr–C(17) bond angles of $96.9(1)^\circ$ and $101.2(2)^\circ$, respectively. The N–Cr–C(17) bond angle in **6.11** ($91.6(2)^\circ$) is slightly smaller compared to the Cr(II) precursor **6.2**, presumably to accommodate the additional iodide ligand. Perhaps the most interesting structural feature of compound **6.11** is the orientation of the chelating ligand backbone, which is clearly bent up towards the Cp ligand to form a boat-like conformation of the metalacycle. This orientation is similar to the Cr(II) precursor **6.2** (Figure 6.4) but is much more pronounced in the Cr(III) iodide complex **6.11** due to the increased coordination number of the metal centre.

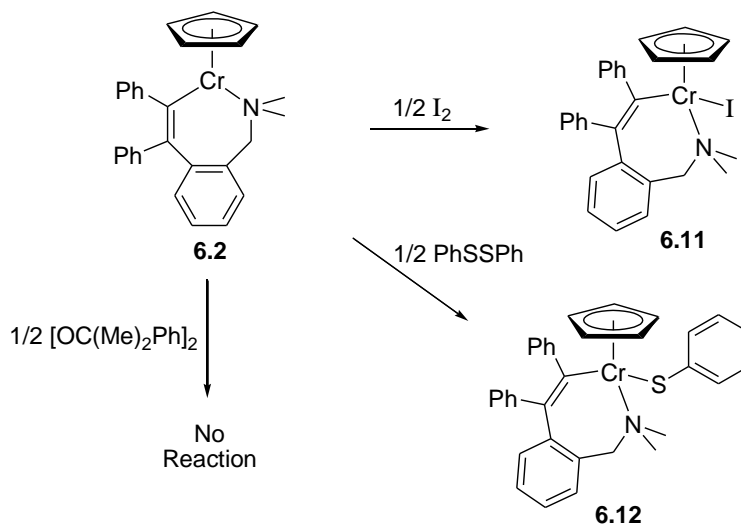


Figure 6.9. Synthesis of Cr(III) $\text{CpCr}[\text{C}(\text{Ph})\text{C}(\text{Ph})\text{C}_6\text{H}_4\text{CH}_2\text{NMe}_2](\text{X})$ compounds by single-electron oxidation of $\text{CpCr}[\text{C}(\text{Ph})\text{C}(\text{Ph})\text{C}_6\text{H}_4\text{CH}_2\text{NMe}_2]$ (**6.2**).

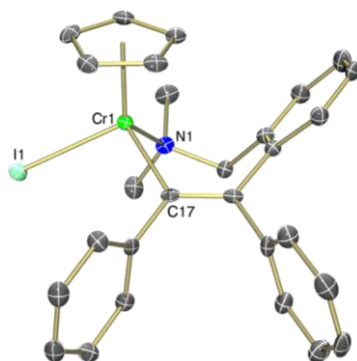


Figure 6.10. Thermal ellipsoid diagram (50%) of **6.11**. All H atoms are omitted for clarity.

Compound **6.2** also reacted with 0.5 equivalents of PhSSPh to form the $\text{CpCr}[\text{C}(\text{Ph})\text{C}(\text{Ph})\text{C}_6\text{H}_4\text{CH}_2\text{NMe}_2](\text{SPh})$ complex **6.12**. The UV-vis spectrum of **6.12** displays an absorption band at 591 nm and two shoulder bands at 360 and 400 nm. The low energy absorption at 591 nm is shifted significantly compared to the SPh compound **6.7** (533 nm), making the two compounds easily distinguishable from one another. Unlike the CpCr benzylamine compound **6.1**, compound **6.2** did not react with dicumyl peroxide to form a Cr(III) alkoxide. The difference in reactivity is attributed to the metal centre in compound **6.2** being more sterically protected compared to compound **6.1**. The Cr(II) CpCr β -diketiminate compounds are also unreactive towards dicumyl peroxide, despite the fact that the Cr(III) alkoxide product **3.7** was prepared by other methods. This is consistent with the previous report that Cr(II) reacts with peroxides via an inner sphere electron transfer mechanism, which is dependent on steric considerations of both the metal centre and the peroxide substrate.¹⁶⁹

In contrast to the preparation of the benzyl (**6.8**) and aryl (**6.10**) compounds, the attempted arylation of the Cr(III) iodide compound **6.11** did not proceed smoothly. Upon addition of the $\text{Mg}(\text{C}_6\text{H}_4\text{Me})_2$ Grignard reagent to a solution of compound **6.11**, an initial colour change to purple was accompanied by an increase in the colour intensity of the solution and the formation of an ionic precipitate, common observations during salt metathesis reactions with both the CpCr β -diketiminate and benzylamine ligand platforms. A further colour change to orange was then accompanied by a significant decrease in the colour intensity of the reaction mixture, forming unidentified products. Further work remains to determine the nature of the decomposition reaction and identification of the reaction product or products.

A second approach was taken in an attempt to prepare a $\text{CpCr}[\text{C}(\text{Ph})\text{C}(\text{Ph})\text{C}_6\text{H}_4\text{CH}_2\text{NMe}_2](\text{Ar})$ complex. The aryl compound **6.10** was treated with $\text{PhC}\equiv\text{CPh}$ to determine whether the insertion reaction would occur to produce the desired

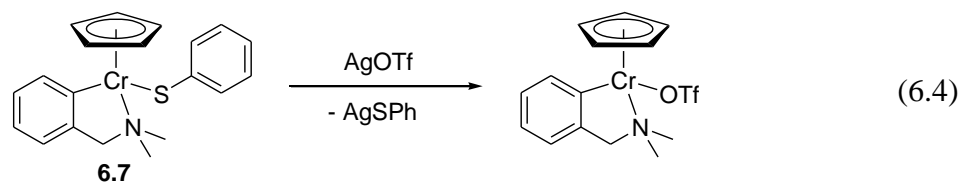
product. Interestingly, both the aryl (**6.10**) and SPh (**6.7**) compounds were completely unreactive towards $\text{PhC}\equiv\text{CPh}$ insertion, even at elevated temperatures (90 °C) with a large excess of $\text{PhC}\equiv\text{CPh}$ (20 equivalents) no reaction was observed over a 48 h period. Although no reaction was observed between the Cr(III) compounds and $\text{PhC}\equiv\text{CPh}$, these results do provide potentially useful insight into the mechanism of alkyne insertion. Only the coordinatively unsaturated Cr(II) compound **6.1** was found to undergo alkyne insertion, while the three-legged piano stool Cr(III) compounds showed no signs of alkyne insertion, despite the fact that the product of alkyne insertion, the Cr(III)–SPh complex **6.12**, was independently synthesized.

6.5 Oxidatively Induced Reductive Elimination

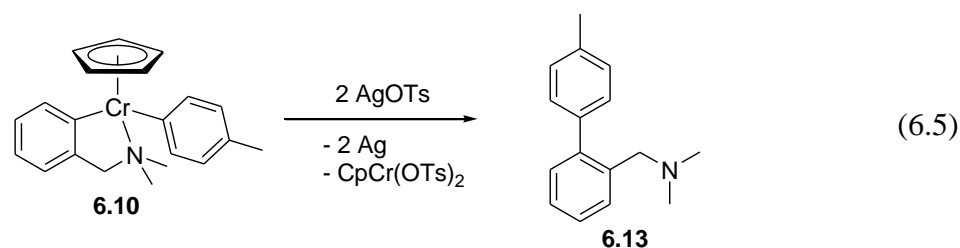
The Cr(III) alkoxide (**6.6**) and SPh (**6.7**) compounds were remarkably thermally robust, showing no signs of decomposition when heated in solution (toluene) at 90–100 °C for 24 h. The benzyl (**6.8**) and aryl (**6.10**) compounds were also stable at elevated temperatures (90 °C), showing no signs of decomposition. The reactions were monitored for changes in their UV-vis spectra; in all cases no changes in the spectra were observed.

Reductive elimination from transition metal compounds is favoured at higher oxidation states.¹⁷ Sanford and co-workers have examined the effect of single-electron oxidation for inducing reductive elimination from a Pd(II) complex (*t*-Bubpy)Pd(Me)₂.¹⁷⁰ The reaction was reported to proceed by initial single-electron oxidation of the Pd(II) to form a Pd(III) intermediate which undergoes disproportionation to form a Pd(IV) intermediate, which reductively eliminates ethane. The single-electron oxidation of Ni(II) compounds has also been examined for carbon–halogen bond formation by reductive elimination from a Ni(III) intermediate.¹⁷¹ In both cases chemical oxidants have been used for oxidation of the organometallic complexes. Cationic silver was an effective oxidant for the Pd(II) system,¹⁷⁰ and has been used extensively herein for the single-electron oxidation of Cr(II) species. We were therefore interested in the potential for Ag(I) to induce oxidation of the highly stable Cr(III) compounds reported in this chapter.

Upon treatment of the Cr(III)–SPh complex **6.7** with a stoichiometric amount of AgOTf, a rapid colour change was observed and the UV-vis spectrum of the reaction mixture closely resembled that of the tosylate compound **6.4**. This suggested that a metathesis reaction with the Ag reagent had occurred, in order to form the $\text{CpCr}(\text{C}_6\text{H}_4\text{CH}_2\text{NMe}_2)(\text{OTf})$ species (eq 6.4), instead of the desired oxidation to form a Cr(IV) species.



A rapid reaction was also observed between the aryl compound **6.10** and AgOTs, in this case the colour change was accompanied by the formation of a silver mirror on the reaction vessel, an indication of the formation silver metal. The use of 2 equivalents of AgOTs produced a blue solution. Upon removal of the THF solvent, the blue solid was sparingly soluble in Et₂O. The blue colour is characteristic of CpCr(X)₂(L) compounds, where X is a halide,^{130,172} and the blue residue is therefore tentatively assigned as CpCr(OTs)₂. The blue solid was also sparingly soluble in C₆D₆, which did, however, contain an organic product that was identified as the reductively coupled compound **6.13**, shown in eq 6.5.



These initial results indicate that, while the Cr(III)–SPh compound **6.7** is not oxidized by Ag(I), the more electron rich aryl complex **6.10** is readily oxidized. The oxidation of **6.10** appears to induce a reductive elimination to form the organic product **6.13** and, presumably, a Cr(II) intermediate, which is oxidized to the CpCr(OTs)₂ species in the presence of a second equivalent of AgOTs. Further work remains to determine the yield for this reaction and to explore the range of potential substrates to be used in this coupling reaction. Although no yield was determined for the formation of **6.13**, the ¹H NMR spectrum of the crude mixture contained only peaks corresponding to the desired product, suggesting that **6.13** is the sole organic product formed and that it should be easily purified by removal of the paramagnetic Cr by-products by simple flash chromatography.

6.6 Experimental Section

General considerations. Protocols were identical to those reported in sections 2.13 and 3.14 using standard Schlenk and glovebox techniques.

Characterization. Protocols were identical to those reported in sections 2.13.

Materials. Protocols were identical to those reported in section 2.13. Additionally, diphenylacetylene, dicumyl peroxide, and benzoyl peroxide were purchased from Aldrich and used as received. *N,N*-dimethylbenzylamine was purchased from Aldrich, degassed by three freeze-vacuum-thaw cycles, and stored under nitrogen prior to use. $\text{Li}[\text{C}_6\text{H}_4\text{CH}_2\text{NMe}_2]$ was prepared by reacting $\text{PhCH}_2\text{NMe}_2$ with 1 equiv of *n*-BuLi in Et_2O .¹⁷³ Upon stirring overnight, the product was isolated by vacuum filtration, rinsed with hexanes, dried under vacuum, and stored under nitrogen. The Grignard reagent $\text{Mg}(\text{C}_6\text{H}_4\text{Me})_2 \cdot 1.89(1,4\text{-dioxane})$ was prepared based on literature procedures.⁶⁴

Synthesis of $\text{CpCr}(\text{C}_6\text{H}_4\text{CH}_2\text{NMe}_2)$ (6.1). CrCl_2 (1.243 g, 10.1 mmol) was suspended in THF (45 mL) in a Schlenk flask. NaCp (5.20 mL of a 2.0 M solution in THF, 10.4 mmol, 1.03 equiv) was added dropwise to the CrCl_2 while stirring at room temperature, followed by the addition of a THF solution of $\text{Li}[\text{C}_6\text{H}_4\text{CH}_2\text{NMe}_2]$ (1.430 g, 10.1 mmol, 1.00 equiv). The reaction mixture rapidly turned dark orange and was allowed to stir overnight. The solvent was removed under reduced pressure, the residue extracted with Et_2O (70 mL), filtered over Celite, and rinsed with Et_2O (4×5 mL). The orange-red solution was concentrated to ~70 mL and cooled to -35°C to yield crystals of **6.1** (1.48 g, 58%) over several days in two crops. UV-vis (toluene; λ_{max} , nm (ϵ , $\text{M}^{-1}\text{cm}^{-1}$)): 325 (2490), 374 (1430), 467 (200).

Synthesis of $\text{CpCr}[\text{C}(\text{Ph})\text{C}(\text{Ph})\text{C}_6\text{H}_4\text{CH}_2\text{NMe}_2]$ (6.2). Compound **6.1** (205 mg, 0.815 mmol) was dissolved in toluene (15 mL). To this solution was added as toluene (2 mL) solution of $\text{PhC}\equiv\text{CPh}$ (147 mg, 0.822 mmol, 1.01 equiv) dropwise. The solution rapidly changed colour from orange to burgundy. After stirring overnight at room temperature, the solvent was removed under reduced pressure, the residue was rinsed with Et_2O , extracted with toluene (15 mL), filtered over Celite, and cooled to -35°C to yield crystals of **6.2** (273 mg, 78%) over several days in three crops. Anal. Calcd for $\text{C}_{28}\text{H}_{27}\text{NCr}$: C, 78.30; H, 6.34; N, 3.26. Found: C, 76.97; H, 6.54; N, 3.11. UV-vis (THF; λ_{max} , nm): 509.

Synthesis of $\text{CpCr}(\text{C}_6\text{H}_4\text{CH}_2\text{NMe}_2)(\text{I})$ (6.3). Compound **6.1** (48.9 mg, 0.195 mmol) was dissolved in Et_2O (10 mL) followed by the addition of an Et_2O (3 mL) solution of I_2 (25.6 mg, 0.101 mmol, 0.52 equiv). The colour intensity of the solution rapidly increased. Upon stirring for 5 min at room temperature, a maroon precipitate formed and the solution became very pale in

colour. After stirring for 4 days the precipitate was isolated by vacuum filtration and dried under vacuum to provide compound **6.3** (61 mg, 83%) as a maroon powder. Anal. Calcd for $C_{14}H_{17}NCrI$: C, 44.46; H, 4.53; N, 3.70. Found: C, 45.70; H, 4.69; N, 3.72. UV-vis (toluene; λ_{max} , nm (ϵ , $M^{-1}cm^{-1}$)): 378 (sh), 430 (sh), 512 (740), 696 (200).

Synthesis of $CpCr(C_6H_4CH_2NMe_2)(OTs)$ (6.4). Compound **6.1** (524 mg, 2.09 mmol) was dissolved in Et_2O (30 mL) followed by the dropwise addition of $AgOTs$ (584 mg, 2.09 mmol, 1.00 equiv) suspended in THF (15 mL). The mixture rapidly changed colour from orange to purple (orange transmitted) and was allowed to stir at room temperature for 2 days. The solvent was removed under reduced pressure, the residue extracted with toluene (25 mL), filtered over Celite, and cooled to $-35\text{ }^{\circ}C$ to yield a burgundy microcrystalline powder of **6.4** (720 mg, 82%) over several days in two crops. Anal. Calcd for $C_{21}H_{24}O_3SNCr$: C, 59.70; H, 5.73; N, 3.32. Found: C, 59.84; H, 5.80; N, 3.19. UV-vis (toluene; λ_{max} , nm (ϵ , $M^{-1}cm^{-1}$)): 365 (650), 418 (470), 499 (910).

Synthesis of $CpCr(C_6H_4CH_2NMe_2)(O_2CPh)$ (6.5): Method A. Compound **6.1** (76.4 mg, 0.304 mmol) was dissolved in THF (8 mL) followed by the addition of AgO_2CPh (69.4 mg, 0.303 mmol, 1.00 equiv) suspended in THF (6 mL). Upon stirring overnight at room temperature, the solution became burgundy (orange transmitted) in colour and the solvent was removed under reduced pressure. The residue was extracted with Et_2O (10 mL), filtered over Celite, and the solution was concentrated to a volume of 3 mL before being cooled to $-35\text{ }^{\circ}C$ for 3 days to provide compound **6.5** (18.4 mg, 16%). Anal. Calcd for $C_{21}H_{22}O_2NCr$: C, 67.73; H, 5.95; N, 3.76. Found: C, 68.00; H, 6.07; N, 3.77. UV-vis (toluene; λ_{max} , nm (ϵ , $M^{-1}cm^{-1}$)): 414 (550), 504 (750).

Method B. Compound **6.1** (30.4 mg, 0.121 mmol) and benzoyl peroxide (16.2 mg, 0.067 mmol, 0.55 equiv) were placed in a Schlenk flask followed by the addition of Et_2O (8 mL). Upon stirring for 5 min at room temperature, the solution became purple (orange transmitted) in colour and was allowed to stir for 2 days. The solvent was removed under reduced pressure, the residue extracted with toluene (8 mL), filtered over Celite, and cooled to $-35\text{ }^{\circ}C$ to yield compound **6.5** (22 mg, 49%) over several days in three crops. The UV-vis spectrum of the product was identical to that of compound **6.5** prepared by method A.

Synthesis of $CpCr(C_6H_4CH_2NMe_2)[OC(Me)_2Ph]$ (6.6). Compound **6.1** (178 mg, 0.706 mmol) and dicumyl peroxide (96.0 mg, 0.355 mmol, 0.50 equiv) were placed in a Schlenk flask followed by the addition of Et_2O (20 mL). Upon stirring overnight at room temperature, the solution became purple in colour, the solvent was removed under reduced pressure, the residue

extracted with hexanes (3 mL), filtered over Celite, and cooled to -35 °C to yield black crystals of **6.6** (155 mg, 57%) over several days in two crops. Anal. Calcd for $C_{23}H_{28}ONCr$: C, 71.48; H, 7.30; N, 3.62. Found: C, 63.12; H, 6.88; N, 3.37. UV-vis (hexanes; λ_{max} , nm (ϵ , $M^{-1}cm^{-1}$)): 432 (530), 579 (400).

Synthesis of $CpCr(C_6H_4CH_2NMe_2)(SPh)$ (6.7). Compound **6.1** (104 mg, 0.415 mmol) was dissolved in toluene (3 mL) followed by the dropwise addition of a toluene (1 mL) solution of PhSSPh (45.5 mg, 0.208 mmol, 0.50 equiv). Upon stirring overnight at room temperature, Et_2O (2 mL) was added to induce precipitation. The solid was isolated by vacuum filtration, rinsed with Et_2O (3×1 mL), and dried under vacuum to provide compound **6.7** (127 mg, 84%) as an analytically pure brown powder. Single-crystals suitable for X-ray crystallography were obtained by Et_2O diffusion into a THF solution of **6.7**. Anal. Calcd for $C_{20}H_{22}NSCr$: C, 66.64; H, 6.15; N, 3.89. Found: C, 66.72; H, 6.14; N, 3.81. UV-vis (toluene; λ_{max} , nm (ϵ , $M^{-1}cm^{-1}$)): 341 (sh), 400 (sh), 533 (550).

Synthesis of $CpCr(C_6H_4CH_2NMe_2)(CH_2Ph)$ (6.8). Compound **6.4** (140 mg, 0.332 mmol) was placed in a Schlenk flask followed by the addition of Et_2O (30 mL) and $ClMgCH_2Ph$ (0.37 mL of a 1.0 M solution in Et_2O , 0.37 mmol, 1.1 equiv). Upon stirring overnight at room temperature, 1,4-dioxane (300 μ L) was added and the mixture was allowed to stir for an additional 1 h before the solvent was removed under reduced pressure. The residue was extracted with hexanes (30 mL), filtered over Celite, and concentrated to a volume of approximately 8 mL before cooling the red solution to -35 °C to yield a black microcrystalline powder of **6.8** (87 mg, 77%) over several days in two crops. Anal. Calcd for $C_{21}H_{24}NCr$: C, 73.66; H, 7.06; N, 4.09. Found: C, 72.56; H, 7.01; N, 3.98. UV-vis (hexanes; λ_{max} , nm (ϵ , $M^{-1}cm^{-1}$)): 390 (sh), 575 (620).

Attempted synthesis of $CpCr(C_6H_4CH_2NMe_2)(CH_2CMe_3)$. Compound **6.4** (81.5 mg, 0.193 mmol) was placed in a Schlenk flask followed by the addition of Et_2O (15 mL) and $Mg(CH_2CMe_3)_2 \cdot 1.05(1,4-dioxane)$ (27.4 mg, 0.106 mmol, 0.55 equiv) with Et_2O (2 mL). Upon stirring overnight at room temperature, the solvent was removed under reduced pressure, the residue extracted with hexanes, filtered over Celite, and the solvent was again removed under reduced pressure. The residue was extracted with a minimum of hexanes (2 mL), filtered over Celite, and cooled to -35 °C to yield black crystals of compound **6.1** (9.0 mg, 19%). The remaining solution was concentrated and cooled again to obtain a second crop of black crystals, identified as compound $(CpCr)_2(\mu-CHCMe_3)(\mu-\eta^3:\kappa^2-C_6H_4CHNMe_2)$ (**6.9**) (2.5 mg, 6%).

Synthesis of $\text{CpCr}(\text{C}_6\text{H}_4\text{CH}_2\text{NMe}_2)(\text{C}_6\text{H}_4\text{Me})$ (6.10). Compound **6.4** (81.0 mg, 0.192 mmol) was placed in a Schlenk flask followed by the addition of Et_2O (15 mL). Upon addition of $\text{Mg}(\text{C}_6\text{H}_4\text{Me})_2 \cdot 1.89(1,4\text{-dioxane})$ (39.2 mg, 0.105 mmol, 0.55 equiv) with Et_2O (2 mL), the reaction mixture rapidly turned purple in colour. After stirring at room temperature for 3 days, the solvent was removed under reduced pressure, the residue extracted with hexanes, filtered over Celite, and concentrated to a volume of approximately 7 mL before cooling the purple (red transmitted) solution to -35°C to yield compound **6.10** (49 mg, 75%) over several days in three crops. Anal. Calcd for $\text{C}_{21}\text{H}_{24}\text{NCr}$: C, 73.66; H, 7.06; N, 4.09. Found: C, 62.21; H, 6.22; N, 3.84. UV-vis (hexanes; λ_{max} , nm (ϵ , $\text{M}^{-1}\text{cm}^{-1}$)): 378 (1210), 393 (1122), 538 (445).

Synthesis of $\text{CpCr}[\text{C}(\text{Ph})\text{C}(\text{Ph})\text{C}_6\text{H}_4\text{CH}_2\text{NMe}_2](\text{I})$ (6.11). Compound **6.2** (218 mg, 0.508 mmol) was dissolved in toluene (15 mL) followed by the addition of a toluene (2 mL) solution of I_2 (65.0 mg, 0.256 mmol, 0.504 equiv). The colour intensity of the reaction mixture rapidly increased upon addition of the I_2 . Upon stirring overnight at room temperature, the solvent was removed under reduced pressure, the residue extracted with toluene (10 mL), filtered over Celite, and layered with hexanes (4 mL) before cooling to -35°C to yield compound **6.11** (17.4 mg). The remaining solution was layered with an additional 4 mL of hexanes and cooled to provide a second crop of **6.11** (225.2 mg). The remaining solution was concentrated and single-crystals suitable for X-ray diffraction were obtained by vapour diffusion of hexanes into the toluene solution of **6.11** (28 mg). A total of 271 mg (96%) was isolated in three crops. Anal. Calcd for $\text{C}_{28}\text{H}_{27}\text{NICr}$: C, 60.44; H, 4.89; N, 2.52. Found: C, 60.67; H, 5.07; N, 2.57. UV-vis (toluene; λ_{max} , nm (ϵ , $\text{M}^{-1}\text{cm}^{-1}$)): 555 (1250), 725 (340).

Synthesis of $\text{CpCr}[\text{C}(\text{Ph})\text{C}(\text{Ph})\text{C}_6\text{H}_4\text{CH}_2\text{NMe}_2](\text{SPh})$ (6.12). Compound **6.2** (105 mg, 0.245 mmol) was dissolved in toluene (3 mL) followed by the dropwise addition of a toluene (1 mL) solution of PhSSPh (27.0 mg, 0.124 mmol, 0.51 equiv). After stirring at room temperature for 2 days, the reaction was filtered over Celite, rinsed with toluene (3×1 mL), and cooled to -35°C to yield a burgundy-brown powder of **6.12** (36 mg, 27%). Anal. Calcd for $\text{C}_{34}\text{H}_{32}\text{NSCr}$: C, 75.81; H, 5.99; N, 2.60. Found: C, 75.78; H, 5.96; N, 2.57. UV-vis (toluene; λ_{max} , nm (ϵ , $\text{M}^{-1}\text{cm}^{-1}$)): 360 (sh), 400 (sh), 591 (770).

Reaction of 6.7 with AgOTf. Compound **6.7** (4.6 mg, 0.013 mmol) was dissolved in toluene (6 mL) followed by the addition of AgOTf (4.2 mg, 0.016 mmol, 1.3 equiv). The solution rapidly turned orange and the colour intensity decreased significantly. Product was identified as $\text{CpCr}(\text{C}_6\text{H}_4\text{CH}_2\text{NMe}_2)(\text{OTf})$ based on UV-vis analysis of the crude reaction mixture: $\lambda_{\text{max}} = 360$ (sh) and 481 nm.

Oxidatively induced reductive elimination. Compound **6.10** (15.1 mg, 0.0441 mmol) was dissolved in THF (4 mL) followed by the addition of AgOTs (25.1 mg, 0.0899 mmol, 2.04 equiv) with THF (2 mL). Upon stirring for 1.5 h at room temperature, the solution became blue in colour and a silver mirror formed on the walls of the reaction vessel. After stirring for an additional 4.5 h, the solvent was removed under reduced pressure, the blue residue was sparingly soluble in both Et₂O and C₆D₆. ¹H NMR analysis of the crude reaction mixture identified the reductively coupled compound **6.13**. ¹H NMR (400.1 MHz, C₆D₆) δ 2.03 (s, 6H), 2.15 (s, 3H), 3.40 (s, 2H), 7.00-7.05 (m, 3H), 7.21-7.30 (m, 3H), 7.68-7.79 (m, 1H). One of the aromatic H signals appears to be overlapping with the residual solvent peak and it was therefore not possible to properly assign the integration.

General procedure for X-ray crystallography. Protocols were identical to those reported in section 2.13.

Chapter 7 Conclusions and Future Work

The CpCr β -diketiminate framework was shown to be an effective platform for studying Cr–C bond homolysis. The rate constants for bond homolysis were elucidated through the use of the radical trapping agent PhSSPh, with the Cr(III) neopentyl and benzyl complexes showing appreciable rates of homolysis at room temperature. The degree of Cr–C bond homolysis was found to be extremely sensitive to steric modifications of both the ancillary and hydrocarbyl ligands. Additionally, the effect of light exposure in inducing metal–carbon bond homolysis in the Cr(III) hydrocarbyl compounds served to underscore both the radical trapping ability of Cr(II) complexes and that photolysis does not necessarily lead to decomposition.

Upon establishing the presence of Cr–C bond homolysis in the Cr(III) complexes, a range of applications were targeted. The Cr(III) neopentyl complex **2.11** was developed as an effective single-component initiator/mediator for the OMRP of VAc, although the utility of the system was ultimately limited due to β -acetate elimination resulting from head-to-head monomer insertion of the growing polymer chains. Although this system did not offer any practical applications for the production of PVAc, it did provide further insight into the interplay between ATRP and OMRP processes.

Initial results for the radical C–C bond formation for organic synthesis were also reported. Intramolecular C–C bond formation was explored using haloacetal substrates. The Cr-catalyzed radical cyclization of bromoacetals was achieved with low catalyst loadings under relatively mild reaction conditions. Cyclization of the chloroacetal substrates was also catalyzed by Cr, although in lower yields, requiring higher catalyst loadings compared to the bromo analogues. Chromium-catalyzed intermolecular C–C bond formation proved to be more challenging, with good yields only being obtained for the synthesis of bibenzyl and $\text{Ph}_3\text{CCH}_2\text{Ph}$.

The higher Cr catalyst loadings required for chloroacetal cyclization is a direct result of the increased carbon-halogen bond strength of the substrates compared to bromo and iodo analogues. Previous work in the Smith group has demonstrated that mixed-aryl β -diketiminate ligands significantly increase the rate of oxidative addition of MeI to the Cr(II) CpCr β -diketiminate system compared to the symmetric ligands reported in this work. Further work in this area could lead to improved catalyst turnover for the chloroacetal radical cyclization that would provide improved reaction yields while simultaneously reducing catalyst loadings and reaction temperatures.

Chromium-catalyzed radical C–P bond formation resulted in the preparation of *c*- $\text{C}_6\text{H}_{11}\text{PPh}_2$ from $\text{Ph}_2\text{P–PPh}_2$ and *c*- $\text{C}_6\text{H}_{11}\text{Br}$. While future work remains to extend the scope of

alkyl halides that could be used to prepare a variety of tertiary phosphines, further extension of this catalytic system to the direct functionalization of elemental phosphorus (P_4) would provide an opportunity to prepare tertiary phosphines directly from P_4 , similar to the Ti-mediated synthesis reported by Cummins and co-workers.¹⁴⁹

The CpCr β -diketiminato catalysts used in this work were extremely air-sensitive in the +2 oxidation state, leading to the formation of oxidized Cr(III) complexes containing strong Cr–O bonds while retaining the Cp and β -diketiminato ligands. A range of methods for regenerating the catalytically relevant Cr(II) species were developed, culminating in the application of those methods for the Cr-catalyzed haloacetal radical cyclization.

Destabilization of the Cr(III) μ -oxo bimetallic species through the use of ortho substituted N-aryl substituents on the β -diketiminato ligand allowed for catalytic oxygen atom transfer leading to PPh_3 oxidation. Catalyst turnover was limited due to intramolecular C–H bond activation of the ortho groups on the β -diketiminato ligand. Replacing the reactive ortho substituted N-aryl substituents with large meta substituted HIPT substituents did not lead to improved catalyst performance due to formation of the stable μ -oxo bimetallic moiety. Therefore, the installation of sterically demanding, yet unreactive, ortho substituted N-aryl substituents on the β -diketiminato ligand could provide an opportunity to improve catalyst performance and stability. For example, the use of 2,6-diphenyl N-aryl substituents would remove the reactive C–H bonds of the previous compounds while providing sufficient steric protection to prevent formation of a bimetallic μ -oxo species, potentially leading to the synthesis of a terminal Cr oxo species $CpCr[(2,6-Ph_2C_6H_3NCMe)_2CH](O)$.

Despite the well-known ability of Cr to catalyze C–C bond formation by non-radical mechanisms, the applications are currently limited to homocoupling reactions, with little development in the area of cross-coupling chemistry. The β -diketiminato ligand of the CpCr β -diketiminato framework was replaced with a deprotonated benzylamine ligand in order to install a reactive Cr–C bond. The methods developed in Chapter 2 for the synthesis of CpCr β -diketiminato hydrocarbyl compounds were then extended to the $CpCr(C_6H_4CH_2NMe_2)$ system. Initial results have demonstrated the potential for heterocoupling by reductive elimination from a Cr(IV) intermediate. Further work remains to explore the range of potential heterocoupling substrates for the formation of not only $C(sp^2)–C(sp^2)$ bonds, but also $C(sp^2)–C(sp^3)$ and $C(sp^2)–C(sp)$ bonds.

References

- ¹ Hartwig, J. F. *Organotransition metal chemistry: from bonding to catalysis*, University Science Books, Sausalito, CA, 2010.
- ² (a) Halpern, J. *Acc. Chem. Res.* **1970**, *3*, 386–392. (b) Bradley, J. S.; Connor, D. E.; Dolphin, D.; Labinger, J. A.; Osborn, J. A. *J. Am. Chem. Soc.* **1972**, *94*, 4043–4044. (c) Lappert, M. F.; Lednor, P. W. *J. Chem. Soc., Chem. Commun.* **1973**, 948–949. (d) Labinger, J. A.; Osborn, J. A.; Coville, N. J. *Inorg. Chem.* **1980**, *19*, 3236–3243. (e) Hall, T. L.; Lappert, M. F.; Lednor, P. W. *J. Chem. Soc., Dalton Trans.* **1980**, 1448–1456. (f) Hill, R. H.; Puddephatt, R. J. *J. Am. Chem. Soc.* **1985**, *107*, 1218–1225.
- ³ Kochi, J. K. *Acc. Chem. Res.* **1974**, *7*, 351–360.
- ⁴ Anet, F. A. L.; Leblanc, E. *J. Am. Chem. Soc.* **1957**, *79*, 2649–2650.
- ⁵ Anet, F. A. L. *Can. J. Chem.* **1959**, *37*, 58–61.
- ⁶ Kochi, J. K.; Davis, D. D. *J. Am. Chem. Soc.* **1964**, *86*, 5264–5271.
- ⁷ Kochi, J. K.; Powers, J. W. *J. Am. Chem. Soc.* **1970**, *92*, 137–146.
- ⁸ Espenson, J. H. *Prog. Inorg. Chem.* **1983**, *30*, 189–212.
- ⁹ van Eldik, R.; Meyerstein, D. *Acc. Chem. Res.* **2000**, *33*, 207–214.
- ¹⁰ van Eldik, R.; Gaede, W.; Cohen, H.; Meyerstein, D. *Inorg. Chem.* **1992**, *31*, 3695–3696.
- ¹¹ Okude, Y.; Hirano, S.; Hiyama, T.; Nozaki, S. *J. Am. Chem. Soc.* **1977**, *99*, 3179–3181.
- ¹² (a) Jin, H.; Uenishi, J.; Christ, W. J.; Kishi, Y. *J. Am. Chem. Soc.* **1986**, *108*, 5644–5646. (b) Takai, K.; Tagashira, M.; Kuroda, T.; Oshima, K.; Utimoto, K.; Nozaki, H. *J. Am. Chem. Soc.* **1986**, *108*, 6048–6050.
- ¹³ Fürstner, A.; Shi, N. *J. Am. Chem. Soc.* **1996**, *118*, 12349–12357.
- ¹⁴ Bandini, M.; Cozzi, P. G.; Umani-Ronchi, A. *Chem. Commun.* **2002**, 919–927.
- ¹⁵ Yamamoto, A.; Ueda, A.; Brémond, P.; Tiseni, P. S.; Kishi, Y. *J. Am. Chem. Soc.* **2012**, *134*, 893–896.
- ¹⁶ Kim, D.-S.; Dong, C.-G.; Kim, J. T.; Guo, H.; Huang, J.; Tiseni, P. S.; Kishi, Y. *J. Am. Chem. Soc.* **2009**, *131*, 15636–15641.
- ¹⁷ (a) Bolm, C.; Legros, J.; Le Paih, J.; Zani, L. *Chem. Rev.* **2004**, *104*, 6217–6254. (b) Cahiez, G.; Moyeux, A. *Chem. Rev.* **2010**, *110*, 1435–1462. (c) Hu, X. *Chem. Sci.* **2011**, *2*, 1867–1886. (d) Yeung, C. S.; Dong, V. M. *Chem. Rev.* **2011**, *111*, 1215–1292. (e) Sun, C.-L.; Li, B.-J.; Shi, Z.-J. *Chem. Rev.* **2011**, *111*, 1293–1314. (f) Jana, R.; Pathak, T. P.; Sigman, M. S.

- Chem. Rev.* **2011**, *111*, 1417–1492. (g) Liu, C.; Zhang, H.; Shi, W.; Lei, A. *Chem. Rev.* **2011**, *111*, 1780–1824.
- ¹⁸ Rudolph, A.; Lautens, M. *Angew. Chem., Int. Ed.* **2009**, *48*, 2656–2670, and references cited therein.
- ¹⁹ Jones, G. D.; Martin, J. L.; McFarland, C.; Allen, O. R.; Hall, R. E.; Haley, A. D.; Brandon, R. J.; Konovalova, T.; Desrochers, P. J.; Pulay, P.; Vicic, D. A. *J. Am. Chem. Soc.* **2006**, *128*, 13175–13183.
- ²⁰ (a) Vechorkin, O.; Proust, V.; Hu, X. *J. Am. Chem. Soc.* **2009**, *131*, 9756–9766. (b) Ren, P.; Vechorkin, O.; von Allmen, K.; Scopelliti, R.; Hu, X. *J. Am. Chem. Soc.* **2011**, *133*, 7084–7095.
- ²¹ Phapale, V. B.; Bunuel, E.; García-Iglesias, M.; Cárdenas, D. J. *Angew. Chem., Int. Ed.* **2007**, *46*, 8790–8795.
- ²² Affo, W.; Ohmiya, H.; Fujioka, T.; Ikeda, Y.; Nakamura, T.; Yorimitsu, H.; Oshima, K.; Imamura, Y.; Mizuta, T.; Miyoshi, K. *J. Am. Chem. Soc.* **2006**, *128*, 8068–8077.
- ²³ Lundin, P. M.; Fu, G. C. *J. Am. Chem. Soc.* **2010**, *132*, 11027–11029.
- ²⁴ Tsou, T.-T.; Loots, M.; Halpern, J. *J. Am. Chem. Soc.* **1982**, *104*, 623–624.
- ²⁵ Halpern, J. *Polyhedron* **1988**, *7*, 1483–1490.
- ²⁶ Espenson, J. H. *Acc. Chem. Res.* **1992**, *25*, 222–227, and references cited therein.
- ²⁷ Luinstra, G. A.; Teuben, J. H. *Organometallics* **1992**, *11*, 1793–1801.
- ²⁸ Daikh, B. E.; Finke, R. G. *J. Am. Chem. Soc.* **1992**, *114*, 2938–2943.
- ²⁹ Poli, R. *Angew. Chem., Int. Ed.* **2006**, *45*, 5058–5070.
- ³⁰ Poli, R. *Eur. J. Inorg. Chem.* **2011**, 1513–1530.
- ³¹ Ouchi, M.; Terashima, T.; Sawamoto, M. *Chem. Rev.* **2009**, *109*, 4963–5050.
- ³² Doherty, J. C.; Ballem, K. H. D.; Patrick, B. O.; Smith, K. M. *Organometallics* **2004**, *23*, 1487–1489.
- ³³ Gibson, V. C.; Newton, C.; Redshaw, C.; Solan, G. A.; White, A. J. P. Williams, D. J. *Eur. J. Inorg. Chem.* **2001**, 1895–1903.
- ³⁴ Champouret, Y.; Baisch, U.; Poli, R.; Tang, L.; Conway, J. L.; Smith, K. M. *Angew. Chem., Int. Ed.* **2008**, *47*, 6069–6072.
- ³⁵ MacLeod, K. C.; Conway, J. L.; Tang, L.; Smith, J. J.; Corcoran, L. D.; Ballem, K. H. D.; Patrick, B. O.; Smith, K. M. *Organometallics* **2009**, *28*, 6798–6806.
- ³⁶ Zhou, W.; Tang, L.; Patrick, B. O.; Smith, K. M. *Organometallics* **2011**, *30*, 603–610.

- ³⁷ Holm, R. H. *Prog. Inorg. Chem.* **1971**, *14*, 241-401.
- ³⁸ Sadique, A. R.; Heeg, M. J.; Winter, C. H. *J. Am. Chem. Soc.* **2003**, *125*, 7774–7775.
- ³⁹ Powers, D. C.; Ritter, T. *Acc. Chem. Res.* ASAP (DOI: 10.1021/ar2001974).
- ⁴⁰ Huang, Y.-B.; Jin, G.-X. *Dalton Trans.* **2009**, 767–769.
- ⁴¹ MacAdams, L. A.; Buffone, G. P.; Incarvito, C. D.; Rheingold, A. L.; Theopold, K. H. *J. Am. Chem. Soc.* **2005**, *127*, 1082–1083.
- ⁴² Ogino, H.; Shoji, M.; Abe, Y.; Shimura, M.; Shimoi, M. *Inorg. Chem.* **1987**, *26*, 2542–2546.
- ⁴³ Olliver, C.; Renaud, P. *Chem. Rev.* **2001**, *101*, 3415–3434.
- ⁴⁴ Sherwood, R. K.; Kent, C. L.; Patrick, B. O.; McNeil, W. S. *Chem. Commun.* **2010**, *46*, 2456–2458.
- ⁴⁵ (a) Carmona, E.; Gutiérrez-Puebla, E.; Marín, J. M.; Monge, A.; Paneque, M.; Poveda, M. L.; Ruiz, C. *J. Am. Chem. Soc.* **1989**, *111*, 2883–2891. (b) Hao, S. K.; Song, J.-I.; Berno, P.; Gambarotta, S. *Organometallics* **1994**, *13*, 1326–1335.
- ⁴⁶ MacLeod, K. C.; Conway, J. L.; Patrick, B. O.; Smith, K. M. *J. Am. Chem. Soc.* **2010**, *132*, 17325–17334.
- ⁴⁷ Theopold, K. H. *Acc. Chem. Res.* **1990**, *23*, 263–270.
- ⁴⁸ Fernandez, I.; Trovitch, R. J.; Lobkovsky, E.; Chirik, P. J. *Organometallics* **2008**, *27*, 109–118.
- ⁴⁹ Culkin, D. A.; Hartwig, J. F. *Acc. Chem. Res.* **2003**, *36*, 234–245.
- ⁵⁰ (a) Huber, T. A.; Macartney, D. H.; Baird, M. C. *Organometallics* **1995**, *14*, 592–602. (b) Derrah, E. J.; Giesbrecht, K. E.; McDonald, R.; Rosenberg, L. *Organometallics* **2008**, *27*, 5025–5032.
- ⁵¹ (a) Fulton, J. R.; Sklenak, S.; Bouwkamp, M. W.; Bergman, R. G. *J. Am. Chem. Soc.* **2002**, *124*, 4722–4737. (b) Oertel, A. M.; Ritleng, V.; Chetcuti, M. J.; Veiros, L. F. *J. Am. Chem. Soc.* **2010**, *132*, 13588–13589.
- ⁵² Blanksby, S. J.; Ellison, G. B. *Acc. Chem. Res.* **2003**, *36*, 255–263.
- ⁵³ Balcells, D.; Clot, E.; Eisenstein, O. *Chem. Rev.* **2010**, *110*, 749–823.
- ⁵⁴ Champouret, Y.; MacLeod, K. C.; Baisch, U.; Patrick, B. O.; Smith, K. M.; Poli, R. *Organometallics* **2010**, *29*, 167–176.
- ⁵⁵ Newcomb, M. *Tertrahedron* **1993**, *49*, 1151–1176.
- ⁵⁶ Fryzuk, M. D.; Leznoff, D. B.; Rettig, S. J. *Organometallics* **1997**, *16*, 5116–5119, and references cited therein.

- ⁵⁷ Nohr, R. S.; Espenson, J. H. *J. Am. Chem. Soc.* **1975**, *97*, 3392–3396.
- ⁵⁸ Hayashibara, K.; Kruppa, G. H.; Beauchamp, J. L. *J. Am. Chem. Soc.* **1986**, *108*, 5441–5443.
- ⁵⁹ Pattenden, G. *Chem. Soc. Rev.* **1988**, *17*, 361–382.
- ⁶⁰ Kirk, A. D. *Chem. Rev.* **1999**, *99*, 1607–1640.
- ⁶¹ (a) Baker, M. V.; Field, L. D.; Hambley, T. W. *Inorg. Chem.* **1988**, *27*, 2872–2876. (b) Schubert, E. M. *J. Chem. Educ.* **1992**, *69*, 62.
- ⁶² Budzelaar, P. H. M.; de Gelder, R.; Gal, A. W. *Organometallics* **1998**, *17*, 4121–4123.
- ⁶³ Cheng, M.; Moore, D. R.; Reczek, J. J.; Chamberlain, B. M.; Lobkovsky, E. B.; Coates, G. W. *J. Am. Chem. Soc.* **2001**, *123*, 8738–8749.
- ⁶⁴ (a) Andersen, R. A.; Wilkinson, G. *J. Chem. Soc., Dalton Trans.* **1977**, 809–811. (b) Dryden, N. H.; Legzdins, P.; Trotter, J.; Yee, V. C. *Organometallics*. **1991**, *10*, 1326–1335.
- ⁶⁵ SAINT, version 7.46A; Bruker Analytical X-ray System: Madison, WI, 1997–2007.
- ⁶⁶ SADABS. *Bruker Nonius area detector scaling and absorption correction*, V. 2.10; Bruker AXS Inc.: Madison, WI, 2003.
- ⁶⁷ (a) SIR97. Altomare, A.; Burla, M. C.; Cammelli, G.; Cascarano, M.; Giacovazzo, C.; Guagliardi, A.; Moliterni, A. G. G.; Polidori, G.; Spagna, A. *J. Appl. Crystallogr.* **1999**, *32*, 115–119. (b) SIR92. Altomare, A.; Cascarano, G.; Giacovazzo, C.; Guagliardi, A. *J. Appl. Crystallogr.* **1993**, *26*, 343–350.
- ⁶⁸ SHELXTL, Version 5.1; Bruker AXS Inc.: Madison, WI, 1997.
- ⁶⁹ Farrugia, L. J. *J. Appl. Crystallogr.* **1997**, *32*, 565.
- ⁷⁰ SQUEEZE. Sluis, P. v. d.; Spek, A. L. *Acta Crystallogr.* **1990**, *A46*, 194–201.
- ⁷¹ Parsons, S.; Gould, G. ROTAX; University of Edinburgh with additions by Cooper, R. (Oxford) and Farrugia, L. (Glasgow), Version Nov 26, 2001.
- ⁷² (a) TWINABS, *Bruker Nonius scaling and absorption for twinned crystals*, V. 2008/2; Bruker AXS Inc.: Madison WI, 2008. (b) TWINABS, *Bruker Nonius scaling and absorption for twinned crystals*, V. 1.05; Bruker AXS Inc.: Madison, WI, 2007.
- ⁷³ (a) Curran, D. P.; Totleben, M. J. *J. Am. Chem. Soc.* **1992**, *114*, 6050–6058. (b) Curran, D. P.; Fevig, T. L.; Jasperse, C. P.; Totleben, M. J. *Synlett* **1992**, 943–961. (c) Curran, D. P.; Gu, X.; Zhang, W.; Dowd, P. *Tetrahedron* **1997**, *53*, 9023–9042. (d) Ogoshi, S.; Stryker, J. M. *J. Am. Chem. Soc.* **1998**, *120*, 3514–3515. (e) Choquette, K. A.; Sadasivam, D. V.; Flowers, R. A., II *J. Am. Chem. Soc.* **2010**, *132*, 17396–17398.

- ⁷⁴ (a) Terao, J.; Saito, K.; Nii, S.; Kambe, N.; Sonoda, N. *J. Am. Chem. Soc.* **1998**, *120*, 11822–11823. (b) Agapie, T.; Diaconescu, P. L.; Mindiola, D. J.; Cummins, C. C. *Organometallics* **2002**, *21*, 1329–1340. (c) Nii, S.; Terao, J.; Kambe, N. *J. Org. Chem.* **2004**, *69*, 573–576. (d) Cossairt, B. M.; Cummins, C. C. *New. J. Chem.* **2010**, *34*, 1533–1536. (e) Trunkley, E. F.; Epshteyn, A.; Zavalij, P. Y.; Sita, L. R. *Organometallics* **2010**, *29*, 6587–6593.
- ⁷⁵ Bridging chromium oxo: (a) Di Vaira, M.; Mani, F. *Inorg. Chem.* **1984**, *23*, 409–412. (b) Bottomly, F.; Paez, D. E.; Sutin, L.; White, P. S.; Köhler, F. H.; Thompson, R. C.; Westwood, N. P. C. *Organometallics* **1990**, *9*, 2443–2454. (c) Noh, S.-K.; Heintz, R. A.; Haggerty, B. S.; Rheingold, A. L.; Theopold, K. H. *J. Am. Chem. Soc.* **1992**, *114*, 1892–1893. (d) Rupp, K. B. P.; Feghali, K.; Kovacs, I.; Aparna, K.; Gambarotta, S.; Yap, G. P. A.; Bensimon, C. *J. Chem. Soc., Dalton Trans.* **1998**, 1595–1605. (e) Huang, H.; Rheingold, A. L.; Hughes, R. P. *Organometallics* **2010**, *29*, 3672–3675. (f) O'Reilly, M. E.; Del Castillo, T. J.; Falkowski, J. M.; Ramachandran, V.; Pati, M.; Correia, M. C.; Abboud, K. A.; Dalal, N. S.; Richardson, D. E.; Veige, A. S. *J. Am. Chem. Soc.* **2011**, *133*, 13661–13673.
- ⁷⁶ Terminal chromium oxo: (a) Budge, J. R.; Gatehouse, B. M. K.; Nesbit, M. C.; West, B. O. *J. Chem. Soc., Chem. Commun.* **1981**, 370–371. (b) Groves, J. T.; Kruper, W. J., Jr.; Haushalter, R. C.; Butler, W. M. *Inorg. Chem.* **1982**, *21*, 1363–1368. (c) Morse, D. B.; Rauchfuss, T. B.; Wilson, S. R. *J. Am. Chem. Soc.* **1988**, *110*, 8234–8235. (d) Hess, A.; Hörz, M. R.; Liable-Sands, L. M.; Lindner, D. C.; Rheingold, A. L.; Theopold, K. H. *Angew. Chem. Int. Ed.* **1999**, *38*, 166–168. (e) Odom, A. L.; Mindiola, D. J.; Cummins, C. C. *Inorg. Chem.* **1999**, *38*, 3290–3295. (f) Hess, J. S.; Leelasubcharoen, S.; Rheingold, A. L.; Doren, D. J.; Theopold, K. H. *J. Am. Chem. Soc.* **2002**, *124*, 2454–2455. (g) Qin, K.; Incarvito, C. D.; Rheingold, A. L.; Theopold, K. H. *J. Am. Chem. Soc.* **2002**, *124*, 14008–14009. (h) Mahammed, A.; Gray, H. B.; Meier-Callahan, A. E.; Gross, Z. *J. Am. Chem. Soc.* **2003**, *125*, 1162–1163. (i) Prem Singh, S.; Venkataramanan, N. S.; Rajagopal, S.; Mirza, S. P.; Vairamani, M.; Rao, P. S.; Velavan, K. *Inorg. Chem.* **2004**, *43*, 5744–5753. (j) Czernuszewicz, R. S.; Mody, V.; Czader, A.; Gałęzowski, M.; Gryko, D. T. *J. Am. Chem. Soc.* **2009**, *131*, 14214–14215. (k) O'Reilly, M.; Falkowski, J. M.; Ramachandran, V.; Pati, M.; Abboud, K. A.; Dalal, N. S.; Gray, T. G.; Veige, A. S. *Inorg. Chem.* **2009**, *48*, 10901–10903. (l) Groysman, S.; Villagrán, D.; Nocera, D. G. *Inorg. Chem.* **2010**, *49*, 10759–10761. (m) Monillas, W. H.; Yap, G. P. A.; Theopold, K. H. *Inorg. Chim. Acta* **2011**, *369*, 103–119.

- ⁷⁷ (a) Qin, K.; Incarvito, C. D.; Rheingold, A. L.; Theopold, K. H. *Angew. Chem. Int. Ed.* **2002**, *41*, 2333–2335. (b) Cho, J.; Woo, J.; Nam, W. *J. Am. Chem. Soc.* **2010**, *132*, 5958–5959. (c) Cho, J.; Woo, J.; Han, J. E.; Kobo, M.; Ogura, T.; Nam, W. *Chem. Sci.* **2011**, *2*, 2057–2062.
- ⁷⁸ MacLeod, K. C.; Patrick, B. O.; Smith, K. M. *Inorg. Chem.* **2012**, *51*, 688–700.
- ⁷⁹ (a) Nichols, P. J.; Fallon, G. D.; Moubarki, B.; Murray, K. S.; West, B. O. *Polyhedron* **1993**, *12*, 2205–2213. (b) Liston, D. J.; Kennedy, B. J.; Murray, K. S.; West, B. O. *Inorg. Chem.* **1985**, *24*, 1561–1567.
- ⁸⁰ Liston, D. J.; West, B. O. *Inorg. Chem.* **1985**, *24*, 1568–1576.
- ⁸¹ Culkin, D. A.; Hartwig, J. F. *J. Am. Chem. Soc.* **2001**, *123*, 5816–5817.
- ⁸² Sun, M.; Mu, Y.; Liu, Y.; Wu, Q.; Ye, L. *Organometallics* **2011**, *30*, 669–675.
- ⁸³ (a) Fürstner, A. *Chem.–Eur. J.* **1998**, *4*, 567–570. (b) Fürstner, A. *Pure Appl. Chem.* **1998**, *70*, 1071–1076.
- ⁸⁴ Fürstner, A.; Hupperts, A. *J. Am. Chem. Soc.* **1995**, *117*, 4468–4475.
- ⁸⁵ Gansäuer, A.; Bluhm, H.; Pierobon, M. *J. Am. Chem. Soc.* **1998**, *120*, 12849–12859.
- ⁸⁶ Shaughnessy, K. H.; Huang, R. *Synth. Commun.* **2002**, *32*, 1923–1928.
- ⁸⁷ Namba, K.; Kishi, Y. *Org. Lett.* **2004**, *6*, 5031–5033.
- ⁸⁸ For studies by Takai and co-workers on the use of catalytic PbCl₂ to activate manganese metal, see: Takai, K.; Ueda, T.; Hayashi, T.; Moriwake, T. *Tetrahedron Lett.* **1996**, *37*, 7049–7052.
- ⁸⁹ Wessjohann, L. A.; Scheid, G. *Synthesis* **1999**, 1–36.
- ⁹⁰ Hansen, K. B.; Leighton, J. L.; Jacobsen, E. N. *J. Am. Chem. Soc.* **1996**, *118*, 10924–10925.
- ⁹¹ Thomas, B. J.; Mitchell, J. F.; Theopold, K. H.; Leary, J. A. *J. Organomet. Chem.* **1988**, *348*, 333–342.
- ⁹² (a) Cotton, A. F.; Daniels, L. M.; Murillo, C. A.; Pascual, I. *J. Am. Chem. Soc.* **1997**, *119*, 10223–10224. (b) Nelson, K. J.; DiPasquale, A. G.; Rheingold, A. L.; Daniels, M. C.; Miller, J. S. *Inorg. Chem.* **2008**, *47*, 7768–7774. (c) Zhu, Q.; Nelson, K. J.; Shum, W. W.; DiPasquale, A.; Rheingold, A. L.; Miller, J. S. *Inorg. Chim. Acta* **2009**, *362*, 595–598.
- ⁹³ Schaus, S. E.; Branalt, J.; Jacobsen, E. N. *J. Org. Chem.* **1998**, *63*, 403–405.
- ⁹⁴ (a) Vaughn, J. W. *Inorg. Chem.* **1981**, *20*, 2397–2402. (b) Díaz, C.; Seguí, A.; Ribas, J.; Solans, X.; Font-Altaba, M.; Solans, A.; Casabó, J. *Transition Met. Chem.* **1984**, *9*, 469–473. (c) Beveridge, K. A.; Bushnell, G. W.; Kirk, A. D. *Acta Crystallogr.* **1985**, *C41*, 899–902.
- ⁹⁵ Schnell, E.; Rochow, E. G. *J. Inorg. Nucl. Chem.* **1958**, *6*, 303–307.

- ⁹⁶ Huacuja, R.; Herbert, D. E.; Fafard, C. M.; Ozerov, O. V. *J. Fluorine Chem.* **2010**, *131*, 1257–1261.
- ⁹⁷ (a) Heintz, R. A.; Ostrander, R. L.; Rheingold, A. L.; Theopold, K. H. *J. Am. Chem. Soc.* **1994**, *116*, 11387–11396. (b) Filippou, A. C.; Schneider, S.; Schnakenburg, G. *Angew. Chem., Int. Ed.* **2003**, *42*, 4486–4489.
- ⁹⁸ Eisenberg, D. C.; Lawrie, C. J. C.; Moody, A. E.; Norton, J. R. *J. Am. Chem. Soc.* **1991**, *113*, 4888–4895.
- ⁹⁹ Colle, T. H.; Glaspie, P. S.; Lewis, E. S. *J. Org. Chem.* **1978**, *43*, 2722–2725.
- ¹⁰⁰ Lai, C.; Kim, Y. I.; Wang, C. M.; Mallouk, T. E. *J. Org. Chem.* **1993**, *58*, 1393–1399.
- ¹⁰¹ McGarrigle, E. M.; Gilheany, D. G. *Chem. Rev.* **2005**, *105*, 1563–1602.
- ¹⁰² Scott, S. L.; Bakac, A.; Espenson, J. H. *J. Am. Chem. Soc.* **1991**, *113*, 7787–7788.
- ¹⁰³ (a) Mayer, J. M. *Acc. Chem. Res.* **1998**, *31*, 441–450. (b) Gunay, A.; Theopold, K. H. *Chem. Rev.* **2010**, *110*, 1060–1081. (c) Warren, J. J.; Tronic, T. A.; Mayer, J. M. *Chem. Rev.* **2010**, *110*, 6961–7001. (d) Mayer, J. M. *Acc. Chem. Res.* **2011**, *44*, 36–46.
- ¹⁰⁴ (a) Bakac, A.; Espenson, J. H. *Acc. Chem. Res.* **1993**, *26*, 519–523. (b) Bakac, A. *J. Am. Chem. Soc.* **2000**, *122*, 1092–1097. (c) Bakac, A. *Inorg. Chem.* **2010**, *49*, 3584–3593.
- ¹⁰⁵ Levina, A.; Lay, P. A. *Coord. Chem. Rev.* **2005**, *249*, 281–298.
- ¹⁰⁶ (a) King, A. R.; Hennessy, E. T.; Betley, T. A. *J. Am. Chem. Soc.* **2011**, *133*, 4917–4923. (b) Cowley, R. E.; Eckert, N. A.; Vaddadi, S.; Figg, T. M.; Cundari, T. R.; Holland, P. L. *J. Am. Chem. Soc.* **2011**, *133*, 9796–9811. (c) Bowman, A. C.; Milsman, C.; Bill, E.; Turner, Z. R.; Lobkovsky, E.; DeBeer, S.; Wieghart, K.; Chirik, P. J. *J. Am. Chem. Soc.* **2011**, *133*, 17353–17369.
- ¹⁰⁷ Dzik, W. I.; Vlugt, J. I. v. d.; Reek, J. N. H.; de Bruin, B. *Angew. Chem. Int. Ed.* **2011**, *50*, 3356–3358.
- ¹⁰⁸ Lu, A.; Zhang, X. P. *Chem. Soc. Rev.* **2011**, *40*, 1899–1909.
- ¹⁰⁹ (a) Knijnenburg, Q.; Gambarotta, S.; Budzelaar, P. H. M. *Dalton Trans.* **2006**, 5442–5448. (b) Zhu, D.; Thapa, I.; Korobkov, I.; Gambarotta, S.; Budzelaar, P. H. M. *Inorg. Chem.* **2011**, *50*, 9879–9887.
- ¹¹⁰ (a) Yandulov, D. V.; Schrock, R. R. *Science* **2003**, *301*, 76–78. (b) Schrock, R. R. *Acc. Chem. Res.* **2005**, *38*, 955–962. (c) Yandulov, D. V.; Schrock, R. R. *Inorg. Chem.* **2005**, *44*, 1103–1117 [erratum p 5542]. (d) Byrnes, M. J.; Dai, X.; Schrock, R. R.; Hock, A. S.; Müller,

- P. Organometallics* **2005**, *24*, 4437–4450. (e) Smythe, N. C.; Schrock, R. R.; Müller, P.; Weare, W. W. *Inorg. Chem.* **2006**, *45*, 7111–7118.
- ¹¹¹ Kenward, A. L.; Ross, J. A.; Piers, W. E.; Parvez, M. *Organometallics* **2009**, *28*, 3625–3628 [erratum p 4898].
- ¹¹² (a) Hiyama, T.; Sawahata, M.; Obayashi, M. *Chem. Lett.* **1983**, 1237–1238. (b) Estévez, R. E.; Justicia, J.; Bazdi, B.; Fuentes, N.; Paradas, M.; Choquesillo-Lazarte, D.; García-Ruiz, J. M.; Robles, R.; Gansäuer, A.; Cuerva, J. M.; Oltra, J. E. *Chem.–Eur. J.* **2009**, *15*, 2774–2791.
- ¹¹³ Monillas, W. H.; Yap, G. P. A.; Theopold, K. H. *Inorg. Chim. Acta* **2011**, *369*, 103–119.
- ¹¹⁴ Dai, X.; Kapoor, P.; Warren, T. H. *J. Am. Chem. Soc.* **2004**, *126*, 4798–4799.
- ¹¹⁵ Lee, J.; Chen, L.; West, A. H.; Richter-Addo, G. B. *Chem. Rev.* **2002**, *102*, 1019–1065.
- ¹¹⁶ Tomson, N. C.; Labios, L. A.; Weyhermüller, T.; Figueroa, J. S.; Wieghardt, K. *Inorg. Chem.* **2011**, *50*, 5763–5776.
- ¹¹⁷ Brown, J. L.; Wu, G.; Hayton, T. W. *J. Am. Chem. Soc.* **2010**, *132*, 7248–7249, and references therein.
- ¹¹⁸ Suzuki, H.; Takiguchi, T.; Kawasaki, Y. *Bull. Chem. Soc. Jpn.* **1978**, *51*, 1764–1767.
- ¹¹⁹ Voronkov, M. G.; Boyarkina, E. V.; Gebel', I. A.; Albanov, A. I.; Basenko, S. V. *Russ. J. Gen. Chem.* **2005**, *75*, 1927–1929.
- ¹²⁰ Matyjaszewski, K.; Woodworth, B. E. *Macromolecules* **1998**, *31*, 4718–4723.
- ¹²¹ (a) Le Grogne, E.; Claverie, J.; Poli, R. *J. Am. Chem. Soc.* **2001**, *123*, 9513–9524. (b) Braunecker, W. A.; Itami, Y.; Matyjaszewski, K. *Macromolecules* **2005**, *38*, 9402–9404. (c) Braunecker, W. A.; Brown, W. C.; Morelli, B.; Tang, W.; Poli, R.; Matyjaszewski, K. *Macromolecules* **2007**, *40*, 8576–8585.
- ¹²² Satoh, K.; Kamigaito, M. *Chem. Rev.* **2009**, *109*, 5120–5156.
- ¹²³ Debuigne, A.; Poli, R.; Jérôme, C.; Jérôme, R.; Detrembleur, C. *Prog. Polym. Sci.* **2009**, *34*, 211–239.
- ¹²⁴ Lu, Z.; Fryd, M.; Wayland, B. B. *Macromolecules* **2004**, *37*, 2686–2687.
- ¹²⁵ Allan, L. E. N.; Perry, M. R.; Shaver, M. P. *Prog. Polym. Sci.* **2012**, *37*, 127–156.
- ¹²⁶ (a) Wayland, B. B.; Poszmik, G.; Mukerjee, S. *J. Am. Chem. Soc.* **1994**, *116*, 7943–7944. (b) Arvanatitopoulos, L. D.; Greuel, M. P.; Harwood, H. J. *Polym. Prep.* **1994**, *35*, 549–550.
- ¹²⁷ Fischer, H.; Radom, L. *Angew. Chem., Int. Ed.* **2001**, *40*, 1340–1371.
- ¹²⁸ Chen, E. Y.-X. *Chem. Rev.* **2009**, *109*, 5157–5214.

- ¹²⁹ (a) Williams, B. S.; Leatherman, M. D.; White, P. S.; Brookhart, M. *J. Am. Chem. Soc.* **2005**, *127*, 5132–5146. (b) Berkefeld, A.; Drexler, M.; Möller, H. M.; Mecking, S. *J. Am. Chem. Soc.* **2009**, *131*, 12613–12622.
- ¹³⁰ (a) Poli, R. *Chem. Rev.* **1996**, *96*, 2135–2204. (b) Fetting, J. C.; Mattamana, S. P.; Poli, R.; Rogers, R. D. *Organometallics* **1996**, *15*, 4211–4222. (c) Mattamana, S. P.; Poli, R. *Organometallics* **1997**, *16*, 2427–2433.
- ¹³¹ de Bruin, B.; Dzik, W. I.; Li, S.; Wayland, B. B. *Chem.–Eur. J.* **2009**, *15*, 4312–4320.
- ¹³² Champouret, Y.; MacLeod, K. C.; Smith, K. M.; Patrick, B. O.; Poli, R. *Organometallics* **2010**, *29*, 3125–3132.
- ¹³³ Shaver, M. P.; Hanhan, M. E.; Jones, M. R. *Chem. Commun.* **2010**, *46*, 2127–2129.
- ¹³⁴ Zakrzewski, J. *Chromatographia* **2004**, *59*, 775–777.
- ¹³⁵ (a) Ueno, Y.; Chino, K.; Watanabe, M.; Moriya, O.; Okawara, M. *J. Am. Chem. Soc.* **1982**, *104*, 5564–5566. (b) Stork, G.; Mook, R., Jr.; Biller, S. A.; Rychnovsky, S. D. *J. Am. Chem. Soc.* **1983**, *105*, 3741–3742.
- ¹³⁶ Salom-Roig, X. J.; Dénès, F.; Renaud, P. *Synthesis* **2004**, 1903–1928.
- ¹³⁷ Vaupel, A.; Knochel, P. *J. Org. Chem.* **1996**, *61*, 5743–5753.
- ¹³⁸ (a) Wakabayashi, K.; Yorimitsu, H.; Oshima, K. *J. Am. Chem. Soc.* **2001**, *123*, 5374–5375. (b) Zhou, L.; Hirao, T. *J. Org. Chem.* **2003**, *68*, 1633–1635. (c) Ohmiya, H.; Yorimitsu, H.; Oshima, K. *J. Am. Chem. Soc.* **2006**, *128*, 1886–1889. (d) Someya, H.; Kondoh, A.; Sato, A.; Ohmiya, H.; Yorimitsu, H.; Oshima, K. *Synlett* **2006**, 3061–3064. (e) Fürstner, A.; Martin, R.; Krause, H.; Seidel, G.; Goddard, R.; Lehmann, C. W. *J. Am. Chem. Soc.* **2008**, *130*, 8773–8787.
- ¹³⁹ (a) Fujita, K.; Nakamura, T.; Yorimitsu, H.; Oshima, K. *J. Am. Chem. Soc.* **2001**, *123*, 3137–3138. (b) Fujita, K.; Yorimitsu, H.; Oshima, K. *Synlett* **2002**, 337–339. (c) Fujita, K.; Yorimitsu, H.; Oshima, K. *Bull. Chem. Soc. Jpn.* **2004**, *77*, 1727–1736. (d) Fujita, K.; Yorimitsu, H.; Oshima, K. *Chem. Rec.* **2004**, *4*, 110–119.
- ¹⁴⁰ (a) Gansäuer, A.; Fleckhaus, A.; Lafont, M. A.; Okkel, A.; Kotsis, K.; Anoop, A.; Neese, F. *J. Am. Chem. Soc.* **2009**, *131*, 16989–16999. (b) Gansäuer, A.; Shi, L.; Otte, M. *J. Am. Chem. Soc.* **2010**, *132*, 11858–11859.
- ¹⁴¹ Giese, B.; Erdmann, P.; Göbel, T.; Springer, R. *Tetrahedron Lett.* **1992**, *33*, 4545–4548.

- ¹⁴² (a) Martin, R.; Buchwald, S. L. *Acc. Chem. Res.* **2008**, *41*, 1461–1473. (b) Fu, G. C. *Acc. Chem. Res.* **2008**, *41*, 1555–1564. (c) Kliegman, S.; McNeill, K. *Dalton Trans.* **2008**, 4191–4201. (d) Zhu, D.; Budzelaar, P. H. M. *Organometallics* **2010**, *29*, 5759–5761.
- ¹⁴³ Liberto, C. M. B.Sc. Thesis, University of British Columbia Okanagan, 2011.
- ¹⁴⁴ (a) Lei, A.; Liu, W.; Liu, C.; Chen, M. *Dalton Trans.* **2010**, 39, 10352–10361. (b) Liu, W.; Cao, H.; Zhang, H.; Zhang, H.; Chung, K. H.; He, C.; Wang, H.; Kwong, F. Y.; Lei, A. *J. Am. Chem. Soc.* **2010**, *132*, 16737–16740.
- ¹⁴⁵ Shrestha, R.; Weix, D. J. *Org. Lett.* **2011**, *13*, 2766–2769.
- ¹⁴⁶ Surry, D. S.; Buchwald, S. L. *Chem. Sci.* **2011**, *2*, 27–50, and references cited therein.
- ¹⁴⁷ Cossairt, B. M.; Piro, N. A.; Cummins, C. C. *Chem. Rev.* **2010**, *110*, 4164–4177.
- ¹⁴⁸ Sato, A.; Yorimitsu, H.; Oshima, K. *J. Am. Chem. Soc.* **2006**, *128*, 4240–4241.
- ¹⁴⁹ Cossairt, B. M.; Cummins, C. C. *New J. Chem.* **2010**, *34*, 1533–1536.
- ¹⁵⁰ Vaillard, S. E.; Mück-Lichtenfeld, C.; Grimme, S.; Studer, A. *Angew. Chem., Int. Ed.* **2007**, *46*, 6533–6536.
- ¹⁵¹ Godfrey, S. M.; McAuliffe, C. A.; Pritchard, R. G. *J. Chem. Soc., Dalton Trans.* **1993**, 371–375.
- ¹⁵² Heppekausen, J.; Stade, R.; Goddard, R.; Fürstner, A. *J. Am. Chem. Soc.* **2010**, *132*, 11045–11057.
- ¹⁵³ Pandey, G.; Rao, K. S. S. P.; Palit, D. K.; Mittal, J. P. *J. Org. Chem.* **1998**, *63*, 3968–3978.
- ¹⁵⁴ Takami, K.; Mikami, S.; Yorimitsu, H.; Shinokubo, H.; Oshima, K. *Tetrahedron* **2003**, *59*, 6627–6635.
- ¹⁵⁵ Ueno, Y.; Moriya, O.; Chino, K.; Watanebe, M.; Okawara, M. *J. Chem. Soc., Perkin Trans. I* **1986**, 1351–1356.
- ¹⁵⁶ Yanada, R.; Koh, Y.; Nishimori, N.; Matsumura, A.; Obika, S.; Mitsuya, H.; Fujii, N.; Takemoto, Y. *J. Org. Chem.* **2004**, *69*, 2417–2422.
- ¹⁵⁷ Lee, H.; Jordan, R. F. *J. Am. Chem. Soc.* **2005**, *127*, 9384–9385.
- ¹⁵⁸ Agapie, T.; Labinger, J. A.; Bercaw, J. E. *J. Am. Chem. Soc.* **2007**, *129*, 14281–14295.
- ¹⁵⁹ (a) Betz, P.; Döhring, A.; Emrich, R.; Goddard, R.; Jolly, P. W.; Krüger, C.; Romão, C. C.; Schönfelder, K. U.; Tsay, Y.-H. *Polyhedron* **1992**, *12*, 2651–2662. (b) Döhring, A.; Emrich, R.; Goddard, R.; Jolly, P. W.; Krüger, C. *Polyhedron* **1992**, *12*, 2671–2680.
- ¹⁶⁰ Jonas, K. *Angew. Chem., Int. Ed. Engl.* **1985**, *24*, 295–311.

- ¹⁶¹ (a) Whitesides, G. M.; Ehmman, W. J. *J. Am. Chem. Soc.* **1970**, *92*, 5625–5640. (b) Uhlig, E. *Organometallics* **1993**, *12*, 4751–4756. (c) Jolly, P. W. *Acc. Chem. Res.* **1996**, *29*, 544–551. (d) Seyferth, D. *Organometallics* **2002**, *21*, 1520–1530. (e) Seyferth, D. *Organometallics* **2002**, *21*, 2800–2820.
- ¹⁶² Smith, K. M. *Curr. Org. Chem.* **2006**, *10*, 955–963.
- ¹⁶³ Angermund, K.; Claus, K. H.; Goddard, R.; Krüger, C. *Angew. Chem., Int. Ed. Engl.* **1985**, *24*, 237–247.
- ¹⁶⁴ Gallant, A. J.; Smith, K. M.; Patrick, B. O. *Chem. Commun.* **2002**, 2914–2915.
- ¹⁶⁵ Edema, J. J. H.; Gambarotta, S.; Meetsma, A.; Spek, A. L. *Organometallics* **1992**, *11*, 2452–2457.
- ¹⁶⁶ (a) Dickieson, L. S. B.Sc. Thesis, University of Prince Edward Island, 2004. (b) Corcoran, L. D. B.Sc. Thesis, University of Prince Edward Island, 2006.
- ¹⁶⁷ (a) Noh, S. K.; Heintz, R. A.; Janiak, C.; Sendlinger, S. C.; Theopold, K. H. *Angew. Chem., Int. Ed. Engl.* **1990**, *29*, 775–777. (b) Heintz, R. A.; Leelasubsharoen, S.; Liable-Sands, L. M.; Rheingold, A. L.; Theopold, K. H. *Organometallics* **1998**, *17*, 5477–5485. (c) Licciulli, S.; Albahily, K.; Fomitcheva, V.; Korobkov, I.; Gambarotta, S.; Duchateau, R. *Angew. Chem., Int. Ed.* **2011**, *50*, 2346–2349.
- ¹⁶⁸ (a) Bhandari, G.; Rheingold, A. L.; Theopold, K. H. *Chem. Eur. J.* **1995**, *1*, 199–203. (b) Mani, G.; Gabbai, F. P. *Angew. Chem., Int. Ed.* **2004**, *43*, 2263–2266.
- ¹⁶⁹ Golstein, S.; Meyerstein, D. *Acc. Chem. Res.* **1999**, *32*, 547–550.
- ¹⁷⁰ Lanci, M. P.; Remy, M. S.; Kaminsky, W.; Mayer, J. M.; Sanford, M. S. *J. Am. Chem. Soc.* **2009**, *131*, 15618–15620.
- ¹⁷¹ Higgs, A. T.; Zinn, P. J.; Simmons, S. J.; Sanford, M. S. *Organometallics* **2009**, *28*, 6142–6144.
- ¹⁷² (a) Bräunlein, B.; Köhler, F. H.; Strauß, W.; Zeh, H. *Z. Naturforsch. B.* **1995**, *50*, 1739–1749. (b) Voges, M. H.; Rømming, C.; Tilset, M. *Organometallics* **1999**, *18*, 529–533. (c) Döhring, A.; Göhre, J.; Jolly, P. W.; Kryger, B.; Rust, J.; Verhovnik, G. P. *J. Organometallics* **2000**, *19*, 388–402. (d) Zhou, W.; Therrien, J. A.; Wence, D. L. K.; Yallits, E. N.; Conway, J. L.; Patrick, B. O.; Smith, K. M. *Dalton Trans.* **2011**, *40*, 337–339.
- ¹⁷³ Manzer, L. E. *J. Am. Chem. Soc.* **1978**, *100*, 8068–8073.

Appendices

Appendix A. Supplementary X-ray Data

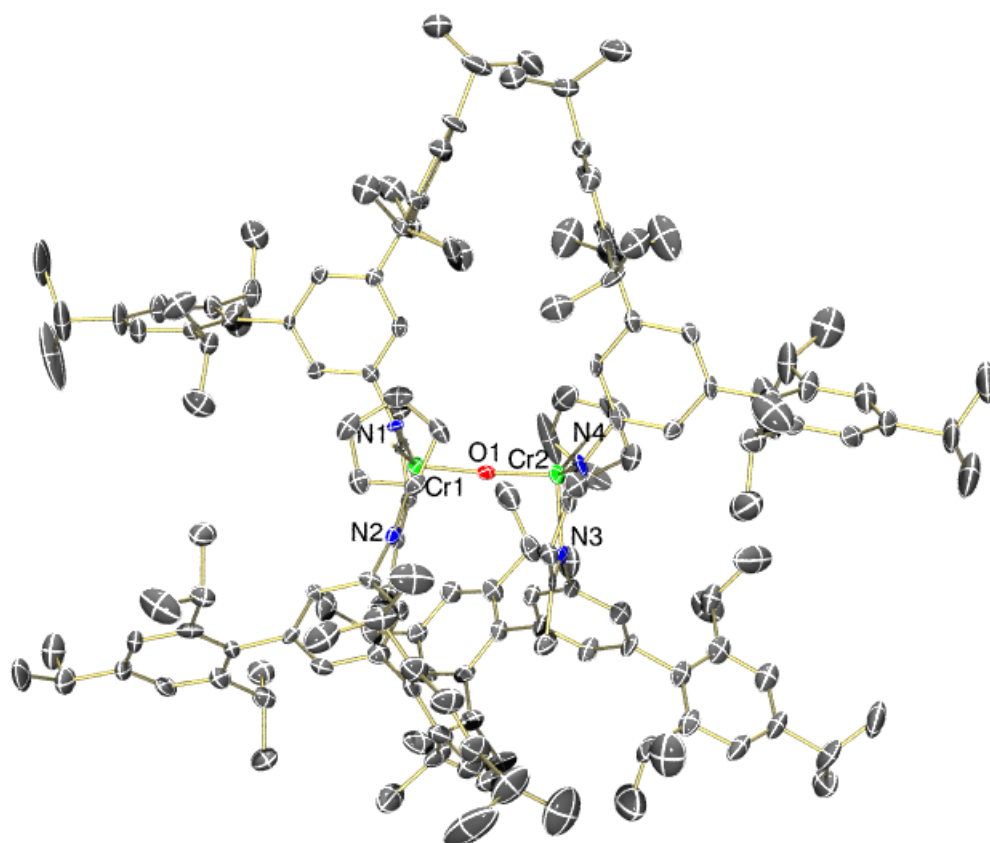


Figure A.1. Thermal ellipsoid diagram (50 %) of **3.11**. All H atoms are omitted for clarity.

Table A.1. Crystal data and refinement parameters for X-ray structures of **2.1a**, **2.2a**, **2.3**, **2.3a**, **2.3b**, and **2.4**.

	2.1a	2.2a	2.3·½C₆H₁₄	2.3a	2.3b	2.4
Formula	C ₂₈ H ₃₄ N ₂ Cr	C ₂₉ H ₃₇ N ₂ Cr	C ₂₉ H ₃₇ N ₂ CrCl	C ₂₈ H ₃₄ N ₂ CrCl	C ₃₀ H ₃₈ N ₂ CrCl	C ₅₆ H ₆₀ N ₄ O ₄ Cr ₂
Formula Weight	450.57	465.61	501.06	486.02	514.07	957.11
Crystal Color, Habit	red, plate	black, plate	black, plate	black, tablet	green, needle	black, irregular
Crystal Dimensions, mm	0.10 x 0.25 x 0.25	0.05 x 0.30 x 0.50	0.12 x 0.26 x 0.45	0.20 x 0.40 x 0.44	0.04 x 0.15 x 0.30	0.15 x 0.43 x 0.56
Crystal System	monoclinic	triclinic	monoclinic	orthorhombic	monoclinic	triclinic
Space Group	<i>C</i> 2/ <i>c</i>	<i>P</i> -1	<i>P</i> 2 ₁ / <i>c</i>	<i>P</i> <i>ca</i> 2 ₁	<i>P</i> -1	<i>P</i> -1
<i>a</i> , Å	16.434(2)	9.4802(10)	13.1109(3)	14.3818(10)	8.0490(18)	10.6263(7)
<i>b</i> , Å	9.3651(11)	11.9897(14)	15.29995(3)	15.2520(10)	11.214(3)	13.4249(9)
<i>c</i> , Å	16.498(2)	12.2729(14)	14.4144(3)	25.8696(19)	15.462(4)	20.7776(13)
α , °	90	70.025(5)	90	90	81.291(7)	104.246(3)
β , °	101.508(4)	79.696(5)	112.818(10)	90	86.346(8)	95.720(3)
γ , °	90	77.347(5)	90	90	74.509(8)	111.945(3)
<i>V</i> , Å ³	2488.2(5)	1271.0(2)	2665.11(10)	5674.5(7)	1329.0(6)	2604.4(3)
<i>Z</i>	4	2	4	8	2	4
D _{calc} , g/cm ³	1.203	1.217	1.249	1.138	1.285	1.220
F ₀₀₀	960	498	1064	2056	546	1008
μ (MoK α), cm ⁻¹	4.76	4.68	5.48	5.13	5.52	4.65
Data Images (no., <i>t</i> /s)	1406, 7	1694, 7	826, 10	1157, 5	941, 20	1700, 10
2 θ _{max}	56.1°	55.0°	55.1°	56.0°	45.6°	56.0°
Reflections measrd	12809	21914	18008	57907	10278	39655
Unique reflcn, R _{int}	2989, 0.034	5785, 0.026	6149, 0.030	13222, 0.042	3437, 0.060	12339, 0.035
Absorption, T _{min} , T _{max}	0.869, 0.954	0.894, 0.977	0.849, 0.936	0.809, 0.902	0.771, 0.978	0.825, 0.933
Obsrvd data (<i>I</i> >2.00 σ (<i>I</i>))	2536	5022	4954	10409	7267	9046
No. parameters	146	296	345	593	317	604
R1, wR2 (F ² , all data)	0.061, 0.136	0.043, 0.094	0.053, 0.113	0.054, 0.090	0.090, 0.144	0.066, 0.126
R1, wR2 (F, <i>I</i> >2.00 σ (<i>I</i>))	0.051, 0.131	0.035, 0.088	0.040, 0.105	0.038, 0.084	0.058, 0.130	0.044, 0.118
Goodness of Fit	1.08	1.06	1.06	1.00	1.04	1.07
Max, Min peak, e ⁻ /Å ³	0.69, -0.36	0.37, -0.30	0.67, -0.49	0.29, -0.32	0.49, -0.48	0.53, -0.45

Table A.2. Crystal data and refinement parameters for X-ray structures of **2.6a**, **2.6b**, **2.7a**, **2.7b**, **2.7c**, and **2.8**.

	2.6a	2.6b	2.7a	2.7b	2.7c	2.8
Formula	C ₃₅ H ₄₁ N ₂ O ₃ SCr	C ₃₇ H ₄₅ N ₂ O ₃ SCr	C ₃₂ H ₄₅ N ₂ SiCr	C ₃₄ H ₄₉ N ₂ SiCr	C ₃₈ H ₅₇ N ₂ SiCr	C ₃₁ H ₃₇ N ₂ Cr
Formula Weight	621.76	649.81	537.79	565.84	621.95	489.63
Crystal Color, Habit	black, irregular	black, prism	black, plate	black, irregular	black, tablet	black, irregular
Crystal Dimensions, mm	0.15 × 0.40 × 0.50	0.27 × 0.35 × 0.55	0.08 × 0.22 × 0.40	0.15 × 0.30 × 0.40	0.15 × 0.55 × 0.55	0.22 × 0.22 × 0.30
Crystal System	monoclinic	triclinic	triclinic	monoclinic	monoclinic	triclinic
Space Group	<i>P</i> 2 ₁ / <i>c</i>	<i>P</i> -1	<i>P</i> -1	<i>P</i> 2 ₁ / <i>n</i>	<i>P</i> 2 ₁	<i>P</i> -1
<i>a</i> , Å	11.3105(7)	10.6913(17)	10.3499(10)	10.8474(11)	16.7572(4)	11.2229(11)
<i>b</i> , Å	16.4180(10)	12.361(2)	11.3640(11)	15.7337(14)	10.4447(2)	14.2255(15)
<i>c</i> , Å	17.7673(11)	13.550(2)	14.9073(15)	18.6138(19)	19.8127(4)	18.197(2)
α , °	90	70.630(5)	100.740(5)	90	90	110.825(3)
β , °	106.560(2)	84.409(6)	104.780(5)	90.495(4)	90.8347(14)	94.326(4)
γ , °	90	82.845(6)	112.521(5)	90	90	95.051(4)
<i>V</i> , Å ³	3162.5(3)	1673.2(5)	1484.7(3)	6848.2(2)	3467.3(1)	6848.2(2)
<i>Z</i>	4	2	2	4	4	4
D _{calc} , g/cm ³	1.306	1.290	1.203	1.183	1.191	1.210
F ₀₀₀	1316	690	578	1220	1348	1044
μ (MoK α), cm ⁻¹	4.65	4.43	4.48	4.22	3.92	4.46
Data Images (no., <i>t</i> /s)	1270, 5	2008, 5	1820, 20	1191, 5	1794, 5	1094, 20
2 θ _{max}	55.8°	55.9°	55.0°	56.1°	56.1°	46.8°
Reflections measrd	32823	35143	24489	42491	63412	26521
Unique reflcn, <i>R</i> _{int}	7544, 0.025	7961, 0.024	6741, 0.033	7688, 0.031	16785, 0.027	7653, 0.039
Absorption, <i>T</i> _{min} , <i>T</i> _{max}	0.819, 0.933	0.801, 0.887	0.778, 0.965	0.884, 0.939	0.844, 0.943	0.785, 0.907
Obsrvd data (<i>I</i> > 2.00 σ (<i>I</i>))	6248	7079	5583	6192	15651	5746
No. parameters	388	404	336	366	759	645
<i>R</i> ₁ , <i>wR</i> ₂ (<i>F</i> ² , all data)	0.049, 0.103	0.038, 0.090	0.051, 0.114	0.049, 0.099	0.040, 0.093	0.084, 0.169
<i>R</i> ₁ , <i>wR</i> ₂ (<i>F</i> , <i>I</i> > 2.00 σ (<i>I</i>))	0.038, 0.096	0.032, 0.085	0.039, 0.106	0.036, 0.091	0.036, 0.090	0.058, 0.152
Goodness of Fit	1.04	1.02	1.04	1.04	1.02	1.07
Max, Min peak, e ⁻ /Å ³	0.89, -0.68	0.40, -0.36	0.45, -0.53	0.33, -0.31	0.33, -0.32	1.00, -0.50

Table A.3. Crystal data and refinement parameters for X-ray structures of **2.10**, **2.10c**, **2.11**, **2.11a**, **2.13**, and **2.14a**.

	2.10	2.10c	2.11	2.11a	2.13	2.14a
Formula	C ₃₀ H ₃₉ N ₂ Cr	C ₃₈ H ₅₅ N ₂ Cr	C ₃₁ H ₄₁ N ₂ Cr	C ₃₃ H ₄₅ N ₂ Cr	C ₂₈ H ₃₂ N ₃ Cr	C ₃₅ H ₄₁ N ₂ Cr
Formula Weight	479.63	591.84	493.66	521.71	462.57	541.70
Crystal Color, Habit	black, plate	black, irregular	black, tablet	black, irregular	black, irregular	black, irregular
Crystal Dimensions, mm	0.08 × 0.36 × 0.42	0.18 × 0.23 × 0.25	0.22 × 0.38 × 0.50	0.15 × 0.20 × 0.33	0.10 × 0.25 × 0.40	0.12 × 0.15 × 0.25
Crystal System	orthorhombic	orthorhombic	orthorhombic	triclinic	triclinic	monoclinic
Space Group	<i>P na</i> 2 ₁	<i>P na</i> 2 ₁	<i>P na</i> 2 ₁	<i>P</i> -1	<i>P</i> -1	<i>C c</i>
<i>a</i> , Å	14.1760(13)	32.4301(13)	14.1980(4)	9.7794(5)	9.1543(7)	16.038(5)
<i>b</i> , Å	13.2281(12)	20.3980(9)	13.7783(5)	11.7808(6)	11.2955(10)	16.383(5)
<i>c</i> , Å	28.386(3)	10.0444(4)	28.1736(13)	14.9206(7)	13.0131(11)	11.162(4)
α , °	90	90	90	106.794(2)	114.359(5)	90
β , °	90	90	90	98.093(2)	95.866(5)	100.889(14)
γ , °	90	90	90	112.487(2)	90.008(5)	90
<i>V</i> , Å ³	5322.9(8)	6644.5(5)	5511.4(4)	1457.90(13)	1218.05(18)	2879.9(15)
<i>Z</i>	8	8	8	2	2	4
D _{calc} , g/cm ³	1.197	1.183	1.190	1.188	1.261	1.249
F ₀₀₀	2056	2568	2120	562	490	1156
μ (MoK α), cm ⁻¹	4.49	3.72	4.36	4.15	4.89	4.23
Data Images (no., <i>t</i> /s)	1609, 30	2475, 20	1073, 10	949, 20	2348, 7	1739, 10
2 θ _{max}	50.6°	60.3°	56.0°	50.8°	55.0°	56.0°
Reflections measrd	52107	199672	55696	14709	23170	25477
Unique reflcn, <i>R</i> _{int}	9541, 0.050	19577, 0.052	10264, 0.049	5213, 0.026	5480, 0.041	6301, 0.030
Absorption, <i>T</i> _{min} , <i>T</i> _{max}	0.800, 0.965	0.852, 0.935	0.746, 0.909	0.880, 0.940	0.794, 0.952	0.873, 0.951
Obsrvd data (<i>I</i> > 2.00 σ (<i>I</i>))	8462	17183	8220	4297	4058	5823
No. parameters	612	764	631	336	295	352
<i>R</i> 1, <i>wR</i> 2 (<i>F</i> ² , all data)	0.067, 0.158	0.045, 0.084	0.062, 0.111	0.050, 0.104	0.068, 0.103	0.036, 0.078
<i>R</i> 1, <i>wR</i> 2 (<i>F</i> , <i>I</i> > 2.00 σ (<i>I</i>))	0.058, 0.152	0.033, 0.078	0.040, 0.097	0.038, 0.097	0.041, 0.090	0.031, 0.075
Goodness of Fit	1.14	1.06	1.06	1.05	1.03	1.03
Max, Min peak, e ⁻ /Å ³	1.47, -0.63	0.38, -0.47	0.49, -0.71	0.55, -0.35	0.53, -0.35	0.25, -0.23

Table A.4. Crystal data and refinement parameters for X-ray structures of **2.14b**, **2.14c**, **2.15**, **2.16**, **2.17**, and **2.18**.

	2.14b	2.14c	2.15	2.16	2.17	2.18
Formula	C ₃₇ H ₄₅ N ₂ Cr	C ₄₁ H ₅₃ N ₂ Cr	C ₃₂ H ₃₅ N ₂ Cr	C ₃₀ H ₃₇ N ₂ Cr	C ₂₈ H ₃₁ N ₂ Cr	C ₃₄ H ₃₉ N ₂ Cr
Formula Weight	569.75	625.85	499.62	477.62	447.55	521.67
Crystal Color, Habit	black, prism	black, prism	black, rod	black, irregular	black, plate	black, irregular
Crystal Dimensions, mm	0.30 × 0.35 × 0.40	0.25 × 0.30 × 0.30	0.28 × 0.36 × 0.50	0.12 × 0.18 × 0.25	0.03 × 0.24 × 0.55	0.12 × 0.15 × 0.15
Crystal System	monoclinic	monoclinic	triclinic	orthorhombic	monoclinic	monoclinic
Space Group	<i>P</i> 2 ₁ / <i>m</i>	<i>P</i> 2 ₁ / <i>c</i>	<i>P</i> -1	<i>P</i> na2 ₁	<i>P</i> 2 ₁ / <i>n</i>	<i>P</i> 2 ₁ / <i>n</i>
<i>a</i> , Å	8.6214(14)	19.3249(5)	9.3624(11)	13.9048(3)	7.853(5)	11.1582(4)
<i>b</i> , Å	19.146(3)	9.0312(2)	12.2408(14)	13.1968(3)	13.783(5)	16.9822(7)
<i>c</i> , Å	9.5494(15)	20.0983(5)	12.6542(3)	28.0798(6)	22.070(5)	15.2142(6)
α , °	90	90	65.485(3)	90	90	90
β , °	102.381(7)	98.6128(10)	89.588(3)	90	90.800(5)	101.161(2)
γ , °	90	90	87.589(3)	90	90	90
<i>V</i> , Å ³	1808.1(3)	3468.1(2)	1318.2(3)	5152.6(2)	2388.6(18)	2828.4(2)
<i>Z</i>	2	4	2	8	4	4
D _{calc} , g/cm ³	1.229	1.199	1.259	1.231	1.245	1.239
F ₀₀₀	610	1348	530	2040	948	1124
μ (MoK α), cm ⁻¹	3.99	3.60	4.57	4.64	4.96	4.29
Data Images (no., <i>t</i> /s)	1081, 10	1570, 10	1320, 15	739, 20	1178, 10	856, 60
2 θ _{max}	56.1°	55.9°	47.6°	55.8°	45.1°	50.9°
Reflections measrd	17472	46664	10444	36839	14768	18196
Unique reflcn, R _{int}	3832, 0.023	8300, 0.023	3967, 0.028	11167, 0.074	3187, 0.073	5199, 0.055
Absorption, T _{min} , T _{max}	0.713, 0.887	0.857, 0.914	0.745, 0.880	0.822, 0.946	0.620, 0.985	0.800, 0.950
Obsrvd data (<i>I</i> >2.00 σ (<i>I</i>))	3308	7324	3429	8144	2641	3563
No. parameters	193	399	322	606	287	338
R1, wR2 (F ² , all data)	0.046, 0.103	0.037, 0.087	0.049, 0.119	0.087, 0.124	0.067, 0.112	0.105, 0.167
R1, wR2 (F, <i>I</i> >2.00 σ (<i>I</i>))	0.037, 0.098	0.032, 0.084	0.040, 0.112	0.051, 0.109	0.047, 0.100	0.065, 0.147
Goodness of Fit	1.05	1.04	1.06	1.01	1.06	1.08
Max, Min peak, e ⁻ /Å ³	0.35, -0.40	0.36, -0.44	0.58, -0.46	0.39, -0.33	0.31, -0.43	0.81, -0.50

Table A.5. Crystal data and refinement parameters for X-ray structures of **2.19**, **3.2**, **3.4**, **3.5**, and **3.6**.

	2.19	3.2	3.4	3.5	3.6
Formula	C ₃₂ H ₃₅ N ₂ SCr	C ₂₆ H ₃₁ N ₂ OCr	C ₂₈ H ₃₃ N ₂ O ₂ Cr	C ₂₆ H ₃₀ H ₂ Cr(C ₈ H ₇ O) _{.899(I).101}	C ₃₀ H ₃₉ N ₂ OCr
Formula Weight	531.68	439.53	481.56	542.52	495.63
Crystal Color, Habit	black, irregular	black, prism	black, irregular	black, irregular	black, prism
Crystal Dimensions, mm	0.12 × 0.22 × 0.46	0.20 × 0.30 × 0.35	0.22 × 0.25 × 0.30	0.12 × 0.22 × 0.37	0.135 × 0.15 × 0.16
Crystal System	monoclinic	monoclinic	monoclinic	triclinic	monoclinic
Space Group	<i>P</i> 2 ₁ / <i>c</i>	<i>P</i> 2 ₁ / <i>n</i>	<i>P</i> 2 ₁ / <i>n</i>	<i>P</i> -1	<i>P</i> 2 ₁ / <i>n</i>
<i>a</i> , Å	9.8834(13)	12.0157(3)	8.2143(12)	9.260(3)	16.302(3)
<i>b</i> , Å	15.9186(19)	15.0102(4)	13.597(2)	12.666(4)	9.0161(16)
<i>c</i> , Å	17.127(2)	13.2704(3)	22.030(3)	13.350(5)	18.449(3)
α , °	90	90	90	67.237(10)	90
β , °	92.837(3)	109.716(1)	90.978(6)	84.384(10)	99.280(4)
γ , °	90	90	90	85.032(10)	90
<i>V</i> , Å ³	2691.2(6)	2253.1(1)	2460.2(6)	1390(1)	2676.2(8)
<i>Z</i>	4	4	4	2	4
<i>D</i> _{calc} , g/cm ³	1.312	1.296	1.300	1.265	1.230
<i>F</i> ₀₀₀	1124	932	1020	561	1060
μ (MoK α), cm ⁻¹	5.26	5.27	4.92	4.40	4.52
Data Images (no., <i>t</i> /s)	936, 5	1067, 10	973, 60	665, 11	967, 60
2 θ _{max}	56.1°	60.1°	45.0°	45.5°	48.3°
Reflections measrd	6487	25873	42299	13751	15747
Unique reflcn, <i>R</i> _{int}	6487, 0.064	6591, 0.027	3174, 0.088	3429, 0.045	4261, 0.041
Absorption, <i>T</i> _{min} , <i>T</i> _{max}	0.629, 0.940	0.821, 0.900	0.608, 0.897	0.750, 0.954	0.866, 0.941
Obsrvd data (<i>I</i> > 2.00 σ (<i>I</i>))	5118	5605	2435	2517	3313
No. parameters	329	357	306	353	312
<i>R</i> ₁ , w <i>R</i> ₂ (<i>F</i> ² , all data)	0.059, 0.125	0.043, 0.100	0.101, 0.194	0.086, 0.118	0.066, 0.112
<i>R</i> ₁ , w <i>R</i> ₂ (<i>F</i> , <i>I</i> > 2.00 σ (<i>I</i>))	0.045, 0.118	0.034, 0.094	0.072, 0.177	0.052, 0.104	0.044, 0.102
Goodness of Fit	1.08	1.04	1.13	1.08	1.06
Max, Min peak, e ⁻ /Å ³	0.46, -0.42	0.47, -0.33	0.61, -0.48	0.45, -0.50	0.34, -0.35

Table A.6. Crystal data and refinement parameters for X-ray structures of **3.8**, **3.10**, **3.11**, **3.12**, and **4.3**.

	3.9	3.10	3.11	3.12	4.3
Formula	C ₂₆ H ₃₀ N ₂ CrF	C ₆₀ H ₇₆ N ₄ O ₂ Cr ₂	C ₁₆₄ H ₂₂₀ N ₄ O ₂ Cr ₂	C ₃₂ H ₃₅ N ₃ CrO	C ₃₄ H ₄₃ O ₃ N ₂ Cr
Formula Weight	441.52	989.25	2367.44	529.63	579.70
Crystal Color, Habit	black, irregular	black, prism	orange, prism	black, prism	black, thin
Crystal Dimensions, mm	0.18 × 0.34 × 0.52	0.10 × 0.17 × 0.25	0.125 × 0.16 × 0.22	0.06 × 0.09 × 0.16	0.075 × 0.20 × 0.25
Crystal System	monoclinic	monoclinic	monoclinic	monoclinic	monoclinic
Space Group	<i>P</i> 2 ₁ / <i>n</i>	<i>P</i> 2/ <i>c</i>	<i>P</i> 2 ₁ / <i>c</i>	<i>P</i> 2 ₁ / <i>n</i>	<i>P</i> 2 ₁ / <i>n</i>
<i>a</i> , Å	12.1594(8)	16.0439(8)	31.054(3)	9.1618(2)	13.7860(5)
<i>b</i> , Å	15.1034(12)	11.9799(5)	18.839(2)	22.4478(5)	16.4769(6)
<i>c</i> , Å	13.2572(10)	27.4399(13)	31.163(3)	13.5023(3)	26.8644(9)
α , °	90	90	90	90	90
β , °	110.146(3)	103.200(2)	111.582(2)	98.3291(11)	102.087(2)
γ , °	90	90	90	90	90
<i>V</i> , Å ³	2285.7(3)	5134.7(6)	16953(3)	2747.6(2)	5967.0(5)
<i>Z</i>	4	4	4	4	8
D _{calc} , g/cm ³	1.283	1.280	0.928	1.280	1.291
F ₀₀₀	932	2112	5152	1120	2472
μ (MoK α), cm ⁻¹	5.23	4.71	1.72	4.46	4.20
Data Images (no., <i>t</i> /s)	1028, 10	1177, 10	824, 90	964, 60	907, 15
2 θ _{max}	56.0°	60.1°	45.1°	55.0°	56.4°
Reflections measrd	26382	58708	83553	22902	52359
Unique reflcn, R _{int}	5442, 0.028	15030, 0.046	21958, 0.127	6212, 0.044	14194, 0.100
Absorption, T _{min} , T _{max}	0.839, 0.910	0.895, 0.954	0.738, 0.979	0.901, 0.974	0.755, 0.969
Obsrvd data (<i>I</i> > 2.00 σ (<i>I</i>))	4464	10647	12172	4343	8321
No. parameters	277	617	1592	398	731
R1, wR2 (F ² , all data)	0.047, 0.099	0.076, 0.122	0.145, 0.231	0.078, 0.108	0.137, 0.184
R1, wR2 (F, <i>I</i> > 2.00 σ (<i>I</i>))	0.034, 0.090	0.046, 0.108	0.085, 0.204	0.044, 0.095	0.074, 0.158
Goodness of Fit	1.04	1.02	0.949	1.01	1.02
Max, Min peak, e ⁻ /Å ³	0.37, -0.36	0.50, -0.35	0.63, -0.56	0.36, -0.35	0.89, -0.58

Table A.7. Crystal data and refinement parameters for X-ray structures of **5.2**, **6.1**, **6.2**, **6.6**, and **6.7**.

	5.2	6.1	6.2	6.6	6.7
Formula	C ₃₄ H ₄₃ N ₂ O ₂ Cr	C ₁₄ H ₁₇ NCr	C ₂₈ H ₂₇ NCr	C ₂₃ H ₂₈ NOCr	C ₂₀ H ₂₂ NSCr
Formula Weight	563.70	251.29	429.51	386.46	360.45
Crystal Color, Habit	black, prism	brown, prism	black, irregular	black, irregular	red, plate
Crystal Dimensions, mm	0.20 × 0.25 × 0.30	0.08 × 0.085 × 0.125	0.15 × 0.15 × 0.25	0.10 × 0.12 × 0.25	0.025 × 0.15 × 0.25
Crystal System	monoclinic	monoclinic	orthorhombic	monoclinic	orthorhombic
Space Group	<i>C</i> 2/ <i>c</i>	<i>P</i> 2 ₁ / <i>n</i>	<i>P</i> <i>na</i> 2 ₁	<i>P</i> 2 ₁ / <i>n</i>	<i>P</i> 2 ₁ 2 ₁ 2 ₁
<i>a</i> , Å	24.9750(6)	6.1939(12)	14.8173(5)	11.8637(5)	6.6572(1)
<i>b</i> , Å	15.3174(4)	12.771(3)	9.6377(3)	14.0753(6)	8.0888(2)
<i>c</i> , Å	15.0963(4)	15.952(3)	15.6977(6)	12.0754(5)	31.8456(7)
α , °	90	90	90	90	90
β , °	91.591(2)	99.188(5)	90	100.629(2)	90
γ , °	90	90	90	90	90
<i>V</i> , Å ³	5772.9(3)	1245.7(7)	2241.7(1)	1981.8(2)	1714.8(1)
<i>Z</i>	8	4	4	4	4
D _{calc} , g/cm ³	1.297	1.340	1.273	1.295	1.396
F ₀₀₀	2408	528	904	820	756
μ (MoK α), cm ⁻¹	4.30	8.90	5.24	5.88	7.87
Data Images (no., <i>t</i> /s)	1561, 10	1208, 10	855, 10	854, 20	2581, 10
2 θ _{max}	55.8°	60.1°	55.9°	56.2°	60.1°
Reflections measrd	39809	14230	18471	15379	51977
Unique reflcn, R _{int}	6895, 0.033	3648, 0.038	5397, 0.044	4764, 0.042	5021, 0.042
Absorption, T _{min} , T _{max}	0.815, 0.918	0.864, 0.931	0.780, 0.924	0.816, 0.943	0.899, 0.981
Obsrvd data (<i>I</i> > 2.00 σ (<i>I</i>))	5542	2934	4490	3478	4680
No. parameters	427	145	271	235	208
R1, wR2 (F ² , all data)	0.051, 0.101	0.052, 0.089	0.051, 0.077	0.078, 0.117	0.038, 0.078
R1, wR2 (F, <i>I</i> > 2.00 σ (<i>I</i>))	0.036, 0.092	0.037, 0.084	0.036, 0.070	0.048, 0.103	0.033, 0.076
Goodness of Fit	1.05	1.03	1.02	1.04	1.10
Max, Min peak, e ⁻ /Å ³	0.63, -0.37	0.99, -0.80	0.35, -0.36	1.15, -0.51	1.01, -0.38

Table A.8. Crystal data and refinement parameters for X-ray structures of **6.9**, **6.10**, and **6.11**.

	6.9	6.10	6.11
Formula	C ₂₄ H ₃₁ NCr ₂	C ₂₁ H ₂₄ NCr	C ₂₈ H ₂₇ NiCr
Formula Weight	437.50	342.41	556.41
Crystal Color, Habit	black, prism	red, plate	black, prism
Crystal Dimensions, mm	0.065 × 0.10 × 0.10	0.06 × 0.10 × 0.12	0.05 × 0.075 × 0.075
Crystal System	orthorhombic	triclinic	monoclinic
Space Group	<i>P</i> <i>na</i> 2 ₁	<i>P</i> -1	<i>P</i> 2 ₁
<i>a</i> , Å	15.4585(23)	8.6032(5)	8.866(2)
<i>b</i> , Å	9.1490(13)	9.9332(5)	14.856(3)
<i>c</i> , Å	14.4789(21)	11.8898(6)	8.982(2)
α , °	90	70.331(3)	90
β , °	90	77.289(2)	96.725(4)
γ , °	90	66.086(2)	90
<i>V</i> , Å ³	2047.7(5)	870.4(1)	1174.9(4)
<i>Z</i>	4	2	2
<i>D</i> _{calc} , g/cm ³	1.419	1.306	1.573
<i>F</i> ₀₀₀	920	362	558
μ (MoK α), cm ⁻¹	10.69	6.56	18.16
Data Images (no., <i>t</i> /s)	1081, 10	2557, 30	1028, 30
2 θ _{max}	60.2°	60.3°	59.7°
Reflections measrd	22648	18392	13181
Unique reflcn, <i>R</i> _{int}	5978, 0.054	5070, 0.025	6623, 0.039
Absorption, <i>T</i> _{min} , <i>T</i> _{max}	0.840, 0.933	0.896, 0.961	0.715, 0.913
Obsrvd data (<i>I</i> > 2.00 σ (<i>I</i>))	5118	4232	5687
No. parameters	249	209	280
<i>R</i> ₁ , <i>wR</i> ₂ (<i>F</i> ² , all data)	0.048, 0.067	0.048, 0.087	0.060, 0.107
<i>R</i> ₁ , <i>wR</i> ₂ (<i>F</i> , <i>I</i> > 2.00 σ (<i>I</i>))	0.034, 0.063	0.032, 0.082	0.045, 0.100
Goodness of Fit	1.02	1.06	1.02
Max, Min peak, e ⁻ /Å ³	0.36, -0.35	0.59, -0.35	2.27, -1.78

Appendix B. ^1H NMR Spectrum of Compound 5.3

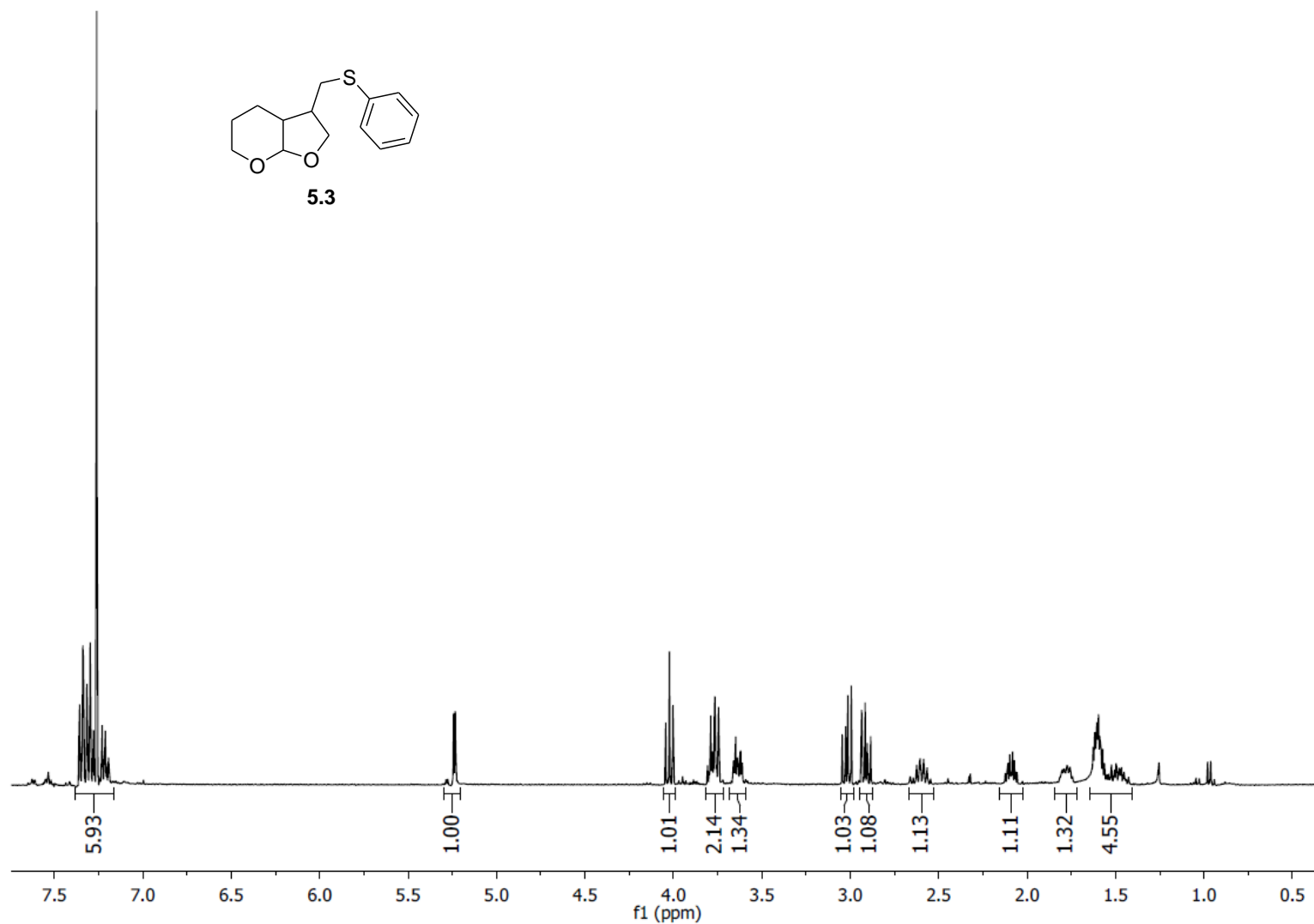


Figure B.1. ^1H NMR (400.1 MHz, CDCl_3) spectrum of compound 5.3.